REPORT DOCUMENTATION PAGE

Form Approved
OMB No. 0704-0188

1. AGENCY USE ONLY (Leave Blank)	2. REPORT DATE	3. REPORT TYPE AND DATES COVERED
	1995	Final

4. TITLE AND SUBTITLE
Multinuclear NMR of Ionomers and Polymer Blends

5. FUNDING NUMBERS

6. AUTHORS
Ellen Margaret O'Connell

7. PERFORMING ORGANIZATION NAME(S) AND ADDRESS(ES)
University of Wisconsin-Madison

AFRL-SR-BL-TR-98-
0005

9. SPONSORING/MONITORING AGENCY NAME(S) AND ADDRESS(ES)
AFOSR/NI
110 Duncan Avenue, Room B-115
Bolling Air Force Base, DC 20332-8080

10. SPONSORING/MONITORING AGENCY REPORT NUMBER

11. SUPPLEMENTARY NOTES

12a. DISTRIBUTION AVAILABILITY STATEMENT
Approved for Public Release

12b. DISTRIBUTION CODE

13. ABSTRACT *(Maximum 200 words)*
See attached.

19980116 142

14. SUBJECT TERMS			15. NUMBER OF PAGES
			16. PRICE CODE
17. SECURITY CLASSIFICATION OF REPORT	18. SECURITY CLASSIFICATION OF THIS PAGE	19. SECURITY CLASSIFICATION OF ABSTRACT	20. LIMITATION OF ABSTRACT
Unclassified	Unclassified	Unclassified	UL

MULTINUCLEAR NMR OF IONOMERS AND POLYMER BLENDS

by

ELLEN MARGARET O'CONNELL

A dissertation submitted in partial fulfillment of the requirements for the degree of

Doctor of Philosophy
(Chemical Engineering)

at the
UNIVERSITY OF WISCONSIN-MADISON
1995

MULTINUCLEAR NMR OF IONOMERS AND POLYMER BLENDS

Ellen Margaret O'Connell
Under the supervision of Professor Thatcher W. Root
and Professor Stuart L. Cooper
at the University of Wisconsin-Madison

Many factors are known to affect the morphology and properties of ionomers, and the role that the cation local environment plays is not well understood. To better understand ionomer morphology, the cation environment in sulfonated and carboxylated ionomers was investigated using ^{23}Na NMR. As many as three environments were seen in polydisperse sulfonated polystyrene (NaSPS): isolated sodium ions at 7 ppm, hydrated ions at 0 ppm, and aggregated ions at –12 to –23 ppm. In monodisperse NaSPS, a fourth peak at –2.7 ppm appeared at ionization levels above 1.2% and molecular weights of at least 35,000. The fraction of sodium ions held in isolated ion pairs decreased to zero while the fraction of ionic species in aggregates increased with increasing sulfonation. As the neutralization level increased, the aggregate peak shifted to higher frequency with incorporation of neutralizing NaOH. These peak positions and trends are explainable in terms of the magnetic and electric field properties of each Na^+ environment.

Effects of sample preparation (solvent casting, humidification and annealing) on the local environment of the sodium ion were determined. NaSPS cast from polar solutions showed more aggregated ions than samples cast from nonpolar solvents. The extent of hydration was followed as a

function of temperature, with more ions residing in aggregates after hydration and dehydration. Finally, annealing at high temperatures led to an increase in the number of isolated ions. Effects of sample processing were partially reversible; the distribution of sodium ions was varied widely using only sample processing.

The investigation into properties of ion-containing polymers was extended to blends of polyurethanes containing interacting groups with small metal-containing molecules. Blends with metal acetates were studied using FTIR, ^{13}C NMR and ^{15}N NMR. Blends with zinc showed improved mechanical properties and peaks shifts in the NMR spectra, indicating complexation. Lesser shifts and lower increases in properties were seen for the blends with magnesium, and no complexation was apparent for the blends containing sodium.

Thatcher W. Root — 8/19/95

Thatcher W. Root — Date

Stuart L. Cooper — 8/19/95

Stuart L. Cooper — Date

Acknowledgments

This thesis would not have been possible without the guidance and support from my coadvisors, Professors Thatcher Root and Stuart Cooper. Despite their differences in research goals and management styles, they always had my best interests at heart. They have assembled excellent research groups within which they encourage exploration of new research areas and ideas. I would particularly like to thank Professor Cooper for having enough faith and trust in all of us to allow our group to remain intact at UW when he moved on to greener (bluer?) pastures.

I would like to thank many of my group members who have contributed to my education here: David Okamoto, Sue Visser, Roger Phillips, Brian Grady, Craig Myers, Rich Goddard, and Eleni Karayianni have taught me polymer characterization techniques and answered my numerous questions. Bob Hergenrother, Jui-Chi Lin, Rich Dickinson, John Coffman, Prahbu Balaraman, Jeff Kobe, Kevin Lewis, and Tracy Perkins have all helped me out in one way or another. Other people who deserve thanks for listening to my complaints and making my stay here more enjoyable are Monica Hart, Frank Skraly, Marty González, Mike(y) Ryan, Mike Lochhead, Mike Cleveland, Cynthia Read, Rod (and Heather) Flemming, and Melanie Goddard. I am grateful for the friendship you have given me.

Special acknowledgment is in order for the departmental staff who helped me out on more than one occasion (too many occasions for some of them!): Becky Torrisi, Janine Jensen, Donna Gabl, Sue Dahms, Linda Caine, Diane Peterson, and Kathy Myhre. Al Hanson, Al Bondioli, and Todd Ninman have also saved the day for me many times. John Cannon deserves

particular thanks for resuscitating my equipment from attacks by a younger group member (he knows who he is!).

I would also like to recognize the sources of funding I have had throughout my stay here. I received fellowship support from the Wisconsin Alumni Research Foundation, the Department of Defense (through the National Defense Science and Engineering Graduate Fellowship Program), and the American Association of University Women. Other laboratory expenses were funded through research grants from the National Science Foundation and the Department of Energy.

Finally, and most importantly, I have to say thank you to my family. My parents, John M.F. and Ann M. O'Connell, have done more to encourage and support me through the years than anyone else. They have always wanted the best for me, and have done everything in their power to open doors in my way. My brother, Larry, has always been there when I needed an escape or a supportive word. Most of all, I would like to thank my husband (a word that still sounds strange!), Douglas Dee, for being understanding and supportive even when he also was working on his Ph.D. There is no one else I would rather spend the rest of my personal and professional life with.

Table of Contents

List of Figures

List of Tables

Chapter One: Introduction

Ionomers are polymers that contain a small number of ionic groups (less than 10-15%) covalently bonded to the polymer backbone. These pendant groups aggregate into ionic domains that form thermally reversible crosslinks.[1,2] The presence of the ionic crosslinks has a strong influence on the physical properties and dominates the behavior of the polymer such that many ionomers, with different polymer backbones, ionic groups, or cations, have enhanced physical properties. Some of the improved physical properties include increases in melt viscosity, tear resistance, modulus, impact strength, oil resistance, and glass-transition temperature.[1] Another advantage of ionomers is the reversibility of the crosslink. At elevated temperatures, thermal dissociation or weakening of the ionic crosslinks occurs, and the polymer can be processed. Processability at high temperatures is an advantage over standard crosslinked systems.

One example of a commercial ionomer is Hycar, a carboxy-terminated telechelic butadiene made by B.F. Goodrich. Hycar, which is used as a thermoplastic rubber, is composed of a low molecular weight chain with functional groups attached at both ends. Telechelic ionomers such as Hycar are often used as model systems because of the regular spacing between the ionic functionalities. Surlyn, another commercial ionomer that is used in the packaging industry, is an ethylene-methacrylic acid copolymer made by Dupont. Other types of ionomers include Nafion, a copolymer of tetrafluoroethylene and perfluorosulfonic acid used as an ion-exchange membrane, and a sulfonated polystyrene random copolymer used by Exxon as a viscosifier for oil-based drilling fluids. These ionomers are shown in

Figure 1-1. While Na^+ ions are the neutralizing cations shown in Figure 1-1, other cations can be utilized. Surlyn and Nafion are semicrystalline copolymers. On the other hand, sulfonated polystyrene is completely amorphous, and may be used to study the solid-state properties of ionomers without the added complexity associated with crystallinity. Another excellent model system is that of the polyurethane ionomers. In these materials the ionic groups can be regularly spaced along the polymer chain, in contrast to the random placement present in samples of commercial sulfonated polystyrene.

Behavior similar to that of ionomers is also exhibited by certain materials composed of blends of metal-containing molecules (either small molecules or ionomers) with polymers containing groups (such as ionic groups, $-NH_2$ groups, or pyridine rings) capable of forming interactions with the added component.[4] These blended polymers also have thermally reversible crosslinks and have the ability to form ion-rich aggregates.

The physical properties of ionomers can be controlled to an extent by modifying the hydrocarbon backbone, the number of ionic groups, the percent of neutralization, or the sample preparation method. Additional degrees of freedom can be gained in ionomer and polymer blends, since the ratios of the blended components and the number of interacting groups can also be varied. As the understanding of the relationships between local structure, polymer morphology, and mechanical properties improves, it will be possible to engineer polymers for use in specific applications.

Because the interacting groups have a dominant effect on the physical properties of ionomers and blends, the nature of the ionic crosslink deserves further study and is the focus of this research. Once the contributions of the

Hycar:

n ≈ 88

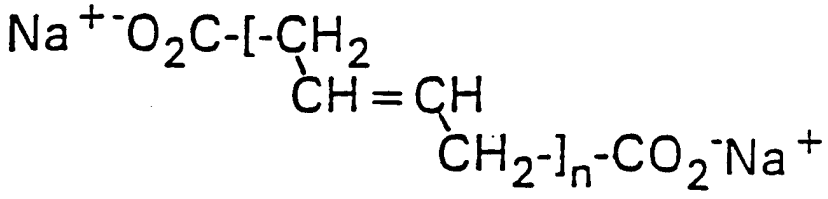

Surlyn:

m/n ≈ 10-30

x ≈ 10^3

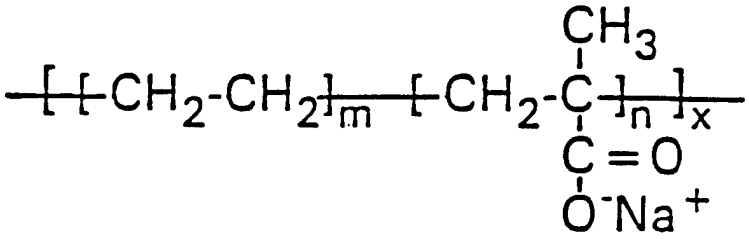

Nafion:

m/n ≈ 5-10

k = 1-3

x unknown

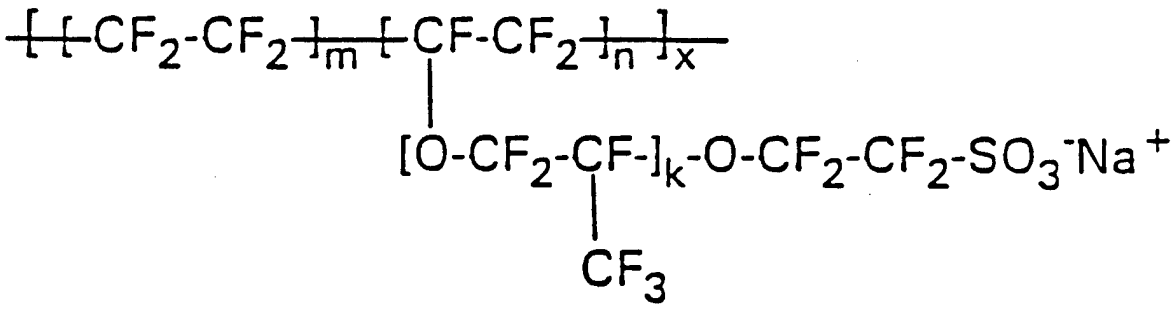

Sulfonated polystyrene (SPS):

m/n ≈ 4-500

x ≈ 10^3-10^4

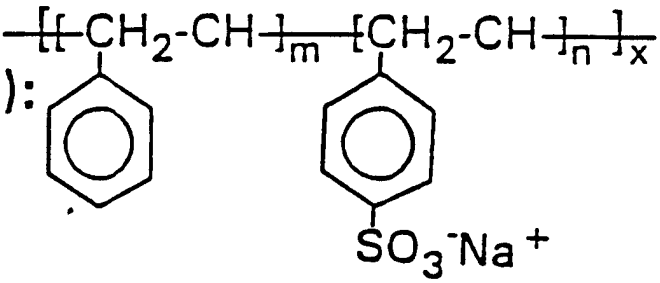

Figure 1-1: Examples of commercial ionomers[3]

ionic groups are better understood, blends of ionomers with polymers that have pendant interacting groups can be studied. In particular, blends of polyurethane ionomers with pyridine-containing polyurethanes would be of interest because of their compatibility and physical properties.

One of the problems with the use of commercial blends is the inability to correlate the sample composition and processing with the resulting physical properties. Understanding the molecular-level interactions within the blend can help link these two areas. Phase separation seems to be a requirement for improved physical properties; however, the interface between two immiscible polymers is often weak.[5] Phase-separated polyurethanes blended with materials which can improve physical properties may overcome these problems.

Nuclear magnetic resonance spectroscopy (NMR) is well-suited for studying ionomers and polymer blends. The technique is site-specific, so it may be used to study the anion or counterion within the ionic aggregate. It can also be used to study the restriction of the nuclei in the area surrounding the aggregate by looking at their motion. Furthermore, NMR is a non-destructive technique, so the sample can be recovered after the experiment.

Other experimental techniques, such as extended x-ray absorption fine structure (EXAFS), have produced a wealth of information on the immediate environment surrounding the cations in ionomers. EXAFS has also been used to determine the number and type of nuclei in the first two coordination shells surrounding the cation. However, the structure and symmetry of the environment is not determined directly. Other techniques, such as electron spin resonance spectroscopy (ESR) and infrared spectroscopy, have probed cation structure in ionomers. The results of these techniques are

complementary to those of NMR. However, NMR can more readily distinguish nuclei which are chemically or structurally different. Also, NMR can be "tuned" to study different nuclei contained in the same material, and can offer information on different microdomains.

This thesis on ionomers has several goals. The first is to study the effect of sample composition on the ^{23}Na NMR properties of sulfonated polystyrene, and through these experiments determine the local morphology of the material. One requirement is to perform a material balance on the sodium ions in the material. This material balance will quantify the number of sodium ions held in aggregates and the number dissolved in the matrix material. Then, the quantity of aggregated material can be related to the mechanical properties of the ionomers. Improved physical properties are expected in ionomers that have more ionic groups aggregating and contributing to crosslinks.

To determine the local morphology of the ionomer it is also necessary to study the structure of the aggregate itself, as well as the structure surrounding the dissolved ion pairs. Lineshape analysis can give information on the environment and the strength of the quadrupole interaction of the ^{23}Na nucleus. The structure of the aggregates is not well-understood, although EXAFS studies have determined it to be fairly disordered in some systems.[6,7] The magnitude of the quadrupolar interaction of a sodium site gives information on the symmetry of the environment surrounding the sodium nucleus and can be used to better understand the structure of the ^{23}Na local environment. Other goals of the research on ionomers include studying the effects of sample preparation (humidification, solvent casting and annealing),

the effects of molecular weight and polydispersity, and the effects of anion type on the local morphology of the ionomers.

Like the ionomers studied in this research, the materials composed of polyurethanes blended with metal-containing salts have been well-characterized through mechanical, thermal, and morphological analysis,[8,9] although not to the extent of the ionomer systems. The goals for the research on this polymer system are twofold: to correlate the effects of blending to changes in the chemical shift and relaxation times for the carbon and nitrogen sites on the pyridine groups that interact with the metal salts and the carbon sites on the acetate group. The results will be used to explain the mechanical and morphological properties acquired from tensile testing and small-angle x-ray scattering. In this way the structure-property relationships of the blends can be determined.

A review of the relevant literature in the fields of ionomers and polymer blends is presented in Chapter 2. In Chapter 3, the experimental procedures used in this study are described, followed by the specific details of the experiments performed. Chapters 4-9 contain the experimental results and discussions of those results for the ionomers and polyurethane blends. Finally, the major conclusions are summarized and recommendations for future work are presented in Chapter 10.

References for Chapter One

1 Eisenberg, A.; King, M. *Ion-Containing Polymers*; Stein, R.S., ed. Academic Press: New York, 1977.

2 Holliday, L. *Ionic Polymers*; Applied Science: London, 1975.

3 Visser, S.A. Ph.D. Thesis, University of Wisconsin-Madison, WI, 1991.

4 Meyer, C.T.; Pineri, M. *J. Polym. Sci., Polym. Phys. Ed.* 1978, **16**, 569.

5 Utracki, L.A.; Weiss, R.A. *Multiphase Polymers: Blends and Ionomers*; American Chemical Society: Washington, D.C., 1989.

6 Ding, Y.S.; Register, R.A.; Yang, C.-Z.; Cooper, S.L. *Polymer*, 1989, **30**, 1221.

7 Register, R.A.; Sen, A.; Weiss, R.A.; Cooper, S.L. *Macromol.* 1989, **22**, 2224.

8 Yang, C.-Z.; Zhang, X.; O'Connell, E.M.; Goddard, R.J.; Cooper, S.L. *J. Appl. Pol. Sci.*, 1994, **51**, 365.

9 Grady, B.P.; O'Connell, E.M., Yang, C.Z.; Cooper, S.L. J. *Polym. Sci. Phys. Ed.* 1994, **32**, 2357.

Chapter Two: Literature Review

A very general overview on the application of NMR techniques to polymer characterization will be presented in the first section of this review. Ionomers will be covered in Sections 2.2 and 2.3, while blends of interacting polymer systems will be discussed in Sections 2.4 and 2.5.

2.1 Polymers and NMR: An Overview

As a non-destructive, site-specific technique, NMR has most commonly been used for routine analysis of chemical compounds. Although the NMR phenomenon was first discovered in 1946,[1,2] extensive application of NMR to solid-state polymers did not begin until 1977, when Schaefer *et al.*[3] used both cross-polarization and magic-angle spinning to enhance the signal intensities in ^{13}C NMR experiments. The applications of NMR to polymers, in both the solution and the solid state, include the determination of chemical structure and conformation, stereoregularity, morphology (phase separation, crystallinity), molecular interactions and polymer dynamics.[4-10]

2.1.1 Proton NMR

Proton (^{1}H) NMR has several advantages, such as the high natural abundance of protons (99.99%) and their short relaxation times. Solution-state ^{1}H NMR is routinely used for identification of chemical structures.[4] Proton NMR of solids is more complicated due to the poor resolution of the corresponding spectra. The ^{1}H NMR spectrum of a solid polymer will generally have only one or two broad, featureless peaks, in contrast to the spectrum of the same polymer in solution, which may have ten to twenty

distinct lines over a 10 ppm range. The severe broadening in solid-state spectra is due to multiple orientation-dependent interactions that obscure the desired information on site identification.

The majority of the work done in the solid state uses multiple-pulse sequences and other specialized pulse routines to selectively eliminate one or more of the confounding factors. One example is the combined rotation and multiple-pulse spectroscopy (CRAMPS) experiment[5] used to study proton relaxation. Another is the Goldman-Shen experiment[11] employed to study spin-diffusion in a phase-separated polymer. However, these are experimentally demanding and have not found widespread application.

2.1.2 Carbon-13 NMR

Solution-state ^{13}C NMR is often used to identify reaction products[12] and to determine polymer microstructure, such as copolymer distribution and stereoregularity[13,14] With solid samples, the technique is still capable of obtaining some of this information,[15] but is more often used to study motions and dynamics.[16] Carbon-13 has a low natural abundance (1.1%) and fairly long relaxation times, which requires long experimental times. However, line-narrowing techniques such as magic-angle spinning, and signal-enhancement techniques such as cross-polarization (CP), can improve signal-to-noise ratios, which shorten experimental times needed.

Many reviews contain detailed discussion of ^{13}C NMR studies of polymers. Discussions on molecular motions,[16] the characteristics of specific types of polymers such as elastomers,[17] and two-dimensional NMR,[18] as well as a number of general books and reviews[5,6,19-23] have been published.

2.1.3 Deuterium NMR

Deuterium (^2H) NMR is well suited to study polymer motions. ^2H is a quadrupolar nucleus with I=1. Because the quadrupolar interaction is dominant, the analysis of spectral lineshapes is relatively straightforward. The lineshape is sensitive to the type of molecular motion, and the nuclear spin relaxation time gives information on timescales of molecular motion.[5] Deuterium nuclei are also of very low natural abundance (0.015%). Therefore, the polymer is often labeled at the sites of interest, to allow for site specificity with the technique. The uses of ^2H NMR in polymers are included in many general NMR and polymer reviews.[5-10] Also, many papers focus on the use of ^2H NMR in glassy polymers and elastomers.[24-28]

2.1.4 Nitrogen-15 NMR

Solid-state ^{15}N NMR has been used only recently in polymer science, due to the low natural-abundance (0.37%) and the long relaxation times of ^{15}N nuclei. The use of ^{15}N-labeled compounds and cross-polarization provides high resolution due to a wide chemical shift range (400 ppm) and the relatively few sites occupied in the polymer (as compared to carbons and protons). The advent of large-volume magic-angle spinning (MAS) systems substantially improved signal-to noise ratios, and made natural-abundance work feasible.[29,30] Although many researchers still use isotopically labeled samples when available,[31-34] some have published work with samples containing natural-abundance levels of ^{15}N.[35-38]

2.2 Ionomers

2.2.1 Models

Several physical and mathematical models have been developed to describe and explain the mechanical and morphological properties of ionomers. Theoretical models, which predict the structure of the aggregate and surrounding chains, have been proposed to describe the mechanical behavior of ionomers. Small-angle x-ray data are usually interpreted in terms of morphological models. A model discussing the existence of multiplets and clusters was proposed by Eisenberg,[39] and this is accepted by a number of researchers.[40,41] However, other researchers[42-44] support instead the idea that some ions are aggregated while others exist as dissolved ion pairs.

Excellent reviews of the structural models are in Mauritz[45] and Eisenberg *et al.*[46] Reviews of the morphological models are included in papers by MacKnight and Earnest,[47] Yarusso and Cooper,[48] and Eisenberg *et al.*[46]

Structure

Eisenberg's model describes qualitatively the two-phase behavior of ionomers which may be inferred from their mechanical properties.[39] The author assumed that an ion pair is the basic structural unit. From thermodynamic arguments for the dipole-dipole attraction of ion pairs in a hydrocarbon matrix and assumptions of steric hindrance due to the pendant groups, Eisenberg proposed an upper limit to the number of ion pairs that could aggregate into a microdomain, or multiplet. These multiplets, which consist only of ionic material, contain a small number (up to eight) of contact ion pairs (Figure 2-1). Eisenberg claims that it is energetically favorable

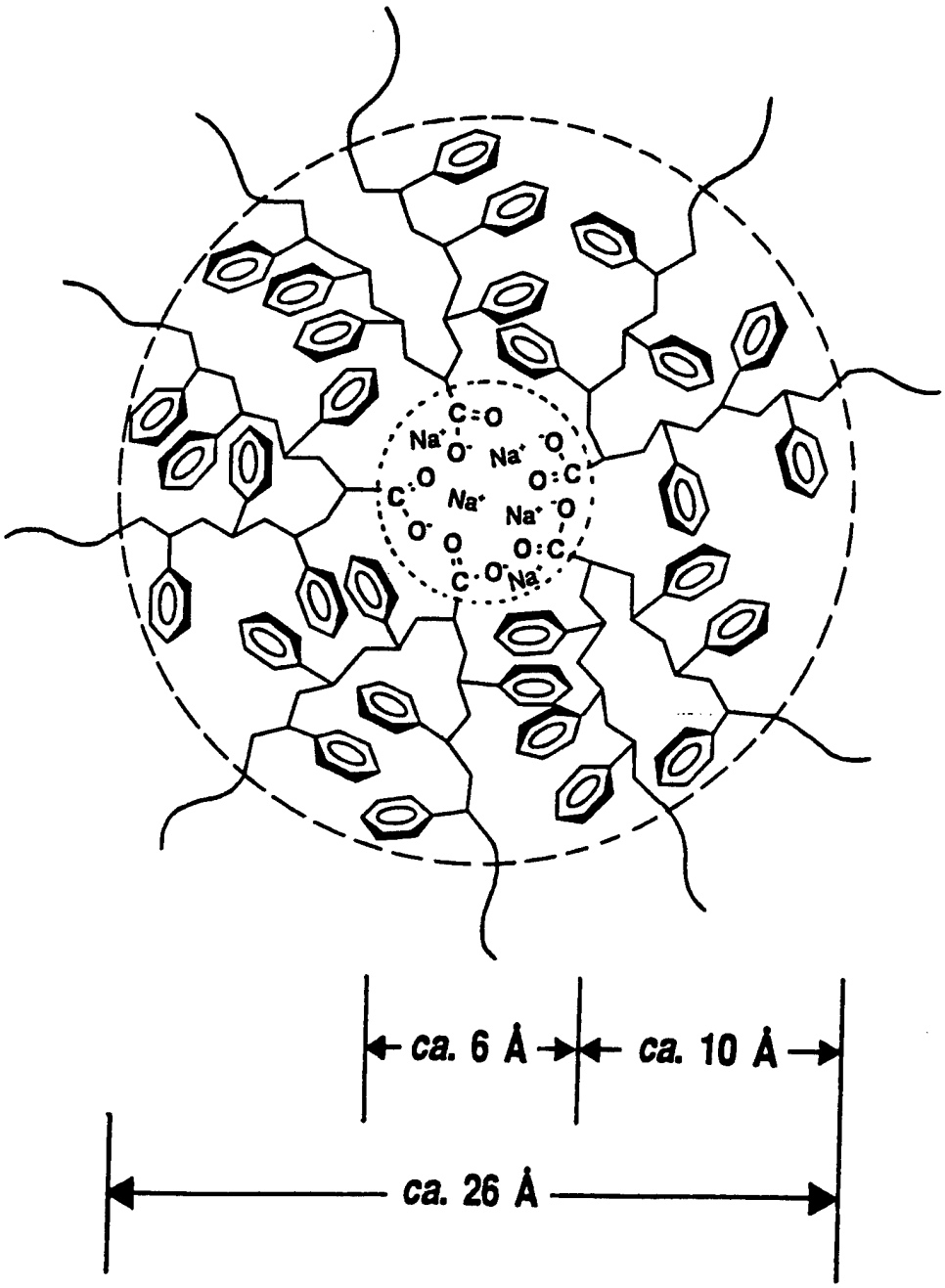

Figure 2-1: Schematic of a multiplet and its corresponding region of restricted mobility[46]

(through electrostatic forces) for these multiplets to form larger groups in which they are separated by thin layers of hydrocarbon. These larger, but still ion-rich, domains are called clusters. The aggregation of ion pairs and multiplets is resisted by the elastic forces of the polymer chains, and the mobility of the chains near the aggregates is reduced. Also, a critical concentration of ion groups is required for the formation of clusters. This is because very dilute concentrations of ion pairs or multiplets have weak attractive forces over long distances as compared to the elastic forces of the chains. The size of a cluster would depend on the balance between the elastic and electrostatic forces. The model also predicts a critical temperature above which the clusters will dissociate.

Eisenberg *et al.*[46] later revised the model of cluster formation to account for inconsistencies in interpreting some mechanical property data on ionomers. The authors proposed that the regions of restricted mobility surrounding the multiplets (which themselves cause an increase in the T_g of the matrix material) overlap at high ion concentrations to form a cluster characterized by a separate T_g. The major modification in this model is that cluster formation is not due to electrostatic interactions between multiplets, but instead is due to the overlap of multiplets at high concentration.

Most structural models are based on Eisenberg's theory of multiplets and clusters. Forsman[49], Dreyfus,[50] and Dayte and Taylor[51] all proposed independent models for describing chain extension in ionomers due to aggregation. Their models are all based on a competition between electrostatic and elastic forces during aggregation. Several attempts to model cluster formation in Nafion have also been published.[52,53]

Lefelar and Weiss[54] offered a crystal-packing argument to explain the differences in mechanical properties and SAXS results between carboxylated and sulfonated ionomers, as well as between ionomers neutralized with monovalent and divalent cations. They proposed that in carboxylated ionomers, the anion packing is based on the cation, while in sulfonated ionomers the anion packing is independent of the cation. In both the carboxylated and sulfonated ionomers, more anions are shared by the monovalent cations than by the divalent cations. Therefore, although the individual dipole-dipole interactions may be stronger in the divalent case, more stress would be required to pull ions from the aggregate in the monovalent case.

Morphology

A large number of models have been proposed to describe the features seen in SAXS patterns of ionomers. The two features commonly seen are a broad peak with a maximum at $q \approx 1\text{-}3$ nm^{-1} and a sharp upturn in intensity at very low q values. The upturn has been attributed to factors such as voids and impurities, which are not related to the ionomer morphology.[55] However, anomalous small-angle x-ray scattering (ASAXS) studies by Ding *et al.*[44] and Register and Cooper[55] have shown that the upturn is due to the ionic character of the polymer.

The source of the ionic peak is the ionic aggregation,[56] but the structure of these aggregates is still not fully understood. The presently accepted SAXS models fall into two categories: those that assign the ionic peak to *intra*particle interference[57-59] and those that claim that the peak is due to *inter*particle interference.[42,48,60,61] A model from each of these

categories will be discussed in detail. Recent studies[41,44,62] have indicated that the *inter*particle model describes the ionomer morphology more completely.

Intraparticle Models

In the intraparticle interference models, the scattering is assumed to be due to the short-range order within the aggregates. In one such model[57] the aggregate is composed of an electron-rich "core" surrounded by hydrocarbon chains. This region is then surrounded by a "shell" of material having a lower electron density than the core, but greater than the hydrocarbon shield and the matrix. (see Figure 2-2a) This "core-shell" model is not physically realistic, since it cannot account for the higher concentration of ions in the shell than in the matrix. The depleted-zone core-shell model,[58] a schematic of which is shown in Figure 2-2b, corrects this deficiency. The ions are assumed to be well-distributed in the matrix initially, but are driven into aggregates by electrostatic forces. As the ion pairs start to aggregate, the areas of the matrix immediately surrounding aggregates are depleted of ionic groups. The peak in the SAXS pattern is due to the preferred distance between the core and the matrix. Although this model qualitatively describes both the SAXS upturn and the scattering peak, it does not adequately fit the SAXS data.[48]

Interparticle Models

In the interparticle models, the aggregates are distributed in the matrix with some degree of order and the ionic peak is due to the scattering between ionic aggregates. The model by Yarusso and Cooper assumes that the ionic aggregates are hard spheres distributed throughout the matrix with liquid-like

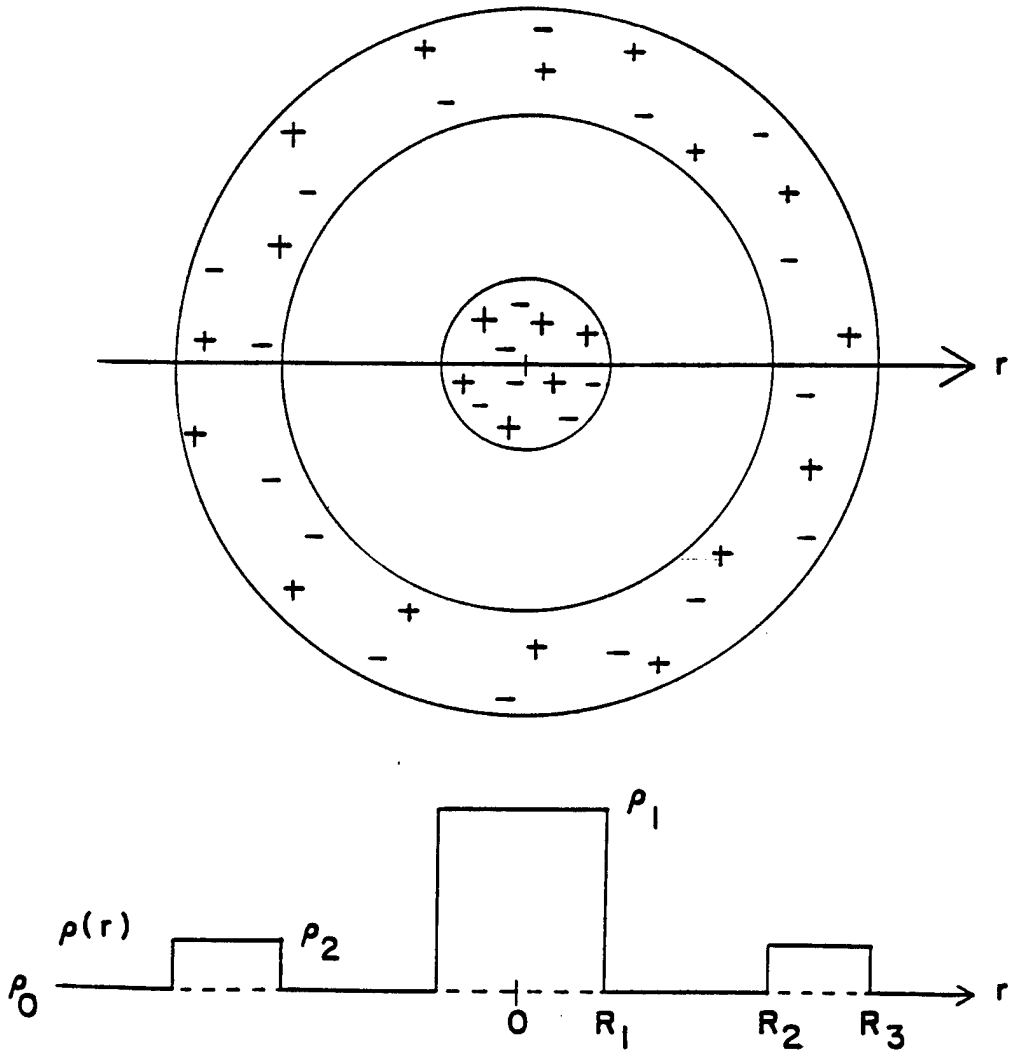

Figure 2-2a: Schematic and electron-density profile for the core-shell model[48]

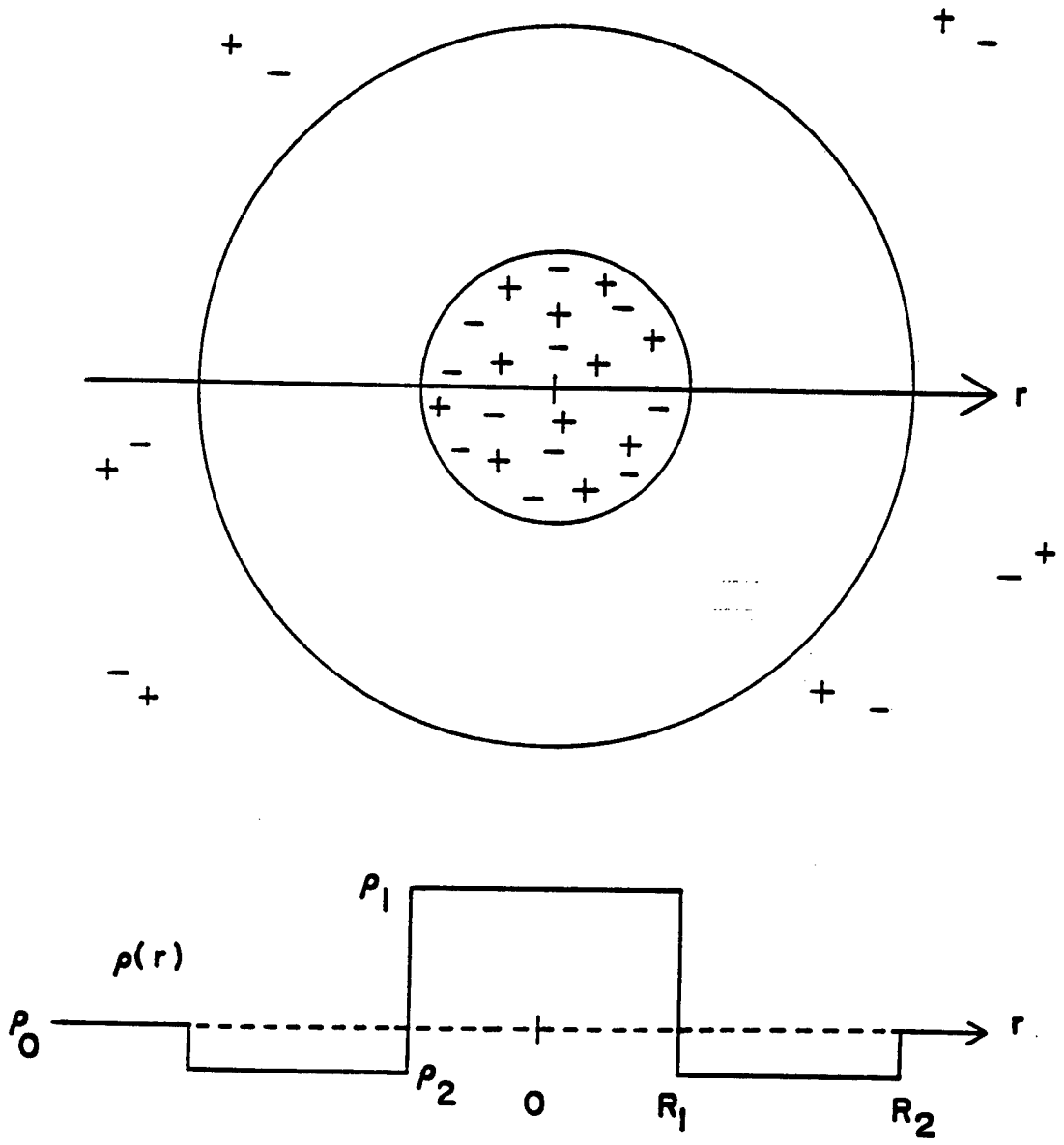

Figure 2-2b: Schematic and electron-density profile for the depleted-zone core-shell model [48]

order.[48] The radius of closest approach between the aggregates is defined by a layer of hydrocarbon chains surrounding, and attached to, the ionic sphere. This model is similar to the depleted-zone core-shell model, but assumes that the scattering is due to interparticle interference. This model fits the data well;[48] a modification by Kinning and Thomas[63] has been shown to give even closer fits to SAXS data.[64,65]

2.2.2 Local Environment

A number of techniques have been used to probe small length scales (< 10 Å) in order to study local environments in an ionomer. Most of these techniques, such as nuclear magnetic resonance (NMR), electron spin resonance (ESR), infrared spectroscopy, and extended x-ray fine structure (EXAFS), study the environment surrounding the cation. Some techniques, such as NMR, can study environments of other nuclei in the system as well. NMR will be discussed in a separate section since it is the emphasis of this research.

Electron Spin Resonance

Electron spin resonance (ESR), also known as electron paramagnetic resonance, has been used to characterize ionomers in the solid-state. The notable features in the ESR spectra of ionomers include the hyperfine structure characteristic of isolated ions in solution. This series of peaks broaden into a featureless line as ion-ion (exchange-interaction) interactions become dominant.[66] A second upfield signal assigned to ion-ion pairs has also been seen in Cu^{2+} spectra, but has been attributed to excess neutralizing agent by some researchers.[67]

The ESR experiment is similar to the NMR experiment in that an applied magnetic field will cause electron spins to align parallel or anti-parallel to the field. In ESR the sample is irradiated with microwaves at a constant frequency while the magnetic field is varied. The magnetic fields used in ESR are also smaller than those used in NMR (10,000 G) because the magnetic moment of an electron is 1800 times greater than that of a proton. Two frequencies commonly used for ESR are the X-band (9500 MHz) and the Q-band (35,000 MHz). Although the sensitivity increases with increasing frequency, there are limitations at high frequencies, such as larger field inhomogeneities.

ESR spectra are usually shown in the derivative form, with signal intensity plotted versus the magnetic field strength. From the spectrum the *g*-factor and hyperfine splitting can be obtained. The *g*-factor is analogous to the chemical shift in NMR, while the hyperfine splitting describes the coupling of electrons with nuclear spin moments. In concentrated systems, electron spin exchange transforms the series of hyperfine lines into a single, broad signal; this exchange occurs when two radicals interact and exchange electrons. Further increases in concentration will narrow this line slightly, a phenomenon which has been termed "exchange narrowing."[68]

Pineri *et al.*[69] first used ESR to study copper-neutralized Hycar and high molecular-weight butadiene-methacrylic acid copolymers neutralized with copper acetate. While SAXS studies showed the presence of clustering, ESR was used to study the structure of the aggregate itself. ESR showed two environments for the Cu^{2+} ion: one signal, with hyperfine structure, was assigned to isolated Cu^{2+} ions, while a second (higher-field) signal was assigned to Cu^{2+}-Cu^{2+} ion pairs (dimers). The second signal intensified as the

percentage of neutralization was increased. Temperature increases decreased the fraction of Cu^{2+}-Cu^{2+} dimers, but increased the signal for isolated ion pairs. The authors suggested that this shows a breaking up of the ion pairs.

Weiss *et al.*[70] and Toriumi *et al.*[71] examined the temperature dependence of the ESR spectrum for Mn^{2+} in Mn-SPS. The authors point out that the ESR exchange interaction occurs at ~ 1-2 mole% sulfonation, which is approximately where the SAXS peak becomes apparent. Since the SAXS peak indicates phase-separation, its appearance suggests clustering. An increase in temperature to 140°C broadened the ESR spectrum of a 0.92% sulfonated sample, as a result of an increase in aggregation. This appears to contradict the results of Pineri *et al.*;[69] however, these studies were performed on ionomers with two types of backbone material which exhibit different behavior with increasing temperature. From spectral simulations, the authors estimated the relative amounts of Mn^{2+} ions present in aggregates at 25°C and at different levels of sulfonation. The authors also stressed that ESR shows aggregation, but not the presence of clusters.

Sen *et al.*[67] examined the ESR and FTIR spectra of Hycar samples neutralized with a mix of copper and sodium acetates. The fully neutralized ionomers with 50% Cu^{2+} and 50% Na^{+} showed a signal typical of isolated copper ions. Ionomers partially neutralized with only 25% or 50% Cu^{2+} showed the signal due to isolated ions, but also had a higher-field signal assigned to Cu^{2+}-Cu^{2+} dimers. However, when the ionomer was exposed to copper acetate for 24 hours (instead of 4 hours), only a broad center peak was present. This suggests that the high-field signal was due to unreacted neutralizing agent.

Other researchers have used ESR to study ionomers. Yamauchi and Yano[72] studied Cu^{2+}-neutralized styrene-methacrylic copolymers with ESR; they saw two strong signals analogous to those seen by Pineri *et al.*, as well as a third environment. Galland *et al.*[73] attempted to quantify the amount of dimers formed in Hycar neutralized with copper. In addition, several studies have been completed on Nafion ionomers.[74,75]

Infrared Absorption Spectroscopy

Infrared absorption (IR) spectroscopy is commonly used to study molecular structure in polymers. In an IR experiment, light is absorbed by the molecules in the sample if the frequency of the radiation is equal to the frequency of a vibration of the molecule. The results are plotted as transmittance versus wavenumber (inverse wavelength), or absorbance versus wavenumber. Assignment of the peaks in absorbance, or bands, with particular molecular vibrations leads to identification of the entire molecule.[66,76] In ionomers, the mid- and far-IR regions (800-4000 cm^{-1} and 100-800 cm^{-1}, respectively) offer the most information about the interactions of the ions with their neighbors.

Mattera and Risen[77] observed the appearance of one absorption band at 120-200 cm^{-1} in the far-IR region of SPS (3.4-16.7% ionization) neutralized with metal cations. The authors attributed this band to cation motion. It shifted to lower wave numbers (lower frequency) as the cation mass increased, and the intensity of the signal improved with dehydration and annealing.

Rouse *et al.*[78] reported far-IR studies on polystyrene methacrylate ionomers. The band at 250 cm^{-1} was due to cation motion, as in the study of

Mattera and Risen;[77] this band is attributed to vibration of aggregates containing only a few ions. However, increasing the level of carboxylate groups and Na^+ counterions led to the appearance of two other bands. One of these was due to weak internal vibrational modes of the polymer, but the other (at 170 cm^{-1}) was attributed to vibrations of aggregates containing many ions. Peiffer *et al.*[79] studied SPS with varying sulfonation levels (1.2-7.2%) and different cations. They saw only one absorbance band in NaSPS, but two in ZnSPS, possibly because the transition-metal ions interact differently with the sulfonate group. Alternatively, the two bands may be due to cation motion either in hydrated and dehydrated sites or in multiplets and clusters. No definitive assignment could be made, but the authors claimed the latter explanation is more likely.

Other studies have focused in the mid-IR range. Andreeva *et al.*[80] studied the IR bands due to the carboxylate ion stretching mode in salts of butadiene methacrylic acid copolymers. The authors observed two bands due to asymmetric stretching vibrations, and assigned them to multiplets and clusters. Some authors, however, suggest that the two bands are due to isolated ion pairs and aggregates.[48] Earnest and MacKnight[81] studied ethylene methacrylate copolymers with IR, but were interested in the temperature dependence of hydrogen bonding in partially-neutralized ionomers. At room temperature all acid groups existed as hydrogen-bonded dimers, but at higher temperatures some dimers dissociated into monomers.

Coleman *et al.*[82] investigated zinc salts of ethylene methacrylic acid copolymers as a function of neutralization level. Based on their IR results on standards and for thermal studies, the authors proposed five local structures for the carboxylate groups that can occur in partially neutralized salts.

However, only one structure, tetracoordinated zinc carboxylate, was found for the fully neutralized ionomer.

Extended X-Ray Fine Structure

The extended x-ray fine structure (EXAFS) technique is used to probe the structural environment within a 5 Å radius of the atom being studied. The EXAFS signal is due to the oscillations of the x-ray absorption line beyond the absorption edge of the cation. The absorption of x-rays causes the ejection of a photoelectron from the absorbing atom, and the oscillations beyond the absorption edge are due to backscattering of the emitted electron off nearby atoms. The information obtained from this experiment includes the number, type, and positions of atoms surrounding the cation.[83,84]

Among the early EXAFS studies on ionomer systems were those by Yarusso *et al.*[85-87] on sulfonated polystyrene (SPS) neutralized with Fe^{2+}, Ni^{2+}, or Zn^{2+}. Two shells, with radii of ~ 2 Å and 3 Å, surrounded the counterion. The inner shell was filled with mostly oxygen and some sulfur atoms, while the outer shell consisted of a few atoms of the metal. The results suggest a certain amount of short-range order in the aggregate. Grady and Cooper[88,89] studied SPS neutralized with Ni^{2+}, Zn^{2+} and Cd^{2+}. The authors proposed structures for NiSPS and ZnSPS and suggested that water must be present in the coordination structure. These authors also studied the effects of stretching on the cation local environments; slight orientation in the stretch direction was noted.[89]

Ding *et al.*[90] studied a series of sulfonated polyurethanes neutralized with various cations. In all cases, the 2-2.3 Å inner shell consisted of oxygen atoms. However, some ions, such as Ni^{2+} and Eu^{3+}, showed clear second

shells consisting of the respective metal, while others, such as Zn^{2+}, did not show a second shell. Sulfur was not found in any case, which the authors attributed to sulfur atoms not being well-ordered.

Galland *et al.*[73] used EXAFS to study ionomers of Hycar neutralized with copper. EXAFS data showed two discernible coordination shells around the Cu atom: an oxygen inner shell and a copper outer shell. The authors concluded that the structure of the copper ion was one of square planar coordination, with the ends of the PBD chains bonded at the corners.

2.2.3 Effects of Sample History

Many different variables can affect the morphology of polymers and ionomers. Among these are the type of ionic group, the choice of neutralizing agent, the ionization and neutralization levels, thermal history, and processing history (such as solution casting and compression molding). Some of the studies that address these areas are discussed in this section.

Type of Anion

Lundberg and Makowski[91,92] compared sodium-neutralized carboxylated polystyrene (NaCPS) and sulfonated polystyrene (NaSPS) at 5% ionization. The melt viscosity of SPS was 1000 times higher than that of CPS, and the ionic association in SPS persisted to higher temperatures. The reduced viscosity of SPS was strongly influenced by the methanol concentration in a cosolvent with xylene, while the viscosity of CPS was unaffected. The authors suggested that the higher polarity of the sulfonate group resulted in stronger ionic associations.

Rigdahl and Eisenberg[93] studied the viscoelastic properties of SPS and compared them to those of sulfonated sodium methacrylate (S-NaMA). Two loss peaks were seen in the tan δ curve. The higher temperature loss peak, assigned to the T_g of clusters, is at a higher temperature in SPS. This is indicative of more stable aggregation.

Visser and Cooper investigated sulfonated and carboxylated polyurethane ionomers (SPU and CPU, respectively) through mechanical studies[94] and SAXS experiments.[65] SPU exhibited higher tensile strengths and increased phase separation compared to CPU. However, CPU showed high modulus values attributed to increased crosslinking efficiency. SAXS patterns showed that the carboxylated ionomers contained larger aggregates. An increase in the number of ionic groups in an aggregate increases the size of the aggregate and the modulus of the carboxylated materials. However, weaker individual ionic associations lead to lower tensile strength.

Yarusso and Cooper[95] examined SAXS patterns of SPS and CPS, and determined that the cluster sizes were almost identical. Weiss[96] concluded that the ionic associations within phosphonate ionomers of EPDM (ethylene-propylene diene monomer terpolymer) and its sulfonated analog are of equivalent strength. MacKnight *et al.* studied carboxylated,[97] phosphonated,[98] and sulfonated[99] polypentenamers; comparisons of the different types of ionic groups were difficult to make, however, because of inconsistencies in synthesis.

Ion Concentration

Makowski *et al.*[100,101] reported studies on S-EPDM of varying sulfonate content. The authors saw increases in melt viscosity, tensile

strength, and modulus, as well as decreases in elongation with increasing sulfonate content. Substantial association was seen at less than 1% sulfonation.

Eisenberg and Navratil[102,103] studied the effects of ion concentration on S-NaMA. At low ion concentrations, time-temperature superposition of stress-relaxation data was obeyed; however, above 6% sulfonation this was no longer true. X-ray studies showed the appearance of an ionic peak at sulfonation levels above 5-6%. The authors determined this to be the critical concentration for cluster formation, or the "cluster point". Bellinger *et al.*[104] noted increases in tensile strength, toughness, fracture properties, of NaSPS as ion content increased. The same research group also determined that fatigue properties decreased as ion content was increased to 5%, after which the fatigue lifetime increased; they attributed this behavior to reaching Eisenberg's "cluster point."[105]

Several SAXS studies have been performed on ionomers with varying ionization levels. In SPS, Peiffer *et al.*[106] observed an ionic peak corresponding to a Bragg spacing of 37 Å in samples above 3% sulfonation. Weiss and Lefelar[107] observed an ionic peak in SPS at sulfonation levels as low as 1.4%. They also observed no scattering peak in a 5.5% sulfonic acid ionomer (HSPS) and only a broad shoulder in 11.5% HSPS.

Williams *et al.*[62] used SAXS to study carboxy-telechelic ionomers. Changing the ion concentration by varying the molecular weight only served to change the distance between ionic domains. Although the authors observed scattering peaks in the SAXS data, they saw no evidence for the existence of clusters, a critical concentration for aggregate formation, or a critical

temperature for aggregate dissociation. Broze *et al.*[108] came to similar conclusions through rheological studies of these same telechelics.

Type of Cation

Navratil and Eisenberg[109] studied the effect of counterion on the viscoelastic relaxation of styrene methylacrylate copolymers. The stress relaxation curves were similar in shape for all samples, but showed variations with cation types. Large ions such as Cs^+ formed less-stable aggregates than smaller ions, such as Na^+, since a lower energy is required to remove an ion pair when the interion distance is larger. Also, values of the rubbery moduli of Ba^{2+}- versus Na^+-neutralized materials suggest that divalent counterions have lower crosslink densities than monovalent cations. However, the transition from the rubbery region to flow (pseudo-rubbery region) is more pronounced for the Ba^{2+} salts, suggesting that divalent cations form aggregates with longer lifetimes than in the monovalent cases. However, the T_g and the critical ion concentration were not affected by the choice of cation. Therefore, it seems that although the choice of cation may affect some physical properties, it does not have a strong influence on the overall structure of the aggregate.

Weiss and Agarwal[110] compared properties for Na^+- and Zn^{2+}-neutralized S-EPDM. The authors reported no difference in T_g between the two materials but did see higher melt viscosities for Na-S-EPDM. Ding *et al.*[111] reported changes in the mechanical behavior with the choice of cation in SPU samples. The authors proposed that the observed differences are due to an "ion-hopping" mechanism in the weaker materials (such as ZnSPU), in which the ions redistribute among the aggregates without dissociation of the

aggregates. This mechanism did not occur in the stronger materials, such as NaSPU. Makowski *et al.*[100,101] reported results for nine different cations in S-EPDM. All cations showed high melt viscosities except for Pb^{2+} and Zn^{2+}; these two cations showed higher elongations and tensile strengths. The authors attributed these results to lower ionic association with Pb^{2+} and Zn^{2+}.

Eisenberg *et al.*[112] found that the critical concentration of ionic groups decreased as the ratio of charge to ion size increased. Following this work and the research of Makowski *et al.*,[100,101] Bagrodia and Wilkes[113] proposed that the covalent character of the counterion should be considered along with the charge-to-size ratio. The authors suggested that Zn^{2+}, which is neither a hard nor a soft acid, has more covalent character than do the other cations (Ca^{2+}, Mg^{2+}, etc.) studied, which are hard acids. Therefore, the ionic associations in Zn^{2+}-neutralized materials are weaker.

Brozoski *et al.*[114] studied IR spectra of Surlyn neutralized with alkali, alkaline earth, and zinc salts. Through an analysis of the most probable chemical structures, the authors interpreted the differences in the spectra of the zinc-neutralized salt from the spectra of the alkali- and alkaline earth-neutralized salts as due to the coordination number of the respective metal complexes. Similar results for Surlyn were observed by Han *et al.*,[115] who proposed two mechanisms for ionomer structure: a multiplet-cluster model for alkali and alkaline earth metals and a coordination-complex model for transition metals. Fitzgerald and Weiss[116] also observed different IR band shifts for SPS neutralized with transition-metal ions rather than other metal ions. These effects were attributed to interactions of the d-electrons of the transition metals with the sulfonate group.

Register *et al.*[117] correlated local order, as studied by EXAFS, and the tensile properties of telechelic ionomers. The authors suggested that certain cations that form ionomers with higher degrees of order have more cohesive aggregates. These tightly bound aggregates cannot relax by ion hopping and, instead, exhibit strain hardening and sample failure. Ding *et al.*[90] and Visser and Cooper[118,119] studied the mechanical properties, SAXS patterns, and EXAFS results for polyurethane ionomers and also observed relationships between tensile properties and local order.

Effects of Partial Neutralization

Arai and Eisenberg[120] investigated the dielectric behavior of 9% ionized S-NaMA with varying degrees of neutralization. The authors saw strong dependencies of dielectric loss and the temperature of the loss peak on the degree of neutralization. Two loss peaks were seen in polymers with high levels of neutralization; the high-temperature loss peak, which depended on the neutralization level, was considered to be the glass-transition temperature of the clustered domains. Yano *et al.*[121] observed similar results in ethylene sodium methacrylate ionomers.

Mohajer *et al.*[122] reported substantially lower modulus values and elongation for a 90% neutralized ionomer than for one neutralized to the equivalence point. Apparently, the acid groups have more covalent than ionic character as compared to the salt groups, and this prevents them from taking part in strong aggregates. Also, Williams *et al.*[62] observed that 80% Mg-neutralized Hycar ionomers swelled more rapidly in water than did the 100% neutralized materials. The authors proposed that acid groups were dissolved in the matrix and allowed for improved water transport through the

hydrocarbon. ESR studies[123] showed that aggregation of the cations was a function of neutralization level in Mn^{2+}-neutralized ionomers at 5.4% ionization. At 99% neutralization, no isolated Mn^{2+} ions existed. Results from SAXS experiments[124,125] suggest that the degree of phase separation increases with increasing degree of neutralization.

Effects of Overneutralization

Makowski *et al.*,[100,101] who investigated S-EPDM neutralized with zinc acetate via viscosity studies, reported a decrease in melt viscosity with overneutralization. The authors attributed this drop to plasticization of the ionic groups by the excess zinc acetate. Similarly, Pésci *et al.*[126] observed decreases in crystallinity of a Mg^{2+}-neutralized semicrystalline ionomer with increasing amounts of Mg^{2+}; the drop in crystallinity was most apparent at magnesium to acetate ratios above unity.

Mohajer *et al.*[122] studied the effects of excess neutralizing agents on the mechanical properties, such as modulus and stress-at-break, of sulfonated telechelic polyisobutylene tri-star ionomers neutralized with either K^+, Ca^+, or Zn^{2+} cations (up to 300% excess neutralization levels). The presence of the excess salts improved the stress attained at high elongation, but did not change its modulus. This seems to contradict the results of Makowski *et al.*; however, these two studies examined different physical properties and temperature ranges. The zinc acetate can act as a reinforcing filler at room temperature, but will act as a plasticizer at high temperature, above its melting point. Since a change in modulus would have indicated a change in the number of crosslink points, it was proposed that overneutralization increases the strength of the ionic associations but not the number of ionic aggregates.

The authors determined that excess neutralizing agent was not held in phase-separated salt domains, because any salt that had crystallized into separate domains would have been removed by vigorous washing.

In a rheological study of the same group of ionomers, Bagrodi *et al.*[127,128] examined the effects of excess neutralizing agent on these K^+-neutralized samples. The melt viscosity of the ionomers neutralized with 100% excess salt was much higher than that of the ionomers neutralized stoichiometrically. Although these results contradict those of Makowski *et al.*, the differences are most likely due to the stronger ionic character of K^+ than Zn^{2+}.[100,113] The authors stressed that these results support their argument that the excess salts are present in the ionic domains and not dispersed in the matrix, since their presence increases the strength of the aggregates and, therefore, the melt viscosity. Vlaic *et al.*[129] noticed similar mechanical and viscoelastic behavior with overneutralization, but did not observe any changes in the local environment through EXAFS experiments. Recently, Kim and Eisenberg[125] noted differences in the tanδ curves for NaSPS neutralized to 100-150% and NaSPS neutralized to 200-300%. At the lower neutralization levels, it is likely that the sodium ion resides near the aggregates while at higher ion content the ions could be phase-separated into NaOH domains.

Effects of Molecular Weight

The effects of molecular weight on the rheological[130,131] and dynamic mechanical properties[131] of ionomers have been reported. Erhardt *et al.*[130] reported effects of molecular weight on the zero-shear viscosity of styrene/butylmethacrylate/potassium methacrylate terpolymers. An ionomer with M_w of 34,000 showed a greater dependence of viscosity on ion

content than did a material with M_w of 145,000. The authors concluded that the ions are much less effective at increasing viscosity when polymer chains are already entangled. Kim *et al.*[131] reported changes with molecular weight in the high-temperature region of dynamic mechanical and rheological experiments for NaSPS and poly(styrene-sodium methacrylate). As molecular weight increased, the high-temperature loss peak (termed "ionic" or "cluster" glass transition) became more well-developed and the onset of flow was delayed to higher temperatures.

Thermal Treatment

Weiss[132] investigated the thermal behavior of SPS as a function of aging time (2 hours-170 days). He suggested that for ionomers quenched from the melt, differential scanning calorimetry (DSC) data showing the appearance of a sub-T_g endotherm with time confirmed a return to equilibrium morphology. Kim and Eisenberg[125] noted small changes in the storage moduli of NaSPS after annealing; the position of the "cluster" peak increased to higher temperature. Galambos *et al.*[133] followed the formation of a SAXS peak with heating in a Mn-SPS sample solution-cast from a THF/water cosolvent. Initially, this material showed no scattering peak, but did show a broad ESR spectrum typical of Mn^{2+} ions in close proximity to each other. At 180°C, a peak appeared with a Bragg spacing of 37 Å, and grew in intensity with temperature. Register *et al.*[134] reported EXAFS results which showed no change in the first coordination shell of the Mn^{2+} ion with the heat treatment; the authors suggested that the result is due to disorder in the aggregates.

Weiss *et al.*,[70] using SAXS and ESR, examined the effect of thermal history on the microstructure of sulfonated polystyrene (SPS). The authors

assumed that clusters were the scattering entities in ionomers. While the SAXS results for Zn^{2+}-neutralized SPS (ZnSPS) and NaSPS and the ESR results for MnSPS were interesting, the findings would have been more conclusive if the authors had compared SAXS and ESR data for MnSPS. This is noteworthy because the changes in SAXS features with thermal treatment were drastically different between NaSPS and ZnSPS. Upon heating to 300°C, the ZnSPS aggregates were partially destroyed, as evidenced by a decrease in SAXS intensity. However, the Bragg spacing, which was determined from the position of the peak maximum, did not change. On the other hand, upon heating the SAXS intensity for NaSPS increased and the peak shifted to lower q values, corresponding to larger Bragg distances. In the ESR studies, some broadening of the hyperfine structure was seen with increasing temperature for all ionomers studied, including those with as low as 0.9 mol% ionization. MnSPS showed exchange interaction and exchange narrowing for the annealed samples, indicating increased aggregation in these samples.

The effect of thermal treatment on a SPU was investigated by SAXS[64,135] in order to observe an aggregate dissociation temperature. Ding *et al.*[64] observed no change in the SAXS pattern of a Cd^{2+}-neutralized material, up to 225°C. However, the SAXS peak for ZnSPU moved to lower q values at temperatures above 175°C, in agreement with the results on ZnSPS.[70] In both cases the intensity of the upturn increased with temperature. In a similar study, Register *et al.*[135] observed no change in the SAXS pattern of NaSPU before sample degradation at high temperatures.

Sample Processing

Sample preparation may significantly affect ionomer morphology. For example, casting Mn-SPS from solutions of different solvents resulted in changes in the scattering peak of the ionomer.[133,136] A cast sample showed a smaller scattering peak than did the compression-molded sample, and a sample cast from a THF/water cosolvent showed no SAXS peak at all. ESR spectra indicated that the Mn^{2+} ions were associated, indicating that isolated ion pairs were not formed.

Ding *et al.*[64,111] studied the effect of sample preparation on SPU ionomers by comparing samples that had been compression molded, cast from DMF, and cast from THF/water. The modulus of the rubbery plateau region was lower for the sample cast from THF/water than for the sample cast from DMF; this was attributed to an increase in dissolved ionic groups and a corresponding decrease in the number of aggregated ionic groups. As the preparation environment became more polar, the SAXS peak and upturn shifted slightly to lower q values, indicating more phase mixing.

2.2.4 Summary

As has been presented, there is an abundance of work published on ionomer systems. Results of some studies seem somewhat contradictory, but the inconsistencies are often due to variations in ionomer backbone, cation type and sample preparation, among other factors, which have been shown to affect the polymer morphology and physical properties. For example, the choice of cation plays an important role in ionomer properties. Monovalent, divalent, and transition metal ions all may have different propensities for

aggregate formation. In that case, studies on one type of ion may not be applicable to other types of ions.

Additionally, the interpretations of experimental results support different physical models. Some investigations, such as certain dynamic mechanical experiments and dielectric spectroscopy studies, support the theory of multiplets and clusters. Other work, such as studies using ESR and Mössbauer spectroscopy, tend to support the existence of dissolved ion pairs and aggregates. Also, results and models based on small-angle x-ray scattering do not clearly support either physical picture.

2.3 Ionomers and NMR

Applications of NMR to ionomers have covered a wide range of studies, including investigations on ionomer miscibility, ionomer crystallinity, and aggregate structure. ^{1}H and ^{13}C NMR have been used to study the effects of ionization on the hydrocarbon matrix, while other nuclei were examined to study the formation and structure of the aggregates.

2.3.1 ^{13}C and ^{1}H and NMR

Many of the NMR studies on ionomers have been done with the polymers in solution. Natansohn and Eisenberg have studied several ionomers[137,138] and ionomer blends[139-142] using ^{1}H and ^{13}C NMR. They used proton NMR to study the interactions between poly(methyl methacrylate co- 4-vinylpyridine) and the acid form of lightly-sulfonated polystyrene (SPS) dissolved in dimethylsulfoxide (DMSO).[139] The authors found that while PMMA and PS are normally incompatible, they can be made compatible by introducing a small number of interacting groups on both

polymer chains. This finding is supported by Natansohn *et al.*, who observed that ionic interactions improved the miscibility of certain polymer blends.[143] Polyurethanes blended with the acid form of SPS were also investigated. The data showed that protons from the sulfonate group are transferred to the polyurethane, forming interactions between the polymers in the blend.[139]

^1H NMR has been used to investigate hydration in ionomers. Sivashinsky and Tanny[144] studied relaxation times for water in Nafion, SPE (chlorosulfonated polyethylene), and SPS. Unfortunately, their T_1 and T_2 relaxation data did not always agree with the standard BPP (Bloenbergen, Purcell and Pound) model, which predicts the temperature-dependence of relaxation of surface-adsorbed water. For Nafion, which showed behavior that could be described by the BPP model, the authors tried to correlate higher values of T_1 with larger values of χ, the Flory-Huggins interaction parameter. In this situation a higher χ means less thermodynamically-favored interactions. This may be the first time that a thermodynamic parameter has been correlated with NMR relaxation in a polymer system. However, the authors were not able to complete work on neutral, or non-ionized, polymers for comparison because of the low solubility of water in the polymer.

Nierzwicki and Rutkowska[145] studied the effects of ionic interactions and crosslinking on the phase separation of polyurethanes. Based on their mechanical and NMR results, the authors concluded that the hard domains became more rigid when ionic groups were incorporated into them. The amount of material in the hard domains increased, while the material in the interface decreased, with increased crosslinking and ionic interactions. It appears, then, that any disruption of the hydrogen bonding within the hard domains is more than compensated for by the ionic associations.

Lu *et al.*[146] used ^{1}H NMR relaxation to study the phase separation of polyurethanes and derivatives of the polyurethanes that contained zwitterion functionality. They measured the spin-lattice relaxation times (T_1), spin-spin relaxation times (T_2), and percentage of protons in each phase. Ionization did not affect proton T_1 times, which were averaged due to spin diffusion. However, from proton T_2 experiments it was found that ionization improved phase separation. ^{13}C cross polarization experiments showed that the chain extender moved from the soft-segment domain to the hard-segment domain as the degree of ionization increased.

Vanhoorne *et al.*[147] synthesized two model ionomers to study the local mobility of chain segments near the ionic aggregates in carboxy-telechelic polystyrene. They selectively deuterated 5 styrene units, either at both ends of the ionomer (DHD) or in the middle (HDH), and studied the CPMAS ^{13}C line width as a function of temperature for the two materials. The HDH material showed a maximum in linewidth verses temperature curves, indicating a relaxation mechanism similar to T_g, 10°C higher than the DHD material. This indicated that local motions near the carboxyl groups were more restricted than those in the center of the chain. In contrast, in non-ionic polystyrene the motion of the chain ends begins 20°C earlier than the rest of the chain.[148]

Belfiore and Shah[149] used NMR to investigate ionomer morphology in Surlyn that had been neutralized with either sodium or zinc. From their ^{13}C NMR data, the authors identified three morphologies that may be present in the partially neutralized copolymer: crystalline ethylene, amorphous ethylene with MMA, and MMA units surrounding metal aggregates. In both NMR and DSC data, decreases in the percent crystallinity with increasing MMA content is apparent. This result is in agreement with a study done by MacKnight *et*

al.,[150] who studied this ionomer by wide-angle x-ray scattering to determine its degree of crystallinity.

2.3.2 ^{31}P and ^{23}Na NMR

^{31}P NMR can be used to characterize ionomers, as was demonstrated by Lindsell *et al.*.[151] The authors used ^{13}C, ^{1}H, and ^{31}P NMR to study a polybutadienyllithium system. These telechelic ionomers are comprised of polybutadiene and terminal quaternary phosphonium groups. The authors did not measure any physical properties but instead used NMR for structure confirmation to show that a new ionomer could be synthesized. Other work with ^{31}P NMR has included proteins and polymers with phosphorus incorporated into the main chain.[152,153]

Only a few research groups have used ^{23}Na NMR to probe local interactions within the ionic groups. Dickinson *et al.*[154] reported ^{23}Na lineshapes of several model compounds, as well as sodium-neutralized Surlyn and SPS. The details of the NMR experiment, unfortunately, are not complete, and the location of the origin in the chemical shift axis is uncertain. The spectrum of a dried 23%-neutralized Surlyn sample showed a broad, featureless line; however, the spectrum of the sample after exposure to water vapor at 93°C showed a narrow peak at -12 ppm as well as the broad line. Similarly, spectra of 100%-neutralized SPS contained a broad line at -40 ppm and a narrow signal at 0 ppm, which grew in intensity with increasing hydration. A 250%-neutralized SPS sample showed a spectrum similar to the hydrated sample. The appearance of this narrow peak could be due to excess sodium ions that are difficult to dehydrate. It is also possible that the sodium ions are in a highly symmetric environment, such as that in NaCl.

Other studies of polymers in solution also show very interesting ^{23}Na results. By investigating the effects of ion content on NMR linewidths of NaSPS, Park *et al.*[155] followed the transition from multiplets to clusters. The "cluster point" was determined to be 5 mol% ionization. These authors also observed that ^{23}Na linewidths increased with ionization level, except at the lowest levels. This increase is caused by the formation of ion aggregates at higher ion concentrations, which reduces the mobility of the sodium ions. The reversal of this trend at low ion concentrations is most likely due to poor solubility in the solvent (DMF). Furthermore, lower degrees of ionization showed more negative (i.e. upfield) chemical shifts, indicative of the effect of solubility on chemical shift. Solid SPS, which is similar to a theta solvent, had the most negative chemical shift, at –11 ppm with respect to aqueous NaOH.

Komoroski and Mauritz[156] studied ion pairing and mobility in a swollen Nafion ionomer, also using ^{23}Na NMR. They observed large chemical shift and linewidth increases when the water content was decreased; these trends were reversed when temperature was increased. It was proposed that more sodium ions are bound to the polymer as the water content decreases. Since the largest changes in linewidth and chemical shift occurred at water concentrations between three and four molecules per sodium ion, this same number of water molecules make up the first hydration sphere of a sodium ion.

There have been several studies of ^{23}Na NMR of polyelectrolytes. Most of these polyelectrolytes consist of polymers complexed with alkali metal salts.[157-162] Spindler and Shriver[157] reported upfield chemical shifts as salt concentration was increased or temperature was decreased. They attributed the upfield shift to ion aggregation. Greenbaum *et al.*[158] studied electrolytes of

poly(propylene oxide) and NaX compounds, where X= I^-, $CF_3SO_3^-$, and others. They determined the ratios of mobile and bound sodium ions by taking the ratio of short and long relaxation times (T_1) of the single peak. ^{23}Na NMR chemical shift of the salt was dependent on temperature and anion type, and precipitation of the salt could be seen by the presence of an additional peak in the spectrum. Similar work was done by Forsyth *et al.*,[159] who studied $NaCF_3SO_3$ in polyurethanes at different salt concentrations and with different plasticizers. Only one species was seen and identified as mobile ions. Increased salt concentrations led to upfield (lower) chemical shifts but decreases in linewidth. Addition of plasticizers led to downfield (higher) shifts and increased linewidths, with no direct correlation to shift. The downfield shifts were attributed to partial solvation, which would decrease cation-anion interactions. Although the changes in linewidth seem counterintuitive, a plot of linewidth versus reduced temperature (T_g/T) showed a maximum near the Larmor frequency (correlation time $\tau_c=1/\omega_L$) and a minimum near the quadrupolar interaction frequency ($\tau_c=1/\omega_L$). A maximum quadrupolar coupling constant of 2 MHz was calculated.

2.4 Interactions in Polymer Blends

Polymers with interacting groups incorporated into them, either as part of the main chain or as pendant groups, can form complexes with other molecules. Some complexes are with low-molecular weight species, such as metal-containing salts blended with pyridine-containing polymers. Others, however, are formed from blending two polymers, such as a pyridine-

containing polymer and an ionomer in its acid or neutralized form. Blends that contain ionomers in their acid form were already discussed in Section 2.3. Other types of blends are discussed below.

2.4.1 Polymer Blends with Metal-Containing Compounds

As was discussed previously, interactions in blended polymers can be due to hydrogen bonding, charge-transfer complexation, ionic interactions, or metal coordination.[163] Any one or a combination of these can lead to interesting and useful changes in the physical properties of the blends as compared to the unmodified polymers. Polymer-metal complexes in blends are particularly interesting because they display behavior similar to ionomers.

Polymer interactions based primarily on metal-coordination chemistry have been studied for many years. For example, the coordination properties of polyethers, such as PEO and PPO with salts dissolved in them, have been investigated.[164,165] Polyesters and nylons have been the focus of other work in this area of research. Dunn and Sansom[166] reported the presence of metal complexes in blends of Nylon-6 with various salts. Based on IR band shifts of the amide groups, they proposed two cation-dependent models for complexation. Similar work was done by Wissburn and Hannon,[167] who blended polymers with nitrate salts. Supported by results from IR studies, the authors proposed a model for complexation in which a divalent metal ion is coordinated to carbonyl oxygens, and to oxygens in the water of hydration. In this model, water also forms hydrogen bonds with ester oxygens, to form a ring structure.

Charlier *et al.*[168] studied polybutadiene terminated with piperazine units and polyisoprene terminated with amine groups. These materials were

blended with $CuCl_2$ or $FeCl_3$. A rubbery plateau region in the dynamic mechanical data appeared after the addition of the metal salts. For the piperazine telechelics, with two nitrogen atoms per piperazine unit which can complex to metals, mechanical and viscoelastic properties were a function of the molar ratio of neutralizing salt to end group (x), and optimum properties occurred at x=1. Therefore, the intermolecular association is strongest at this ratio. This result is surprising because Cu^{2+} and Fe^{3+} have been shown to coordinate to four amino groups (x=0.5). Instead, the metal atoms coordinate to the piperazine nitrogen groups and chlorine atoms, forming a complex network. The variation of the properties with molar ratio x shows that the rigidity of the material can be adjusted by varying the blend ratios.

Polymer-metal interactions have also been used to improve miscibility in polymer blends. Molnár and Eisenberg[169] found an optimum composition for a homogeneous material in blends of Li-SPS and a polyamide. Lu and Weiss[170] reported decreases in intensity of the SAXS peak for ZnSPS in a blend with nylon-6 that indicated solvation of the ionic domains. Strong transition-metal complexation was observed between the amide groups and the metal sulfonate. Rutkowska and Eisenberg[171] reported that addition of HSPS to a polyurethane led to a two-phase system; the HSPS and polyurethane hard segments were contained in one phase, and the polyurethane soft segments were in another phase.

Xue and Schlick[172] studied the ESR spectra of amine-terminated Hycar complexed with copper salts. Multiple Cu^{2+} sites were present but there was no evidence for the existence of dimers, in contrast to studies on carboxy-terminated Hycar ionomers.[69] The authors saw line-broadening with increasing Cu^{2+} content, which suggests aggregation. This behavior is similar

to that of ionomers. As ion concentration increased, the number of nitrogen ligands interacting with a cation decreased; particularly, at high ion concentrations (three times the stoichiometric amount) the cations appeared to form domains completely unconnected to the amine groups. This result suggests that at high concentrations the salt domains act as fillers, and not as additional crosslinks. The fact that salt is not incorporated into the matrix itself may explain the experimental observation that the T_g's of some polymers are relatively unaffected by the addition of high amounts of salt.

2.4.2 Blends with Pyridine-Containing Polymers

Studies with pyridine groups incorporated into a polymer have been undertaken by many research groups. For instance, Agnew[173] found evidence for an average stoichiometry of two pyridine rings to one zinc atom in Zn^{2+}-neutralized poly(4-vinylpyridine) (P4VP). Meyer and Pineri[174-177] demonstrated iron complexation in a terpolymer of butadiene, styrene, and P4VP. By using Mössbauer spectroscopy, SAXS, and electron microscopy, the authors obtained evidence for three different iron complexes (aggregates 50%, dimers 30%, singlets 20%).

In another study, Peiffer *et al.*[163] characterized blends of P4VP copolymers and Zn^{2+}-neutralized sulfonated EPDM using melt viscosity measurements and IR absorption. Their results suggested coordination in 1:1 stoichiometric blends for Zn^{2+}- and Cu^{2+}-neutralized blends. Apparently, both the presence of the sulfonate group (which behaves like another metal ligand) and the steric hindrance of the chains prevented the system from obtaining same ratio determined by Agnew. Further work[178] showed that strong coordination was present with transition metal ions, but not with sodium or

magnesium ions. Therefore, for these systems the mode of interaction was described to be transition-metal complexation with the pyridine-nitrogen lone pair.

Lu and Weiss[179] studied the solution behavior of mixtures of neutralized SPS and poly(styrene-co-4-vinylpyridine). They found interactions in blends with alkali and alkaline earth metals as well as with transition metals. The authors proposed a schematic of the intermolecular complex in which the cation is solvated by a relatively polar solvent, which allows coordination between the pyridine nitrogen and the sulfonate oxygen. It was suggested that the intermolecular complex for alkali or alkaline earth metal blends can be described by this solvated-ion scheme, which relies on the electrostatic fields of the cations for interaction. On the other hand, the formation of ion pairs is favored in transition-metal complexes, indicating a mechanism of metal-ligand coordination bonding. This type of coordination would be stronger than electrostatic interactions. For the former types of ions, the ratio of vinylpyridine groups to sulfonate groups varied with solvent polarity, which suggests competition between the solvent and the sulfonate group for complexation with the pyridine nitrogen.

Jacovic *et al.*[180] observed coordination complexes at molar ratios of pyridine to zinc of close to 2:1, in agreement with other researchers who report coordination at stoichiometric ratios as well.[181,182] The complexed copolymers had higher values of T_g and higher rubbery plateau moduli than did the unmodified copolymers. These types of increases in T_g and plateau modulus have been seen in ionomer systems as well,[47] indicating parallel behavior in the two systems.

Polymer-metal interactions have also been used to improve miscibility in polymer blends. Douglas *et al.* [183] observed a mixed phase in blends of SPS and copolymers containing pyridine groups. However, because the authors found no differences in the miscibilities of the acid- and Zn^{2+}-neutralized form of SPS, they concluded that the presence of crosslinks, rather than the specific nature of the interaction, is more important in the formation of a compatible blend. For these blends, IR studies have shown molecular-level interactions.[184]

2.5 Polymer-Metal Interactions and NMR

Polyurethanes, ionomers, and other multiblock polymers are well-suited for NMR studies since the phase-separated domains usually have different motional characteristics. Soft segments, for example, have linewidths and relaxation behavior typical of liquids, while the hard domains are more suited for enhancement by cross polarization and usually have longer relaxation times. Incorporation of a complexing agent into the system restricts motion immediately around the interacting groups, and should affect nuclear relaxation times and, possibly, chemical shifts of nearby nuclei.

NMR has been used to study many types of interacting systems such as those with hydrogen-bonding,[185] ion-dipole interactions,[186] charge-transfer complexation,[187] ionic interactions,[188] and polymer-metal interactions.[189,190] These different interactions can be expected to change the phase structure in some polymer blends and modify their physical properties. In terms of relating interactions in polymer blends to those in

ionomers, the specific case of polymer-metal interactions is the most applicable.

Gao *et al.*[191] used $T_{1\rho}(H)$ and $T_1(H)$ experiments to study miscibility in a system of a polyamide and Na- or LiSPS; the authors observed better miscibility in blends with the latter due to stronger interactions between Li^+ ions and the polyamide. The authors referred to work showing that Li^+ interacts with amide groups mostly strongly of all the alkali metals. Kwei *et al.*[192] reported downfield ^{13}C chemical shifts in the carbonyl and methylene (adjacent to nitrogen) groups of a polyamide when it was blended with ZnSPS, indicating a Zn:N complex. Zhang *et al.*[193] used CP/MAS ^{13}C NMR to study blends of deuterated HSPS and a copolymer with polyvinylpyridine. The deuterated polystyrene showed no signal in the CP/MAS spectrum because no protons were near carbons. However, after blending with the pyridine-containing polymer, signals from the styrene carbons were observed, indicating close proximity of the two chain types.

Belfiore *et al.*[194,195] studied transition-metal complexes in ionomeric blends composed of either P2VP or P4VP and partially Zn^{2+}-neutralized Surlyn. When Surlyn and P4VP are blended, a peak appears at ~180 ppm; this is due to partially-neutralized carboxylic acid carbons near Zn^{2+} ions, which complex with the pyridine nitrogen's lone pair. This peak is missing when P2VP is used in place of P4VP, which suggests that steric hindrance prevents complexation. The fact that the carbon resonances from the acid carbonyl (185 ppm) and the non-complexed Zn^{2+}-neutralized carbonyl (189 ppm) are still seen suggests a phase-separated system. Mechanical data from tensile testing support this conclusion.

In a continuation of this study, Belfiore *et al.*[189,195] reported transition-metal coordination in both model compounds and polymer blends. The authors looked at blends of P4VP and several zinc salts (acetate, laurate, and stearate). ^{13}C NMR spectra of the carbonyl group in zinc acetate showed a shift from 185 ppm (crystalline) to 179 ppm in blends containing at least 28 mole % zinc acetate. It was suggested that the peak shift was due to complexation with the pyridine nitrogen. Although the authors claimed to see similar changes in the peaks of the pyridine ring carbons, no spectra were shown. Blends with zinc laurate and zinc stearate with P4VP showed peaks at both 181 and 185 ppm, indicating that both amorphous and crystalline phases of the zinc salt were present. No evidence for complexation was seen in blends with magnesium acetate. This was attributed to the preferential complexation of magnesium, a hard acid, to acetate or water instead of to the pyridine nitrogen, a weak base.

References for Chapter Two

1 Bloch, F.; Hansen, W.W.; Packard, M. *Phys Rev.* 1946, **69**, 127.

2 Purcell, E.M.; Torrey, H.C.; Pound, R.V. *Phys. Rev.* 1946, **69**, 37.

3 Schaefer, J.; Stejskal, E.O.; Buchdahl, R. *Macromol.* 1977, **10**, 384.

4 Bovey, F.A. *Polym. Eng. Sci.* 1986, **26**, 1420.

5 Komoroski, R.A., ed. *High Resolution NMR Spectroscopy of Synthetic Polymers in Bulk,* VCH Publishers: Deerfield Beach, Fl., 1986.

6 Randall, J.C., ed. *NMR and Macromolecules*; American Chemical Society: Washington, D.C., 1984.

7 Speiss, H.W. *Annu. Rev. Mater. Sci.* 1991, **21**, 131.

8 Jelinsky, L.W. *C&EN*, 1984, November, 26.

9 Sillescu, H. *Makromol. Chem., Macromol. Symp.* 1986, **1**, 39.

10 Fedotov, V.D.; Schneider, H., in *NMR-Basic Principles and Progress*, Diehl, P.; Fluck, E.; Günther, H.; Kosfeld, R.; Seelig, J., eds., Vol. 21; Springer-Verlag: New York, 1989.

11 Assink, R.A. *Macromol.* 1978, **11**, 1233.

12 Delides, C.; Pethrick, R.A.; Cunliffe, A.V.; Klein, P.G. *Polymer*, 1981, **22**, 1205.

13 Tonelli, A.E.; Schilling, F.C. *Acc. Chem. Res.* 1981, **14**, 233.

14 Randall, J.C. *Polymer Sequence Determination*; Academic Press: New York, 1977.

15 Jelinski, L.W. *Chemtech* 1986, March, 186.

16 Slichter, W.P. in *NMR-Basic Principles and Progress*, Diehl, P.; Fluck, E.; Kosfeld, R., eds., Vol. 4; Springer-Verlag: New York, 1971.

17 Kinsey, R. *Rubber Chem. Tech.* 1990, **63**, 407.

18 Kessler, H.; Gehrke, M.; Griesinger, C. *Angew. Chem.* 1988, **27**, 490.

19 Voelkel, R. *Angew. Chem.* 1988, **27**, 1468.

20 Axelson, D.E.; Russell, K.E. *Prog. Polym. Sci.* 1985, **11**, 221.

21 Laupretre, F. *Prog. Polym. Sci.* 1990, **15**, 425.

22 Yu, T; Guo, M. *Prog. Polym. Sci.* 1990, **15**, 825.

23 Harris, R.K.; Packer, K.J.; Say, B.J. *Makromol. Chem., Suppl.* 1981, **4**,117.

24 Kintanar, A.; Jelinski, L.W.; Gancarz, I.; Koberstein, J.T. *Macromol.* 1986, **19**, 1876.

25 Röber, S.; Zachmann, H.G. *Polymer* 1992, **33**, 2061.

26 Kornfield, J.A.; Speiss, H.W.; Nefzger, H.; Hayen, H.; Eisenbach, C.D. *Macromol.* 1991, **24**, 4787.

27 Speiss, H.W. in *NMR-Basic Principles and Progress*, Diehl, P.; Fluck, E.; Kosfeld, R., eds., Vol. 15; Springer-Verlag: New York, 1978.

28 Speiss, H. W. *Pure & Appl. Chem.* 1985, **57**, 1617.

29 Zhang, M; Maciel, G.E. *J. Magn. Res.* 1989, **85**, 156.

30 Zhang, M; Maciel, G.E. *Anal. Chem.* 1990, **62**, 633.

31 Duff, D.W.; Maciel, G.E. *Macromol.* 1991, **24**, 387.

32 Hatfield, G.R.; Maciel, G.E. *J. Phys. Chem.* 1988, **92**, 4620.

33 Fyfe, C.A.; Niu, J.; Rettig, S.J.; Burlinson, N.E. *Macromol.* 1992, **25**, 6289.

34 Mathias, L.J.; Johnson, C.G. *Macromol.* 1991, **24**, 6114.

35 Powell, D.G.; Sikes, A.M.; Mathias, L.J. *Polymer* 1991, **32**, 2523.

36 Live, D.H.; Radhakrishnan, I.; Misra, V.; Patel, D. *J. Am. Chem. Soc.* 1991, **113**, 4687.

37 Chaloner-Gill, B.; Euler, W.B.; Roberts, J.E. *Macromol.* 1991, **24**, 3074.

38 Kricheldorf, H.R. *J. Macromol. Sci.-Chem.* 1980, **A14**, 959.

39 Eisenberg, A. *Macromol.* 1970, **3**, 147.

40 Fitzgerald, J.J.; Weiss, R.A.; *Rev. Macromol. Chem. Phys.* 1988, **C28**, 99.

41 Moore, R.B.; Bittencourt, D.; Gauthier, M.; Williams, C.E.; Eisenberg, A. *Macromol.* 1991, **24**, 1376.

42 Marx, C.L.; Caufield, D.F.; Cooper, S.L. *Macromol.* 1973, **6**, 344.

43 Squires, E.; Painter, P.; Howe, S. *Macromol.* 1987, **20**, 1740.

44 Ding, Y.S.; Hubbard, S.R.; Hodson, K.A.; Register, R.A.; Cooper, S.L. *Macromol.* 1988, **21**, 1698.

45 Mauritz, K. *Rev. Macromol. Chem. Phys.*, 1988, **C28**, 65.

46 Eisenberg, A.; Hird, B.; Moore, R.B. *Macromol.* 1990, **23**, 4098.

47 MacKnight, W.J.; Earnest, T.R.; *J. Polym. Sci., Macromol. Rev.* 1981, **16**, 41.

48 Yarusso, D.J.; Cooper, S.L. *Macromol.* 1983, **16**, 1871.

49 Forsman, W.C.; *Macromol.* 1982, **15**, 1032.

50 Dreyfus, B. *Macromol.* 1985, **18**, 284.

51 Datye, V.K.; Taylor, P.L. *Macromol.* 1985, **18**, 1479.

52 Hsu, W.Y.; Gierke, T.D. *Macromol.* 1982, **15**, 101.

53 Mauritz, K.A.; Rogers, C.E. *Macromol.* 1985, **18**, 483.

54 Lefelar, J.A.; Weiss, R.A. *Macromol.* 1984, **17**, 1145.

55 Register, R.A.; Cooper, S.L. *Macromol.*, 1990, **23**, 310.

56 Wilson, F.C.; Longworth, R.; Vaughan, D.J.; *Polym. Prepr.* 1968, **9**, 505.

57 MacKnight, W.J.; Taggart, W.P; Stein, R.S. *J. Polym. Sci., Polym. Symp.* 1974, **45**, 113.

58 Fujimara, M.; Hashimoto, T.; Kawai, H.; *Macromol.* 1981, **14**, 1309.

59 Roche, E.J.; Stein, R.S.; Russell, T.P., MacKnight, W.J. *J. Polym. Sci., Polym. Phys. Ed.* 1980, **18**, 1497.

60 Binsberger, F.L.; Kroon, G.F. *Macromol.* 1973, **6**, 145.

61 Lee, D.C.; Register, R.A.; Yang, C.-Z.; Cooper, S.L. *Macromol.* 1988, **21**, 998.

62 Williams, C.E.; Russell, T.P.; Jerome, R.; Horrion, J. *Macromol.* 1986, **19**, 2877.

63 Kinning, D.L.; Thomas, E.L. *Macromol.* 1984, **17**, 1712.

64 Ding, S.Y.; Register, R.A.; Yang, C.-Z.; Cooper, S.L. *Polymer*, 1989, **30**, 1213.

65 Visser, S.A.; Cooper, S.L. *Macromol.* 1991, **24**, 2584.

66 Drago, R.S. *Physical Methods for Chemists*, 2nd Ed.; Sauders College Publishing: Orlando, FL, 1992.

67 Sen, A.; Weiss, R.A.; Oh, J.; Frank, H.A. *Polym. Prepr.* 1987, **28**, 220.

68 Bersohn, M.; Baird, J.C. *An Introduction to Electron Paramagnetic Resonance*; W.A. Benjamin, Inc.: New York, 1966.

69 Pineri, M.; Meyer, C.; Levelut, A.M.; Lambert, M. *J. Polym. Sci., Polym. Phys. Ed.* 1974, **12**, 115.

70 Weiss, R.A.; Lefelar, J.; Toriumi, H. *J. Polym. Sci., Polym. Lett. Ed.* 1983, **21**, 661.

71 Toriumi, H.; Weiss, R.A.; Frank, H.A. *Macromol.* 1984, **14**, 2104.

72 Yamauchi, J.; Yano, S. *Makromol. Chem.* 1978, **179**, 2799.

73 Galland, D.; Belakhovsky, M.; Medrignac, F.; Pineri, M.; Vlaic, G.; Jerome, R. *Polymer*, 1986, **27**, 883.

74 Alonso-Amigo, M.G.; Schlick, S. *J.Phys. Chem.* 1986, **90**, 6353.

75 Vasquez, R.; Avalos, J.; Volino, F.; Pineri, M.; Galland, D. *J. Appl. Polym. Sci.* 1983, **28**, 1093.

76 Kemp. D.S.; Vellaccio, F. *Organic Chemistry*; Woth Publishers, In.: New York, 1980.

77 Mattera, V.D.; Risen, W.M. *J. Polym. Sci., Polym. Phys. Ed.* 1984, **22**, 67.

78 Rouse, G.B.; Risen, W.M.; Tsatsas, A.T.; Eisenberg, A. *J. Polym. Sci., Polym. Phys. Ed.* 1979, **17**, 81.

79 Peiffer, D.G.; Hager, B.L.; Weiss, R.A.; Agarwal, P.K.; Lundberg, R.D. *J. Polym. Sci., Polym. Phys. Ed.* 1985, **23**, 1869.

80 Andreeva, E.D.; Nikitin, V.N.; Boyartchuk, Y.M. *Macromol.* 1976, **9**, 238.

81 Earnest, T.R; MacKnight, W.J. *Macromol.* 1980, **13**, 844.

82 Coleman, M.M.; Lee, J.Y.; Painter, P.C. *Macromol.* 1990, **23**, 2339.

83 Fay, M.J.; Proctor, A.; Hoffman, D.P.; Hercules, D.M. *Anal. Chem.* 1988, **60**, 1225A.

84 Teo, B.K. *EXAFS: Basic Principles and Data Analysis*; Springer-Verlag: New York, 1986.

85 Yarusso, D.J.; Cooper, S.L.; Knapp, G.S.; Georgopoulos, P. *J. Polym. Sci., Polym. Lett. Ed.* 1980, **18**, 557.

86 Yarusso, D.J.; Ding, Y.S.; Pan, H.K.; Cooper, S.L. *J. Polym. Sci., Polym. Phys. Ed.* 1984, **22**, 2073.

87 Ding, Y.S.; Yarusso, D.J.; Pan, H.K.; Cooper, S.L. *J. Appl. Phys.* 1984, **56**, 2396.

88 Grady, B.P.; Cooper, S.L. *Macromol.* 1994, **27**, 6627.

89 Grady, B.P.; Cooper, S.L. *Macromol.* 1994, **27**, 6635.

90 Ding, Y.S.; Register, R.A.; Yang, C.-Z.; Cooper, S.L. *Polymer*, 1989, **30**, 1221.

91 Lundberg, R.D.; Makowski, H.S. *Polym. Prep.* 1978, **19**, 287.

92 Lundberg, R.D.; Makowski, H.S., in *Ions in Polymers*; American Chemical Society: Washington, D.C., 1980.

93 Rigdahl, M.; Eisenberg, A. *J. Polym. Sci., Phys. Ed.* 1981, **19**, 1641.

94 Visser, S.A.; Cooper, S.L. *Macromol.* 1991, **24**, 2576.

95 Yarusso, D.J.; Cooper, S.L.; *Polymer*, 1985, **26**, 371.

96 Weiss, R.A. *J. Polym. Sci., Polym. Chem. Ed.* 1980, **18**, 2887.

97 Sanui, K.; Lenz, R.W.; MacKnight, W.J.; *J. Polym. Sci., Polym. Chem. Ed.* 1974, **12**, 1965.

98 Rahrig, D.; Azuma, C.; MacKnight, W.J. *J. Polym. Sci., Polym. Phys. Ed.* 1978, **16**, 59.

99 Rahrig, D.; MacKnight, W.J., in *Ions in Polymers*; American Chemical Society: Washington, D.C., 1980.

100 Makowski, H.S.; Lundberg, R.D.; Westerman, L.; Bock, J., in *Ions in Polymers*; American Chemical Society: Washington, D.C., 1980.

101 Agarwal, P.K.; Makowski, H.S.; Lundberg, R.D. *Macromol.* 1980, **13**, 1679.

102 Eisenberg, A.; Navratil, M. *Macromol.* 1973, **6**, 604.

103 Eisenberg, A.; Navratil, M. *Macromol.* 1974, **7**, 90.

104 Bellinger, M.; Sauer, J.A.; Hara, M. *Macromol.* 1994, **27**, 1407.

105 Hara, M.; Jar, P.-Y.; Sauer, J. *Macromol.* 1988, **21**, 3183.

106 Peiffer, D.G.; Weiss, R.A.; Lundberg, R.D. *J. Polym. Sci., Polym. Phys. Ed.* 1982, **20**, 1503.

107 Weiss, R.A.; Lefelar, J.A. *Polymer*, 1986, **27**, 3.

108 Broze, G.; Jerome, R.; Teyssie, P.; *J. Polym. Sci., Polym. Phys. Ed.* 1983, **21**, 2205.

109 Navratil, M.; Eisenberg, A. *Macromol.* 1974, **7**, 84.

110 Weiss, R.A.; Agarwal, P.K. *J. Appl. Polym. Sci.* 1981, **26**, 449.

111 Ding, Y.S.; Register, R.A.; Yang, C.-Z.; Cooper, S.L. *Polymer*, 1989, **30**, 1203.

112 Eisenberg, A.; Matsuura, H.; Tsutsui, T.; *J. Polym. Sci., Polym. Phys. Ed.* 1980, **18**, 479.

113 Bagrodia, S.; Wilkes, G.L. *Polym. Bull.* 1984, **12**, 389.

114 Brozoski, B.A.; Coleman, M.M.; Painter, P.C. *Macromol.* 1984, **17**, 230.

115 Han, K.; Williams, H.L. *J. Appl. Polym. Sci.* 1991, **42**, 1845.

116 Fitzgerald, J.J.; Weiss, R.A., in *Coulombic Interactions in Macromolecular Systems*; American Chemical Society: Washington, D.C., 1986.

117 Register, R.A.; Foucart, M.; Jerome, R.; Ding, Y.S.; Cooper, S.L. *Macromol.* 1988, **21**, 1009.

118 Visser, S.A.; Cooper, S.L. *Polymer*, 1992, **33**, 920.

119 Visser, S.A.; Cooper, S.L. *Polymer*, 1992, **33**, 930.

120 Arai, K.; Eisenberg, A. *J. Macromol. Sci., Phys.* 1980, **B17**, 803.

121 Yano, S.; Fujiwara, Y.; Kato, F.; Aoki, K.; Koizumi, N. *Polymer J.* 1981, **13**, 283.

122 Mohajer, Y.; Bagrodia, S.; Wilkes, G.L.; Storey, R.F.; Kennedy, J.P. *J. Appl. Polym. Sci.* 1984, **29**, 1943.

123 Takei, M.; Tsujita, Y.; Simada, S.; Ichihara, H.; Enokida, M.; Takizawa, A.; Kinoshita, T. *J. Polym. Sci., Polym. Phys. Ed.* 1988, **26**, 997.

124 Moudden, A.; Levelut, A.M.; Pineri, M. *J. Polym. Sci., Polym. Phys. Ed.* 1977, **15**, 1707.

125 Kim, J.-S.; Eisenberg, A. *J. Polym. Sci., Phys. Ed.* 1995, **33**, 197.

126 Pésci, Z.S.; Szmercsanyi, I.V.; Cser, F.; Varga, J.; Belina, K. *J. Polym. Sci., Polym. Phys. Ed.* 1981, **19**, 703.

127 Bagrodia, S.; Pisipati, R.; Wilkes, G.L.; Storey, R.F.; Kennedy, J.P. *J. Appl. Polym. Sci.* 1984, **29**, 3065.

128 Bagrodia, S.; Tant, M.R.; Wilkes, G.L.; Kennedy, J.P. *Polymer*, 1987, **28**, 2207.

129 Vlaic, G.; Williams, C.; Jerome, R.; Tant, M.R.; Wilkes, G.L. *Polymer*, 1988, **29**, 173.

130 Erhardt, P.F.; O'Reilly, J.M.; Richards, W.C.; Williams, M.W. *J. Polym. Sci. Symp.* 1974, **45**, 139.

131 Kim, J.S.; Yoshikawa, K.; Eisenberg, A. *Macromol.* 1994, **27**, 6347.

132 Weiss, R.A. *J. Polym. Sci., Polym. Phys. Ed.* 1982, **20**, 65.

133 Galambos, A.F.; Stockton, W.B.; Koberstein, J.T.; Sen, A.; Weiss, R.A.; Russell, T.P. *Macromol.*, 1987, **20**, 3094.

134 Register, R.A.; Sen, A.; Weiss, R.A.; Cooper, S.L. *Macromol.* 1989, **22**, 2224.

135 Register, R.A.; Yu, X.-H.; Cooper, S.L. *Polym. Bull.* 1989, **22**, 565.

136 Fitzgerald, J.J; Kim, D.; Weiss, R.A. *J. Polym. Sci., Polym. Lett. Ed.* 1986, **24**, 263.

137 Simmons, A.; Natansohn, A.; Eisenberg, A. *J. Polym. Sci., Polym. Chem. Ed.* 1987, **25**, 2221.

138 Natansohn, A.; Eisenberg, A. *Can. J. Chem.* 1987, **65**, 1873.

139 Natansohn, A.; Eisenberg, A. *Macromol.* 1987, **20**, 323.

140 Natansohn, A.; Rutkowska, M.; Eisenberg, A. *Polymer*, 1987, **28**, 885.

141 Natansohn, A.; Rutkowska, M.; Eisenberg, A. *J. Polym. Mater.* 1987, **4**, 9.

142 Natansohn, A.; Rutkowska, M.; Eisenberg, A. *Polym. Eng. Sci.* 1987, **27**, 1504.

143 Natansohn, A.; Murali, R.; Eisenberg, A. *Chemtech*, 1990, (July), 418.

144 Sivashinsky, N.; Tanny, G.B. J. Appl. Polym. Sci. 1981, **26**, 2625.

145 Nierzwicki, W.; Rutkowska, M. *Polym Comm.* 1986, **27**, 327.

146 Lu, X.; Wang, Y. *Polym Comm.* 1991, **32**, 426.

147 Vanhoorne, P.; Jérôme, R.; Teyssié, P.; Lauprêtre, F. *Macromol.* 1994, **27**, 2548.

148 Kornfield, J.A.; Chung, G.-C.; Smith, S.D. *Macromol.* 1992, **25**, 4442.

149 Belfiore, L.A.; Shah, R.J. *Polym. Sci. Mater. Eng.* 1986, **54**, 490.

150 MacKnight, W.J.; Taggart, W.P.; McKenna, L.; *J. Polym. Sci., Symp.* 1974, **46**, 83.

151 Lindsell, W.E.; Radha, K.; Souter, I.; Stewart, M.J. *Polymer*, 1990, **31**, 1374.

152 Gard, J.K.; Gard, D.R.; Burquin, J.C.; Callis, C.F. *Chemtech*, 1989, November, 698.

153 Murano, M.; Hongo, T. *Polym. Prepr.* 1978, **19**, 256.

154 Dickinson, L.C.; MacKnight, W.J.; Connelly, J.M.; Chien, J.C.W. *Polym. Bull.* 1987, **17**, 459.

155 Park, J.K.; Park, B.K.; Ryoo, R. *Polym. Eng. Sci.* 1991, **31**, 873.

156 Komoroski, R.A.; Mauritz, K.A.; *J. Am. Chem. Soc.* 1978, **100**, 7486.

157 Spindler, R; Shriver, D.F. *J. Amer. Chem. Soc.* 1988, **110**, 3036.

158 Greenbaum, S.G.; Pak, Y.S.; Wintersgill, M.C.; Fontanella, J.J. *Solid State Ionics*, 1988, **31**, 241.

159 Forsyth, M.; Smith, M.E.; Meakin, P.; MacFarlane, D.R. *J. Polym. Sci., Phys. Ed.* 1994, **32**, 2077.

160 Lemmon, J.P.; Kohnert, R.L.; Lerner, M.M. *Macromol.* 1993, **26**, 2767.

161 Newman, J.K.; McCormick, C.L. *Macromol.* 1994, **27**, 5114.

162 Wieczorek, W.; Such, K.; Chung, S.H.; Stevens, J.R. *J. Phys. Chem.* 1994, **98**, 9047.

163 Peiffer, D.G.; Duvdevani, I.; Agarawal, P.K.; Lundberg, R.D. *J. Polym. Sci., Polym. Lett. Ed.* 1986, **24**, 581.

164 Rabek, J.F.; Lucki, J.; Qu, B.J.; Shi, W.F. *Macromol.* 1991, **21**, 836.

165 Manning, J.; Frech, R. *Polymer*, 1992, **33**, 3487.

166 Dunn, P.; Sansom, G.F.; *J. Appl. Polym. Sci.* 1969, **13**, 1657.

167 Wissburn, K.F.; Hannon, M.J. *J. Polym. Sci., Polym. Phys. Ed.* 1975, **13**, 223.

168 Charlier, P.C.; Jerome, R.; Teyssie, P.; Ultracki, L.A. *Macromol.* 1990, **23**, 3313.

169 Molnar, A.; Eisenberg, A. *Macromol.* 1992, **25**, 5774.

170 Lu, X.; Weiss, R.A.; *Macromol.* 1992, **25**, 6185.

171 Rutkowska, M.; Eisenberg, A. *Macromol.* 1984, **17**, 821.

172 Xue, H.; Schlick, S. *Macromol.* 1992, **25**, 4437.

173 Agnew, N.H.; *J. Polym. Sci., Polym. Chem. Ed.* 1976, **14**, 2819.

174 Meyer, C.T.; Pineri, M. *J. Polym. Sci., Polym. Phys. Ed.* 1975, **13**, 1057.

175 Pineri, M.; Meyer, C.; Bourret, A. *J. Polym. Sci., Polym. Phys. Ed.* 1975, **13**, 1881.

176 Meyer, C.T.; Pineri, M. *J. Polym. Sci., Polym. Phys. Ed.* 1978, **16**, 569.

177 Meyer, C.T.; Pineri, M. *Polymer*, 1976, **17**, 382.

178 Agarwal, P.K.; Duvdevani, I.; Peiffer, D.G.; Lundberg, R.D. *J. Polym. Sci., Polym. Phys. Ed.* 1987, **25**, 839.

179 Lu, X.; Weiss, R.A. *Macromol.* 1991, **24**, 5763.

180 Jacovic, M.S.; Perovic, I. MacKnight, W.J.; Lenz, R.W. *J. Appl. Polym. Sci.* 1988, **35**, 903.

181 Bekturov, E.A.; Bimenda, L.A. *Adv. Polm. Sci.* 1981, **41**, 99.

182 Tsuchida, E.; Abe, K. *Adv. Polm. Sci.* 1982, **45**.

183 Douglas, E.P.; Sakurai, K.; MacKnight, W.J. *Macromol.* 1991, **24**, 6776.

184 Sakurai, K.; Douglas, E.P.; MacKnight, W.J. *Macromol.* 1992, **25**, 4506.

185 Cheng, C.; Belfiore, L.A. *Polymer News*, 1990, **15**, 39.

186 Hara, M.; Eisenberg, A. *Macromol.* 1984, **17**, 1335.

187 Natansohn, A.; Simmons, A. *Macromol.* 1989, **22**, 4426.

188 Zhang, X.; Natansohn, A.; Eisenberg, A. *Macromol.* 1990, **23**, 412.

189 Belfiore, L.A.; Pires, A.T.; Wang, Y.; Graham, H.; Ueda, E. *Macromol.* 1992, **25**, 1411.

190 Mishra, L.; Singh, V.K.; Ran, V.J. *Spectr. Acta.* 1992, **48A**, 751.

191 Gao, Z.; Molnar, A.; Morin, F.; Eisenberg, A. *Macromol.* 1992, **25**, 6460.

192 Kwei, T.K.; Dai, Y.K.; Lu, X.; Weiss, R.A. *Macromol.* 1993, **26**, 6583.

193 Zhang, X.; Natansohn, A.; Eisenberg, A. *Macromol.* 1990, **23**, 412.

194 Belfiore, L.A. *Polym. Prepr.* 1988, **29**, 17.

195 Belfiore, L.A.; Graham, H.; Ueda, E. *Macromol.* 1992, **25**, 2935.

Chapter Three: Experimental Methods

The following is a description of techniques that have been used in this research. The first three experiments are standard methods of polymer characterization and the fourth, small-angle x-ray scattering, is commonly used to study ionomers and other phase-separated polymers. These techniques will be used to support evidence obtained using nuclear magnetic resonance spectroscopy, which is the primary method of analysis used in this research. Following the descriptions of the experimental techniques are the details of the procedures used in this study.

EXPERIMENTAL METHODS

3.1 Stress-Strain Experiments

Stress-strain experiments, or tensile tests, are commonly used to determine a sample's physical characteristics, such as its stiffness, resistance to elongation or breaking, and ultimate strength. In a typical experiment, the sample is pulled at a constant rate of elongation and a transducer measures the resulting force on the sample. The engineering strain is defined as $\Delta L/L_0$, where ΔL is the change in length and L_0 is the initial length of the sample. Results are plotted as engineering stress σ (force divided by initial area) versus engineering strain ε.[1,2]

Some of the characteristics of a stress-strain curve are shown in Figure 3-1.[3] The modulus, E, or stiffness, is defined as the slope of the curve near the origin (at low levels of strain). A yield point is often seen in polymeric

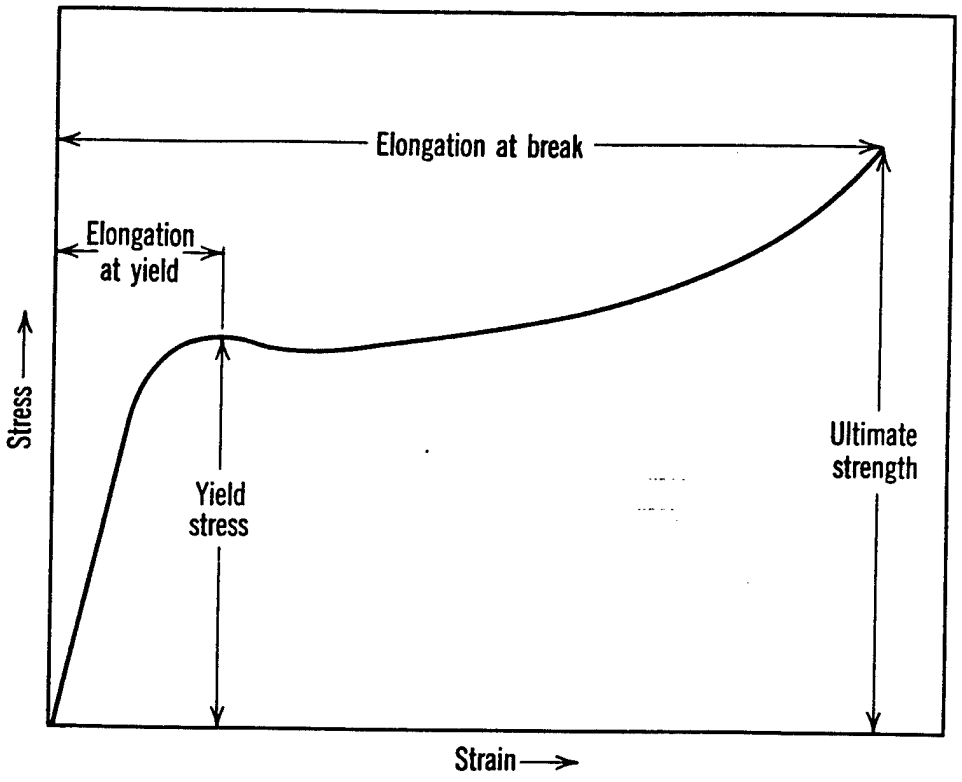

Figure 3-1: Example of a stress-strain curve [3]

materials.[4] At low elongations (before yield) increased amounts of stress can be applied to the polymer with little elongation. However, beyond the yield point only a small amount of additional applied stress is necessary to substantially elongate the polymer. The yield point might be the point at which crystalline domains break apart or at which molecular-level interactions, such as metal complexation,[5] are overcome. The domains due to molecular interactions or crystallinity act like physical crosslinks; once they are pulled apart, the polymer exhibits plastic deformation. At high levels of elongation, the slope of the stress-strain curve may increase sharply. This is known as strain hardening, and is due to either stress-induced crystallization of chain segments or the finite extensibility of the chains. Sample failure occurs after this phenomenon.

3.2 Infrared Spectroscopy

Infrared spectroscopy (IR) is one of the most commonly used spectroscopic techniques in polymer science. Its main advantages are that it is quick, sensitive, and relatively easy to use. Its main disadvantage is in quantitative measurements, which are not as straightforward. In an IR experiment, a beam of infrared light is passed through a sample and the intensity of the transmitted light (I) relative to the intensity of the initial beam (I_0) is measured. The molecules will absorb light if the energy of the light is the same as the frequency of the molecular vibration. If the vibration causes a change in dipole moment, then an an IR band will appear at the frequency of the vibration. The types of vibrations that lead to absorption of IR energy are bond stretching, bond bending, and internal rotations.[6,7] The

data is presented as transmittance (% I/I_0) or absorbance (log I_0/I) versus wavenumber (cm^{-1}) or wavelength (wavenumber =1/wavelength).

There are three regions to infrared data, near-IR, mid-IR, and far-IR. The mid-IR is 400-4000 cm^{-1} and is the typical range for organic molecules such as polymers. IR studies of ionomers have also been done in the far-IR ($\leq$ 400 cm^{-1}), which is sensitive to vibrations of the cations.[8]

3.3 Viscometry

Viscometric measurements are well-established for characterizing polymers in solution. Fluid flows through a tube and the time for the polymer solution to flow a given distance (t) is compared to that of the solvent (t_0). The specific viscosity is the increase in viscosity of the solution due to the presence of the polymer and is defined as $\eta_{sp} = (\eta\ \eta_0)/\eta_0 \approx (t - t_0)/t_0$,[3] where η_0 is the viscosity of the solvent. In the dilute concentration regime, the Huggins equation[9,10] is obeyed:

$$\eta_{sp}/c = [\eta] + k_1[\eta]^2 c \qquad (3\text{-}1)$$

where η_{sp} is the specific viscosity, c is the concentration, $[\eta]$ is the intrinsic viscosity, and k_1 is the Huggins constant. The viscosity molecular weight (M_v) is obtained from the intercept of above equation, $[\eta]$, through the Mark-Houwink equation:[11]

$$[\eta] = kM_v^a \qquad (3\text{-}2)$$

where k and a are constants for a given polymer-solvent combination.

3.4 Small-Angle X-Ray Scattering

Small-angle x-ray scattering (SAXS) is one of the more commonly used techniques for studying the morphology of ionomers and other phase-separated polymers.[12,13] X-rays are scattered by inhomogeneities in the material on the order of the wavelength of the x-ray (~ 1 Å). To study larger-scale (10-1000 Å) inhomogeneities, Bragg's law requires that small angles be used:

$$2d\sin\theta=n\lambda \qquad (3\text{–}3)$$

where n is an integer, d is the distance between scattering centers, 2θ is the scattering angle, and λ is the wavelength of the x-rays. In a typical SAXS experiment, 2θ is less than 6°. The intensity of the scattered radiation is proportional to the square of the difference in the electron densities in the material. In ionomers, the electron density difference is between the matrix hydrocarbon and the ionic domains. The results of a SAXS experiment are plotted as intensity versus the wave vector q:[14]

$$q=(4\pi/\lambda)\sin\theta\,. \qquad (3\text{-}4)$$

The main feature in a SAXS pattern of an ionomer is a broad maximum in intensity usually centered at a 2θ angle of 4°. Although the origin of this peak is still being debated,[8] it is generally considered to be due to interparticle interference. The position of the peak is related to the Bragg spacing between inhomogeneities ($d=2\pi/q$); this spacing is generally 20-50 Å. A second feature

commonly seen in ionomers is an upturn at very low q values. Although the origin of this feature is also in dispute, it is probably be due to the large-scale inhomogeneities in the distribution of ionic material in these systems. The size of the aggregates and their separation, along with other information, can be determined from a fit of the SAXS pattern to a given mathematical model.

3.5 Nuclear Magnetic Resonance

Nuclear magnetic resonance (NMR) is a non-destructive technique that can be used to examine the local environment of a nucleus. The primary NMR characteristics of a nucleus, which may be different for each type of site, are chemical shift, lineshape, relaxation time, and quadrupole moment. In this section, the origin of the NMR signal, interactions, and relaxation will be discussed.[15-23]

3.5.1 Basic Phenomenon

In order for a nucleus to have an NMR signal the nuclear spin quantum number, I, must be non-zero. The value of I is quantized and can only take on values of 0, 1/2, 1, 3/2, 2, etc. The actual number of energy levels is $2I+1$. Dipolar nuclei, for which $I=1/2$, have two spin states. In the absence of a magnetic field, these two states are degenerate and the spins do not have a preferred orientation. However, in a static magnetic field B_0, the degeneracy is split and the spins align either parallel or anti-parallel to the field. The energy splitting is proportional to the strength of the magnetic field:

$$\Delta E=(h/2\pi)\gamma B_0=(h/2\pi)\omega_L \qquad (3\text{-}5)$$

where h is Plank's constant and γ is the gyromagnetic ratio of the nucleus. This ratio is a constant for a particular type of nucleus and is defined by the ratio of the magnetic moment, μ, to the nuclear spin quantum number:

$$\gamma=(2\pi/h)\mu I \qquad (3\text{-}6)$$

The resonance frequency of the spin transitions ω_L is called the Larmor or angular precession frequency.

The populations of the two states are governed by a Boltzmann distribution. Because more spins are in the lower level than in the upper level, a net magnetization exists along the direction of the static field; the small population difference is the origin of the signal observed in NMR experiments.

Radiofrequency (*rf*) pulses are used to excite transitions in the nuclear spins and allow the observation of magnetization in the *xy* plane. The pulse usually tips the magnetization 90°, from the z-axis into the xy plane. Other tip angles can also be used. As will be shown, carefully chosen tip angles are necessary for quantitative information in quadrupolar work. The tip angle can be calculated from the equation:

$$\theta_{tip}=\gamma B_1 t \qquad (3\text{-}7)$$

The time t is the pulse time or pulse width. The frequency describing the rate of tip is ω_1 and the corresponding magnetic field due to the pulse is B_1.[20,21]

3.5.2 Interactions

In solid-state systems, there are a number of interactions that contribute to the chemical shifts, lineshapes, and relaxation times. These include scalar coupling, dipolar, and chemical shift anisotropy interactions; there is also a quadrupolar interaction present for nuclei with $I > 1/2$. Often, one interaction is dominant in a system. Scalar coupling will not be discussed in this report, however, scalar coupling is studied frequently in solution-state proton NMR, where the splittings caused by the interaction can be resolved.[20] In solids, scalar coupling is usually unresolvable or is eliminated by high-power proton decoupling, which will be discussed later.

The dipolar interaction is the major reason for the broad spectra observed for dipolar nuclei in the solid state. In fact, a large dipole-dipole interaction may hide any available chemical-shift information. The dipole-dipole interaction causes the ^{13}C nuclei to feel a component of the proton local magnetic fields, which increases the broadening in the spectrum. It is a through-space interaction that depends on the magnitude of the magnetic moments, the dipolar distance, and the relative orientation of the dipoles to each other and to the static magnetic field. In solution, this interaction is averaged to zero by the isotropic motion of the molecules. In solids, it can be averaged to zero by spinning the sample at a particular angle, called the magic angle, which will be discussed later.

The interaction due to chemical-shift anisotropy (CSA) depends on both the type of nucleus and the environment surrounding the nucleus. The electrons surrounding a nucleus partially shield it from the static magnetic field, with the degree of shielding determined by the number of electrons present and their spatial distribution. The orientational dependence of

shielding for a single species may be larger than the differences in average shielding for chemically distinct species. Since all molecular orientations are possible in a solid, the spectral lineshape, or powder pattern, covers a large range of chemical shifts. In polymers, the CSA patterns of all the different carbon sites overlap, ranging from 750 Hz to 10 kHz in width, and prevent any resolution of the individual sites. However, in solution, the differences in shielding are again averaged by the isotropic motion of the molecules. As before, the anisotropy in solids can be removed by spinning at the magic angle.

Magic-angle spinning (MAS) reduces or removes interactions that complicate the NMR spectrum. Both CSA and dipole-dipole interactions are functions of the form $3\cos^2\theta - 1$, where θ is the angle between the static magnetic field and the interaction vector. For $\theta=54.74°$ this factor is zero, and the effects of the interaction on the spectrum are eliminated. This yields a relatively narrow line with the isotropic chemical shift normally seen in solution-state NMR. Sidebands may appear at integral multiples of the spinning speed due to the time-dependent portion of the CSA, if the CSA is larger than the spinning speed. If enough sidebands are present, they can be used to reconstruct the original CSA pattern, which contains information on the electronic and/or molecular structure around the nucleus[24] Spinning at rates greater than half the width of the CSA pattern should cause the intensity of the sidebands to be negligible.

A second technique, high-power proton decoupling, is required to prevent broadening by the dipolar interaction. Radiofrequency radiation at the ^1H Larmor frequency saturates the protons by causing rapid precession. This averages the effective dipolar magnetic field seen by the ^{13}C nuclei and

decouples two nuclei. In solids, a B_1 field of 20-75 kHz (~ 5-20 Gauss)[20] is normally needed to average the ^{13}C-^{1}H interaction. ^{13}C-^{13}C interactions can be neglected because of the very low natural abundance (1.1%) of ^{13}C. Residual line broadening can be seen if ^{1}H-^{13}C dipolar decoupling is incomplete. Even after dipolar decoupling and MAS have been employed, the solid-state lineshapes are still 10-100 times greater than those in the solution state because of magnetic field inhomogeneities and other residual interactions. However, these MAS spectra with dipolar decoupling are usually of adequate resolution for polymer studies.

3.5.3 Relaxation

Relaxation studies are most commonly used to examine molecular motion in both solids and liquids. There are three relaxation times discussed in NMR studies of polymers in the solid-state. These are the spin-lattice relaxation time T_1, the spin-lattice relaxation time in the rotating frame $T_{1\rho}$, and the spin-spin relaxation time T_2. Each of these relaxation times is affected by the various interactions discussed in the previous section, and the degree to which the local motion of the nucleus modulates them. Each relaxation time indicates the magnitude of the interactions fluctuating at characteristic frequencies, with T_1 sensitive to 10-100 MHz motions (methyl group rotation), $T_{1\rho}$ depending on 10-50 kHz motions (chain rotations), and T_2 responding to very low frequency motions. In polymers, relaxation data have been useful in studying crystal structure, phase separation, and chain dynamics. NMR relaxation data are particularly useful due to the site-specificity of the experiment. The relationships between relaxation times,

molecular motion, and mechanical properties will help us better understand polymer properties and allow us to design new polymers more systematically.

All relaxation times measure the return of the magnetization to some equilibrium value after it has been perturbed. T_2 governs a purely entropic relaxation in the *xy* plane. A small T_2 value implies that the interaction among spins is efficient. In polymers, proton T_2 is most often measured since the ^1H signal is easily observed. Although $T_2(H)$ values have been reported in the polyurethane and ionomer literature, they measure the average relaxation of all protons in a given domain of the sample and are not specific to individual sites; therefore, they will not be emphasized in this research.

T_1 is the time constant for recovery of z-magnetization to its equilibrium value. As it returns to equilibrium, the nuclear dipole transfers its excess energy to its surroundings, or lattice. When molecular motion causes a fluctuating magnetic field with a frequency close to the Larmor frequency of the nucleus (10-100 MHz), the energy transfer is more efficient and T_1 times tend to be small. For a one-component system, T_1 relaxation is described by:

$$M(t)=M_0\left(1-\exp\left(-\frac{t}{T_1}\right)\right), \qquad (3\text{-}8)$$

where M_0 is the equilibrium value of the magnetization. For solids, $T_1 >> T_2$ and is generally the limiting factor in an experiment, in terms of the length of time of an experiment. T_1 is normally measured by an inversion-recovery or a saturation-recovery pulse sequence. In phase-separated polymers, such as the polyurethanes and ionomers in this research, the latter pulse sequence is

normally used as a more efficient method for sampling the wide range of relaxation times present due to the two motional regimes.

The third relaxation time, $T_{1\rho}$, is sensitive to motions in the kilohertz range of frequencies. In the rotating frame, the frame of reference follows the Larmor frequency, and the field created by the *rf* pulse (B_1 field) determines the energy scale of interest. The magnetization, which was originally determined by the large B_0 field, decays exponentially to its equilibrium value in a field of magnitude B_1.

In some cases, two or more relaxation times are necessary to describe the relaxation behavior of the system. This is particularly true in phase-separated systems where the various phases have very different motional characteristics. Under these circumstances, the relative amounts of material and the magnitude of the motions in each phase are determined from the percentage of signal described by each relaxation time and the value of the relaxation time itself.

3.5.4 Cross-Polarization

Cross-polarization (CP) is a signal-enhancement technique that uses a spin reservoir of a high-abundance nucleus, such as a proton reservoir, to improve the signal of a low-abundance nucleus, such as ^{13}C. This is accomplished through thermal contact of the spin reservoirs. CP is possible when the warmer reservoir of ^{13}C nuclei comes into contact with the colder proton reservoir.[20,25] This energy transfer occurs when both types of nuclei are simultaneously irradiated so that cross-relaxation in the rotating frame is an energy-conserving process (the Hartmann-Hahn condition):[26]

$$\omega_{1H}=\omega_{1C}, \text{ or } \gamma_H B_{1H}=\gamma_C B_{1C} \qquad (3\text{-}9)$$

In the above relation, ω_{1H} and ω_{1C} are the frequencies of the B_1 field for the proton and carbon nuclei, respectively.

In other words, when the Hartmann-Hahn condition is fulfilled, ^1H and ^{13}C nuclei can exchange energy through mutual spin flips, since they precess at identical frequencies in the rotating frame. As energy is exchanged, a new equilibrium is approached, one in which in which the carbons have a "colder" spin temperature. The spin temperature is related to the population difference between the energy levels (and therefore the NMR signal):

$$\frac{N_u}{N_l} = \exp\left(-\frac{\Delta E}{kT_s}\right), \qquad (3\text{-}10)$$

where T_s is the spin temperature, N_u and N_l are the spin populations of the upper and lower levels, respectively, and k is the Boltzmann constant.[23] As the spin temperature decreases, the population difference increases and the observed signal is enhanced.

The pulse delay is the time delay after data acquisition during which the magnetization returns to equilibrium along the z-axis. In a normal T_1 experiment, this time is determined by $T_1(C)$. However, in a cross-polarization experiment, the pulse delay is determined by the rate of recovery of proton magnetization because the observed magnetization originates from the protons. Since $T_1(H)$ is usually less than $T_1(C)$, often by one or two orders of magnitude, this represents a substantial savings in experimental time.

Equivalently, this offers a significant improvement in the signal-to-noise ratio for a given experimental time.

The maximum signal enhancement is governed by the gyromagnetic ratios of the two nuclei; the maximum enhancement available to ^{13}C nuclei from protons is 4. The actual enhancement is affected by the contact time, which is the length of time that the two reservoirs are matched. Generally, the optimum contact time is longer for the polyurethane soft-segment carbons than for the hard-segment carbons. This is because the soft segments are more mobile and, as a result, the dipolar interaction is reduced. Therefore, cross-polarization is less efficient for soft-segment carbons.

The cross-polarization technique was first combined with magic angle spinning and high-power proton decoupling by Schaefer *et al.* in 1977.[27] These researchers used CP/MAS to determine $T_{1\rho}(C)$ relaxation times of glassy polymers. They correlated $T_{1\rho}$ to the mechanical property of impact strength. The ability of a polymer to absorb an impact is related to its ability to dissipate energy through molecular motions. For effective energy dissipation, the frequencies of motion must be in the same range as the frequency of the impact, which is in the range 10-100 kHz. $T_{1\rho}$ was determined to be inversely related to impact strength. Small $T_{1\rho}$ values, which indicate a high level of kilohertz-frequency motions, lead to high impact strength. Since this study, CP/MAS has since become a standard technique for improving signal-to-noise ratios in ^{13}C NMR studies of polymers.

3.5.5 Quadrupolar Nuclei

Nuclei with spin quantum number $I > 1/2$ possess a quadrupole moment in addition to the dipole moment. Examples include ^{23}Na, ^{2}H, and

^{14}N. Because of the quadrupole moment, the nuclei are sensitive to electric field gradients around the nucleus. The quadrupolar interaction, which generally dominates the lineshape and relaxation behavior of the nucleus, is sensitive to the nature of bonding of the nucleus. For example, the number of ligands, the symmetry of the ligands, and the type of ligands to which the nucleus is bonded all affect the quadrupolar interaction.[16,28] This interaction can also be influenced by the presence and structure of nearby molecules, as well as by the formation of complexes. The quadrupole coupling constant (QCC)=e^2Qq/h,[29] is a measure of the strength of the interaction and is very dependent on the symmetry of the surrounding charge distribution. For example, in ^{23}Na NMR, a sodium environment of six oxygen atoms gives a QCC of ~ 600 kHz, while in $Na_2S_2O_3 \cdot 5H_2O$ (where the sodium environment is five oxygen atoms and one sulfur atom) the asymmetric environment yields a QCC of 2258 kHz.[30]

Finally, MAS cannot remove the effects of quadrupole interaction because it does not have an orientation dependence of the form $3\cos^2\theta - 1$ (where θ is the angle between the magnetic field and the sample). This creates the need for the use of other techniques. The current approach uses tip angles smaller than 90°, as discussed below. More information about quadrupolar nuclei can be found in many reference books and review articles.[30,31]

For a nucleus with $I > 1/2$, the magnitude of the field due to the quadrupolar interaction can range from zero to several megahertz.[32] Since the radiofrequency pulse is about a 50 kHz field, the field due to the quadrupole (ω_Q or B_Q) be comparable or greater. In the case of a very large quadrupole moment, the *rf* field will not be able to tip, or nutate, the spin

vector into the *xy* plane, and the vector component of signal which does appear on the *xy* plane will be a function of the quadrupolar interaction. For a sample containing several chemical sites with different nutation behavior, the ratios of the observed intensities between species will not be quantitative. A stack plot demonstrating this phenomenon is shown in Figure 3-2.[32] As t_1 is varied (where $\omega_{rf}t_1=\theta_{tip}$), the intensity of the peak at 0 kHz (NaCl; QCC=0) steadily increases while the peak at −1.5 kHz ($NaNO_2$; QCC=1.1 MHz) reaches a maximum and starts to decay. The ratio of the two species as determined from the ratio of the areas of the peaks will vary with tip angle, so that the correct composition of the material cannot be determined.

For very small tip angles, the effect of ω_Q is negligible and the resulting spectrum gives quantitative information on the number of species present. Samoson and Lippmaa[33] determined that for quantitative work, the tip angle must satisfy the following condition:

$$(I + 1/2)\omega_{rf}t_1 \leq \pi/6 \qquad (3\text{-}11)$$

For ^{23}Na, I=3/2 and the maximum tip angle for uniform excitation is θ=15°. So, in order to count the number of ^{23}Na spins in a given sample accurately, the tip angle must be set correctly. On the other hand, in order to obtain information on the precession frequency of the quadrupolar nucleus, experiments which vary the tip angle come into play.

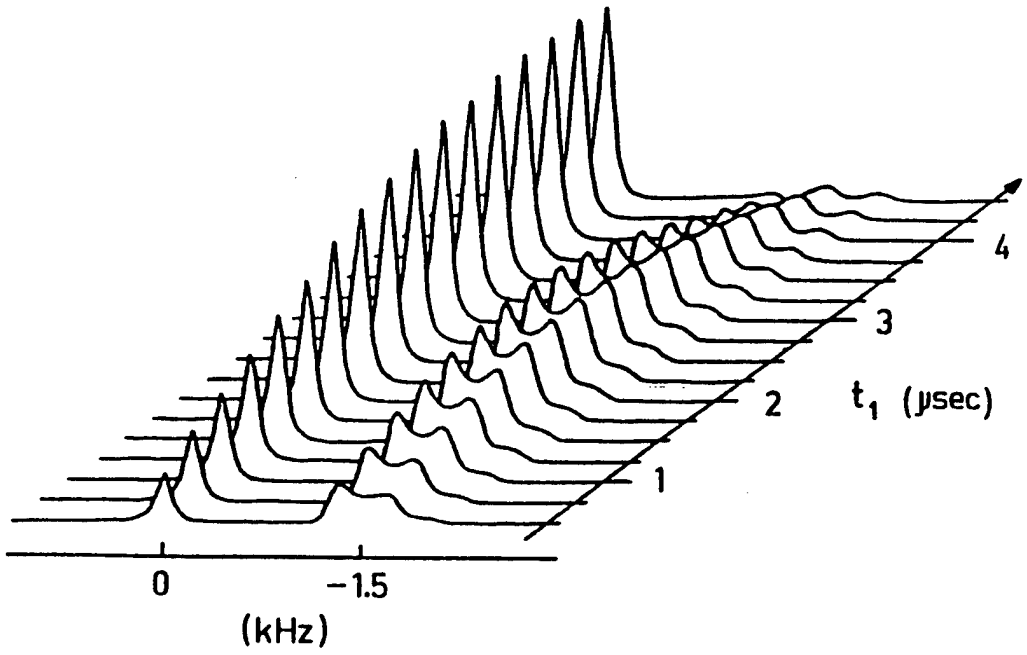

Figure 3-2: Stacked plot of ^{23}Na NMR intensity versus pulse length for a mixture of NaCl(s) and $NaNO_2$(s)[32]

EXPERIMENTAL DETAILS

3.6 Materials

3.6.1 Ionomers

Polydisperse sulfonated polystyrene (HSPS) and sodium-neutralized sulfonated polystyrene (NaSPS) were provided by Drs. Robert D. Lundberg and Dennis G. Peiffer of the Exxon Research and Engineering Corporation. The synthesis of these materials has been described elsewhere.[34] The structure of the material is shown in Figure 1-1. The number average molecular weight of the materials was 106,000 and $M_w/M_n = 2.7$. Materials are identified as NaSPS-X, where X is the percent of styrene groups that are sulfonated; NaSPS-1.7 is a sample having 1.7% of the available styrene groups sulfonated. Samples studied as received from Exxon, without any additional processing, are identified as the "original, uncast" samples, or "bulk" samples. Monodisperse sodium-neutralized sulfonated polystyrene (MNaSPS) ionomers were synthesized as described in the literature.[34] Sulfonation was carried out for one hour at 50°C; acid forms of the ionomers were neutralized with NaOH at 50°C. The ionomer was isolated via steam stripping, dried under air for 12 hours, and dried under vacuum at 60°C for 24 hours. Sulfur content was determined through Dietert sulfur analysis. The sulfonation level reported here is based on this analysis. The molecular weights, sulfonation levels, and sample identification for the monodisperse SPS samples used in this study are shown in Chapter 7. Unless otherwise specified, all polymer samples and reference compounds were dried under vacuum at room temperature for 2-7 days to remove residual water.[35] It is

likely that drying below the glass transition temperature (T_g) of the ionomer does not completely remove all water molecules from the aggregates; however, more rigorous drying above T_g affects the local morphology[36] and microstructure[37] of the ionomer.

The materials studied in the section *Effect of Neutralization Level* in Chapter 4 were synthesized in the following manner: the acid form of SPS (HSPS) was dissolved in a 95% tetrahydrofuran (THF) /5% water solution, and NaOH(aq) was added dropwise. Sodium content is characterized by the ratio (NaOH/sulfonic acid sites) x 100%; this ratio is labeled percent neutralization even at values greater than 100%. For the highest neutralization levels, above 180%, the solution was cloudy (showing micellar characteristics) but homogeneous. The resulting neutralized ionomers were dried at 65°C in air for 24 hours, then under vacuum at room temperature for 48-168 hours. These samples were not precipitated or steam-stripped to ensure that all NaOH remained in the polymer. All other SPS samples were received in the sodium form.

To prepare the humidified samples reported in Chapters 4 and 6, the ionomers were suspended over beakers of deionized water held at 40°C, 60°C, or 80°C, loosely covered, for 72 hours. Solution-cast samples for Chapters 5 and 6 were prepared from ~0.1–2.5 wt% solutions, with the solvent evaporation over 24-72 hours (depending on solvent) at 50°C. Samples were then placed under vacuum at room temperature for complete drying. Solutions of monodisperse NaSPS in Chapter 7 were made with 95/5 THF/water to a concentration of 0.5 wt% or, in the case of the ionomer blends, in 90/10 THF/methanol or 90/10 THF/water at $\leq$ 0.1 wt%. Blends of monodisperse polystyrenes were synthesized by adding the two ionomer

solutions dropwise and stirring for several hours following blending. The resulting solutions were dried at room temperature in air and under vacuum for several days. Heat-treated samples in Chapter 6 were dried under vacuum at 25°C before being heated to 140°C, 160°C, or 180°C. Some thermally-treated samples showed slight discoloration; however, no evidence of significant degradation was noted. The presence of residual solvent (e.g. tetrahydrofuran) was apparent in the NMR spectrum as a sharp peak at roughly -1 ppm, which could be removed by drying.

NaSPS polyelectrolyte (M_w=77,400; M_w/M_n=1.10; ion content 4.7 meq/g) was obtained from Polysciences, Inc. Sodium chloride (NaCl), sodium hydroxide (NaOH), sodium nitrite ($NaNO_2$), sodium toluene sulfonate ($CH_3C_6H_4SO_3Na$), sodium dodecyl sulfate ($CH_3(CH_2)_{11}OSO_3Na$), Acid Yellow 29, Amberlyst-15® ion-exchange resin, toluene, methanol, dimethylformamide (DMF), and tetrahydrofuran (THF) were obtained from Aldrich and used as received.

The carboxylated materials in Chapter 8 were made by several different synthesis routes. The sampled identified as NaSPS were synthesized by Professor X. Yu of Nanjing University via a post-polymerization process detailed by Lundberg and Makowski.[38] The polystyrene backbone was lithiated with butyllithium tetramethylethylene diamine in cyclohexane. A gel was recovered, dissolved in THF, and reacted with a solution of carbon dioxide in THF. The ionomer was neutralized with NaOH. The starting polystyrene has M_n~100,000 and M_w/M_n~1.9. The samples identified as HCPS (or VBA-X where X is the percent of carboxyl groups) were synthesized by Professor Yu through copolymerization of styrene and vinyl benzoic acid, as described by Tomita and Register.[39] A

standard polystyrene (VBA-0) was also synthesized. The molecular weights of the VBA copolymers were determined through viscometric experiments in THF. The carboxy-telechelic polystyrene ionomers were synthesized by Professor R. Jérôme of the University of Liège, Belgium via a procedure described previously.[40] The ionomer was made through an anionic polymerization for a low molecular weight distribution and the functionality was determined to be >1.95 from titration of the acid end groups. The polyurethane ionomers were synthesized by Susan Visser at the University of Wisconsin. Details of the procedure have been published elsewhere.[41] The base polyurethane was composed of a 1:1 ratio of toluene diisocyanate (TDI) and poly (propylene oxide), M_n=1000. The ionomers were synthesized by removing the urethane hydrogen with NaH and reacting the resulting material with either propane sultone or propiolactone.

3.6.2 Polyurethane Blends

The polyurethanes were synthesized by Professor Chang-Zheng Yang of Nanjing University using a two-step addition reaction. The materials are based on 3/2/1 or 2/1/1 molar ratios of diphenylmethane 4,4'-diisocyanate (MDI), N,N-bis (2-hydroxyethyl)isonicotinamide (BIN), and poly (tetramethylene oxide) (PTMO, MW=1000). The complete synthesis procedure has been reported.[5] The polyurethanes were then blended with a stoichiometric amount of metal acetate (zinc, magnesium or sodium); the molar ratio of pyridine to acetate was 1:1 for all blends. Materials are identified as XX-##, where XX is PU for the base polyurethane or the metal cation for the blends, and ## is the weight fraction of MDI units (29% for 2/1/1 and 35% for 3/2/1 mole ratios).

Isocyanate:chain-extender 1:1 hard segment-only materials were synthesized in a manner similar to that used for the polyurethanes. BIN was dissolved anhydrous DMAc under a dry nitrogen gas purge flow and stirred constantly. The solution was heated to 60°C and the catalyst (dibutyltin dilaurate) and the isocyanate (MDI, already dissolved in anhydrous DMAc) were added. The reaction was stirred for 1 hour at 65°C, then for 2-3 hours at 80°C. The polymer solution was allowed to cool to room temperature, then was precipitated in a large volume of water. The polyurethane product was soaked in water overnight, filtered, dried in a oven at 60°C for several hours, and dried in a vacuum oven at 60°C for 1 week. The IR spectrum showed that all the isocyanate groups had been reacted with hydroxyl groups. The 1:1 MDI/butanediol (BD) hard segment material was synthesized in an equivalent manner by Richard Goddard of the University of Wisconsin. Residual DMF was seen as an IR band at 1666 cm^{-1}, as ^{13}C NMR peaks at 31, 36, and 162 ppm, or as a ^{15}N NMR peak at –260 ppm. DMF could be removed by drying at 65°C for ~1 week for the polyurethanes conatining soft segments and 80°C for ~ 3 weeks for the hard segment- only materials.

3.7 Experimental Protocol

Materials for uniaxial stress-strain experiments were cast from 5 wt% solutions of DMF onto Teflon dishes. Data were obtained on an Instron Model TM using a crosshead speed of 0.5 in/min. The Instron was interfaced to a personal computer for automatic data acquisition. Samples were cut with an ASTM D1708 die. Data are reported as engineering stress and are the average of 3 or more tests.

Infrared spectra on the pyridine-containing polyurethanes were acquired using a Mattson GL-5020 spectrometer using a MCT detector. The resolution was 2 cm^{-1} and the number of scans acquired varied from 16 to 64. Samples were cast from 1 wt% solutions of either THF or DMF directly onto KBr plates. The film thickness was controlled so that the absorbance of the material was less than 1, which is the range in which the Beer-Lambert law is valid.[6]

The experiments were performed using an AVS 300 Schott-Geräte viscometer measuring station. A KPG Ubbelohde capillary viscometer, size #53103, was set into the measuring stand in a temperature-controlled water bath. The size of the capillary was chosen based on the viscosity range of interest. The temperature of the water bath was controlled to 0.05°C. Flow times were always greater than 200 seconds; the Hagenbach corrections for the specific capillary used were applied. The values obtained from this experiment were kinematic viscosities. Mark-Houwink parameters were taken from Wagner;[42] $k=14.1x10^{-3}$ dl/g and a=0.70.

Small angle x-ray scattering (SAXS) ionomer samples were either compression molded for 4 minutes at 190°C and 9000 psi or were cast from a 2.5 wt% solution onto a liquid gallium surface. Polyurethanes were compression molded for 4 minutes at 150°C. SAXS patterns were acquired on a Kratky camera with CuK_{α} X-rays from an Elliot GX-21 rotating anode generator with a nickel filter; data were collected using a Braun OED-50M linear position detector. The data were corrected for sample absorption of x-rays, parasitic scattering, detector sensitivity, and detector linearity. Low count rates were used so no correction for dead time was necessary. Sample intensities were converted to an absolute scale using a Lupolen standard;

cholesterol myristate was used to determine the sample-to-detector distance. The data were desmeared using the method of Lake[43] and background scattering was accounted for using the Bonart method.[44] The data are presented as I/I_eV versus the scattering vector q, where I is the scattered intensity, I_e is the scattered intensity of a single electron, V is the scattering volume, and $q=4\pi\sin\theta/\lambda$ (2θ is the scattering angle; λ is the wavelength of the x-rays, 1.54Å).

Solution-state ^1H NMR experiments were performed on a Bruker AC 300 machine operating at 300.13 MHz. Samples were spun at 15-20 Hz. VBA-0 and VBA-6 were dissolved in d_8-THF; the internal reference was tetramethylsilane. The frequency range was 20 ppm.

For the ionomers, ^{23}Na FTNMR spectra were acquired at 79.2 MHz on a Chemagnetics CMC-300A spectrometer. The frequency axis was set using an external reference of NaCl(s), which has with chemical shift δ=7.1 ppm relative to the standard NaCl(aq) solution. All solid samples were run in zirconia rotors using magic angle spinning (typically 5 kHz) and high power proton decoupling. To achieve uniform excitation, which permits quantitative analysis of the peak areas, the samples were run with a pulse width of 1.2 μs (corresponding to a 12.7° tip).[28,33] A pulse delay of 10 s was necessary to obtain fully-relaxed spectra; some spectra were obtained using shorter pulse delays so more scans could be acquired. These spectra are labeled in the figure captions. Supporting data were collected on a Bruker AM-500 spectrometer (located at the National Magnetic Resonance Facility at Madison, NMRFAM) running at 132 MHz. The spinning speed for these runs was 2.8 kHz.

NMR spectra of the polyurethanes were acquired on the Chemagnetics CMC-300A spectrometer at 75.4 MHz for ^{13}C NMR and 30.3 MHz for ^{15}N NMR. ^{13}C NMR spectra were acquired in a 7.5 mm probe using zirconia rotors; magic angle spinning (typically 5 kHz), cross polarization, and high power proton decoupling were employed. The secondary reference was the methyl carbon of hexamethylbenzene, which is δ=17.3 ppm from tetramethylsilane (TMS). ^{15}N NMR spectra were obtained using a 9.5 mm probe and Delrin rotors. Cross polarization, high power proton decoupling, and magic angle spinning (typically 2-3 kHz) were employed. The frequency axis was set using an external reference of glycine, which has with chemical shift $\delta = -350$ ppm relative to the standard CH_3NO_2. Pulse delays of 5 s were used for all cross-polarized spectra.

References for Chapter 3

1 Sperling, L.H. *Introduction to Physical Polymer Science*; John Wiley and Sons: New York, 1986.

2 Allcock, H.R.; Lampe, F.W.; *Contemporary Polymer Chemistry*, 2nd ed.; Prentice Hall, Inc.: Englewood Cliffs, New Jersey, 1990.

3 Billmeyer, F.W. *Textbook of Polymer Science*; 3rd. ed.; John Wiley & Sons: New York, 1984.

4 Speckhard, T.A.; Cooper, S.L. *Rubber Chem. Tech.* 1986, **59**, 405.

5 Yang, C.-Z.; Zhang, X.; O'Connell, E.M.; Goddard, R.J.; Cooper, S.L. *J. Appl. Pol. Sci.*, 1994, **51**, 365.

6 Koenig, J.L. *Spectroscopy of Polymers*; American Chemical Society: Washington, D.C., 1992.

7 Drago, R.S. *Physical Methods for Chemists*, 2nd Ed.; Sauders College Publishing: Orlando, FL, 1992.

8 Fitzgerald, J.J.; Weiss, R.A.; *Rev. Macromol. Chem. Phys.* 1988, **C28**, 99.

9 Huggins, M.L. *J. Am. Chem. Soc.* 1942, **64**, 2716.

10 *Polymer Handbook*, 3rd ed.; Brandrup, J.; Immergut, E.H., eds.; John Wiley and Sons: New York, 1989.

11 Hiemenz, P.C. *Polymer Chemistry*; Marcek Dekker, Inc.: New York, 1984.

12 Utracki, L.A.; Weiss, R.A. *Multiphase Polymers: Blends and Ionomers*; American Chemical Society: Washington, D.C., 1989.

13 Stein, R.S. *Pure & Appl. Chem.* 1991, **63**, 941.

14 Glatter, O.; Kratky, O. *Small-Angle X-Ray Scattering*; Academic Press: New York, 1982.

15 Slichter, W.P. in *NMR-Basic Principles and Progress*, Diehl, P.; Fluck, E.; Kosfeld, R., eds., Vol. 4; Springer-Verlag: New York, 1971.

16 Slichter, C.P. *Principles of Magnetic Resonance*, 3rd Ed.; Springer-Verlag: New York, 1990.

17 Kinsey, R. *Rubber Chem. Tech.* 1990, **63**, 407.

18 Bovey, F.A. *Polym. Eng. Sci.* 1986, **26**, 1420.

19 Voelkel, R. *Angew. Chem.* 1988, **27**, 1468.

20 Komoroski, R.A., ed. *High Resolution NMR Spectroscopy of Synthetic Polymers in Bulk*, VCH Publishers: Deerfield Beach, Fl., 1986.

21 Fukushima, E.; Roeder, S.B.W. *Experimental Pulse NMR*; Addison-Wesley Publishing Co., Inc.: Reading, MA, 1981.

22 Akitt, J.W. *NMR and Chemistry*, 2nd Ed.; Chapman and Hall: New York, 1983.

23 Farrar, T.C. *Introduction to Pulse NMR Spectroscopy*; The Farragut Press: Madison, WI, 1989.

24 Herzfeld, J.; Berger, A.E. *J. Chem. Phys.* 1980, **73**, 6021.

25 Pines, A.; Gibby, M.G.; Waugh, J.S. *J. Chem. Phys.* 1973, **59**, 569.

26 Hartmann,S.R.; Hahn, E.L. *Phys. Rev. B*, 1962, **12**, 2042.

27 Schaefer, J.; Stejskal, E.O.; Buchdahl, R. *Macromol.* 1977, **10**, 384.

28 Lippmaa, E.; Samoson, A.; Magi, M. *J. Am. Chem. Soc.* 1986, **108**, 1730.

29 Pfeifer, H. in *NMR-Basic Principles and Progress*, Diehl, P.; Fluck, E.; Kosfeld, R., eds., Vol. 15; Springer-Verlag: New York, 1972

30 Semin, G.K.; Babushkina, T.A.; Yakobson, G.G., *Nuclear Quadrupole Resonance in Chemistry*; John Wiley & Sons: New York, 1975.

31 Cohen, M.H.; Reif, F. *Solid State Phys.* 1957, **5**, 321.

32 Man, P.P. *J. Mag. Res.* 1988, **77**, 148.

33 Samoson, A.; Lippmaa, E. *Phys. Rev. B*, 1983, **28**, 6567.

34 Makowski, H.S.; Lundberg, R.D.; Singhal, G.S. U.S. Pat. 3,870,841 to Exxon Research and Engineering Company, 1975.

35 Toriumi, H.; Weiss, R.A.; Frank, H.A. *Macromol.* 1984, **14**, 2104.

36 Chapter 6

37 Weiss, R.A.; Lefelar, J.A. *Polymer*, 1986, **27**, 3.

38 Lundberg, R. D.; Makowski, H.S. *Am. Chem. Soc. Adv. Chem.* 1980, **187**, 21.

39 Tomita, H.; Register, R.A. *Macromol.* 1993, **26**, 2791.

40 Broze, G.; Jérôme, R.; Teyssié, P. *Macromol.* 1982, **15**, 920.

41 Visser, S.A.; Cooper, S.L. *Macromol.* 1991, **24**, 2576.

42 Wagner, H.L. *J. Phys. Chem. Ref. Data.* 1985, **14**, 1101.

43 Lake, J.A. Acta Cryst. 1967, **23**, 191.

44 Bonart, R. Müller, E.H. *J. Macromol. Sci., Phys.*, 1974, **B10**, 177.

Chapter Four: Ionomers: Effects of Sample Composition

4.1 Introduction

As discussed in Chapter 1, ionomers have been defined as polymers that contain a small number of ionic repeat units. Small-angle X-ray studies (SAXS) have shown that the ion pairs aggregate into ion-rich domains that are microphase-separated from the ion-poor matrix.[1-3] This aggregation is due to the incompatibility of the ion pairs and the non-polar hydrocarbon matrix. However, some of the ion groups remain outside these aggregates as isolated ion pairs. The most direct evidence for these isolated groups comes from electron spin resonance studies (ESR), which show hyperfine structure for polymers with isolated ions of copper (II) or manganese (II).[4,5] No direct evidence has been shown for isolated ions of monovalent cations such as sodium; however, anomalous SAXS (ASAXS) studies have suggested that a low-angle upturn in SAXS patterns of ionomers is due to an inhomogeneous distribution of isolated ions or ionic aggregates.[6,7]

Several nuclear magnetic resonance (NMR) probes have been used to study ionomers, including ^{19}F studies of perfluorosulfonate membranes,[8,9] as well as numerous proton[10-13] and carbon[14,15] studies to determine the effects of ionization, complexation, and water content on the mobility of the ionomer chains. Direct NMR studies of the counterions such as solid-state ^{23}Na NMR have been relatively rare.[16-18] One preliminary study by Dickinson *et al.*[16] examined sodium in Surlyn® and 5% sulfonated polystyrene (SPS). In both types of ionomers a broad peak was seen and attributed to the aggregated ions. After humidification or overneutralization, a second, sharper peak appeared downfield.

The ionomer chosen for these studies is sulfonated polystyrene, which has no crystallinity or phase separation in the homopolymer that would serve to complicate the interpretation of spectra. Additionally, the ionic content can be varied readily without changes to molecular weight or matrix composition. The morphology[2,3,6,19-21] and physical properties[19,22] of SPS have been studied in detail, including the effects of ion content,[3,19] water uptake,[2,23] and thermal history.[19,21,24] The strong base of macroscopic results invites studies that focus on the microscopic explanation for these materials' behavior.

Because ionic groups have such a strong effect on the physical properties of ionomers, the nature of the ionic crosslink was the focus of much of the research in this thesis. Among the many compositional and processing parameters that influence the physical properties of ionomers, this chapter deals with the effects of the number of ionic groups and the percent of neutralization on the local environment of the sodium ion. As described below, ^{23}Na NMR can observe directly the sodium ions held in different environments. Thermal history, solvent treatment, and other sample preparation steps are also major influences on the ionomer microstructure and physical properties, and the effects of these variables will be described in later chapters.

4.2 Results and Discussion

4.2.1 Reference Compounds

Several reference compounds were examined to establish characteristic spectral lineshapes for different ^{23}Na environments.

Figure 4-1 shows the spectra of solid sodium chloride and sodium nitrite. The sodium chloride spectrum is characterized by a Lorentzian lineshape with no quadrupolar features present. The sodium nuclei in NaCl are held in symmetric octahedral sites, leading to a cancellation of the electric field gradient. In contrast, $NaNO_2$ has a crystal structure of lower symmetry and shows a distinct powder pattern that can be simulated using the method of Kundla *et al.*,[25] with QCC=1.5 MHz and η=0.1.

Amberlyst-15® ion-exchange resin is polymeric HSPS and non-crystalline, and thus might be expected to behave similarly to NaSPS. However, it is a covalently crosslinked resin with a much higher sulfonation level than the SPS ionomers. It is expected that the mobility of the polymer chains in the resin would be greatly restricted as compared to NaSPS due to these crosslinks. Figure 4-2 shows the spectra of sodium-neutralized Amberlyst-15®. Initially obtained in the acid form, the neutralization level of this resin was varied from 1.5% to 150% of the available sulfonate groups. The spectrum of the 3.4% exchanged resin shows a broad, featureless peak centered around – 24 ppm. This peak shifts downfield and broadens with neutralization level; the dramatic shift in the center of gravity seen in the 150% neutralized material is most likely due to excess sodium hydroxide present as amorphous NaOH-rich domains. The peak does not have the obvious quadrupolar features that can be seen in the $NaNO_2$ spectrum. This is probably caused by a combination of factors, the most significant being inhomogeneous broadening due to the distribution of sodium sites and near-neighbor interactions in the sample.

As the sodium content increases the peak breadth increases and the peak begins to shift downfield, particularly above 100% exchange. For a

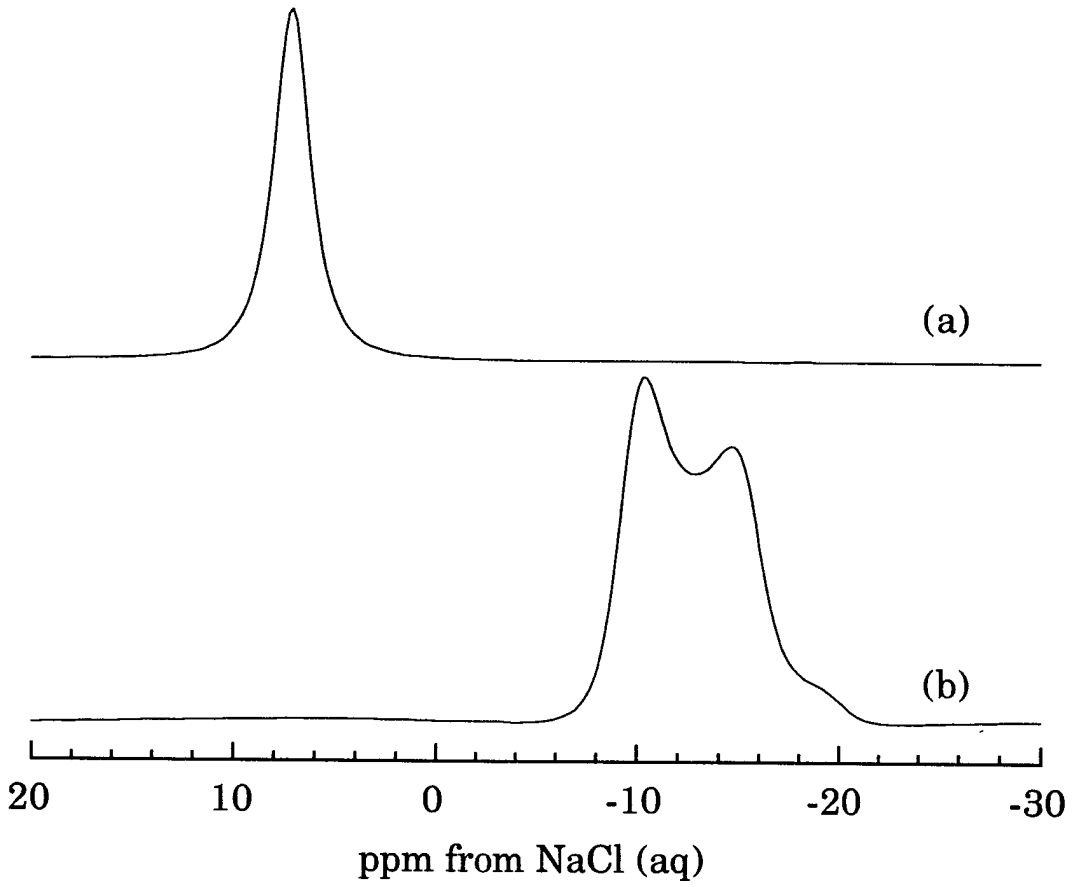

Figure 4-1: Solid-state ^{23}Na NMR spectra of a) NaCl and b) $NaNO_2$

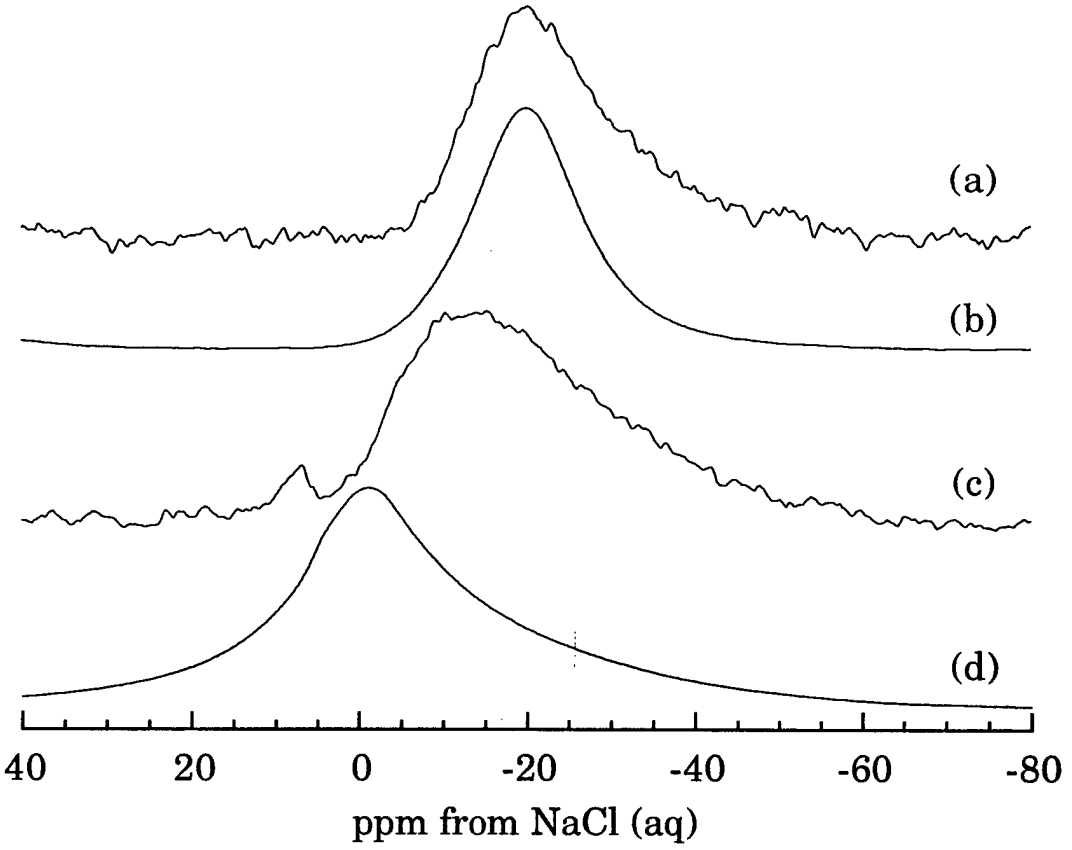

Figure 4-2: NMR spectra of Amberlyst-15 ion-exchange resin, exchanged with NaOH to a) 3.4% b) 40% c) 84% and d) 150% neutralization levels.

single sodium ion, second-moment calculations using the Van Vleck formula[26] show that the broadening of the sodium line is due to increasing numbers of sodium-sodium interactions. A single sodium ion surrounded by three oxygen atoms at 2.5 Å has a non-spinning width at half height of 0.2 ppm, while a sodium ion surrounded by three oxygen atoms at 2.5 Å and a second sodium ion at 4 Å has a non-spinning width at half height of 2.5 ppm–an order of magnitude increase. Also, the broadening due to quadrupolar interactions with like nuclei can be calculated using a modified version of the Van Vleck formula.[27,28] For a sodium-sodium distance of 4 Å this factor would add 2.3 or 2.2 ppm of peak broadening for nuclei in equivalent or inequivalent sites, respectively. The nearby sodium ions and the presence of trace waters of hydration would also increase the asymmetry of the environment surrounding the sodium ion, leading to a wider line. Finally, as was mentioned earlier, the distribution of sodium cations in the aggregate will cause additional, inhomogeneous broadening.

4.2.2 Peak Identification in NaSPS

Figure 4-3 shows a schematic diagram of the morphology of NaSPS. The black circles represent ion-rich domains termed aggregates. These aggregates may also contain hydrocarbon chains and trace amounts of water. The aggregates have a distribution of sizes (with an average diameter of 1-2 nm) and have been shown to be spherical in shape.[29] In addition to the aggregates, it is assumed that there are also some isolated ion pairs distributed throughout the hydrocarbon matrix which, in the case of a monovalent cation such as sodium, do not contribute to the crosslinking of the hydrocarbon chains.

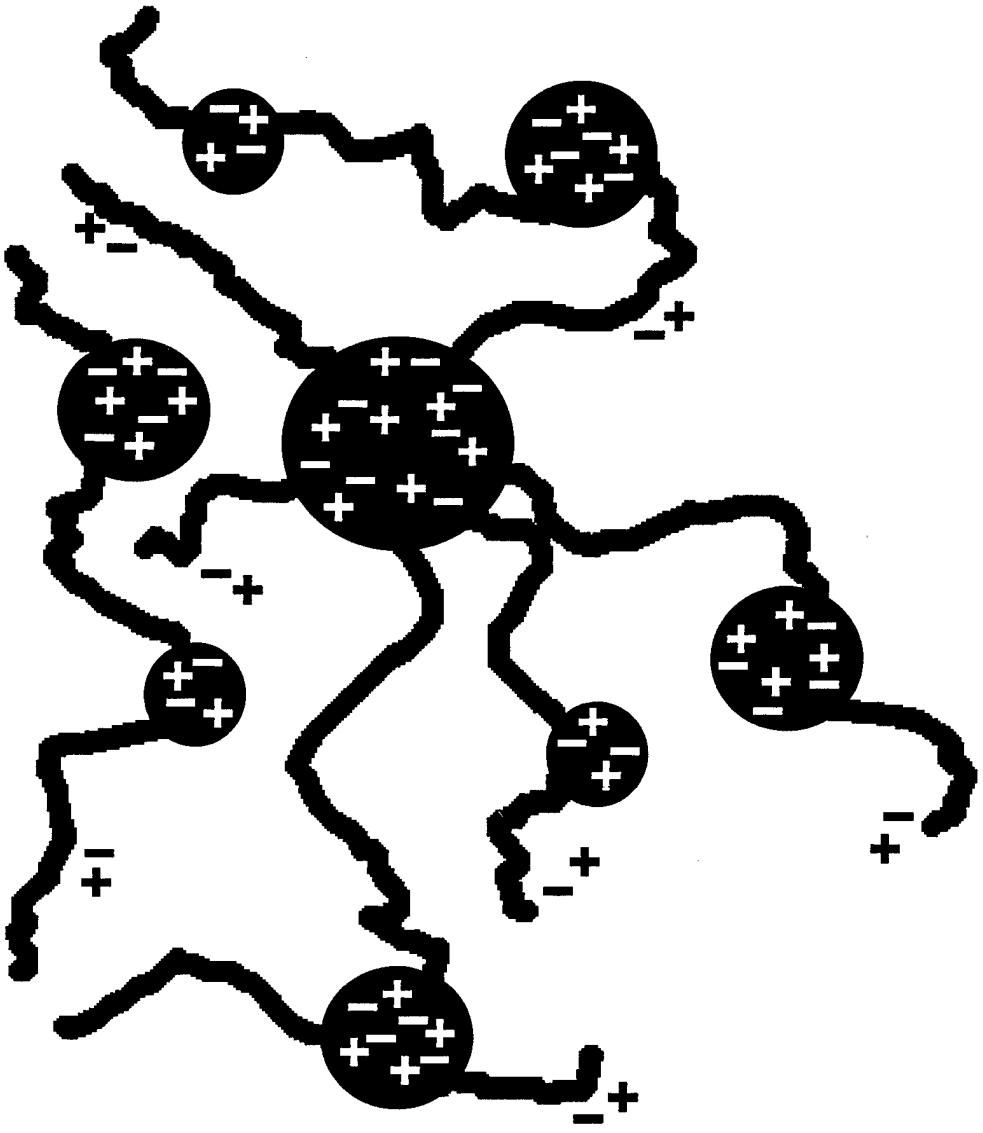

Figure 4-3: Schematic of the morphology of sodium-neutralized sulfonated polystyrene (NaSPS).

Figure 4-4 shows the spectrum of NaSPS at a sulfonation level of 1.7%. The ionomer was allowed to equilibrate in air for an extended period of time. This spectrum contains three Na^+ species shown by sharp peaks at 0 ppm and 7 ppm, and a broad peak at –12 ppm. These are associated with three different sodium environments that have been identified through the use of reference compounds, QCC calculations, and experiments presented later in this paper. The three environments seen in this spectrum have been assigned to sodium-sulfonate ion pairs i) fully hydrated at 0 ppm, ii) isolated at 7 ppm, and iii) aggregated at –12 to –23 ppm.

Hydrated Sodium Ions

The peak at 0 ppm is due to hydrated sodium ions. The sodium ion is in a symmetric tetrahedral environment when surrounded by water molecules as $Na(H_2O)_4^+$.[17,30,31] Hydrating the sample resulted in an increase in the intensity of the 0 ppm peak, and drying the sample under vacuum removed the peak completely. When the ion is hydrated the electric field gradient at the nucleus is zero and the resulting line is narrowed. This peak position is the same as that for aqueous sodium ions.[31,32]

Isolated Sodium Ions

The peak at 7 ppm has not been observed previously. We have assigned this peak to isolated sodium ions dispersed throughout the polymer matrix. A reference compound, Acid Yellow 29, supports this assignment. This dye is a large molecule that is only 4% sodium by weight, and because of its bulky structure is expected to produce isolated Na^+ ions in the solid state. Acid Yellow 29 shows two peaks (Figure 4-5), one at 7 ppm and a

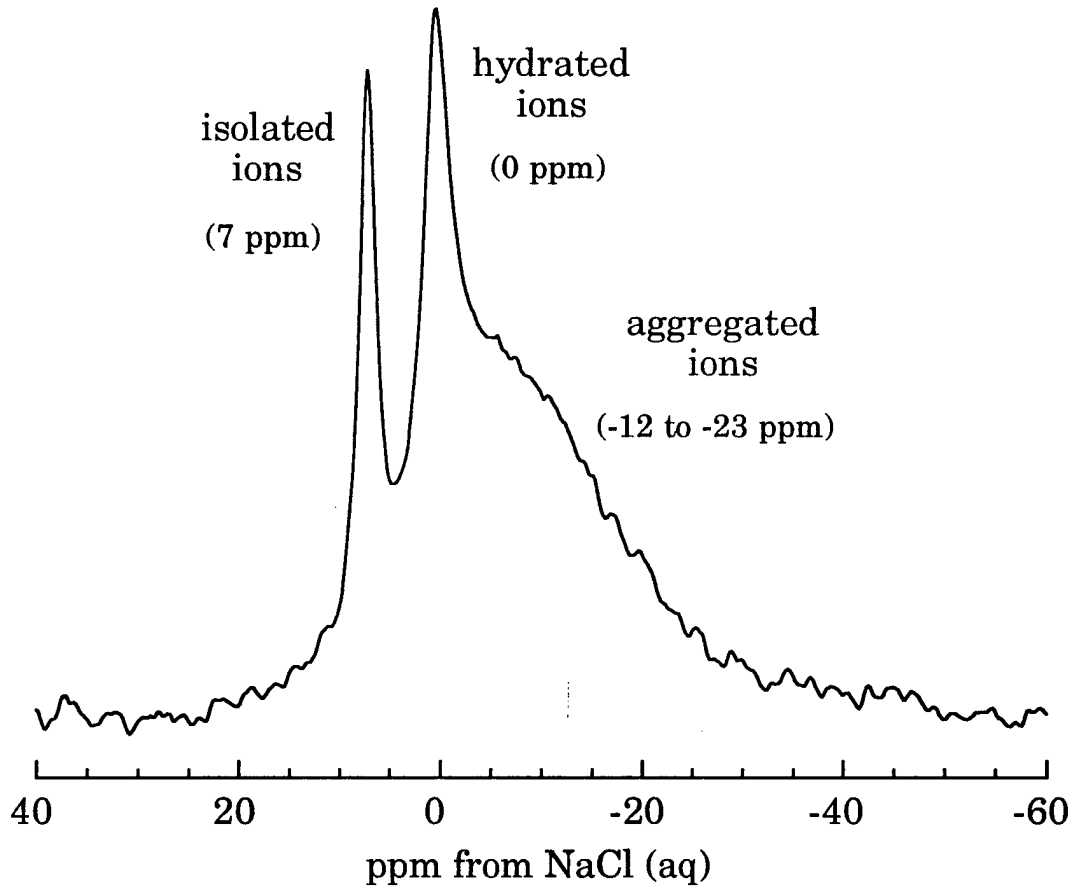

Figure 4-4: NMR spectrum of NaSPS–1.7. The ionomer was exposed to the atmosphere before the experiment, and the spectrum is not fully relaxed.

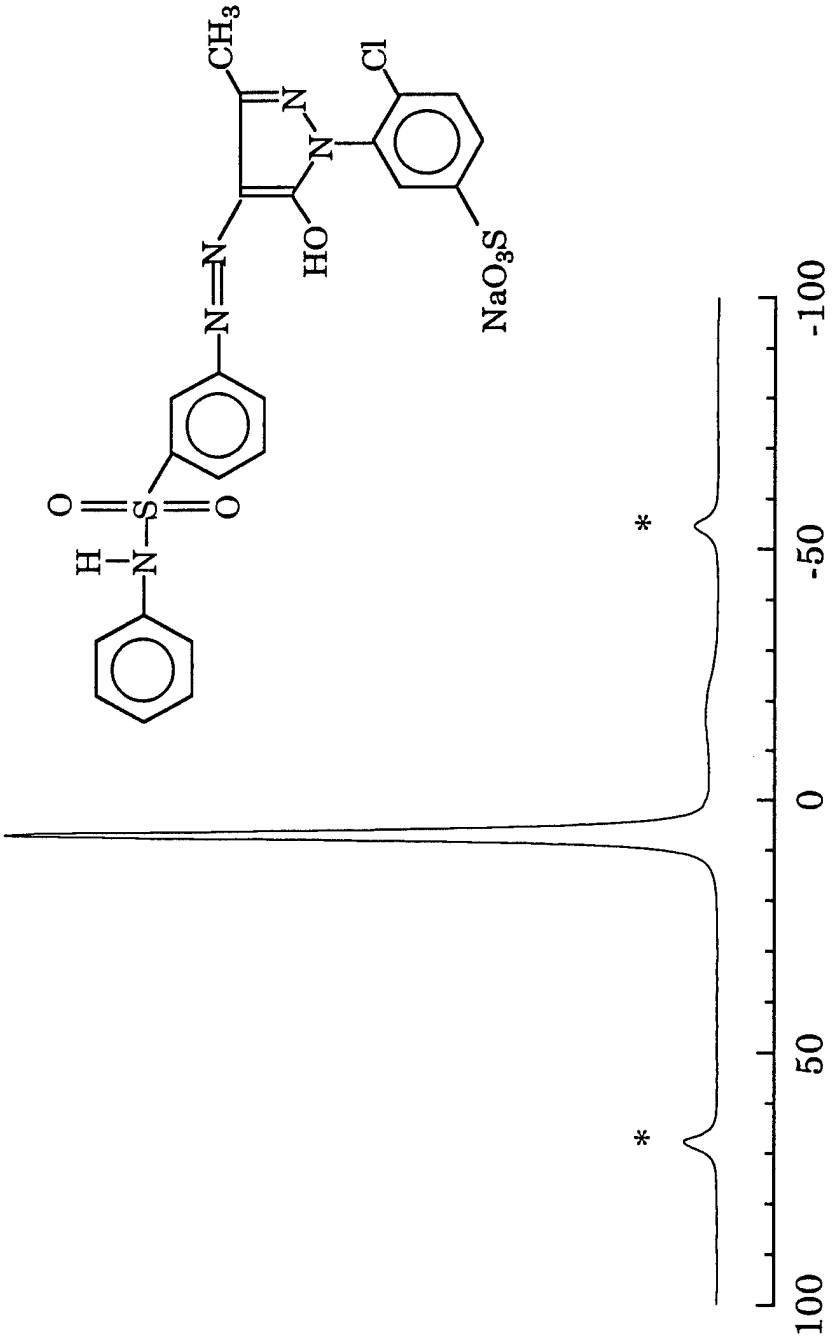

Figure 4-5: Structure and NMR spectrum of Acid Yellow 29.
Spinning sidebands are denoted by asterisks (*).

broad peak of relatively low intensity (10% of the total area) at –20 ppm. The similarity of this spectrum with those of the ionomers is in the positions of the peaks themselves, while the intensities of the peaks in the dye are consistent with the xpectation that most sodium ions are isolated in a predominantly hydrocarbon environment.

In the ionomers and Acid Yellow 29, the Na^+ in isolated ion pairs interacts with a single sulfonate group, but the geometry of the $R–SO_3^-$ group produces only a small residual electric field gradient at the sodium site so the NMR line is narrow. An estimation of the quadrupolar strength, assuming a tetrahedral geometry, is calculated as follows:

$$QCC = \frac{e^2qQ}{h} = \frac{(eQ)(eq)}{h} \qquad (4\text{-}1)$$

$$eq = V_{zz} = \frac{e}{r^3}\left(\frac{3\cos^2\Theta - 1}{2}\right). \qquad (4\text{-}2)$$

In these equations h is Planck's constant, e is an elementary charge, Q is the electric quadrupole moment, r is the Na–O distance in the $SO_3^-Na^+$ group, and Θ is the angle between the Na–O vector and the principal axis of the SO_3^- group. Typical values of S–O distance (r = 1.45Å) and angles (Θ = 74°) and Na–O distance (r = 2.26-2.7 Å) were taken from structures of related, well-studied compounds.[33-35] The resulting QCC is approximately 160 kHz and is relatively insensitive to the choice of r within the range given above. Simulations of the MAS quadrupolar lineshape of a sodium ion with this QCC were done using a program based on the work of Kundla *et al.*[25] The results are shown in Figure 4-6, which shows the predicted spectrum, with

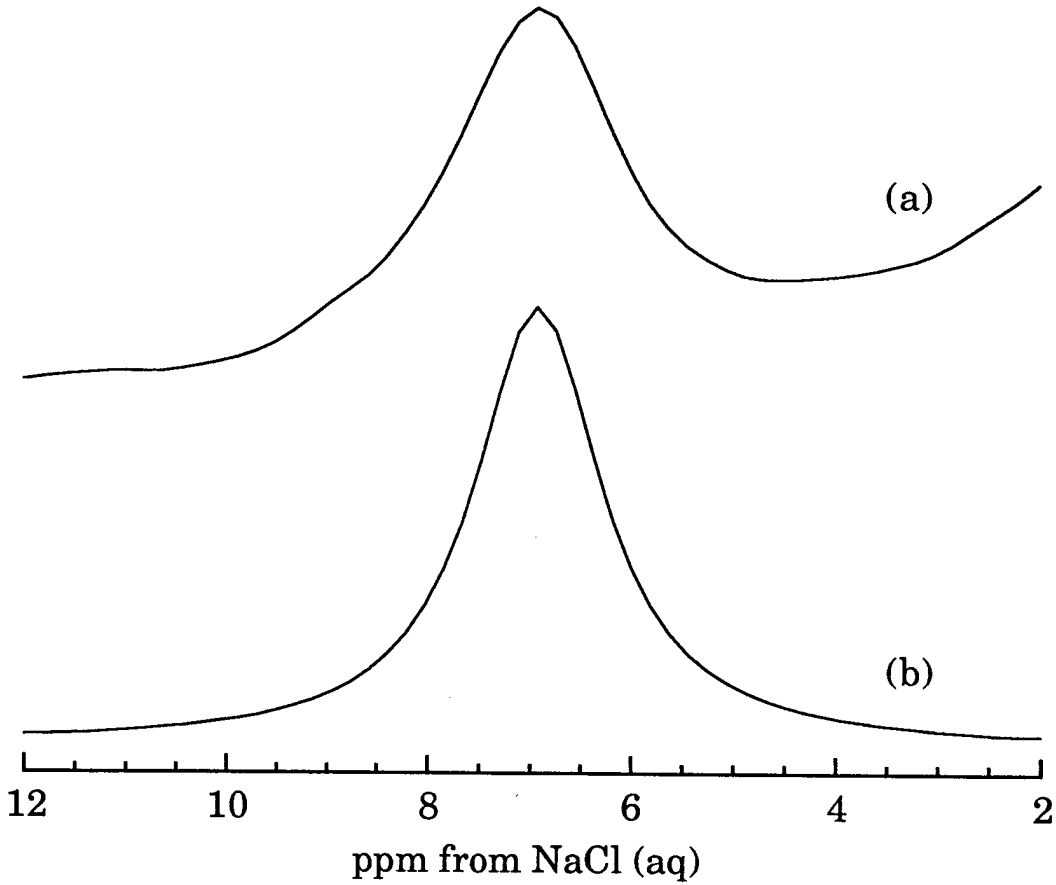

Figure 4-6: a) NMR peak due to isolated sodium ions in NaSPS–1.7 and b) simulated spectrum of an isolated sodium ion, aligned with the peak in NaSPS.

~1.1 ppm of additional Lorentzian broadening applied, and aligned with the actual NMR spectrum for 1.7% NaSPS. Both the observed and modeled peaks are ~160 Hz (= 2 ppm) wide under spinning conditions, indicating that this model for the isolated Na^+–RSO_3^- ion pairs is reasonable. Additional spectra obtained at 132 MHz show no shift in the position of this peak, confirming that the quadrupole coupling is small.

The existence of isolated ions has been reported previously in ESR studies that have probed the local environment of paramagnetic ions.[30,36-39] These studies have concentrated primarily on Mn(II)- and Cu(II)-exchanged ionomers. Ionomers neutralized with divalent ions exhibit behavior very different from ionomers with monovalent ions,[19,40-43] such as longer extension of the rubbery plateau region,[42] better fatigue resistance,[43] and different morphological behavior during annealing.[19] Isolated ions are more likely in a system containing divalent ions, in which the metal ion has two polymer chains tethered to it and is less able to aggregate into ion-rich microdomains.[44] Other authors[45-47] have suggested that there are different mechanisms for ionomer structure for materials neutralized with alkali and alkaline earth metals as compared to those neutralized with transition metals. The support for this view comes primarily from differences in the infrared spectra of ionomers. SPS neutralized with Mn^{2+} showed isolated ions in the ESR spectrum even at 5.5% sulfonation;[48] however, as will be shown in a later section, SPS neutralized with sodium ions contain no isolated ions above about 4% sulfonation level. Thus, the data in this chapter support the view that monovalent ions (Na^+) and divalent

transition-metal ions (studied with ESR) are distributed differently in ionomers.

Aggregated Sodium Ions

The final peak in NaSPS is centered around –17 ppm for NaSPS–4.2 and shifts with ion concentration. This environment is characterized by a broad, asymmetric peak showing a second-order quadrupolar shift. A similar peak was seen in a study by Dickinson *et al.*,[16] in which spectra of 5% NaSPS at 52.9 MHz were reported. The position of the broad peak was ~ –40 ppm and it was assigned to aggregated sodium ions. This peak shift as a function of spectrometer frequency is due to the strength of the quadrupolar coupling of the sodium ions. The center of gravity of a lineshape shifts with frequency as follows:[49]

$$\sigma_{CG} = \sigma_{CS} + \sigma_{QS}\,, \tag{4-3}$$

$$\text{with}\quad \sigma_{QS} = -\frac{3}{40}\frac{QCC^2}{\omega_L{}^2}\frac{I(I+1)-9m(m-1)-3}{I^2(2I-1)^2}\left(1+\frac{\eta^2}{3}\right), \tag{4-4}$$

where σ_{CG} is the center of gravity of the lineshape, σ_{CS} is the true chemical shift, σ_{QS} is the quadrupolar shift, ω_L is the Larmor frequency, I is the spin quantum number of the nucleus (I=3/2 in the case of sodium), m is the transition level, and η is the asymmetry parameter. In the calculations below, η is assumed to be zero for convenience. The maximum possible value of η=1 will cause at most a 15% change in the calculated QCC values.

The SPS 4.2% sample was run at 132 MHz on a Bruker AM-500 spectrometer and compared to the results obtained at 79.2 MHz. Both are

shown in Figure 4-7. The breadth of the peak base in the spectrum taken at higher frequency is due to spinning sidebands, which could not be spun far enough away from the peak itself due to equipment limitations. However, at the higher magnetic field the aggregate peak is narrowed and less asymmetrical, and so the center of gravity of the peak can be roughly approximated using a Lorentzian peak centered at –10.2 ppm. Using this value in combination with the value of –17 ppm observed at 79.2 MHz, the quadrupolar coupling constant for SPS 4.2% was calculated to be 1.6 MHz. This value is an order of magnitude larger than that found for isolated ions and indicates that the Na^+ ions in aggregates are not merely complexed to a single SO_3^- group in a symmetric geometry.

The width and shift of the peak assigned to aggregated sodium ions can be compared to those of sodium toluene sulfonate (STS) and sodium dodecyl sulfate (SDS), two smaller molecules with chemical structures similar to that of the ionomer. STS was chosen because its chemical structure is nearly identical to that of the SPS monomer, and SDS was chosen for its long-chain hydrocarbon, which may allow for easier aggregation than the bulky ring of STS. Figure 4-8 shows the spectra of both sodium toluene sulfonate and sodium dodecyl sulfate plotted above a spectrum of NaSPS 6.0%. Both small molecules show distinct lineshapes in the range of interest, but with much less homogeneous broadening than was seen in the ionomers and the ion-exchange resins. The STS spectrum can be fitted to a QCC of 2.75 MHz and an η of 0.2. Both the center of gravity and the quadrupolar coupling constant of the broad ionomer peak are in the range of those found for STS and SDS.

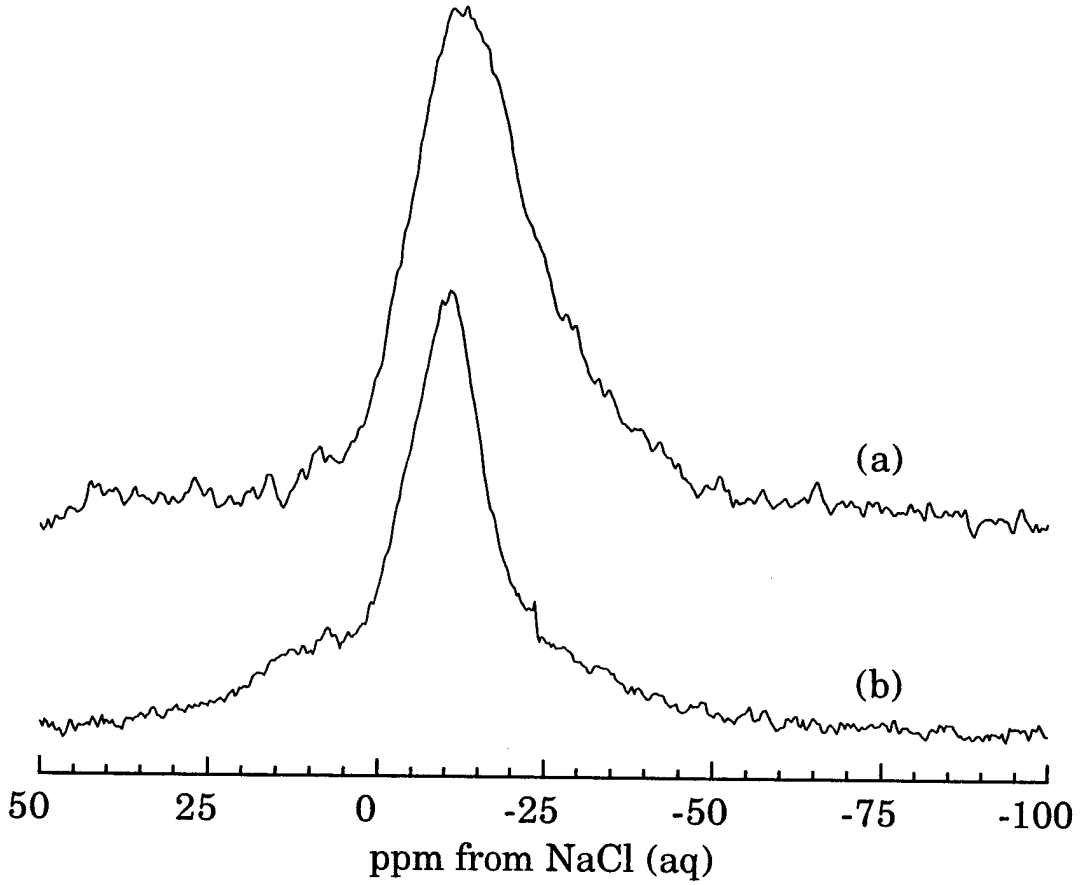

Figure 4-7: NMR spectra of NaSPS–4.2, a) collected at 79.2 MHz and b) collected at 132 MHz.

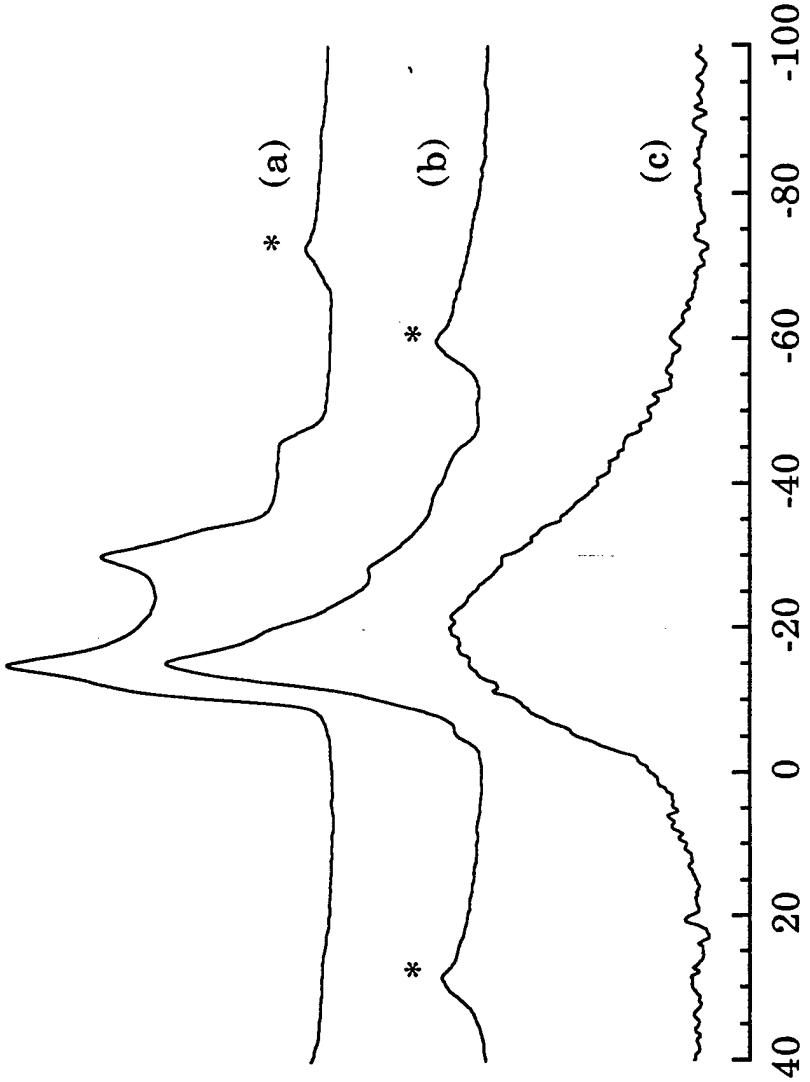

Figure 4-8: NMR spectra of a) sodium toluene sulfonate, b) sodium dodecyl sulfate, and c) NaSPS–6.0. Spinning sidebands are denoted by asterisks (*).

The structure of STS is considered to be similar to that of ionic aggregates,[50] and there is a general similarity of the shape, width, QCC, and position of the NaSPS peak with the peak shown for STS. Therefore, as in the study of Dickinson *et al.*,[16] this peak is assigned to sodium ions held in aggregates and which are subject to nearby interactions with other sodium ions and sulfonate groups. Different types of aggregated ions, such as dimers, trimers and larger aggregates, are not resolvable, and all are represented by the broad NMR peak. The interactions lead to increased line width, as was discussed for the ion exchange resins in Section 4.2.1, Reference Compounds. Due to the nature of the material, these interactions are assumed to be ionic, either as ionic bonds or nearby charges that polarize the electrons of the sodium ion. The individual sodium ions exhibit large quadrupolar coupling constants due to the asymmetric environment of the aggregate and the proximity of other ionic species.

4.2.3 Effects of Changing Sample Composition

Effect of Humidification

An NaSPS sample with an ionization level of 1.7% was dried under vacuum to remove residual water. The resultant ^{23}Na NMR spectrum consists of two peaks, at 7 and –12 ppm (Figure 4-9a). The same sample was subsequently humidified, producing a single hydrated NMR peak at 0 ppm, as shown in Figure 4-9b. With humidification, all sodium ions exist in the fully hydrated form, $Na(H_2O)_4^+$.[19,30] In this form, sodium ions in aggregates are far enough from other sodium ions (> 10 Å) that no homonuclear broadening is observed. In addition, all sites have equivalent symmetrical local environments after water has complexed with the Na^+ ions and it is not

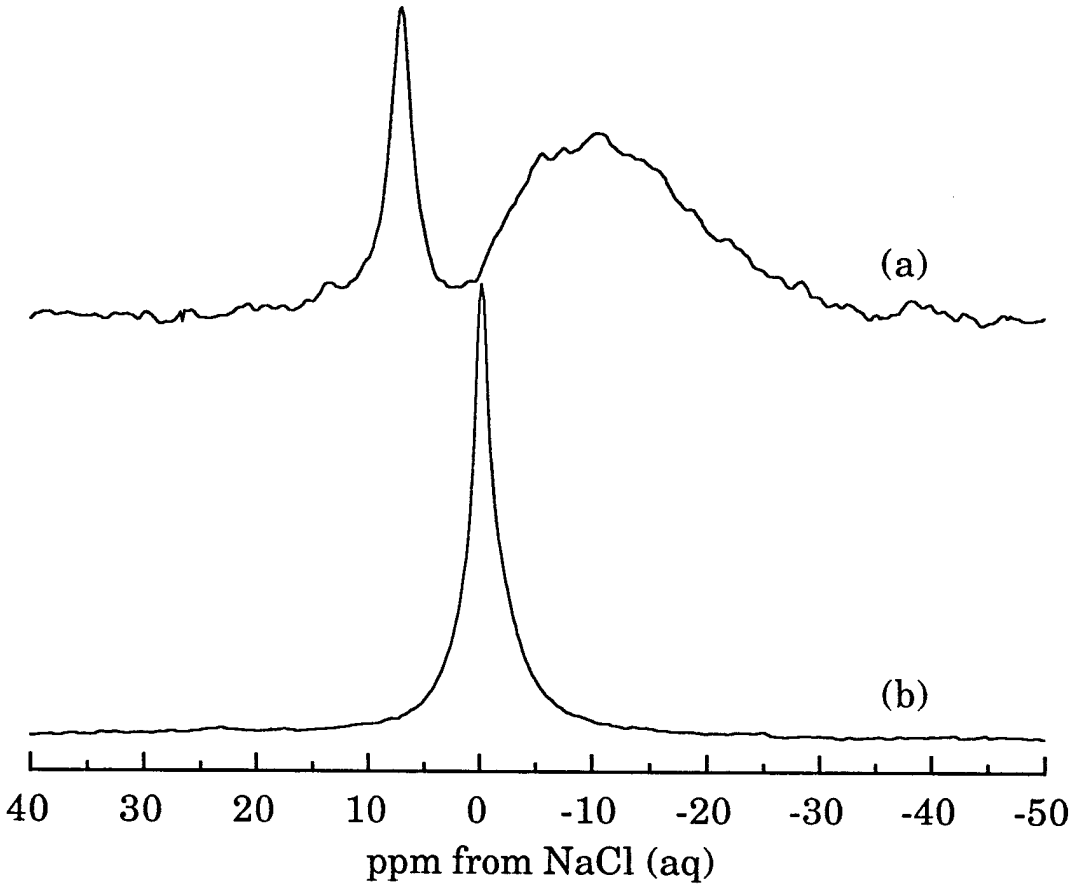

Figure 4-9: NMR spectra of NaSPS–1.7 a) dried under vacuum at room temperature and b) humidified at 80°C for 72 hours.

possible to determine from the spectra whether the species outside the hydration sphere are hydrocarbons (polymer chains) or ionic groups. These results show that even in a glassy matrix such as polystyrene, all sodium ions are available for hydration and that hydration completely frees sodium ions from interactions with any neighboring sulfonate counterions. Whether the aggregates continue to exist in a swollen form or whether they disperse into the matrix, it is clear that hydration greatly weakens the ion-ion interactions and so reduces the accompanying properties of the ionically crosslinked polymer.

Effect of Ionization Level

One of the goals of the present ^{23}Na NMR investigation was to determine a method for producing a mass balance on the sodium ions (*i.e.* fraction contained in aggregates versus fraction isolated). This has been accomplished by systematically varying the ionic concentration of the material. The effect of ionization level on the fraction of sodium ions in each environment is shown in Figure 4-10. The ratio of isolated to aggregated sodium ions clearly varies with ionization level; as the sulfonation level increases, fewer isolated ions are present. This is likely because the distance between sulfonate groups decreases at higher ionization levels. The attractive force between dipoles depends inversely on the fourth power of the distance between the ion groups, so the sodium sulfonate ion pairs are more likely to aggregate at higher ion concentrations. Consequently, the number of ion pairs dispersed throughout the hydrocarbon matrix decreases as the ionization level increases. The results of Figure 4-10 show that at some ionic concentration between 3.0 and 4.2%, the attractive forces are strong enough

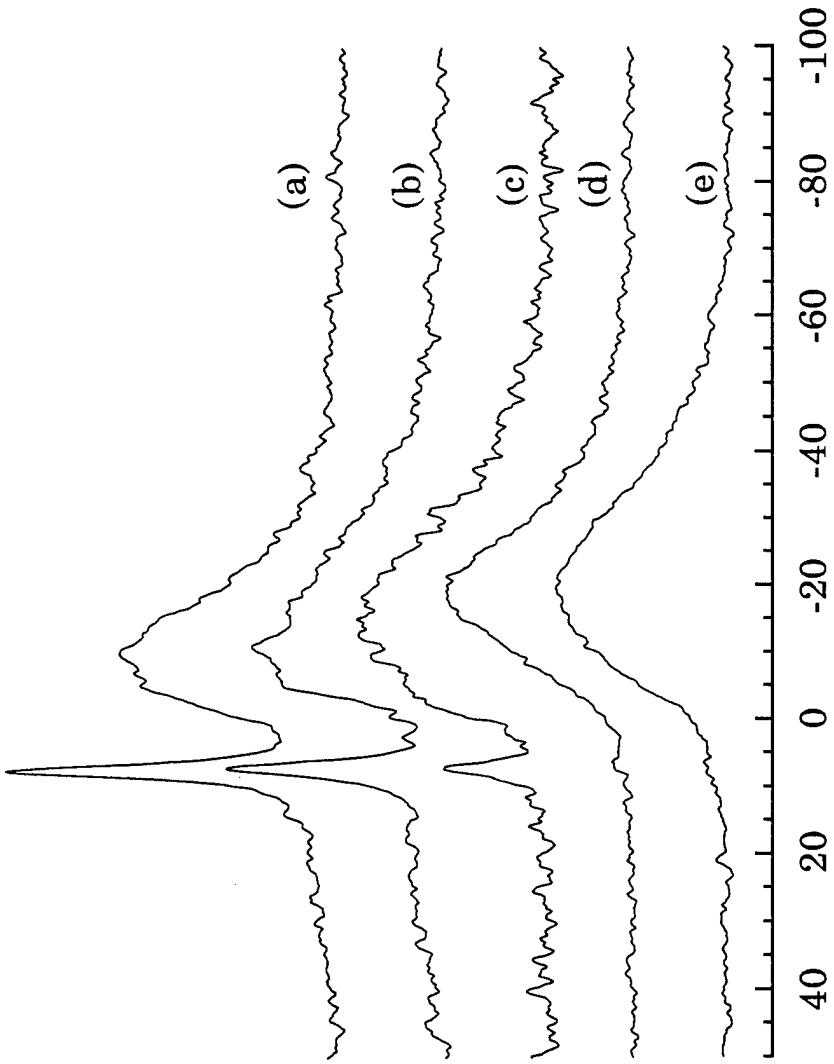

Figure 4-10: The effect of ionization level on the NMR spectrum of NaSPS: a) 1.7% b) 2.65% c) 3.0% d) 4.2% e) 6.0%.

that all ion pairs are held in aggregates. It should be noted that an "aggregated" sodium ion, as recognized by NMR, is any sodium ion that is not completely isolated from other sodium ions on the NMR length scale of ~ 10Å. A recent study has shown a transition point in tensile properties of NaSPS at the same ion concentration as we see the disappearance of isolated ions. Bellinger *et al.*[51] noted a small increase in tensile strength and toughness when increasing ion content below about 4%, and steeper increase in these properties at 4% and above. Additionally, the ion content above which the full extension of the rubbery plateau occurs in dynamic mechanical experiments is 3.5%.[52] It appears that the transition point in the tensile and mechanical properties is related to the loss of isolated ions, and therefore a greater efficiency of the ions as crosslinks.

Figure 4-11 shows the shift of the center of gravity with sulfonation level for the aggregated sodium ions. The peak shifts gradually upfield with increasing ion content. According to theory (equation 4-3), a shift to more negative frequency at constant field (ω_L) is due to a higher value of the quadrupolar coupling constant. This is consistent with results from spectra obtained at the higher field of 132 MHz: the aggregate peak in SPS 1.7% shifted less with frequency than did the peak in SPS 4.2%, indicating a lower QCC value for the sample with a lower ionization level. QCC is dependent on the environment surrounding the sodium ion, such as the symmetry of the site, the number of atoms surrounding the sodium ion, and the distances between the sodium ions and the surrounding atoms. Therefore, an increase in the QCC could be due to an increased number of ions held in the aggregate, closer packing between atoms, less symmetrical packing of atoms, or a combination of these factors.

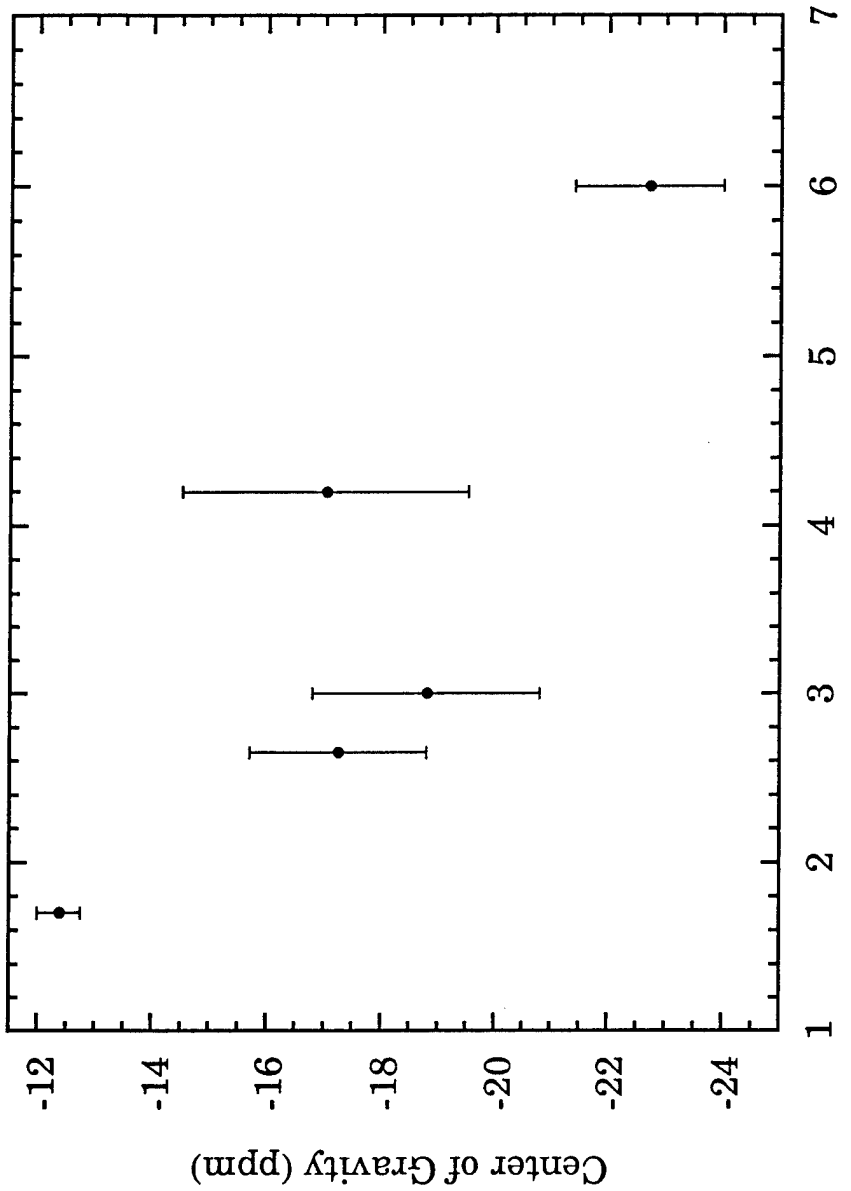

Figure 4-11: The center of gravity of the aggregate peak versus ionization level for NaSPS.

In a previous SAXS study of NaSPS the interparticle aggregate scattering peak was absent for the ionomer at 1.7% sulfonation, but present at ionization levels above 4%.[3] A later study[19] showed relatively weak and broad scattering peaks with a characteristic distance of ~ 4 nm for ionomers sulfonated to 1.4 and 2.3%. Differences in the results of the two studies may be due to different sample preparation techniques. The scattering peaks are indicative of phase separation in the ionomer. The SAXS and NMR studies indicate that the electron density difference necessary for the formation of the ionomer peak in SAXS is barely present at this low sulfonation level, despite the aggregation of the sodium ions that can be seen with ^{23}Na NMR. The results of even minimal aggregation are apparent in the increases in tensile properties of 1% NaSPS compared to those of unmodified polystyrene.[51]

SAXS results have shown that the scattering peak has more intensity and becomes more well-defined (less broad) as the ionization level increases, indicating better phase separation and less variation in the sizes of the aggregates.[3,19] The NMR findings are consistent with these results since better phase separation is due to the migration of isolated ions, dimers, and other small multiplets into larger aggregates. In turn, this migration would increase the electric fields and field gradients of the sodium ions involved. Additionally, steric hindrance from the tethered polymer chains would likely prevent symmetric packing inside the aggregate.

Effect of Neutralization Level

The acid form of 3.4% SPS was neutralized to levels of 30-370%. The resulting ^{23}Na NMR spectra are shown in Figure 4-12. The spectra show

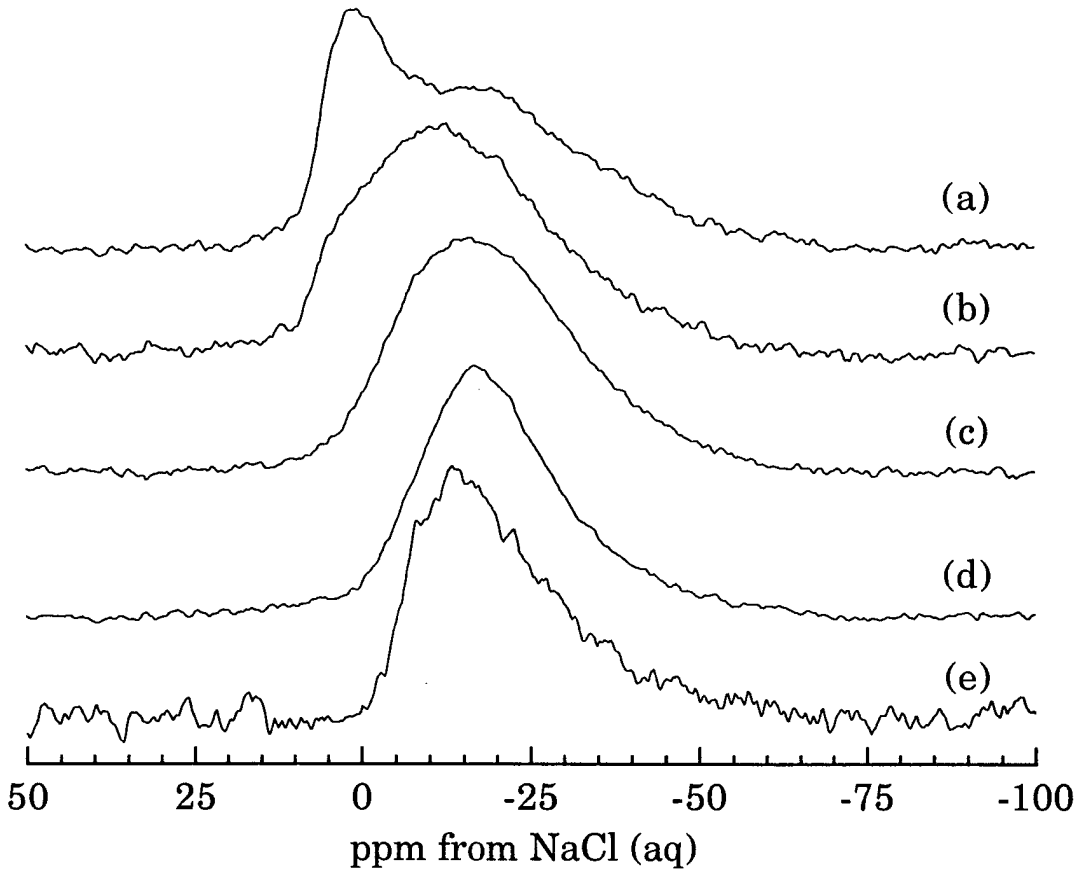

Figure 4-12: The effect of neutralization level on the ^{23}Na NMR spectrum for NaSPS at 3.4% sulfonation level: a) 370% b) 180% c) 110% d) 72% e) 31%.

that no isolated ions are present in NaSPS 3.4%, as was the case for higher sulfonation levels (Figure 4-10). In addition, the centers of gravity of the SPS 3.4% samples do not fall between the shifts for NaSPS 3.0 and 4.2 in Figure 4-11. Both deviations are attributed to solvent effects, which will be discussed in Chapter 5.

Increasing the neutralization level in NaSPS 3.4% gives results analogous to those seen for the ion-exchange resins (Figure 4-2); the width of the sodium peak increases with neutralization level and the center of gravity of the NMR line shifts downfield (higher ppm) as neutralization is increased past 100%. Figure 4-13 shows the shift in the center of gravity of the sodium peak as a function of neutralization level.

The level of neutralization has been shown to affect the mechanical[53,54] and rheological[55,56] properties of ionomers. Polymers neutralized below the equivalence point have exhibited poor mechanical properties[53] and increased water uptake.[57] On the other hand, the addition of excess neutralizing agent has been shown to increase the value of the stress at high elongations, while keeping the value of Young's modulus constant. This has been interpreted as an increase in the strength of ionic domains without a corresponding increase in their number. Therefore, it was proposed that the excess neutralizing agent remains trapped in the ionic aggregates and stabilizes the crosslinks.[53,56] This view has been supported by EXAFS studies of zinc-neutralized telechelic butadiene, which show no evidence of phase-separated zinc acetate.[58] These EXAFS studies also found no change in the environment of the zinc cation as the percent of overneutralization increased from 10% to 100%. In a study on the fatigue behavior of overneutralized SPS,[54] samples with up to 100% excess NaOH

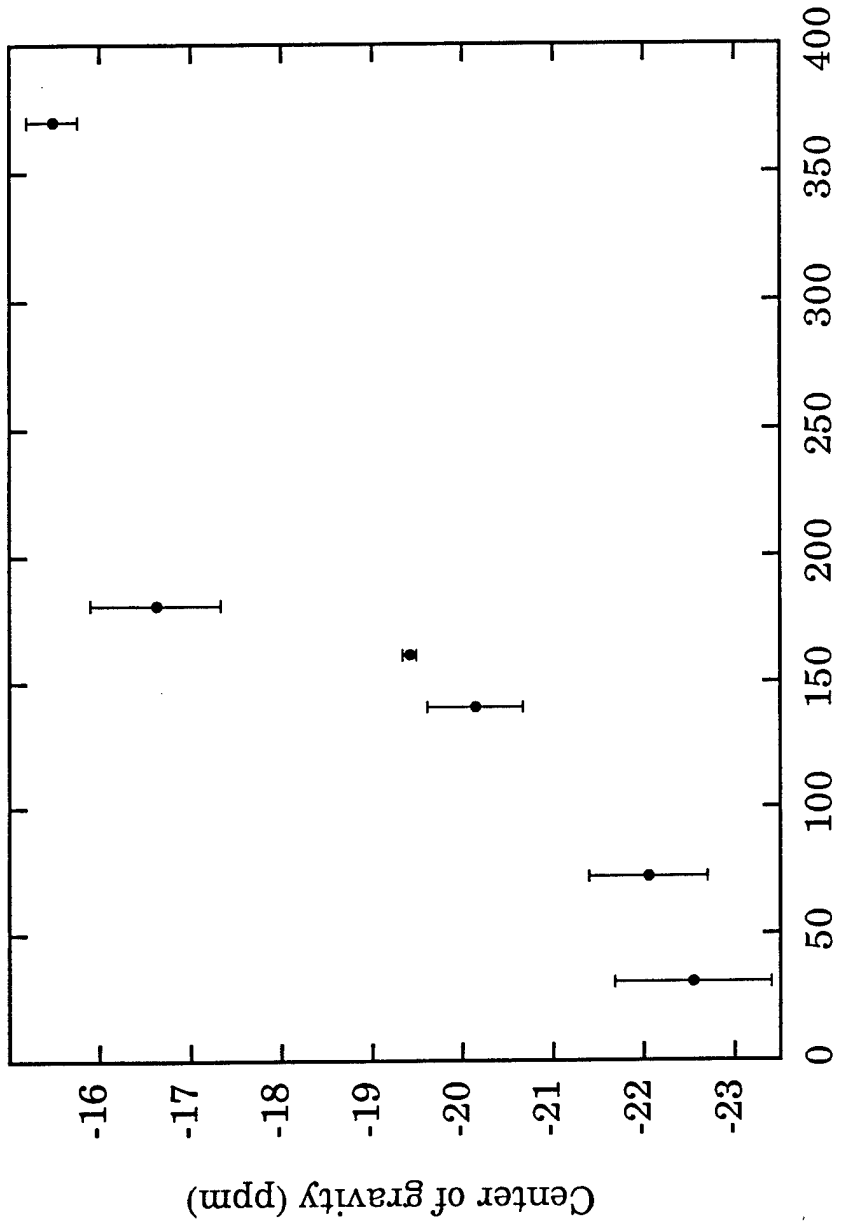

Figure 4-13: Center of gravity of the aggregate peak versus neutralization level for NaSPS–3.4.

displayed longer fatigue life than those exactly neutralized; however, those samples neutralized to 300% excess showed poor fatigue properties. It was determined that the excess NaOH in these highly overneutralized samples was held in phase-separated particles that were seen in SEM micrographs. Additionally, Weiss *et al.*[59] reported only slight improvement in tensile properties for poly(styrene-ethylene/butylene-styrene) neutralized with zinc to 200%, and a drastic decrease in properties for the sodium ionomer at the same neutralization level. In summary, previous studies have shown that excess neutralizing agent can increase mechanical properties; however, at high enough levels additional agent decreases tensile properties and shortens fatigue life. The question unanswered in prior studies has been exactly where the excess neutralizing agent lies within the ionomer at the different neutralization levels.

The ^{23}Na NMR results for neutralization levels below ~150-200% show that the excess neutralizing agent is within the aggregates, since no additional peak due to NaOH is seen in the spectra; for comparison, a spectrum of crystalline NaOH is shown in Figure 4-14. However, in this composition range the ^{23}Na NMR data do show some change in the sodium environment with increased amounts of neutralizing agent, as indicated by the changes in peak position and width. Finally, a spectrum of NaSPS 3.4% neutralized to 370% contains an additional peak due to phase-separated NaOH. Although the peak position is nearly the same as that of the fully hydrated sodium ion, the width is 2-3 times larger. The position of the new peak is comparable to bulk NaOH (Figure 4-14), but the sharp features present in the crystalline NaOH are not observed. Therefore, these new, principally NaOH domains are not fully crystalline and differ markedly from

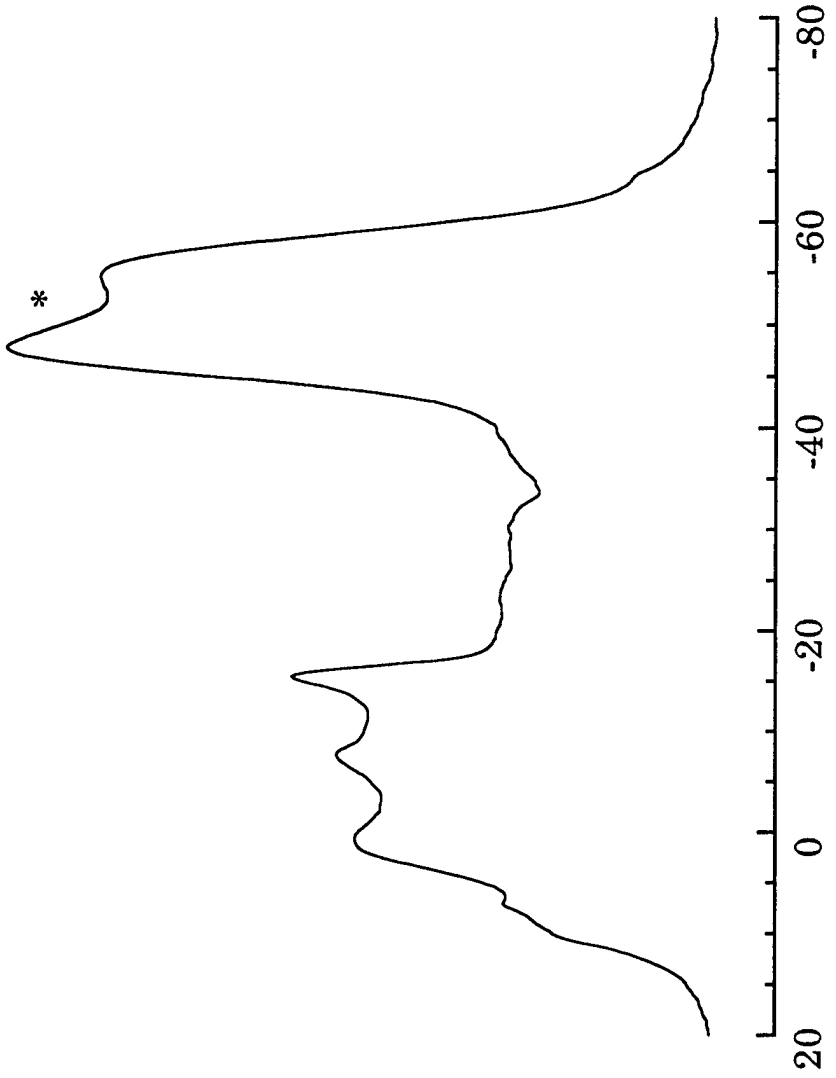

Figure 4-14: NMR spectrum of crystalline NaOH.
A spinning sideband is denoted by an asterisk (*).

bulk NaOH. The peak contains roughly 21% of the total amount of sodium in the ionomer. The remainder of the sodium appears in the modified aggregate peak, indicating that these aggregates can contain approximately two NaOH units for every sodium-sulfonate pair before additional NaOH produces this new peak near 0 ppm.

The NMR data reconcile some of the discrepancies among the results of other studies. At low levels of overneutralization, the excess neutralizing agent is held in the ionic aggregates, where it strengthens the crosslinks and increases aggregate size. However, at high enough levels the aggregates can no longer contain the additional NaOH, and the excess collects into phase-separated domains that act as defects. For NaSPS–3.4, the threshold for NaOH defect formation is quite high, occurring between 200% and 370% neutralization.

4.3 Conclusions

^{23}Na magic-angle spinning NMR has been used to characterize the environment of sodium ions incorporated into sulfonated polystyrene ionomers. This technique can measure the distribution of sodium ions based on quantitative detection of those held in aggregates and those dispersed throughout the matrix. Different Na^+ environments produce characteristic NMR peaks, with a 7 ppm peak due to isolated ions, a 0 ppm peak representing hydrated ions, and a broad peak at –12 to –23 ppm produced by sodium ions in aggregates. Since isolated monovalent ions do not contribute to crosslinking, NMR is a useful technique in determining the efficiency of ionic crosslinking of the pendant sulfonate groups.

^{23}Na NMR can also follow the changes in the ion distribution as a function of humidification, ionization level, and neutralization level. With humidification of 1.7% NaSPS at 80°C, all sodium ions are held in hydrated sites, $Na(H_2O)_4^+$, demonstrating that all ion pairs – isolated or aggregated – are readily hydrated. As the ionization level is increased, the fraction of ions in isolated sites decreases to zero. Finally, as neutralization level increases at a given sulfonate content, the broadening and downfield shift of the NMR peak assigned to aggregated sodium ions shows that the aggregates continue incorporating sodium well beyond the neutralization equivalence point. At very high levels of overneutralization, a new peak at 0 ppm indicates sodium ions present in domains of excess NaOH that no longer contribute to improved physical properties.

References for Chapter Four

1 Yarusso, D.J.; Cooper, S.L. *Macromol.* 1983, **16**, 1871.

2 Yarusso, D.J.; Cooper, S.L.; *Polymer*, 1985, **26**, 371.

3 Peiffer, D.G.; Weiss, R.A.; Lundberg, R.D. *J. Polym. Sci., Polym. Phys. Ed.* 1982, **20**, 1503.

4 Bersohn, M.; Baird, J.C. *An Introduction to Electron Paramagnetic Resonance*; W.A. Benjamin, Inc.: New York, 1966.

5 Westra, S.W.T.; Lyte, J.C. *J. Mag. Res.* 1979, **34**, 475.

6 Ding, Y.S.; Hubbard, S.R.; Hodson, K.A.; Register, R.A.; Cooper, S.L. *Macromol.* 1988, **21**, 1698.

7 Register, R.A.; Cooper, S.L. *Macromol.*, 1990, **23**, 310.

8 Schlick, S.; Gebel, G.; Pineri, M.; Volino, F. *Macromol.* 1991, **24**, 3517.

9 Boyle, N.G.; McBrierty, V.J.; Eisenberg, A. *Macromol.* 1983, **16**, 80.

10 Natansohn, A.; Eisenberg, A. *Macromol.* 1987, **20**, 323.

11 Natansohn, A.; Rutkowska, M.; Eisenberg, A. *Polymer*, 1987, **28**, 885.

12 Nierzwicki, W.; Rutkowska, M. *Polym Comm.* 1986, **27**, 327.

13 Lu, X.; Wang, Y. *Polym Comm.* 1991, **32**, 426.

14 Belfiore, L.A.; Shah, R.J. *Polym. Sci. Mater. Eng.* 1986, **54**, 490.

15 Yang, Y.; Wang, D.; Qui, J.; Qian, B.; Wang, H. *Chinese J. of Polym. Sci.* 1992, **10**, 113.

16 Dickinson, L.C.; MacKnight, W.J.; Connelly, J.M.; Chien, J.C.W. *Polym. Bull.* 1987, **17**, 459.

17 Komoroski, R.A.; Mauritz, K.A.; *J. Am. Chem. Soc.* 1978, **100**, 7486.

18 Park, J.K.; Park, B.K.; Ryoo, R. *Polym. Eng. Sci.* 1991, **31**, 873.

19 Weiss, R.A.; Lefelar, J.A. *Polymer*, 1986, **27**, 3.

20 Galambos, A.F.; Stockton, W.B.; Koberstein, J.T.; Sen, A.; Weiss, R.A. *Macromol.* 1987, **20**, 3094.

21 Register, R.A.; Sen, A.; Weiss, R.A.; Cooper, S.L. *Macromol.* 1989, **22**, 2224.

22 Hara, M.; Jar, P.; Sauer, J.A. *Polymer*, 1991, **32**, 1622.

23 Yang, S.; Sun, K.; Risen, W.M. *J. Polym. Sci., Phys. Ed.* 1990, **28**, 1685.

24 Hara, M.; Jar, P.; Sauer, J.A. *Polymer*, 1991, **32**, 1380.

25 Kundla, E.; Samoson, A.; *Lippmaa, E. Chem. Phys. Lett.* 1981, **83**, 229.

26 Van Vleck, J.H. *Physical Review*, 1948, **74**, 1168.

27 Cohen, M.H.; Reif, F. *Solid State Phys.* 1957, **5**, 321.

28 Kambe, K.; Ollom, J. *J. Phys. Soc.* Japan, 1956, **11**, 50.

29 Li, C.; Register, R.A.; Cooper, S.L. *Polymer*, 1989, **30**, 1227.

30 Maeda, M.; Ohtaki, H. *Bull. Chem. Soc. Japan*, 1975, 48, 3755.

31 Jardetzky, O.; Wertz, J.E. *J. Am. Chem. Soc.* 1960, 82, 318.

32 Mason, J., ed. *Multinuclear NMR*; Plenum Press: New York, 1987.

33 Barnes, C.L.; Hawkinson, S.W. *Acta Cryst.* 1980, B36, 2431.

34 Chetkina, L.A.; Sobolev, A.N. *Acta Cryst.* 1977, B33, 2751.

35 Arora, S.K.; Sundaralingam, M. *Acta Cryst.* 1971, B27, 1293.

36 Pineri, M.; Meyer, C.; Levelut, A.M.; Lambert, M. *J. Polym. Sci., Polym. Phys. Ed.* 1974, **12**, 115.

37 Yamauchi, J.; Yano, S. *Makromol. Chem.* 1978, **179**, 2799.

38 Galland, D.; Belakhovsky, M.; Medrignac, F.; Pineri, M.; Vlaic, G.; Jerome, R. *Polymer*, 1986, **27**, 883.

39 Alonso-Amigo, M.G.; Schlick, S. *J.Phys. Chem.* 1986, **90**, 6353.

40 Lefelar, J.A.; Weiss, R.A. *Macromol.* 1984, **17**, 1145.

41 Navratil, M.; Eisenberg, A. *Macromol.* 1974, **7**, 84.

42 Hara, M; Jar, P.; Sauer, J.A. *Polymer*, 1991, **32**, 1625.

43 Hara, M; Jar, P.; Sauer, J.A. *Macromol.* 1990, **23**, 4465.

44 Mattera, V.D.; Risen, W.M. *J. Polym. Sci., Polym. Phys. Ed.* 1986, **24**, 753.

45 Brozoski, B.A.; Coleman, M.M.; Painter, P.C. *Macromol.* 1984, **17**, 230.

46 Brozoski, B.A.; Coleman, M.M.; Painter, P.C. *Macromol.* 1984, **17**, 1591.

47 Han, K.; Williams, H.L. *J. Appl. Polym. Sci.* 1991, **42**, 1845.

48 Toriumi, H.; Weiss, R.A.; Frank, H.A. *Macromol.* 1984, **14**, 2104.

49 Samoson, A. *Chem. Phys. Lett.* 1985, **119**, 25.

50 Sakuri, K.; Douglas, E.; MacKnight, W.J. *Macromol.* 1993, **26**, 208.

51 Bellinger, M; Sauer, J.A.; Hara, M. *Macromol.* 1994, **27**, 1407.

52 Hird, B.; Eisenberg, A. *Macromol.* 1992, **25**, 6466.

53 Mohajer, Y.; Bagrodia, S.; Wilkes, G.L.; Storey, R.F.; Kennedy, J.P. *J. Appl. Polym. Sci.* 1984, **29**, 1943.

54 Hara, M; Jar, P.; Sauer, J.A. *Macromol.* 1990, **23**, 4964.

55 Makowski, H.S.; Lundberg, R.D.; Westerman, L.; Bock, J., in *Ions in Polymers*; American Chemical Society: Washington, D.C., 1980.

56 Bagrodia, S.; Pisipati, R.; Wilkes, G.L.; Storey, R.F.; Kennedy, J.P. *J. Appl. Polym. Sci.* 1984, **29**, 3065.

57 Williams, C.E.; Russell, T.P.; Jerome, R.; Horrion, J. *Macromol.* 1986, **19**, 2877.

58 Vlaic, G.; Williams, C.; Jerome, R.; Tant, M.R.; Wilkes, G.L. *Polymer*, 1988, **29**, 173.

59 Weiss, R.A.; Sen, A.; Pottick, L.A.; Willis, C.L. *Polymer*, 1991, **32**, 2785.

Chapter Five: Ionomers: Effects of Solution Casting

5.1 Introduction

In the previous chapter, ^{23}Na NMR results on NaSPS showed that sodium ions in polystyrene ionomers are found in up to three environments: isolated, aggregated and hydrated. The distribution of ions between aggregated and isolated sites was a function of the sample composition, *i.e.* the levels of ionization and neutralization. In this chapter it is shown that sample processing, specifically casting from solvents, also changes the ion distribution.

Many solution studies have been done on SPS ionomers in solvents of varying polarity.[1-12] In these studies, polymer solutions in low polarity solvents show association behavior while those in high polarity solvents do not. Electron spin resonance (ESR) studies of manganese-neutralized SPS (MnSPS) at 2.25% sulfonation showed both isolated and associated Mn^{2+} ions when the polymer was in a THF solution (primarily associated), but only isolated ions in a DMF solution.[2,3] Also, increasing the amount of methanol in a toluene/methanol solution of MnSPS, or adding water to a THF solution, increased the fraction of non-interacting (isolated) Mn^{2+} ions.[2] The presence of isolated ions indicates that the polar solvent (DMF, water, or methanol) was able to solvate the cation, removing all associations with other Mn^{2+} ions.

Although the ESR data indicate that DMF and the cosolvents toluene/methanol and THF/water are able to solvate cations, of the three only DMF and THF/water solutions show polyelectrolyte behavior for the SPS ionomers.[4,5] A THF/methanol solution has been shown to lack polyelectrolyte behavior as well.[6] The existence of polyelectrolyte behavior in the THF/water

cosolvent also depends on the ratio of the solvents; polyelectrolyte behavior is seen when the volume fraction of water is greater than 3%.[4,6] The investigators proposed that solvation results in an equilibrium between dissociated and aggregated ions.[10-12] In this scheme, the equilibrium focuses solely on the interaction between the solvent and the ionic groups. The direction in which the equilibrium shifts will therefore depend on the strength of the solvent-ionic group interaction and the concentration of polar cosolvent. For example, Lantman *et al.*[7-9] have shown that dissolving NaSPS in DMF leads to dissociation of the sodium from the sulfonate group; in THF the $Na^+SO_3^-$ group remains primarily associated.

Weiss *et al.*,[13,14] showed changes in the SAXS patterns of MnSPS at 7.6% sulfonation cast from solvents of increasing polarity. The intensity of the SAXS peak decreased as the polarity of the casting solvent increased, and the scattering peak completely disappeared in a sample cast from a 90/10 THF/water cosolvent. In all materials, however, the ESR spectra indicated that all Mn^{2+} ions were fully aggregated, even in the absence of the SAXS peak. In this chapter, related work is presented on the distribution of ions in the solid polymer films after solvent casting. Since the distribution of ions in solution is a function of the solvent polarity, it would be expected that the distribution in the resulting cast film would also be affected by the choice of solvent.

5.2 Results and Discussion

5.2.1 Effect of Solution Casting

The concentration of polymer in the casting solution affects the fraction of isolated ions found in the cast sample. Figure 5-1 shows samples cast from 90/10 THF/water solutions at 2.5, 1.0, 0.5, and 0.1 wt%. Materials cast from 2.5 wt% DMF and 0.5 wt % DMF showed the same trend. In all cast samples the final fraction of isolated ions is lower than in the original, uncast (bulk) sample. The two samples cast from higher concentration solutions have nearly the same fraction (~19%, compared to 30% in the original material), while the sample cast from the solution of lowest concentration shows far fewer isolated ions (Table 5-1). Lundberg and Phillips[6] have presented plots of reduced viscosity versus polymer concentrations for NaSPS-1.7 in THF/water solutions of varying ratios. Increases in reduced viscosity at low concentrations were seen for a 90/10 mixture of THF and water. The upward curvature began between 0.5 wt% and 1 wt% solutions, which is the point at which the significant decrease in the fraction of isolated ions is seen in Figure 5-1. A dependence of ionomer properties on sample history has been reported previously.[15] Solutions of NaSPS-1.7 isolated (freeze-dried) from dilute solutions of dioxane displayed lower melt viscosities and higher solubilities in xylene than solutions of NaSPS-1.7 isolated from more highly concentrated solutions. These freeze-dried samples are expected to retain the morphology of NaSPS in solution, while the solution-cast samples in this study do not.

The effect of the ratio of polar to nonpolar components in the cosolvent was studied for the samples cast from THF/methanol and THF/water. Figure 5-2 shows NaSPS-1.7 cast from a 1 wt% solution of THF/water at different

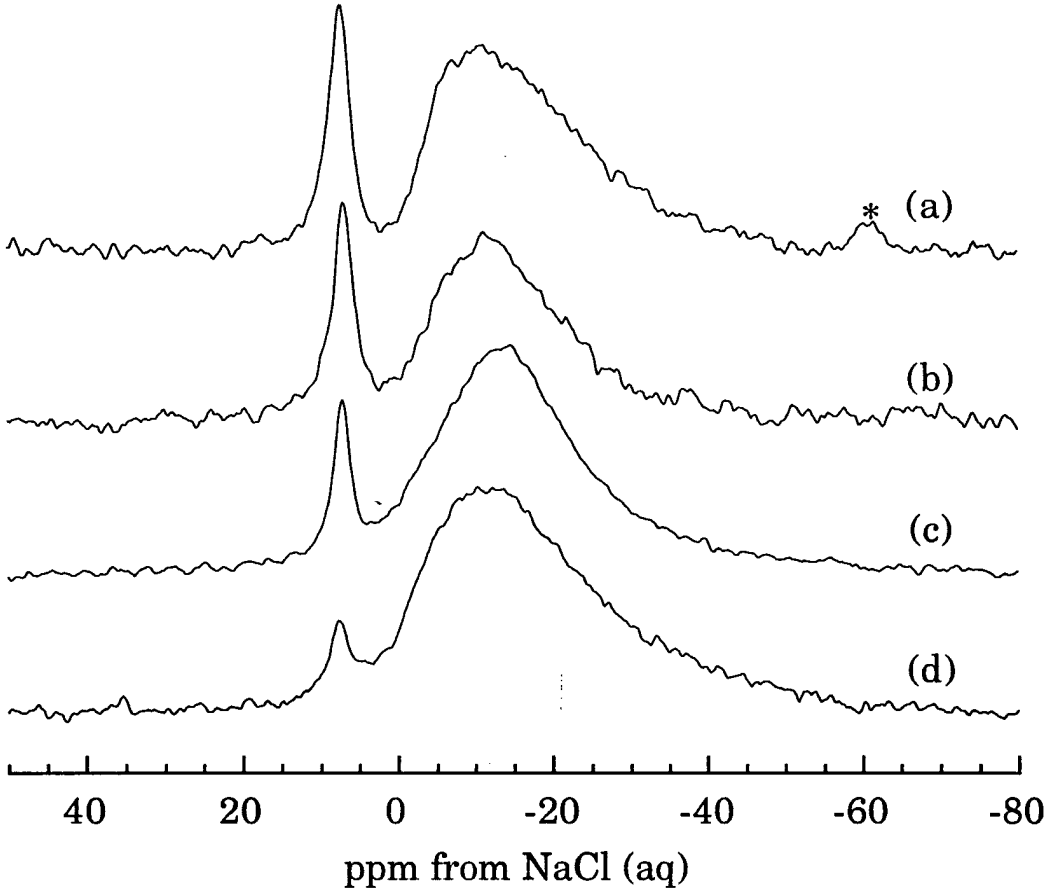

Figure 5-1: NMR spectra of NaSPS–1.7 cast from solutions of 90/10 THF/water at several polymer concentrations: a) 2.5 wt%, b) 1.0 wt%, c) 0.5 wt% and d) 0.1 wt%. Spinning sidebands are denoted by asterisks (*).

Table 5-1: THF/water influence on isolated Na^+ in films

90/10 THF/Water		1 wt% NaSPS in Solution	
NaSPS Concentration (wt%)	% Isolated Ions	THF/Water Ratio	% Isolated Ions
2.5	22	99/1	28
1.0	19	95/5	20
0.5	11	90/10	19
0.1	6		

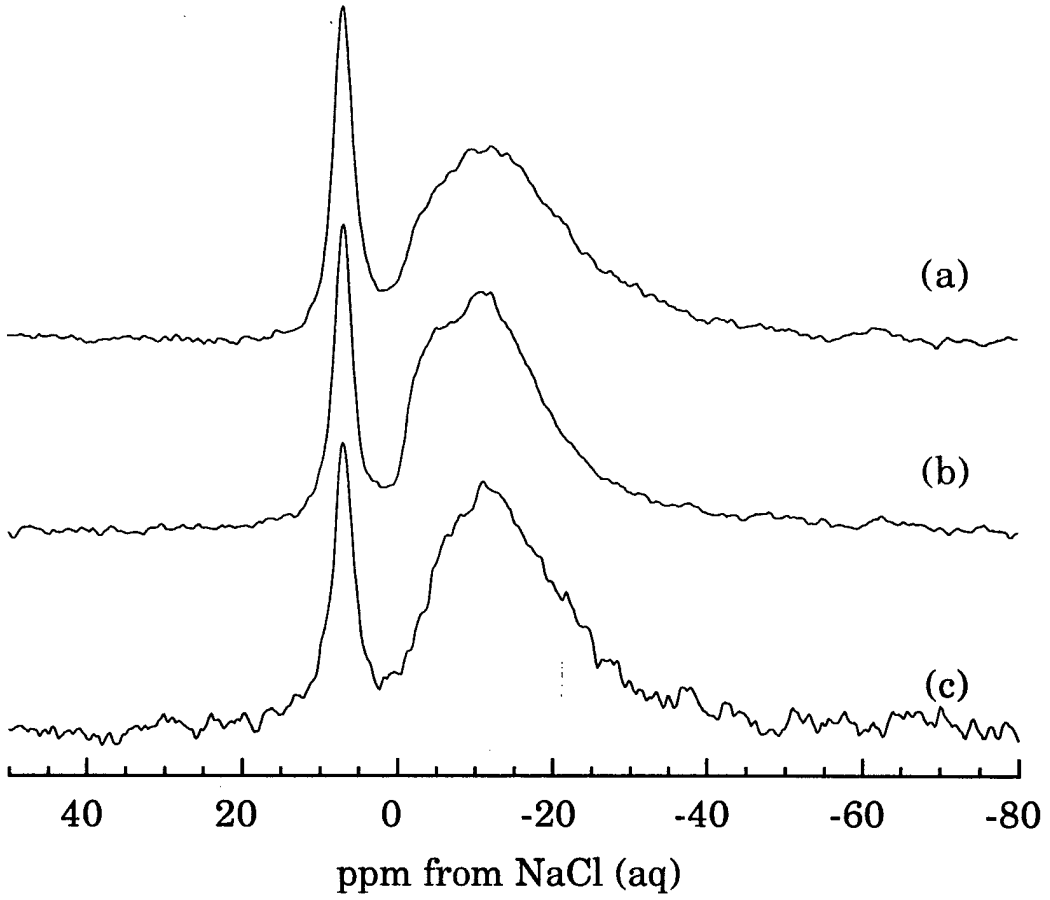

Figure 5-2: NMR spectra of NaSPS–1.7 cast from a 1.0 wt% solution of THF/water at several cosolvent ratios: a) 99/1, b) 95/5, c) 90/10.

cosolvent ratios. The fraction of isolated ions decreases as the percentage of water in the solution increases (Table 5-1). The sample cast from 99/1 THF/water has approximately the same fraction of isolated ions as the original uncast sample. Comparison of the fractions of isolated ions in a sample cast from a 95/5 cosolvent and in one cast from a 90/10 cosolvent shows them to be nearly identical. This is consistent with results from reduced viscosity studies.[4,6] A solution of 97/3 THF/water showed no polyelectrolyte behavior, but solutions of 95/5 and 90/10 THF/water showed the distinct increases in reduced viscosity at low concentrations. THF/methanol samples (95/5 and 90/10), which do not show polyelectrolyte behavior,[6] produced cast samples with NMR spectra that showed nearly identical amounts of isolated ions (30% and 27%, respectively). These quantities were nearly equivalent to the value for the original, uncast sample (30%).

Figure 5-3 shows NaSPS-1.7 cast from several different solvents: toluene/methanol, THF, THF/methanol, DMF, and THF/water. Table 5-2 contains the fractions of isolated and aggregated ions in these samples, as well as the "average" dielectric constant of the solvents used. The average value of the dielectric constant for the mixtures is only a guide; it is likely that specific interactions between the polar cosolvent and the ionic groups overwhelm the effect of overall solvent polarity.[6] The samples cast from THF and THF/methanol show few changes compared to the 30% isolated ions seen for the uncast sample, while NaSPS cast from toluene/methanol actually shows a slight increase in the fraction of isolated ions. The samples cast from the more polar solvents show substantially fewer ions in isolated sites. As the polarity of the casting solvent increases, the fraction of isolated ions in the

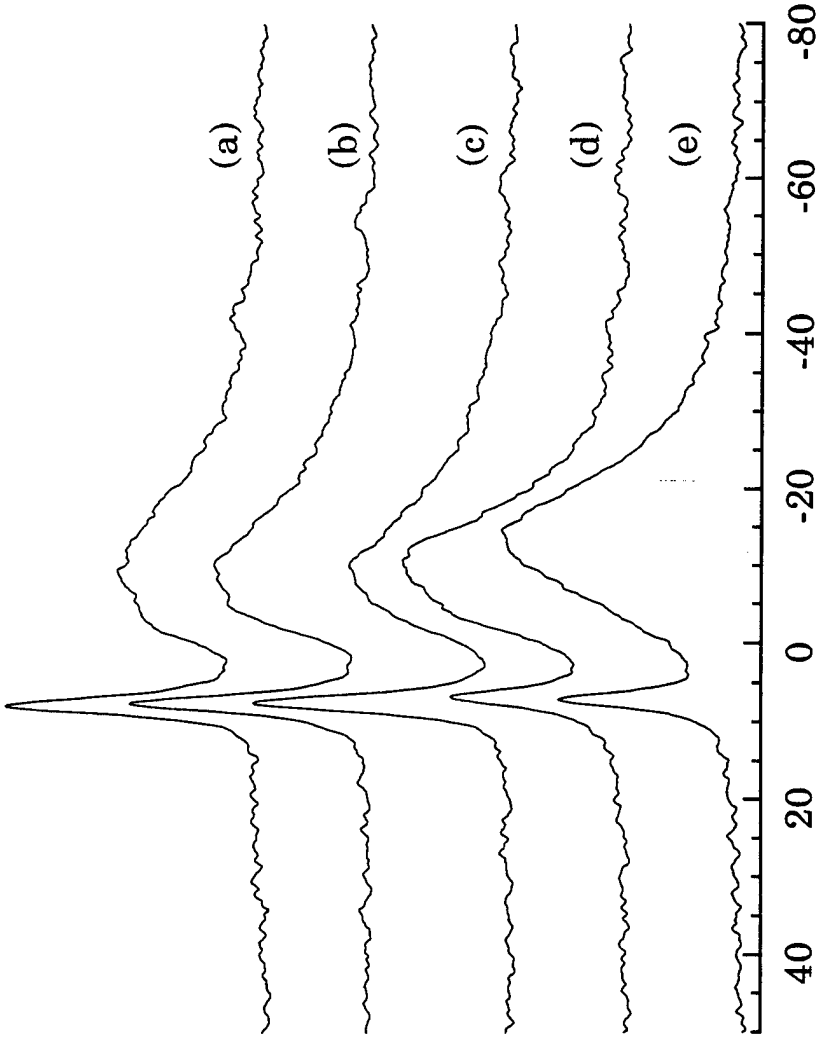

Figure 5-3: NMR spectra of NaSPS–1.7 cast from 0.5% solutions of a) 90/10 toluene/methanol, b) THF, c) 90/10 THF/methanol, d) DMF, and e) 90/10 THF/water.

Table 5-2: Fractions of Na^+ ions for NaSPS-1.7%, cast from different solvents

Solvent†	Effective dielectric constant*	Isolated ions (7 ppm)	Aggregated ions (-12 ppm)
no treatment	–	0.30	0.70
90% toluene/ 10% methanol	5.4	0.36	0.64
THF	7.6	0.27	0.73
90% THF/ 10% methanol	10.1	0.27	0.73
90% THF/ 10% water, 1 wt%	14.7	0.19	0.81
90% THF/ 10% water	14.7	0.11	0.89
DMF	36.7	0.11	0.89

† 0.5 wt% except as indicated

* For mixed solvents, this is estimated as the average of the dielectric constants of the pure solvents weighted by the volume fractions.

cast material decreases by 2/3. The more polar solvents dissociate the aggregates and solvate the isolated ions. During the evaporation of the solvent or cosolvent, the chains are able to rearrange and form new aggregates. This results in a decrease in the fraction of isolated sodium ions. Additionally, in the sample cast from THF/water solution, the aggregate peak has shifted to higher frequency. This shift has been found to be smaller for samples cast from solutions of higher concentration (1 wt% or higher).

SAXS patterns for NaSPS-1.7 compression molded and cast from THF and THF/water are shown in Figure 5-4. At this sulfonation level it is difficult to obtain the electron density contrast necessary to see a scattering peak,[16] and no peak is seen for the compression-molded sample or the sample cast from THF, which, from the previous arguments, should have a morphology nearly identical to that of the bulk ionomer. There is scattered intensity over the q-range of interest, but the pattern decays smoothly with no evidence of an interference peak. The sample cast from THF/water, however, does show changes in the SAXS pattern, with some evidence of a scattering peak being formed in the range q = 1 to 2 nm^{-1}. It is possible that the change in the SAXS pattern is due to a change in electron density difference between the aggregates and the matrix, which in turn is due to the increased aggregation of the sodium ions upon casting from THF/water.

At higher sulfonation levels more complete aggregation is obtained, and solvent casting appears to have less of an effect on the local morphology. Figure 5-5 shows the NMR spectra of bulk NaSPS-4.2, cast from DMF, cast from a toluene/methanol solution, and cast from a 90/10 THF/water mixture. The resulting spectra show the same features for all samples. No isolated ions are created by casting, and there is no substantial shift in the aggregate

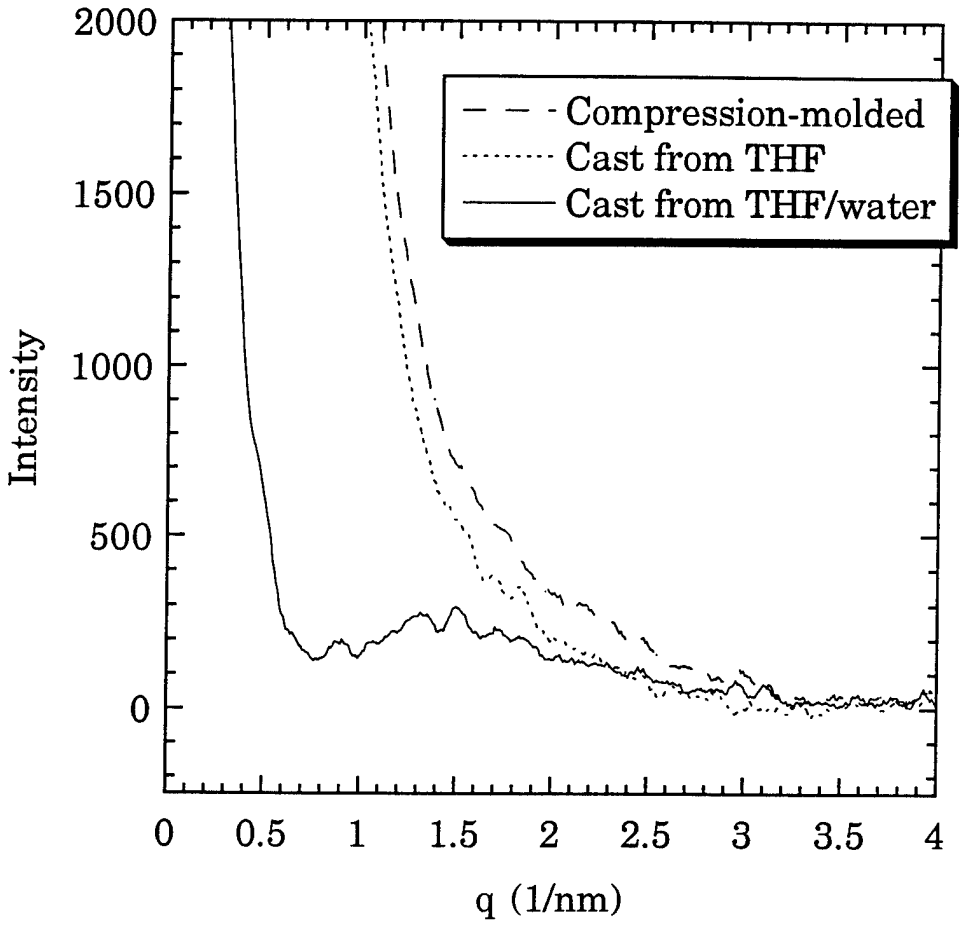

Figure 5-4: SAXS patterns for NaSPS–1.7 compression molded, cast from a 2.5 wt% solution of THF, and cast from a 2.5 wt% solution of 95/5 THF/water.

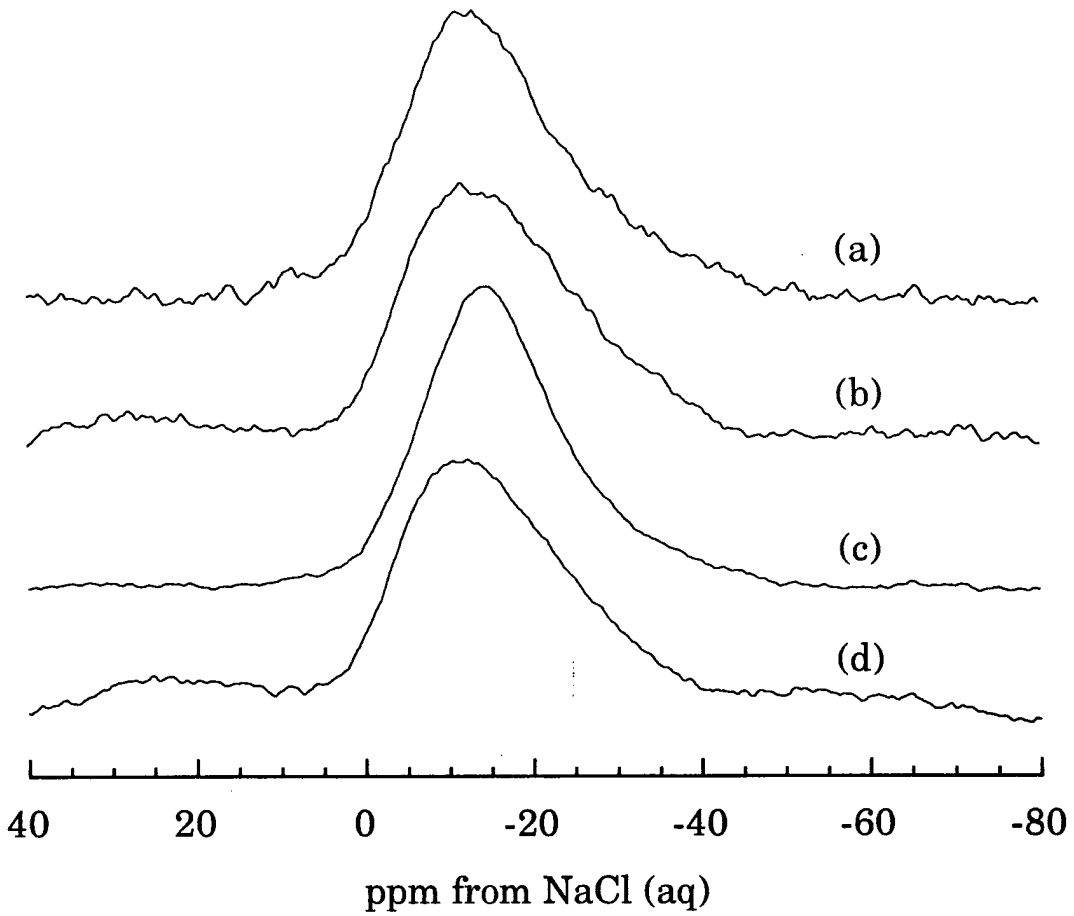

Figure 5-5: NMR spectra of NaSPS–4.2: a) dried under vacuum, b) cast from 90/10 toluene/methanol, c) cast from DMF, and d) cast from 90/10 THF/water.

peak. At this ion content, ion-pair interactions are strong enough to ensure that all ions reside in aggregates regardless of solvent history. Therefore, in terms of the local morphology probed by NMR, there is no difference between casting NaSPS-4.2 from a nonpolar solvent and a polar solvent. Fitzgerald and Weiss[2] reported that NaSPS cast from several solvents retained the characteristic SAXS scattering peak, in contrast to their work on MnSPS. The SAXS patterns of NaSPS-4.2 compression molded and cast from THF and 95/5 THF/water solutions are shown in Figure 5-6. All samples show the characteristic interference peak.

The structure of the ionomer in solution is quite different in the solvents THF (relatively nonpolar) and DMF (polar). In THF, the ionomer mimics its bulk conformation, and most of the ions are associated.[7-9] When the THF is evaporated, the distribution of ions will remain mostly unchanged from the bulk. In DMF, the ions are fully solvated, the aggregates are dissociated and the ionomer acts like a polyelectrolyte.[4,7-9] As the polar solvent is evaporated, the ions are driven into the polar environment of the aggregates.

In the THF/water cosolvent, the water solvates the cations and evaporates more slowly than THF, permitting the ions to reaggregate. Water also solvates Na^+ ions much more easily than methanol, which would lead to more mobility in the cations in THF/water solutions compared to THF/methanol solutions; Lundberg found that more than 10 wt% methanol was needed for 50% solvation of NaSPS-4.2 while only 0.6 wt% water in THF was required.[17] In the equilibrium of aggregated and dissociated species proposed by Lundberg,[10,11] he states that only when the alcohol-ionic group association is stronger than the ionic group self-association will the addition of alcohol dissociate the aggregates. In this case, methanol in moderate

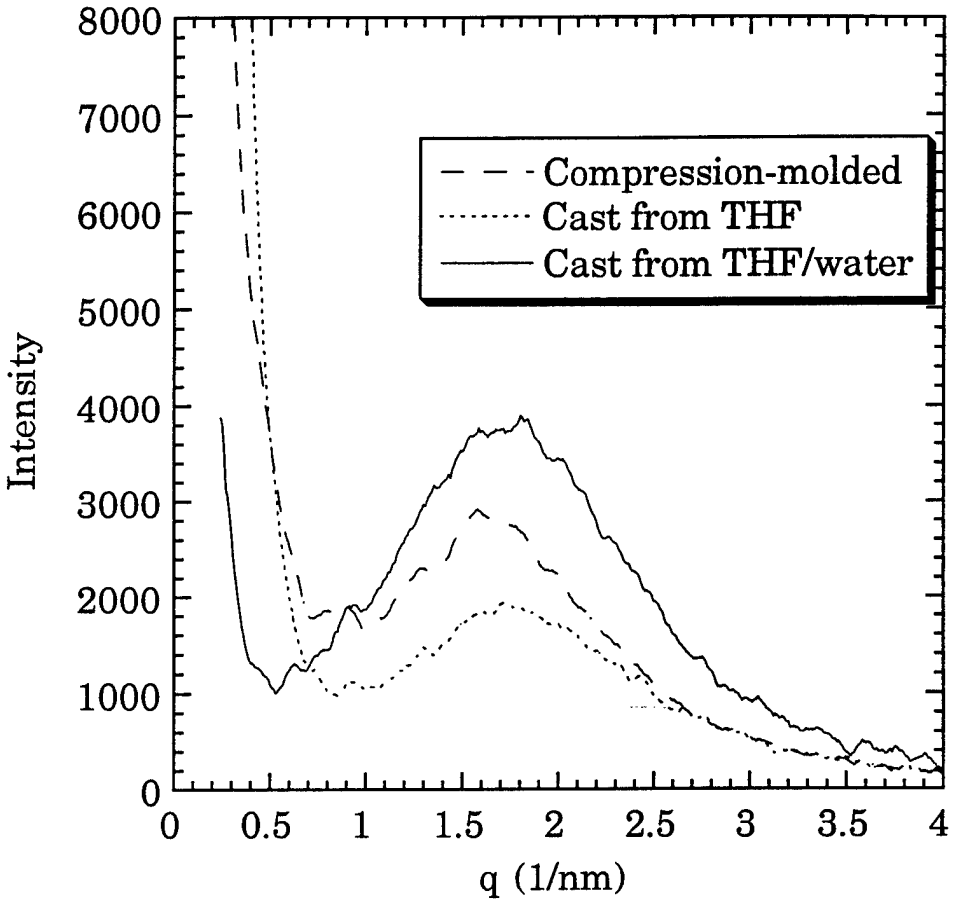

Figure 5-6: SAXS patterns for NaSPS–4.2 (a) compression molded, (b) cast from a 2.5% solution of THF, and (c) cast from a 2.5% solution of 95/5 THF/water.

amounts is not enough to dissociate the aggregates; however, the more strongly solvating cosolvent water is. Lundberg also reported more isolated sodium ions in THF/water solutions than in toluene/methanol solutions,[6] indicating that more ion pairs are fully dissociated when water is the cosolvent.

The rate of evaporation of the two solvents may also affect the final aggregation of the sodium ions. Table 5-3 shows the boiling points for the two polar and two nonpolar solvents. In mixtures of methanol and toluene the polar solvent evaporates much faster than the non-polar solvent, and the solvated chains transport some ions into the organic phase. In mixtures of THF and water, the polar solvent evaporates much slower than the non-polar solvent and solvated ionic groups will be driven to aggregate. In the case where the boiling points of the cosolvents are nearly identical, such as in THF/methanol mixtures, in which the methanol weakly solvates the ionic groups, the final cast sample will show little change from the original ionomer.

The NaSPS samples that show the largest extent of redistribution are those cast from the more polar solvents. Ionomers in these solutions show both isolated ions in ESR studies and polyelectrolyte behavior in viscometric and light scattering studies. Therefore, the ion pairs must be completely dissociated from any other ion pairs in order to permit local rearrangement of the pairs during solvent evaporation. When the polar solvent is the highest-boiling component, NMR spectra of the cast samples show the lowest quantities of isolated ion pairs remaining in the solid state, so the polar cosolvent can cause tremendous changes in aggregation or distribution.

Table 5-3: Boiling points for solvents used in mixed-solvent systems

Solvent	Boiling Point (°C)
methanol	65
THF	66
water	100
toluene	110

5.2.2 Reversibility of the Effects of Solution Casting

Sample processing can lead to changes in the distribution of sodium ions among different morphological sites in the ionomer and to changes in the aggregate peak position of the processed ionomer compared to the original sample. NMR studies indicate that all changes are reversible to some degree.

The sample cast from 1 wt% 90/10 THF/water (Figure 5-2c) was recast from several solvents to determine if the changes in morphology were reversible. Casting from THF and THF/methanol did not substantially affect the local morphology of the ionomer; as was seen in the study on the original, uncast NaSPS, these solvents produce cast samples that mimic the bulk morphology of the ionomer before it is put into solution. However, the samples recast from toluene/methanol and DMF showed distinct changes (Figure 5-7). Casting from DMF decreased the fraction of isolated ions, similar to what was seen in Figure 5-3, but the fraction of isolated ions decreased to 3%. Casting from toluene/methanol increased the fraction of isolated ions to 29% and also shifted the position of the aggregate peak. The peak is much more narrow than in the uncast sample, and its center of gravity is at a higher ppm value. It appears that the upfield shift in the aggregate peak caused by casting from THF/water can be reversed by this choice of solvent.

5.3 Conclusions

Solution casting has a significant effect on the morphology of NaSPS at low sulfonation levels. The distribution of ions shifts for samples cast from relatively polar solvents (DMF, THF/water), in which the aggregates are dissociated and the isolated ions are solvated while in solution. Upon slow evaporation of the solvent the ions form new aggregates and substantially

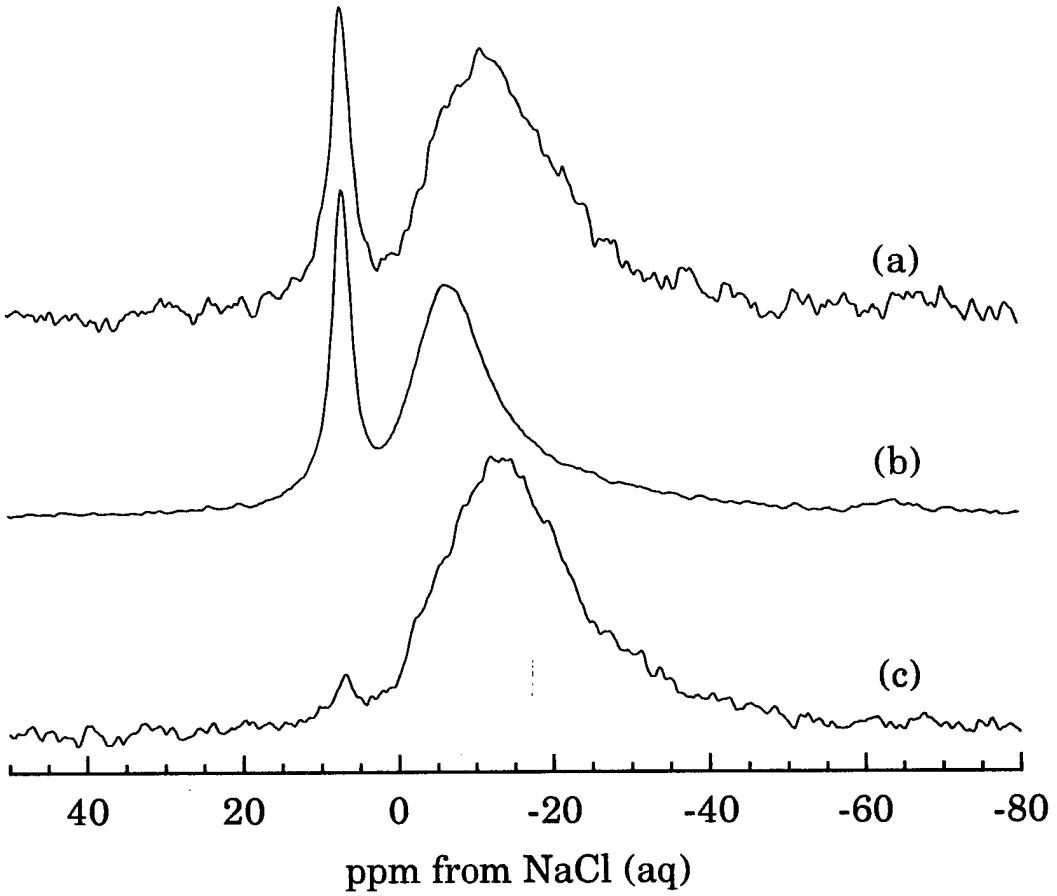

Figure 5-7: NMR spectra of NaSPS–1.7: a) cast from a 1 wt% solution of 90/10 THF/water, b) sample (a) recast from a 1 wt% solution of 90/10 toluene/methanol, and c) sample (a) recast from a 1 wt% solution of DMF.

fewer isolated ions are present. Casting from relatively nonpolar solvents (THF, THF/methanol) did not drastically change the morphology of the original, uncast ionomer, although casting from toluene/methanol mixtures slightly increased the fraction of isolated ions.

The effects of solution casting on the local morphology of NaSPS appear to be reversible; the choice of casting solvent can allow for variation in the extent of ion aggregation in a given ionomer sample. These findings suggest that the local morphology of the ionomer at low sulfonation levels can be tailored to the desired specifications solely through sample processing. At higher sulfonation levels (4.2%), ion proximity is high enough that aggregation is seen for all processing conditions tested, and solvent character has no detectable effect on local morphology.

References for Chapter Five

1 Fitzgerald, J.J.; Weiss, R.A. *Rev. Macromol. Chem. Phys.* 1988, **C28**, 99.

2 Fitzgerald, J.J.; Weiss, R.A. *J. Polymer Sci., Phys. Ed.* 1990, **28**, 1719.

3 Weiss, R.A.; Fitzgerald, J.J.; Frank, H.A.; Chadwick, B.W. *Macromol.* 1986, **19**, 2085.

4 Lundberg, R.D; Phillips, R.R. *J. Polym. Sci., Phys. Ed.* 1982, **20**, 1143.

5 Weiss, R.A.; Lundberg, R.D.; Turner, S.R. *J. Polym. Sci., Polym. Chem. Ed.* 1985, **23**, 549.

6 Lundberg, R.D.; Phillips, R.R., in *Coulombic Interactions in Macromolecular Systems*, Eisenberg, A.; Bailey, F., eds. American Chemical Society: Washington, D.C., 1986.

7 Lantman, C.W.; MacKnight, W.J.; Peiffer, D.G.; Sinka, S.K.; Lundberg, R.D. *Macromol.* 1987, **20**, 1096.

8 Lantman, C.W.; MacKnight, W.J.; Higgins, J.S.; Peiffer, D.G.; Sinka, S.K.; Lundberg, R.D. *Macromol.*, 1988, **21**, 1339.

9 Lantman, C.W.; MacKnight, W.J.; Sinka, S.K.; Peiffer, D.G.; Lundberg, R.D.; Wignall, G.D. *Macromol.*, 1988, **21**,1344.

10 Lundberg, R.D. *Polymer Prepr.* 1978, **19**, 455.

11 Lundberg, R.D.; Makowski, H.S. *J. Polym. Sci., Polym. Phys. Ed.* 1980, **18**, 1821.

12 Tant, M.R.; Wilkes, G.L. *JMS-Rev. Macromol. Chem. Phys.* 1988, **C28**, 1.

13 Galambos, A.F.; Stockton, W.B.; Koberstein, J.T.; Sen, A.; Weiss, R.A. *Macromol.* 1987, **20**, 3091.

14 Fitzgerald, J.J.; Kim, D.; Weiss, R.A. *J. Polym. Sci., Polym. Lett. Ed.* 1986, **24**, 263.

15 Lundberg, R.D., Phillips, R.R. *J. Polym. Sci., Polym. Lett. Ed.* 1984, 22, 377.

16 Peiffer, D.G.; Weiss, R.A.; Lundberg, R.D. *J. Polym. Sci., Polym. Phys. Ed.* 1982, **20**, 1503.

17 Lundberg, R.D., in *Structure and Properties of Ionomers*, Pineri, M.; Eisenberg, A., eds. D. Reidel Publishing Co.: Dordrecht, Holland, 1987.

Chapter Six: Ionomers: Effects of Humidification and Annealing

6.1 Introduction

The ^{23}Na NMR results in Chapter 4 showed that sodium ions in SPS are found in up to three environments: isolated ions (7 ppm), fully hydrated ions (0 ppm), and aggregated ions (–12 to –23 ppm). The peaks were identified through the use of reference compounds and quadrupolar coupling constant calculations. In Chapter 5, the effects of solvent casting on the site distributions and local morphology were discussed. The largest extent of redistribution occurred for samples cast from more polar solvents, such as dimethylformamide and tetrahydrofuran/water mixtures. Casting from these solvents resulted in a larger fraction of the sodium ions residing in aggregates. Additionally, in Chapter 4 it was shown that both the isolated and aggregated ions attracted water molecules, and all ions could be held in the fully hydrated state, $Na(H_2O)_4^+$. In this chapter it is shown that the effects of other processing variables on the local environment of the sodium ions can be as significant as the effects of composition. Specifically, the effects of humidification and thermal treatment are presented here.

6.2 Results and Discussion

6.2.1 Effect of Humidification and Drying

One goal of this study is to establish the role of water in ionomer processing and how it relates to the final distribution of ions in a sample. Previous studies have indicated that water remains trapped in the aggregates even after thorough drying.[1] Addition of water also affects the morphology of

ionomers, as indicated by a shift of the SAXS scattering peak to smaller angles,[2-5] or by the disappearance of the scattering peak.[4,5] The presence of water may also partially dissociate the ions,[6] weakening the ionic crosslinks, resulting in decreased mechanical properties.[7] Hydration can also affect the local structure of the aggregates, as has been shown using extended x-ray absorption fine structure (EXAFS),[8] NMR,[9,10] and Fourier transform infrared spectroscopy (FTIR).[11-14]

To better understand the role of water in material processing, humidification experiments have been conducted. The ^{23}Na NMR spectrum of dry NaSPS at 1.7% sulfonation consists of two peaks, at 7 and –12 ppm (Figure 6-1a). The relaxation times of these two peaks are roughly 6 and < 0.5 sec, respectively. Thus, any exchange between these two sites must occur no faster than 1 every 6 seconds. The same sample subsequently humidified at 80°C produced a single hydrated NMR peak at 0 ppm, as seen in Figure 6-1b. Following this, the humidified sample was redried at room temperature in air, producing again isolated and aggregated Na^+ environments (Figure 6-1c), but with a different distribution among the sites. This redistribution is due to exchange between the isolated and aggregated sodium ions during humidification. With the humidification, all sodium ions are converted to the fully hydrated form, $Na(H_2O)_4^+$. This indicates that all sodium ions, even those bound in aggregates, are available for hydration. A comparison of dry NaSPS–1.7 with a sample equilibrated with humid room-temperature air (Figure 6-2) shows that the aggregate peak shifts downfield when the ionomer is partially hydrated. This is likely due to swelling of the aggregates by water. Such swelling would decrease the strength of the

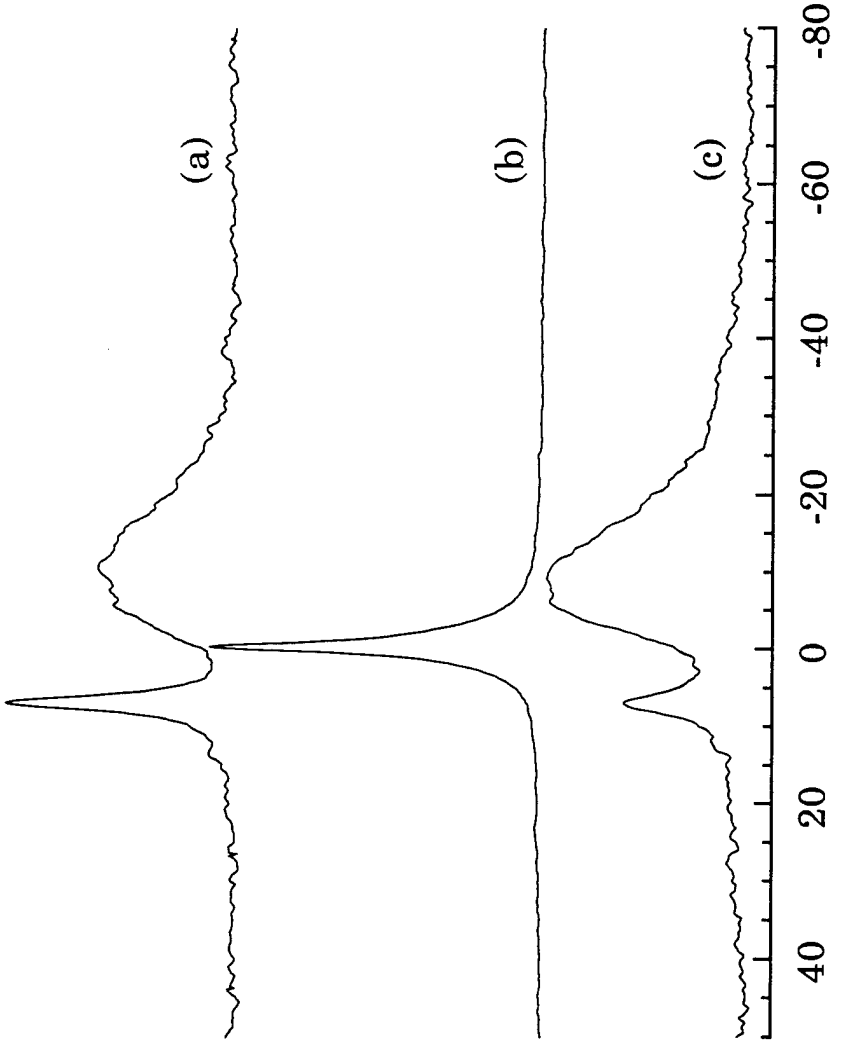

Figure 6-1: NMR spectra of NaSPS at 1.7% sulfonation: a) dried under vacuum at room temperature, b) hydrated at 80°C, and c) redried in air at room temperature.

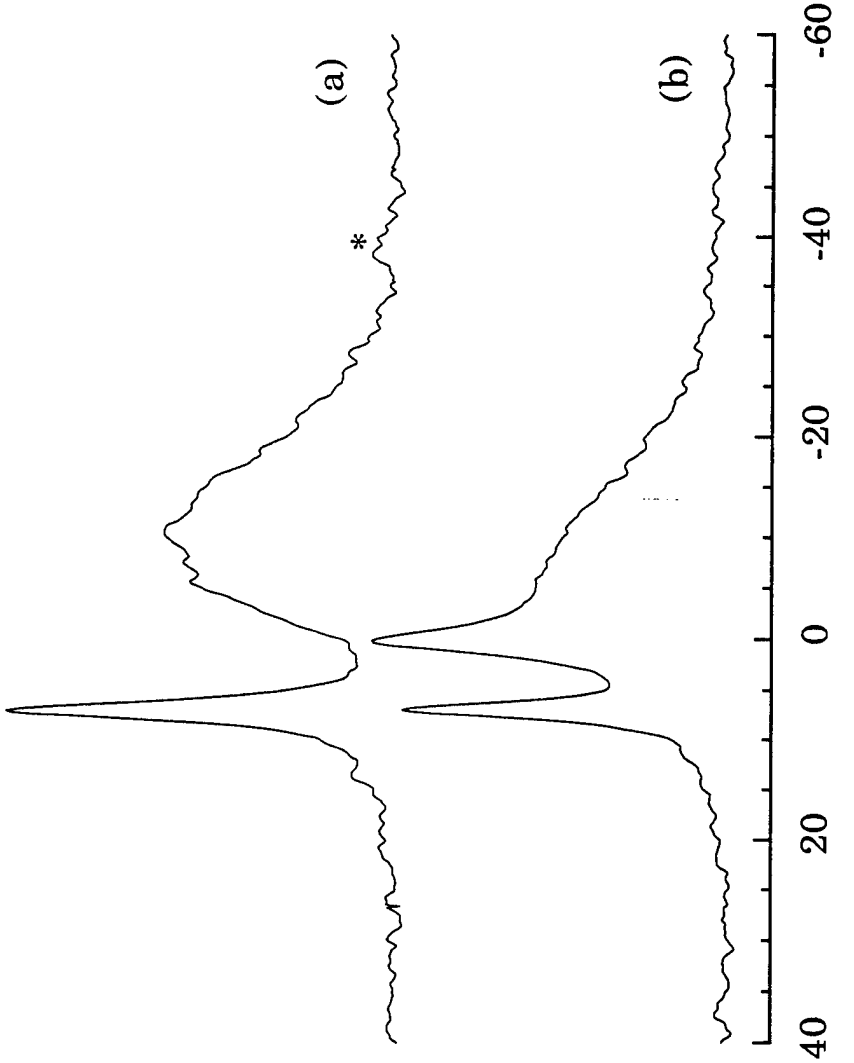

Figure 6-2: NMR spectra of NaSPS–1.7 a) dried under vacuum and b) equilibrated with room temperature air. Spinning sidebands are denoted by asterisks (*).

quadrupolar interaction, both from the increased site symmetry for $Na(H_2O)_4^+$ and because of the increased distance between Na^+ nuclei.

Figure 6-3 shows NaSPS–1.7 after humidification at three different temperatures: 40°C, 60°C, and 80°C. As the temperature of humidification increases the fraction of isolated ions decreases until it becomes negligible. At lower temperatures (40°C), hydration is not complete and the peak due to isolated ions, while decreased in magnitude, is still present. Additionally, the peak corresponding to aggregated ions (initially at –12 ppm) has broadened to include the hydrated ions (the intensity at 0 ppm). Comparison of this spectrum, which is of a sample humidified at 40°C for 72 hrs, with that in Figure 6-2, which is of a sample equilibrated in humid air at room temperature for an extended period of time, indicates that hydration is a slow process and, in the case of the 40°C sample, is only partially complete after 72 hrs. The peak indicating isolated ions decreases more quickly than the aggregate peak; unhydrated aggregated sodium ions are still apparent in the 60°C spectrum (as seen in the inset) but the peak indicating isolated ions has vanished. At this temperature all isolated ions are hydrated, but some small number of the aggregated ions is still unaffected by the humidity. This is particularly interesting since at 60°C the amount of water present in the sample (calculated from weight loss after drying) corresponds to ~14% of the original sample mass. This mass is more than 10 times the amount of water needed for the stoichiometric level of Na^+:H_20=1:4. Even with an excess of water, complete hydration of all aggregated ions only occurs above 60°C. Comparing the peak widths of the samples humidified at 60°C and at 80°C, it is apparent

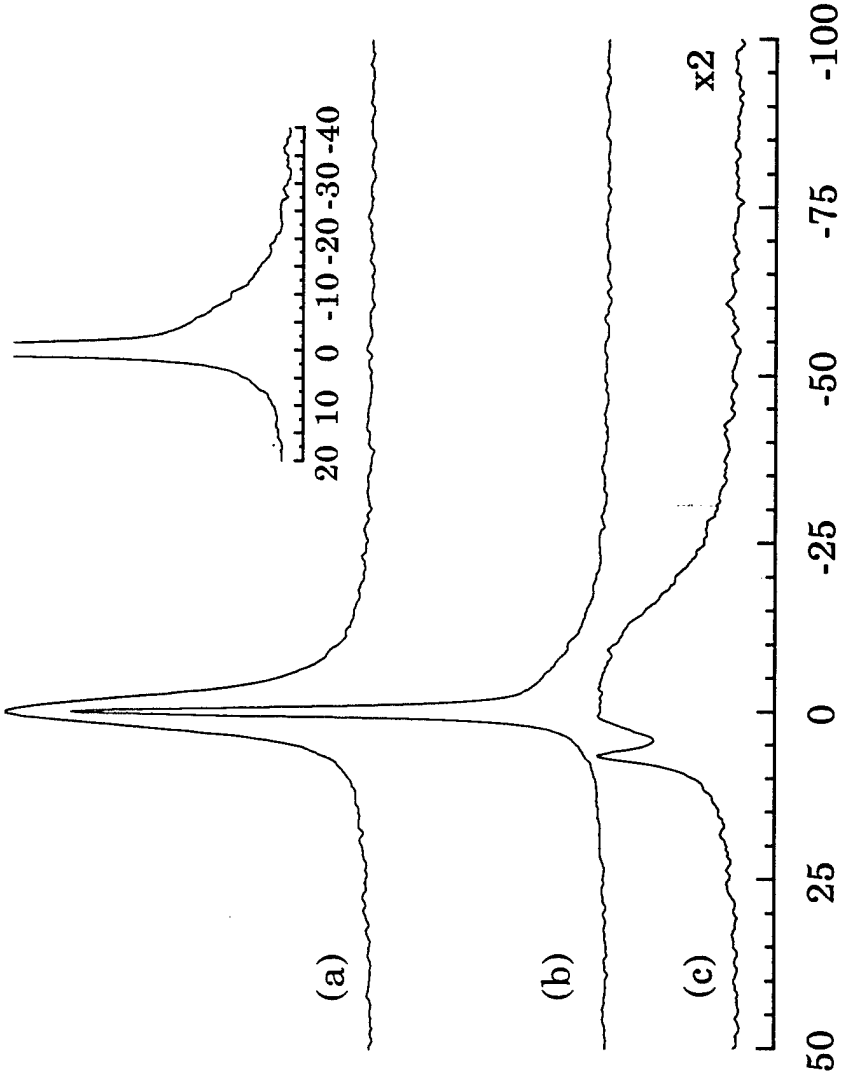

Figure 6-3: NMR spectra of NaSPS–1.7 after humidification at three temperatures: a) 80°C, b) 60°C, and c) 40°C. The inset shows 3(b) on an expanded scale.

from the broader peak at 80°C that more exchange between isolated and aggregated sodium ions is occurring in the sample humidified at the higher temperature.

Detailed examination of the hydration/dehydration transient provides further insight into changes in NaSPS with humidification. Figure 6-4 shows the NaSPS sample humidified at 40°C for the first few hours of the NMR experiment, which is conducted by spinning the sample in dry air. The fraction of isolated sodium ions increases during the first three hours of the experiment, after which the value is stable. The increase in the number of isolated ions is probably due to drying of the sample by exposure to the air used during sample spinning (MAS). This transient provides insight into the transport of water out of the ionomer. The growth of the isolated ion peak is due to a decrease in the humidified ions, which are held in the broadened, higher-field peak. This fraction of hydrated isolated ions loses waters of hydration readily, and over a fairly short period of time. Thus the isolated ions are both hydrated and dehydrated more readily than ions in aggregates. The isolated ions appear to be very changeable and readily accessible.

Figure 6-5 shows the three NaSPS samples when dried at room temperature after humidification at the different temperatures used above. More sodium ions are aggregated in the final dried ionomer for samples humidified at the higher temperatures. At the lower humidification temperature (40°C), at which hydration of the isolated ions was not complete, there is no noticeable change in the fraction of isolated ions in the final dried sample as compared to the untreated material. Humidification at this temperature apparently hydrates the ions in their environment, but no net transport of ions occurs. Therefore, this distribution of Na^+ locations is a

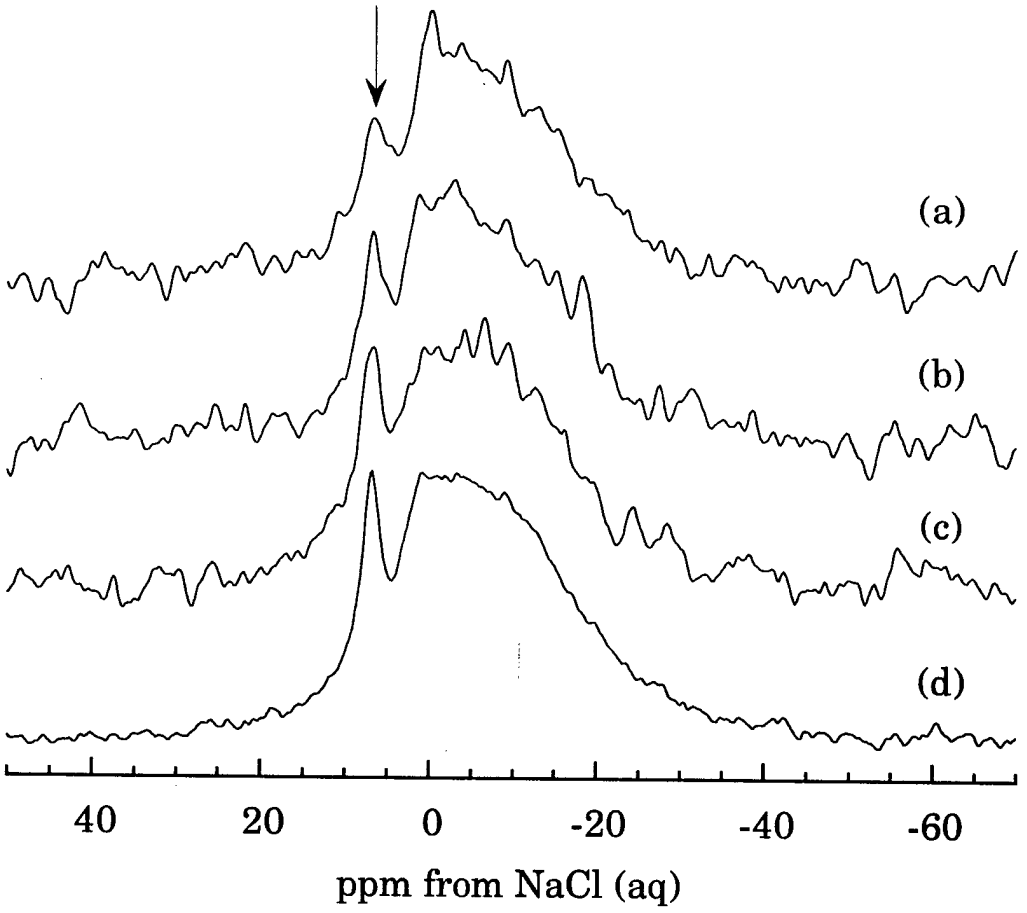

Figure 6-4: NMR spectra of the first few hours of the NMR experiment on NaSPS–1.7 humidified at 40°C: a) first hour (400 scans); b) second hour (400 scans); c) third hour (400 scans); d) final spectrum (8992 scans).

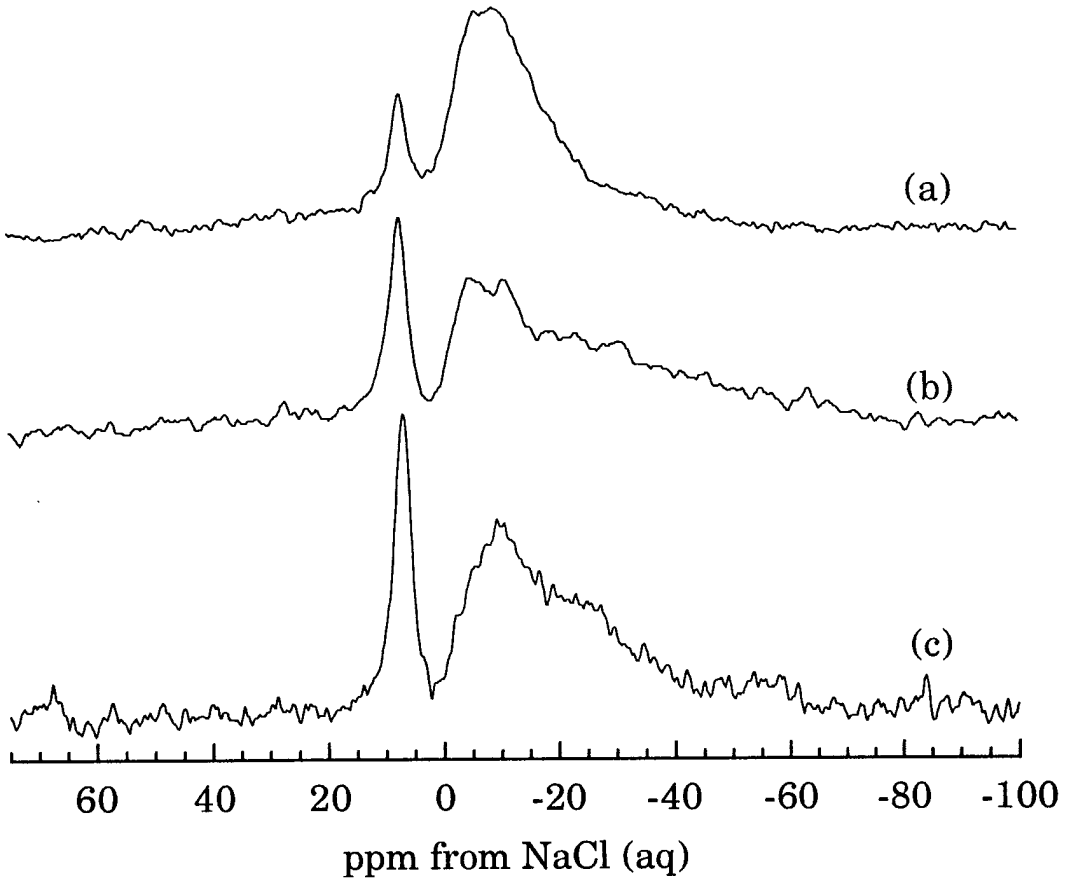

Figure 6-5: NMR spectra of NaSPS–1.7 a) dried at room temperature immediately after humidification at a) 80°C (dried in air) b) 60°C (dried under vacuum), and c) 40°C (dried under vacuum).

reproducible but non-equilibrium state. Above this temperature, the local morphology is altered by humidification and subsequent drying. These results indicate that hydration and disruption of the aggregates is needed to permit global reorganization and to produce the observed aggregation of previously isolated sites. Ishioka[12] also noted reversibility with respect to water content in the FTIR spectra of the carboxylated ionomer ethylene methacrylate partially neutralized with zinc, but at 60°C. The difference in the temperatures at which the changes are still reversible is probably due to a combination of changes in anion groups, counterions, and backbone polymers. In NaSPS, complete humidification (80°C) allows for rearrangement of the ions in the polymer matrix. In turn, this rearrangement leads to an increase in the number of aggregated ions on drying. Since the local morphology of the final dried sample depends on the extent of hydration, then the amount of physical cross-linking (or aggregation) can be controlled by the choice of humidification temperature.

Cooper *et al.* have presented SAXS results for humidified zinc-neutralized SPS[2] and ethylene-methacrylate copolymers.[4] To account for changes such as a peak shift to lower q values on addition of water (where Bragg spacing $d=2\pi/q$), they postulated that the fraction of aggregated ions might change when the sample is swelled; hydrated ionic species in the matrix would have increased mobility and tend to aggregate. In this study, we have shown that redistribution of the sodium ions is exactly what is occurring during hydration. Complete hydration of isolated ions and some hydration of pre-existing aggregates is required to provide this increased mobility.

6.2.2 Effect of Annealing

Previous studies on thermal treatment of ionomers have shown morphological changes with annealing.[1,15,16] These studies have indicated that the behavior of ionomers is a function of the neutralizing cation. For example, after treatment at temperatures above the matrix glass transition, SAXS patterns of NaSPS showed increased phase separation while SAXS curves of ZnSPS showed increases in phase mixing.[16]

In this study, the NaSPS samples have been subjected to thermal treatment to study more thoroughly the kinetics of formation and dissociation of the aggregates. Samples of NaSPS–4.2 were heated to 140°C, 160°C and 180°C and quenched to room temperature. NMR spectra of one sample before and after annealing at 160°C for 24 hrs are shown in Figure 6-6. The heat treatment affects the aggregates, as is demonstrated through an upfield shift of the peak's center of gravity from ~ –17 ppm to ~ –23 ppm. This shift indicates a change in the structure of the aggregate. Since the shift is to lower frequency, it is likely that some of the aggregates are becoming more well-ordered. One reason for the improvement in order could be the loss of loosely-held interfacial ions from the aggregate.

Accompanying the aggregate peak shift is an increase in the intensity of the 7 ppm peak, indicating some dissociation of aggregates and the formation of isolated R-$(SO)_3^-$ /Na^+ ion pairs. This is a different result than was seen in electron spin resonance studies of MnSPS,[1] in which annealing caused increased aggregation, not dissociation. However, SPS ionomers neutralized with Mn^{2+} and Na^+ may have qualitatively different behavior as a consequence of the metal valence and the number of polymer-bound anions with which it interacts. Such qualitative differences have also been seen in

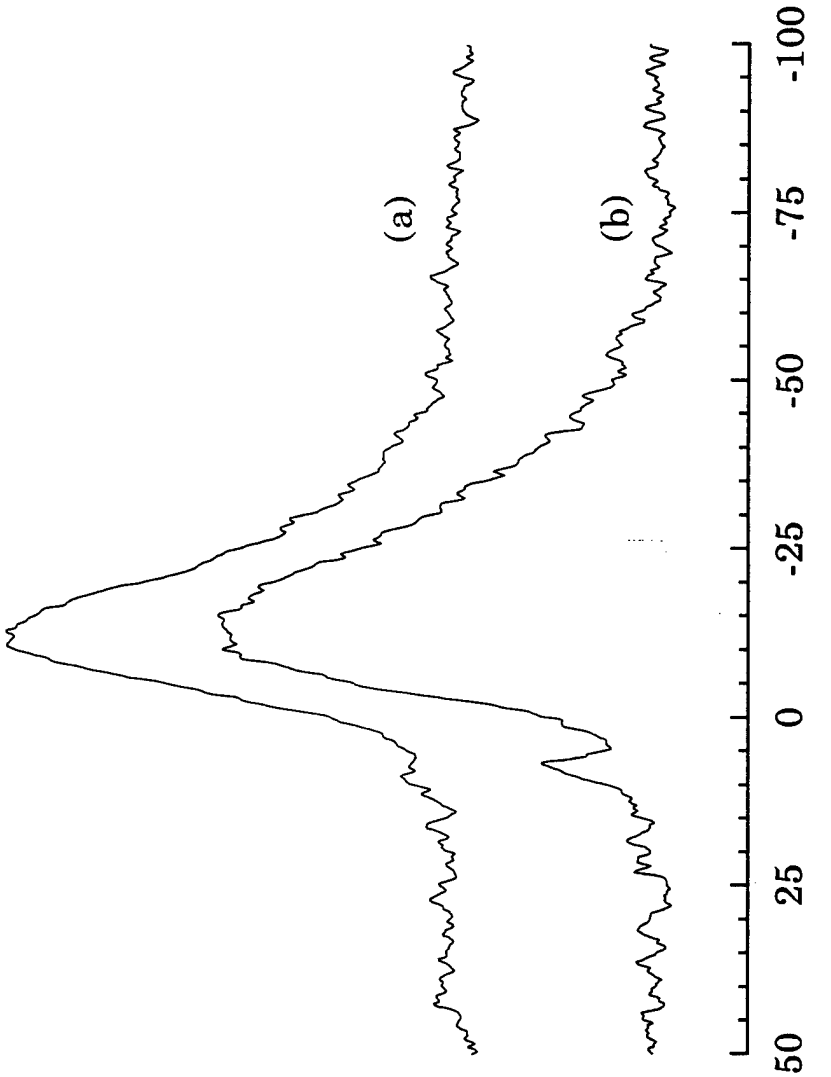

Figure 6-6: NMR spectra of NaSPS–4.2 a) before and b) after annealing at 160°C for 24 hours.

the effects of solvent casting on these two materials.[17,18] Previous studies have shown differences in behavior between ionomers neutralized with mono- and divalent cations,[13,19-21] and one group of researchers suggested that the behavior could be due to differences in counterion packing within the aggregates.[22]

The fraction of isolated ions, which is a measure of the level of dissociation, can be tracked as a function of annealing time at the three temperatures. This variation in the fraction of isolated ions with annealing time is shown in Figure 6-7. The rate equation for dissociation of aggregated sodium ions (A) to isolated sodium ions (I), assuming a reversible process and a first-order rate expression, is:

$$A \leftrightarrows I$$

$$\frac{dI}{dt} = -k_a I + k_d A \qquad (6\text{-}1)$$

but $I_0=0$ and $I+A = A_0$. The resulting solution is:

$$\frac{I(t)}{A_0} = \frac{k_d}{k_d+k_a}\left(1-e^{-(k_d+k_a)t}\right) = \frac{K_{eq}}{1+K_{eq}}\left(1-e^{-k_a(1+K_{eq})t}\right) \qquad (6\text{-}2)$$

since $K_{eq}=k_d/k_a$. Fitting the data from the annealing experiments ($\frac{I(t)}{A_0}$ vs. t) yields the values for K_{eq} and k_a for each of the three temperatures given in Table 6-1. The heat of reaction for dissociation can be determined from the temperature variation of the equilibrium constant using the Clausius-Clapeyron expression:

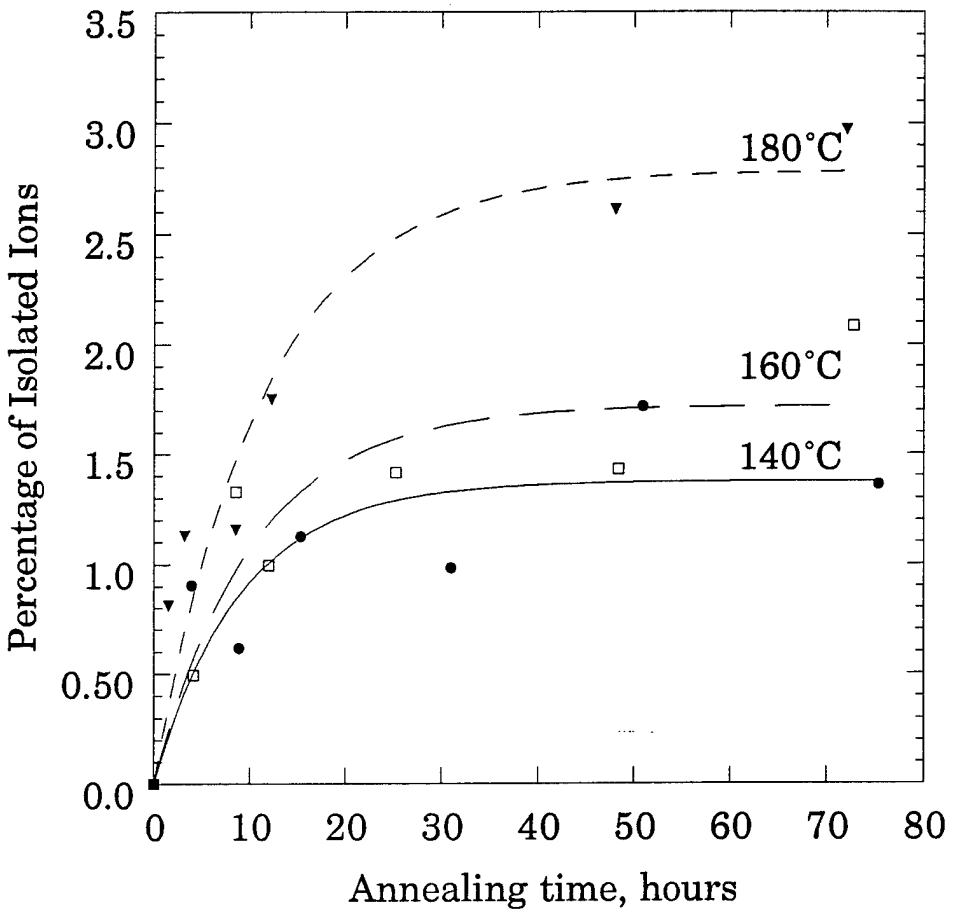

Figure 6-7: Fraction of total intensity of the NaSPS–4.2 peak from isolated ions as a function of annealing time, for three temperatures: 180°C (▲), 160°C (□), and 140°C (●). Lines correspond to fitting the data to a first-order expression, as described in the text.

Table 6-1: Kinetic parameters for the association/dissociation of Na^+ in SPS

Temperature (°C)	$k_d \times 10^3$ (1/hr)	k_a (1/hr)	$K_{eq} \times 10^2$
140	1.51±0.64	0.108±0.054	1.4±0.9
160	1.67±0.49	0.095±0.034	1.8±0.8
180	1.91±0.58	0.069±0.027	2.8±1.4

$$\ln(K_{eq}) = \frac{-\Delta H}{RT} + \frac{\Delta S}{R} \qquad (6\text{-}3)$$

Since the range of temperatures is limited, and there is substantial scatter in the data, the trends should be stressed more than the absolute numbers. The heat of reaction (ΔH) is determined to be +6.3 ± 1.4 kcal/mol, which is stronger than a hydrogen bond but weaker than a primary bond. The formation of isolated ions pairs is thus endothermic, as expected. The entropy change is determined to be +6.7 ± 3.2 cal/mol-K. The Arrhenius activation energies in the forward and reverse directions are $E_{a,d}$ = 2.2±0.2 and $E_{a,a}$ = –3.9±1.2 kcal/mol, respectively. These values are substantially lower than those reported by Hird and Eisenberg (40-54 kcal/mol), who determined activation energies for NaSPS from dynamic storage modulus data at varying frequencies.[23] However, this discrepancy is due to differences in the processes being monitored by each technique. In the mechanical tests, the activation energy for large-scale motion of the polymer chains near the aggregate would be directly measured, and this is certainly expected to be larger than that measured by ^{23}Na NMR, which looks directly at only individual sodium ions.

It is apparent from the data in Figure 6-7 and Table 6-1 that the equilibrium constant, K_{eq}, increases with temperature, which is consistent with the endothermic reaction in equation 6-1. Although there is substantial scatter in the data in Figure 6-7, it appears that k_a decreases with increasing temperature. This behavior would indicate a negative apparent $E_{a,a}$. Negative activation energies are rare, and this value probably signifies the presence of a multi-step process instead of simple association/dissociation,

including such factors as energy of the polymer chains, exclusion of water from the aggregate, or differences in the energy requirements for removing sodium ions from the edge of an aggregate and the energy requirements for removing ions from the center of an aggregate. Higher-order reactions do not describe the trends in the data as well as the first-order reaction, nor do they lead to a positive value of $E_{a,a}$.

One possibility for the complexity in the reassociation step involves temperature-dependent levels of water in the aggregates. As was discussed above, the presence of water can affect the local structure,[8,12-14,24] morphology[2,4,5,25] and physical properties[7] of a sample. Drying NaSPS–4.2 at 25°C does not lead to any isolated ions, based on NMR results, but probably does not lead to complete drying of the ionomer, either. Heating the sample to a higher temperature, above the glass transition temperature of the ionomer (~120°C), leads to the presence of a small fraction (~1-4%) of isolated ionic groups. The ionomer matrix has become more mobile at higher temperatures, and allows more ion transport than it did at temperatures below T_g. Therefore, since chain rearrangement occurs at the high temperatures required for complete drying, separating the effects of water removal and chain motion on the local morphology of the cations is not possible.

The fraction of isolated ions created by thermal treatment is small and is unlikely to affect the mechanical properties of these ionomers. However, small changes in the distribution of ions may complicate investigations of the local and larger-scale morphology of the ionomer even for the materials with higher sulfonation levels, where most ions are in aggregates. Cations such as sodium have intrinsically low scattering contrast in SAXS. Therefore, small

changes in the number of isolated ions could affect the electron density difference necessary for contrast in SAXS studies. Additionally, small changes could affect the average cation environment as seen in EXAFS studies of these materials, so consistency in sample preparation is of utmost importance when using sensitive characterization techniques.

6.2.3 Reversibility of the Effects of Sample Processing

Solvent casting, humidification, and thermal treatment have been shown to affect the local morphology of an ionomer through changes in the distribution of sodium ions in different morphological sites, and through changes in the aggregate peak shape and position. NMR studies have also shown that none of these changes are permanent; original ion distributions can be restored to some extent.

Two of the NaSPS-4.2 samples annealed to high temperature were cast from solution, one from toluene/methanol and one from THF/water, to determine if casting would return the samples to their original morphologies. The results are shown in Figures 6-8 and 6-9. In Figure 6-8, it is apparent that casting an annealed sample from a 90/10 mixture of THF/water at 0.5 wt% completely removes the isolated ions that were created from thermal treatment. Additionally, the aggregate peak is narrowed compared to the thermally treated sample; the center of gravity shifted downfield ~ 5 ppm following solvent casting. Comparison of the cast sample with the bulk NaSPS–4.2 (Figure 6-6a) shows that this treatment returns the aggregated peak to its original position. So, the effects of thermal treatment on the isolated ions can be removed with this solvent. Interestingly, a similar sample cast from a 1 wt% solution of 95/5 THF/water showed narrowing of the

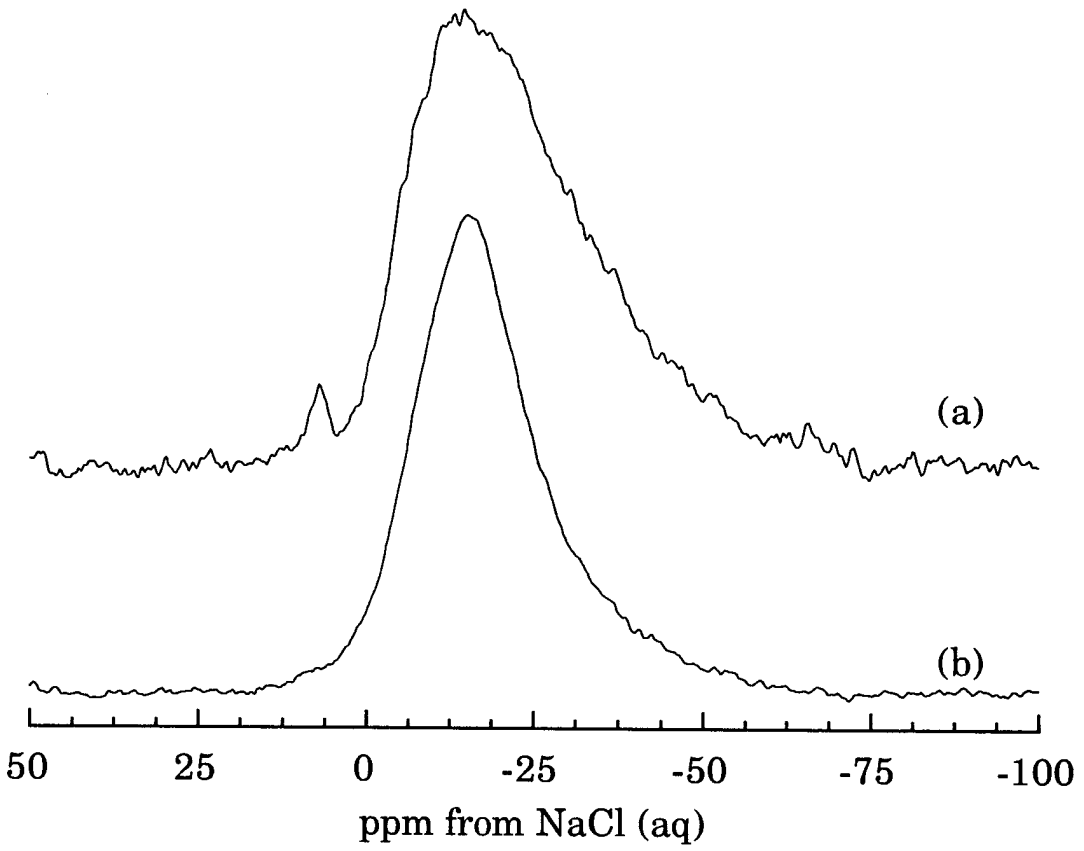

Figure 6-8: NMR spectra of NaSPS–4.2: a) annealed at 160°C for 24 hours and b) sample (a) cast from a 0.5 wt% solution of 90/10 THF/water.

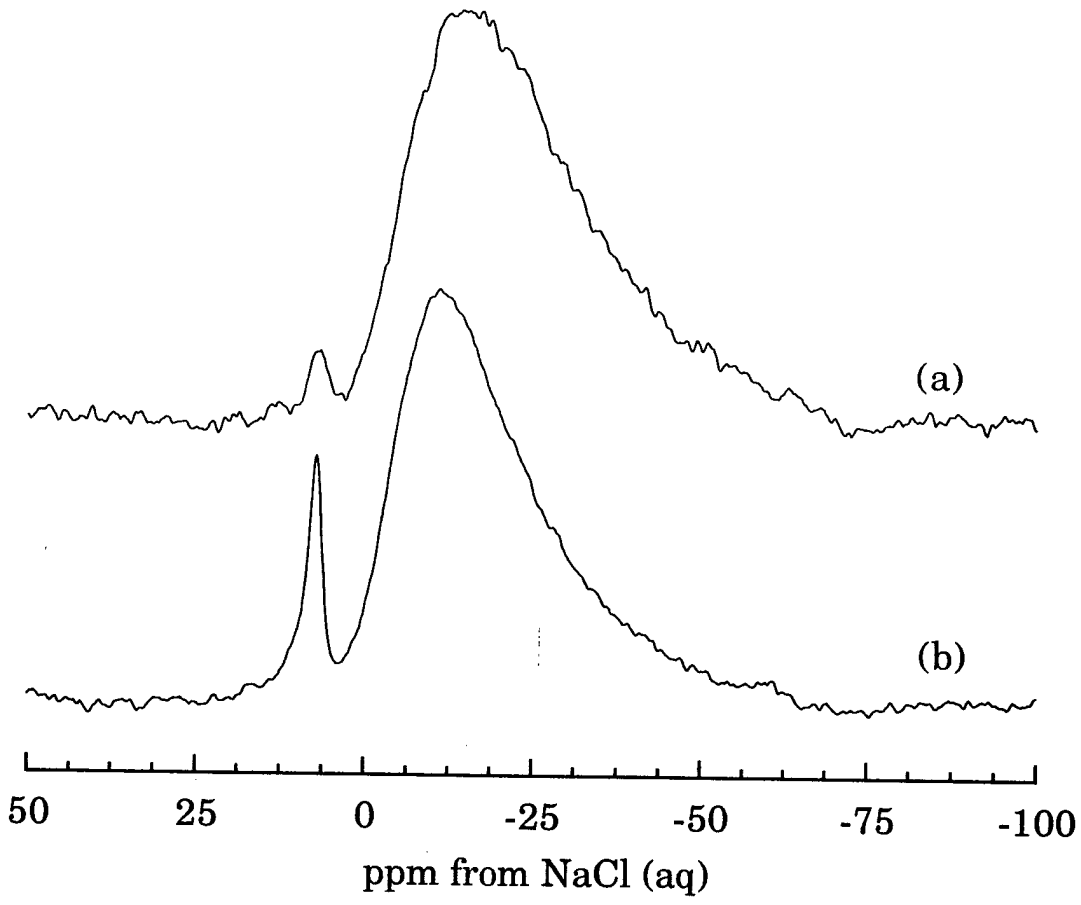

Figure 6-9: NMR spectra of NaSPS–4.2: a) annealed at 160°C for 48 hours, and b) sample (a) cast from a 0.5 wt% solution of 90/10 toluene/methanol.

aggregate peak but the peak due to isolated ions remained intact. In Figure 6-9, the annealed sample cast from 90/10 toluene/methanol at 0.5 wt% showed a dramatic increase in the fraction of isolated ions. The aggregate peak also shows less intensity in its low-ppm tail, similar to the result in Figure 6-8, and the center of gravity of the peak is shifted downfield about 5 ppm. NaSPS–1.7 samples cast from toluene/methanol have also shown an increase in the number of isolated ions; in the preceding chapter, the effects of solvent processing on NaSPS–1.7 were presented. For cosolvents in which the polar solvent is the higher-boiling component (such as THF/water mixtures), the resulting cast sample contains a larger fraction of aggregated ions. For cosolvents in which the non-polar component is the higher-boiling solvent (such as toluene/methanol mixtures), the polar component evaporates sooner, and the remaining non-polar solvent prohibits aggregation of "stranded" ions during drying and therefore produces more isolated ions. Figures 6-8 and 6-9 show this behavior for annealed NaSPS–4.2. The presence of isolated ions in the sample before casting is an important factor; the original, unannealed NaSPS–4.2 sample contains no isolated ions, and the corresponding sample cast from toluene/methanol also contains no isolated ions (Chapter 5).

The effects of sample preparation on the structure of ionomers in toluene solutions has been discussed by Vanhoorne *et al.*[26] The researchers obtained SAXS patterns of barium sulfonato polystyrene ionomers in toluene; the samples were either concentrated from the synthesis solution or isolated from the synthesis solution by distillation of the solvent, dried at 160°C under vacuum, and dissolved in toluene. The latter sample displayed a more homogeneous solution, i.e. a more narrow distribution of interaggregate

spacing. Therefore, the ionomer structure formed in solution is related to the sample processing history.

Thermal treatment has been shown to increase the fraction of isolated ions in the case of NaSPS–4.2, and this treatment should also increase the fraction of isolated ions in a sample cast from a polar solvent, in which the fraction of isolated ions was decreased through the solvent casting procedure. Figure 6-10 shows NaSPS–2.65 in a series of sequential treatments: as received, cast from 95/5 THF/water, then annealed at 160°C, and then recast from 95/5 THF/water. The fraction of isolated ions for each step in the processing is given in Table 6-2. The cast sample shows the expected decrease in the fraction of isolated ions as compared to the original, bulk sample. Following heating, this sample shows a dramatic increase in the fraction of isolated ions, which is much greater than the increase caused by heating the uncast NaSPS–4.2 sample (Figure 6-6). When the 2.65% sulfonation sample was recast, the fraction of isolated ions again decreased, although not to the amount present in the original sample or after the first casting.

If the ionomer chains in THF/water solution were fully separated and randomly located in solution, then the spectra in Figures 6-10b and 6-10d would be equivalent, since the bulk morphology prior to dissolution would be inconsequential. However, this is not the case for NaSPS–2.65, and this result leads to the possibility that the chains have a certain degree of order in solution. Ise *et al.*[27-30] have studied ordering in polyelectrolyte solutions using small-angle X-ray scattering (SAXS). These authors propose that the SAXS peak seen for a wide range of polyelectrolyte concentrations (1-16 wt%) is due to interparticle interference. THF/water solutions of ionomers at low

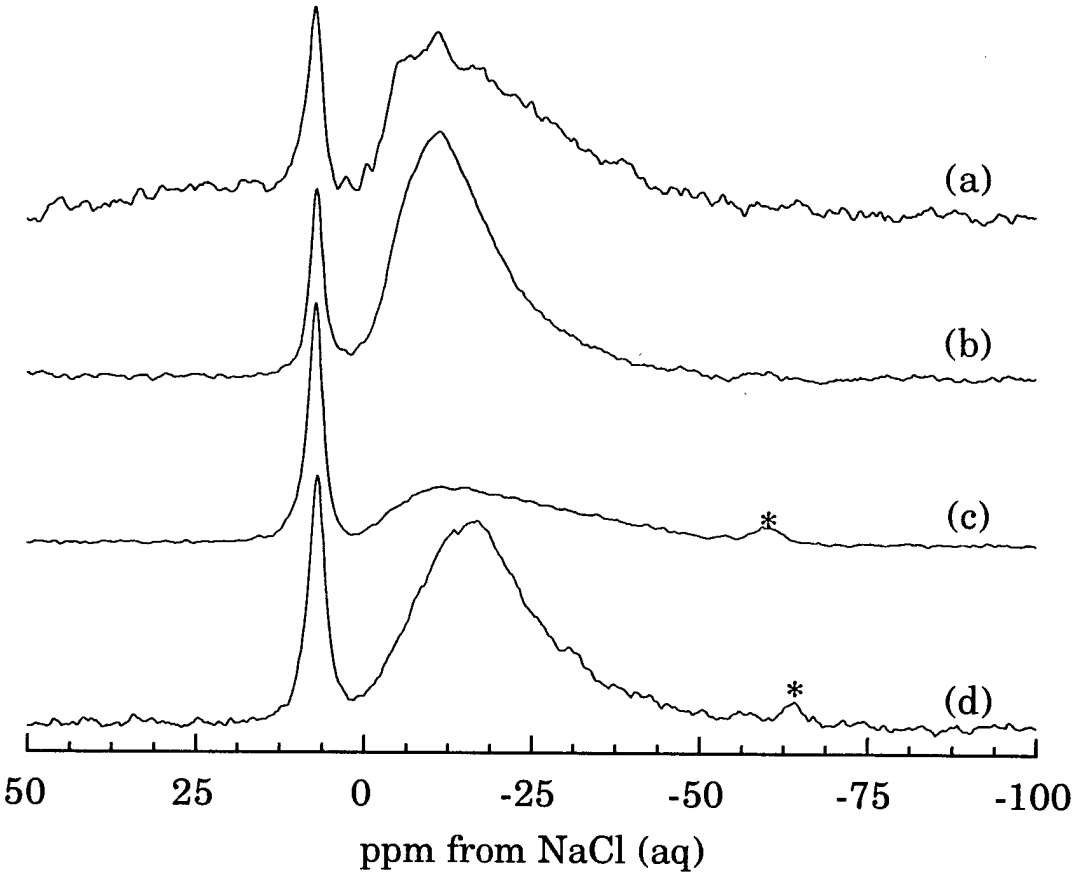

Figure 6-10: NMR spectra of NaSPS–2.65 a) dried under vacuum, b) cast from 0.5 wt% solution of 95/5 THF/water, c) sample (b) annealed at 160°C for 24 hrs, and d) sample (c) cast from THF/water. (*) are spinning sidebands.

Table 6-2: Fraction of isolated ions in processed samples of NaSPS 2.65%

Sample Processing	% Isolated Ions
as received	16
cast from 95/5 THF/water at 0.5 wt%	13
cast, then annealed at 160°C for 24 hours	47
cast, annealed, then cast from 95/5 THF/water at 0.5 wt%	20

concentrations show polyelectrolyte behavior in viscosity experiments.[31] A type of ordering similar to that seen in polyelectrolytes would impose a type of "memory" on the ionomer and could account for the differences in the spectra shown in Figures 6-10b and 6-10d.

Both humidification and thermal treatment can allow for variation in the extent of ion aggregation in a given ionomer sample. Subsequent treatments can alter the ionomer local structure to yet another morphology. The effects of these treatments on the local morphology of NaSPS can be restored to some degree. The deliberate manipulation of these treatments produced the large changes seen here, which can be as large as the changes caused by sulfonation level. Inadvertent changes can produce comparable variations in production materials or other experimental studies, and may be a cause of variable behavior in experimental results.

6.3 Conclusions

Sample processing (humidification, solvent casting, and thermal history) has a significant effect on the morphology of NaSPS. Humidification can affect the distributions of ions in a sample. At a high enough temperature, all ions are hydrated. All sites have equivalent symmetrical local environments, and it is not possible to determine from the spectra whether the environment outside the hydration sphere is hydrocarbon matrix (polymer chains) or ionic groups. When the temperature is high enough (60°C or 80°C), rearrangement of the polymer-bound ionic groups accompanies humidification. On subsequent drying, the fraction of ions in aggregates is higher than in the unmodified ionomer. Also, isolated ions are more readily hydrated and dehydrated at lower temperatures than are aggregated ions.

Annealing NaSPS at high temperatures leads to some dissociation of the aggregates, which can be seen through the formation of isolated ions. Additionally, the peak position of the aggregate peak shifts about 5 ppm upfield, indicating some restructuring in the aggregates. Measurements of the fraction of isolated ions at different temperatures and times followed a reversible first-order rate expression and yielded a heat of reaction of 6.3 ± 1.4 kcal/mol.

The effects of thermal treatment were shown to be reversible to some degree in this system. Therefore, the local morphology of an ionomer can be tailored to the needs of a specific application. One ionomer can be used repeatedly; its morphology can be altered without variations in the chemistry of the system, allowing for less sample-to-sample variation in a study. Additionally, this preparation-dependent variation and its control are clearly important factors to understand in using ionomers exposed to varying environments.

References for Chapter Six

1 Toriumi, H.; Weiss, R.A.; Frank, H.A. *Macromol.* 1984, **14**, 2104.

2 Yarusso, D.J.; Cooper, S.L.; *Polymer*, 1985, **26**, 371.

3 Longworth, R.; Vaughn, D.J. *Nature*, 1968, **218**, 85.

4 Marx, C.L.; Cooper, S.L. *Macromol.* 1973, **6**, 344.

5 MacKnight, W.J.; Taggart, W.P.; Stein, R.S. *J. Polym. Sci., Symp. Ser.* 1974, **45**, 113.

6 Fitzgerald, J.J.; Weiss, R.A. *Rev. Macromol. Chem. Phys.* 1988, **C28**, 99.

7 Weiss, R.A.; Sen, A.; Pottick, L.A.; Willis, C.L. *Polymer*, 1991, **32**, 2785.

8 Goddard, R.J.; Grady, B.P.; Cooper, S.L. *Macromol.* 1994, **27**, 1710.

9 Dickinson, L.C.; MacKnight, W.J.; Connelly, J.M.; Chien, J.C.W. *Polym. Bull.* 1987, **17**, 459.

10 Komoroski, R.A.; Mauritz, K.A.; *J. Am. Chem. Soc.* 1978, **100**, 7486.

11 Fitzgerald, J.J.; Weiss, R.A., in *Coulombic Interactions in Macromolecular Systems*, Eisenberg, A.; Bailey, F., eds. American Chemical Society: Washington, D.C., 1986.

12 Ishioka, T. *Polymer J.* 1993, **11**, 1147.

13 Brozoski, B.A.; Coleman, M.M.; Painter, P.C. *Macromol.* 1984, **17**, 230.

14 Brozoski, B.A.; Coleman, M.M.; Painter, P.C. *Macromol.* 1984, **17**, 1591.

15 Register, R.A.; Sen, A.; Weiss, R.A.; Cooper, S.L. *Macromol.* 1989, **22**, 2224.

16 Weiss, R.A.; Lefelar, J.A. *Polymer*, 1986, **27**, 3.

17 Chapter 5

18 Galambos, A.F.; Stockton, W.B.; Koberstein, J.T.; Sen, A.; Weiss, R.A. *Macromol.* 1987, **20**, 3091.

19 Weiss, R.A.; Agarwal, P.K. *J. Appl. Polym. Sci.* 1981, **26**, 449.

20 Navratil, M; Eisenberg, A. *Macromol.* 1974, **7**, 84.

21 Han, K.; Williams, H.L. *J. Appl. Polym. Sci.* 1991, **42**, 1845.

22 Lefelar, J.A.; Weiss, R.A. *Macromol.* 1984, **17**, 1145.

23 Hird, B.; Eisenberg, A. *Macromol.* 1992, 25, 6466.

24 Ding, Y.S.; Register, R.A.; Nagarajan, M.R.; Pan, H.K.; Cooper, S.L. *J. Polym. Sci., Phys. Ed.* 1988, **26**, 289.

25 Ishioka, T.; Kobayashi, M. *Macromol.* 1990, **23**, 3183.

26 Vanhoorne, P.; Van den Bossche, G.; Fontaine, F.; Sobry, R.; Jerome, R.; Stamm, M. *Macromol.*, 1994, **27**, 838.

27 Ise, N,; Okubo, T.; Yamamoto, K.; Kawai, H.; Hashimoto, T.; Fujimura, M.; Hiragi, Y. *J. Am. Chem. Soc.* 1980, **102**, 7901.

28 Ise, N,; Okubo, T.; Kunugi, S.; Matsuoka, H.; Fujimura, M.; Ishii, Y. *J. Chem. Phys.*, 1984, 81, 3294.

29 Ise, N. *Angew. Chem.* 1986, 25, 323.

30 Ise, N.; Matsuoka, H.; Ito, K.; Yoshida, H.; Yamanaka, J. *Langmuir*, 1990, 6, 296.

31 Lundberg, R.D.; Phillips, R.R., in *Coulombic Interactions in Macromolecular Systems*, Eisenberg, A.; Bailey, F., eds. American Chemical Society: Washington, D.C., 1986.

Chapter Seven: Ionomers: Effects of Polydispersity in Molecular Weight

7.1 Introduction

The viscoelastic[1-9] and tensile[10,11] behavior of linear, monodisperse polymers has been the subject of numerous studies. However, the behavior of polydisperse materials is less well understood. Many researchers have chosen to study blends of two or more well-characterized monodisperse materials in order to understand the effects of polydispersity.[2,6,12-15] In many cases, the relaxation behavior was simply the superposition of the viscoelastic behavior of the two monodisperse materials. Jackson and Winter[12] have reviewed a number of models used for predicting the behavior of bidisperse blends and have used a generalized linear blending rule to describe data on polystyrene blends.

Polydispersity has been shown to affect shear moduli (G', G"),[2,4,16,17] stress relaxation moduli,[6] compliance,[2,14,18] dielectric spectra,[19] melt viscosity,[2-5,8,11,15] tensile properties,[10,11,16] and self-diffusion.[20,21] Researchers have also investigated the effects of molecular weight and dispersity of polymer chains between crosslinks in network systems.[22-24] Above the critical entanglement molecular weight, narrow-distribution polystyrenes show two distinct relaxations in shear experiments while polydisperse materials show only a broad distribution of relaxation times.[1,2] Materials with very large molecular weight distributions exhibit non-Newtonian flow at lower shear rates than the corresponding narrow-distribution polymers.[5,8,17] In terms of bulk properties, the tensile strengths and elongations of monodisperse polystyrenes are higher than those of

polydisperse materials at the same weight-average molecular weights (M_w); the reverse behavior is seen with respect to M_n.[10,11]

Influences of molecular weight in telechelic ionomers have also been studied.[25-27] The effects are more complicated in these systems because varying the molecular weight in a telechelic ionomer also changes the ion content. Additionally, different ion types will play varied roles in viscoelastic and mechanical behavior. Jérôme and Broze[25] studied telechelic Mg-neutralized polyisoprene ionomers and reported decreases in G' as the molecular weight increased from 7,000 to 36,000, as would be expected since the ion content is decreasing in this range. However, as the molecular weight was increased further to 69,000, the values of G' increased. They attributed this behavior to an increased density of entanglements. Tant *et al.*[26] reported increases in mechanical properties (stress-strain properties) and decreases in creep rates as molecular weight increased for Ba-neutralized polyisoprene telechelic ionomers. The authors concluded that, in this case, the effects of ionic groups are less significant than the effects of entanglements.

The effects of molecular weight on properties in random ionomer systems have received less attention than similar studies looking at the effects of ion content or ion type. However, investigations on the rheological[28,29] and dynamic mechanical properties[29] of ionomers have been reported. Erhardt *et al.*[28] reported effects of molecular weight on the zero-shear viscosity of styrene/butylmethacrylate/potassium methacrylate terpolymers. An ionomer with M_w of 34,000 showed a greater dependence of viscosity on ion content than did a material with M_w of 145,000. The authors concluded that the ions are much less effective at increasing viscosity when polymer chains are already entangled; the entanglements control the viscous

behavior of the material more so than the ionic groups. Kim *et al.*[29] reported changes with molecular weight in the high-temperature region of dynamic mechanical and rheological experiments of sodium-neutralized sulfonated polystyrene and poly(styrene-sodium methylacrylate). As molecular weight increased, the high-temperature loss peak (termed "ionic" or "cluster" glass transition) became more well-developed and the onset of flow was delayed to higher temperatures. These changes were particularly noticeable for very low molecular weights (M_n=21,000) and were much less dramatic in the sulfonated ionomer than in the carboxylated material.

One of the most commonly studied ionomers is sulfonated polystyrene. Many of the previous studies of SPS have been completed using polydisperse ionomers. However, more recently monodisperse SPS ionomers have been studied, particularly investigations of the solution behavior of these systems using viscometry, light scattering and neutron scattering techniques.[30-36] A recent small-angle x-ray scattering (SAXS) study[37] has indicated differences in solid-state morphology between SPS samples of different polydispersities.

7.2 Results and Discussion

Sodium-neutralized sulfonated polystyrene materials studied previously were complicated systems. These were ionically cross-linked, polydisperse, entangled materials. It is possible to reduce the number of parameters by choosing monodisperse polymers above and below the molecular weight at which entanglements occur in polystyrene (M_c~31,200-38,000).[4] In this way, the effects of molecular weight and polydispersity on the fraction of sodium ions participating in crosslinking can be determined.

The effect of polydispersity on the local environments of the sodium ions in sulfonated polystyrene (termed 'local morphology' in this chapter) has not been studied previously. In fact, if SPS is a random ionomer with the ionic groups randomly spaced along the hydrocarbon chain, the initial expectation would be that chain polydispersity should have very little effect on aggregate morphology. However, a previous SAXS study[37] showed differences in the breadth and position of the SAXS interference peak for samples of differing polydispersity. Since the SAXS peak is generally attributed to the presence of ionic domains, it appears that the domains are different in these two materials.

7.2.1 Effects of Molecular Weight and Ion Content in Monodisperse NaSPS

The molecular weights and sulfonation levels for the monodisperse sulfonated polystyrene materials are shown in Table 7-1. Figure 7-1 shows the NMR spectra of monodisperse NaSPS samples with M_n~105,000 and a range of ion contents. Each spectrum shows a distinct peak at –2.7 ppm. The fraction of the total intensity in this peak decreases slightly as ion content increases for materials of constant molecular weight. The broad peak due to aggregated ions becomes more distinguishable as ion content increases, probably signifying more order in the aggregates at higher ion contents. The 1.2% sulfonated sample does not show enough resolution to determine the fraction of intensity in any peak. However, it is interesting to note that only at this low ion content is a substantial amount of the NMR intensity present around 7 ppm, which is the chemical shift assigned to isolated sodium ions. At this ion content, many ions are too far apart to aggregate together and are left dispersed throughout the polystyrene matrix as isolated $Na^+SO_3^-$ ion pairs.

Table 7-1: Number-average molecular weight and ionization level for monodisperse sulfonated polystyrene materials.

Sample Name	M_n	% Sulfonation	Number of Entanglements/ Chain
M1-100	105,000	1.2	5.5
M2-100	105,000	2.7	5.5
M3-100	105,000	3.6	5.5
M5-100	105,000	5.1	5.5
M2-1.8m	1,800,000	2.3	95
M3-900	900,000	3.2	47
M4-35	35,000	4.2	1.8
M6-9	9,000	5.9	0.5
PE-100	87,000	100	4.6

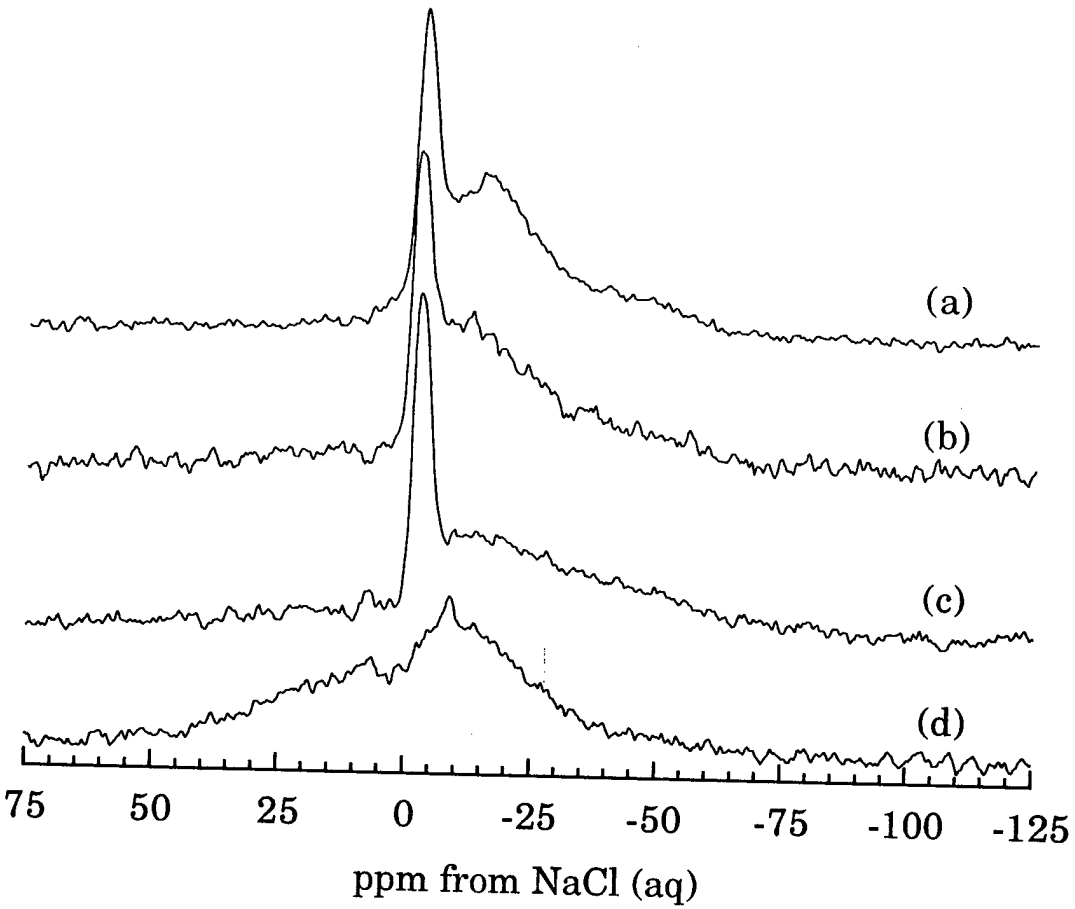

Figure 7-1: NMR spectra of MNaSPS with Mn=105,000.
Ion contents are: a) 5.1%; b) 3.6%; c) 2.7%; d) 1.2%.
Figure 1(d) was acquired with a pulse delay of 0.5 s.

The intensity at this chemical shift dramatically decreases as ion content increases, and isolated sites are barely observed at 2.7% ion content. In contrast, isolated ions persist past 3.0% ion content in polydisperse NaSPS (Chapter 4).

Figure 7-2 shows the spectra of the NaSPS samples with different molecular weights. The lowest molecular weight ionomer, M_n=9,000, shows no distinct –2.7 ppm peak at all. Additionally, the ionomer with M_n=35,000 has less intensity in the narrow peak than the other ionomers studied. The fraction of intensity represented by the –2.7 ppm peak for all monodisperse samples is plotted as a function of ionization level and molecular weight in Figure 7-3. The peak appears only above the entanglement length of polystyrene, and it accounts for 15-18% of the overall sodium intensity of the sample for molecular weights above 35,000. Kim *et al.*[29] have shown that molecular weight effects in ionomers are less apparent above M_n~100,000, similar to the behavior reported here. Erhardt *et al.*[28] have suggested that the effects of chain entanglements and ionic groups on ionomer behavior are interrelated. Additionally, Tant *et al.*[26] have stated that, at high enough molecular weights, the effect of molecular weight (or more precisely, entanglements) on telechelic ionomers outweighs the effects of ionic interactions. Finally, Onogi *et al.* showed that properties of nonionic polystyrene become less sensitive to molecular weight above M_n~100,000.[1,10,14] In summary, the effects of molecular weight begin to outweigh the effects of ion contents at high enough M_n, and plateau at $M_n \geq 100{,}000$. These conclusions are consistent with the data presented here; it appears that once the molecular weight of the polymer is high enough for entanglements, the effect of ion content on the ^{23}Na NMR spectra is less

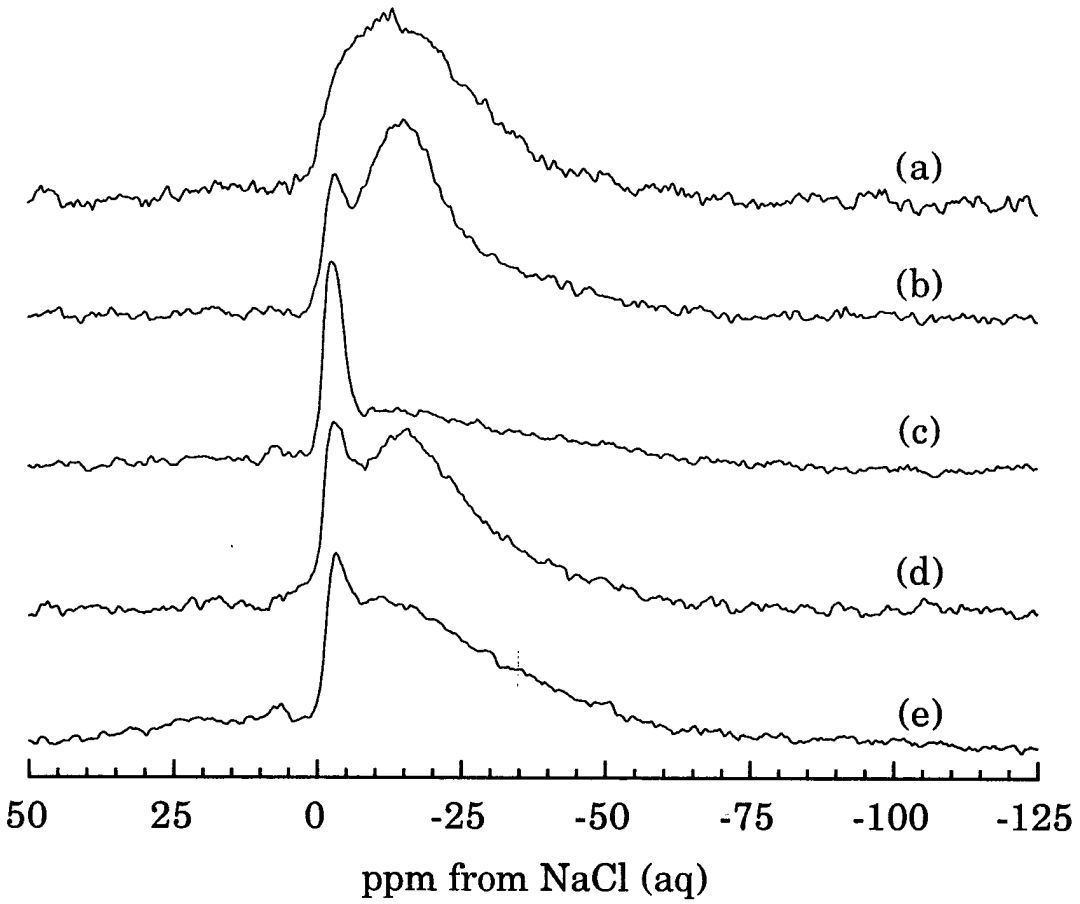

Figure 7-2: NMR spectra of MNaSPS at five different ion contents and molecular weights: a) M6-9 b) M4-35 c) M2-100 d) M3-900 e) M2-1.8m. Figure 7-2e was aquired with a 1s delay. A spectrum with a 10s delay was similar.

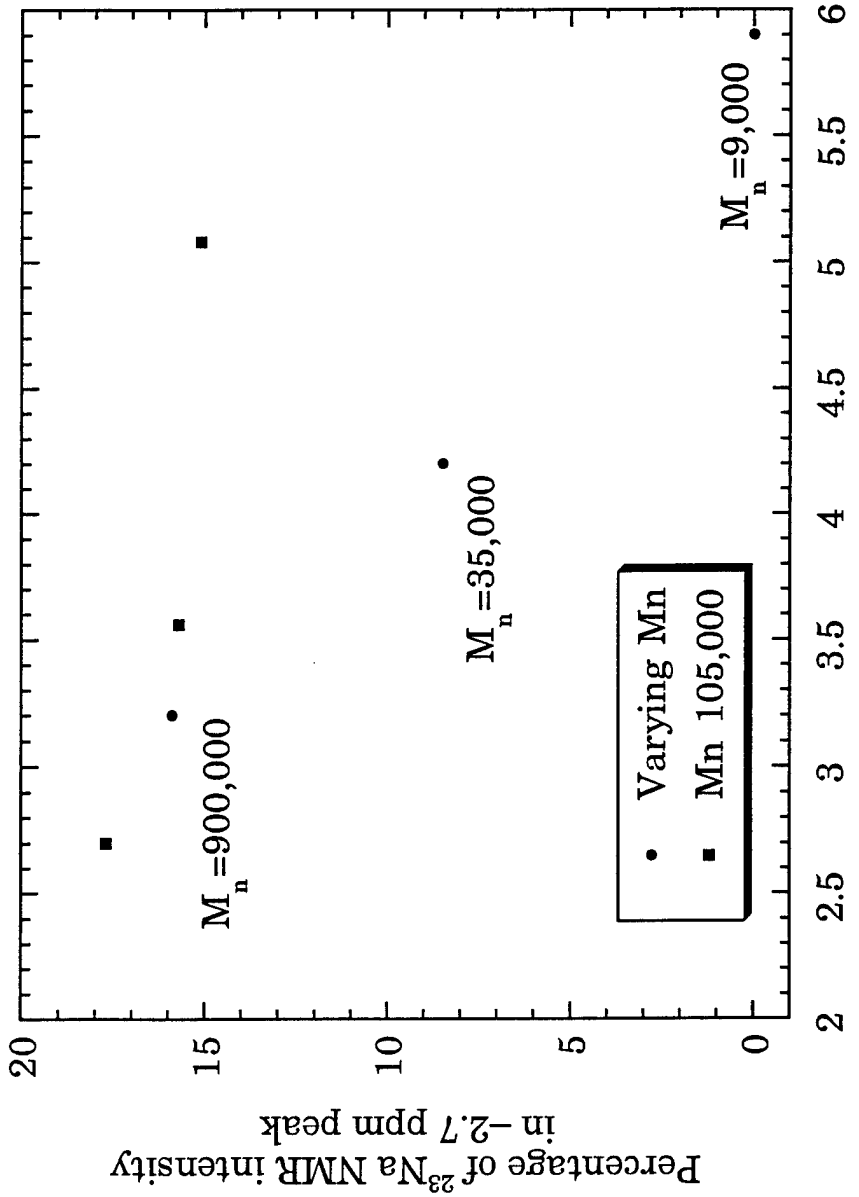

Figure 7-3: Fractions of NMR intensity due to the –2.7 ppm peak for several monodisperse sulfonated polystyrene ionomers.

significant. In this case, the presence or absence of entanglements causes changes in the environments in which the sodium ions reside. Much larger effects of ion content were seen for polydisperse NaSPS materials (Chapter 4), in which a portion of polymer chains are below the entanglement molecular weight.

7.2.2 Effects of Polydispersity in NaSPS

Molecular weight has been shown to affect ionomer properties,[28,29] particularly below the molecular weight needed for entanglements. Therefore, it is not unexpected that polydispersity would play a role as well. In order to determine the effects of polydispersity on the local environment of the sodium ions, ^{23}Na NMR studies of poly- and monodisperse polystyrene were undertaken.

^{23}Na NMR spectra of polydisperse NaSPS have been discussed in Chapters 4-6. The NMR spectrum of monodisperse NaSPS at 2.7% ionization (M2-100) is shown in Figure 7-4 with the corresponding spectrum of polydisperse NaSPS ionized to 2.7% (NaSPS–2.7). The materials have similar values of M_n and have most of their sodium cations in aggregates, as seen from the broad peak near –15 ppm. The most noticeable difference between the two spectra is the presence of a relatively narrow (~5–5.5 ppm wide) peak at –2.7 ppm only in the monodisperse sample. Also, the fraction of isolated ions, represented by the intensity at 7 ppm, is much lower in the monodisperse material.

The ^{23}Na NMR spectrum of a sulfonated polystyrene polyelectrolyte (M_n~87,000) is shown in Figure 7-5. This polyelectrolyte is equivalent to a fully sulfonated monodisperse polystyrene sample. It is apparent from the

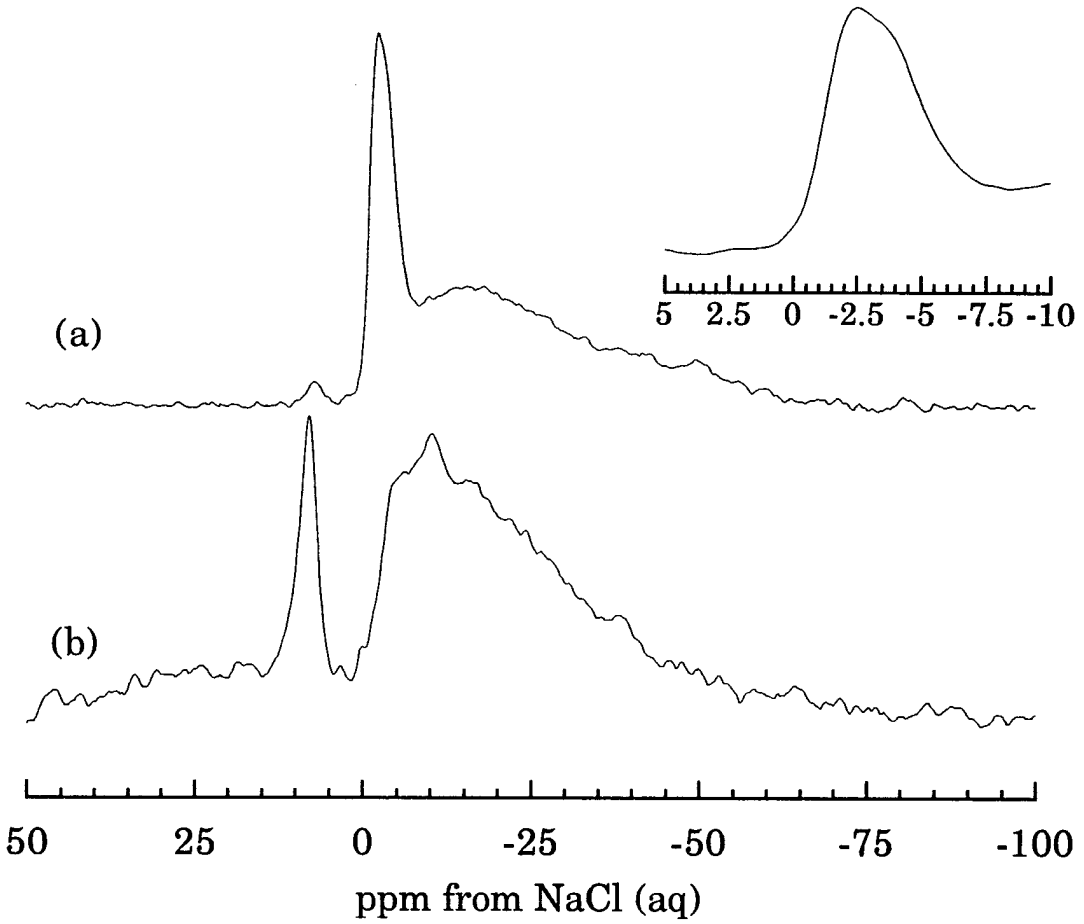

Figure 7-4: Comparison of a) monodisperse and b) polydisperse NaSPS at 2.7% ionization and M_n~105,000. The inset is the –2.7 is the peak in 7-4a.

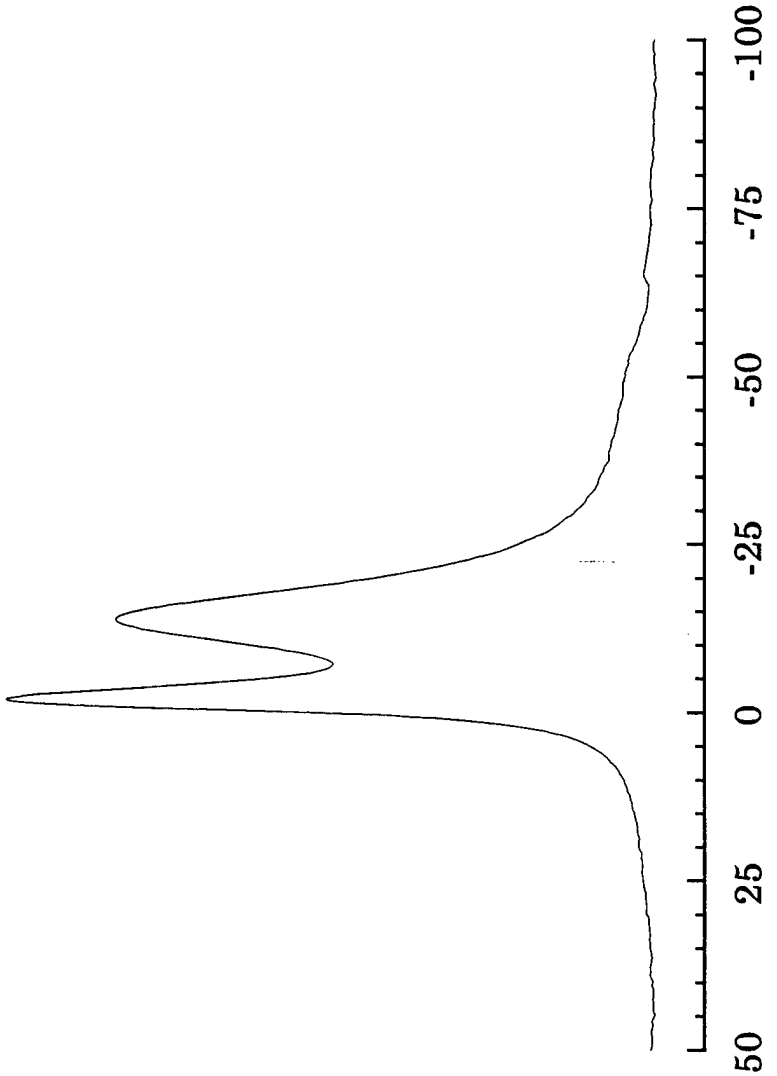

Figure 7-5: NMR spectra of a sodium-neutralized sulfonated polystyrene polyelectrolyte. M_n=87,000.

spectrum that at complete ionization this additional NMR peak at –2.7 ppm persists. The fraction of sodium ions represented by this peak is ~18%, which is at the upper end of the range shown in Figure 7-3.

The origin of this –2.7 ppm peak is certainly of interest. In principle, the peak could be due to differences in chemistry (initiators or contaminants) between the monodisperse and polydisperse ionomers or due to differences between the morphologies of the two materials. Based on a number of reasons, we believe that this peak has a morphological cause.

There are several possible explanations for the presence of the –2.7 ppm peak in the monodisperse sample. The first is the presence of excess neutralization agent, excess water, or an extraneous product. However, the sample is neutralized with NaOH, and Chapter 4 the peak for excess NaOH was identified at 0 ppm. The ionomers are dried under vacuum, and in Chapters 4 and 6, the peak due to humidified sodium ions appeared at 0 ppm, and did not appear in samples dried under vacuum. The asymmetry present in the –2.7 ppm peak (Figure 7-4 inset) is not apparent in the peak due to hydrated sodium ions. This –2.7 ppm peak was also seen for the commercial polyelectrolyte, which was synthesized in a manner different from our procedure. Additionally, as will be discussed shortly, the peak can be removed through solvent casting. Therefore, the peak is not due to excess NaOH, water, or an additional component.

The second possibility is that the differences in the polymerization of the two types of polystyrene affect the ionization reaction. The particular initiator in the monodisperse polystyrene might contribute to preferential sulfonation of the chain ends. If this were the case, however, the difference in the intensities of the –2.7 ppm peaks in the samples with M_n=105,000 and

M_n=900,000 should be much greater than it is, since the former has nine times as many chain ends per unit mass as the latter. Most likely, then, the peak is not due to chain ends.

The last possibility to consider is that the origin of the peak is due to morphological changes in material structure. This is most likely for two reasons. The peak does not appear in materials below the entanglement length of polystyrene, and is of lower intensity in materials near the entanglement length. Also, as is shown below, the peak is not removed through casting from a THF/methanol, but can be removed by casting from a THF/water solution. Each of these factors indicate that this peak is due to morphological constraints, such as steric hindrance of isolated ions, in the as-prepared monodisperse sulfonated polystyrene. This is considered further in section 7.2.5, Discussion.

7.2.3 Effects of Sample Preparation

The effects of solvent casting on the local morphology of polydisperse NaSPS ionomers have been studied in detail in Chapter 5. Casting NaSPS samples from low concentrations of 90/10 or 95/5 THF/water mixtures resulted in dramatic decreases in the fraction of isolated ions present in the material. In these solvents and concentrations the ionic groups are fully solvated[38] and the ionomers exhibit polyelectrolyte behavior, indicated by a sharp increase in reduced viscosity at decreasing concentrations.[39] Slow evaporation of the solvent allows for rearrangement of the chains and the formation of a new morphology. Presumably, similar morphological changes will occur when MNaSPS is cast from similar solvent mixtures. Two ionomer systems, M1-100 and M2-100, were cast from 95/5 THF/water to determine

the effects of the polar cosolvent on the morphology of these ionomers. The results are shown in Figures 7-6 and 7-7 for the 1.18% and 2.7% sulfonated ionomers, respectively. Additionally, the monodisperse ionomers are compared to the corresponding polydisperse ionomers prepared by similar casting procedures. It is apparent that solvent effects are substantial in these systems: the peak at –2.7 ppm is reduced to a shoulder in the case of M2-100 and the fraction of signal near 7 ppm is reduced considerably for M1-100. Similar results were seen in an earlier study of solvent effects on polydisperse NaSPS,[53] in which casting from THF/water permitted local rearrangement of the sodium ions into aggregates. Therefore, the THF/water cosolvent appears to be an effective medium for permitting local rearrangement of sodium ions in mono- and polydisperse NaSPS ionomers.

It is particularly interesting to note the differences between cast samples of the monodisperse and polydisperse NaSPS at equivalent ionization and molecular weight, NaSPS–2.7 and M2-100 (Figure 7-7). In parallel with the results for the uncast samples, the monodisperse ionomer has substantially fewer isolated ions than the polydisperse material, as shown by the intensities at 7 ppm. This indicates that the cast monodisperse samples have more sodium ions in aggregates, where they participate in crosslinking. Results in Chapters 5 and 6 have indicated that differences in ion distributions in NaSPS could be due to different sample histories. In this case, the different local morphologies seen here are not due to material processing since the preparations were equivalent.

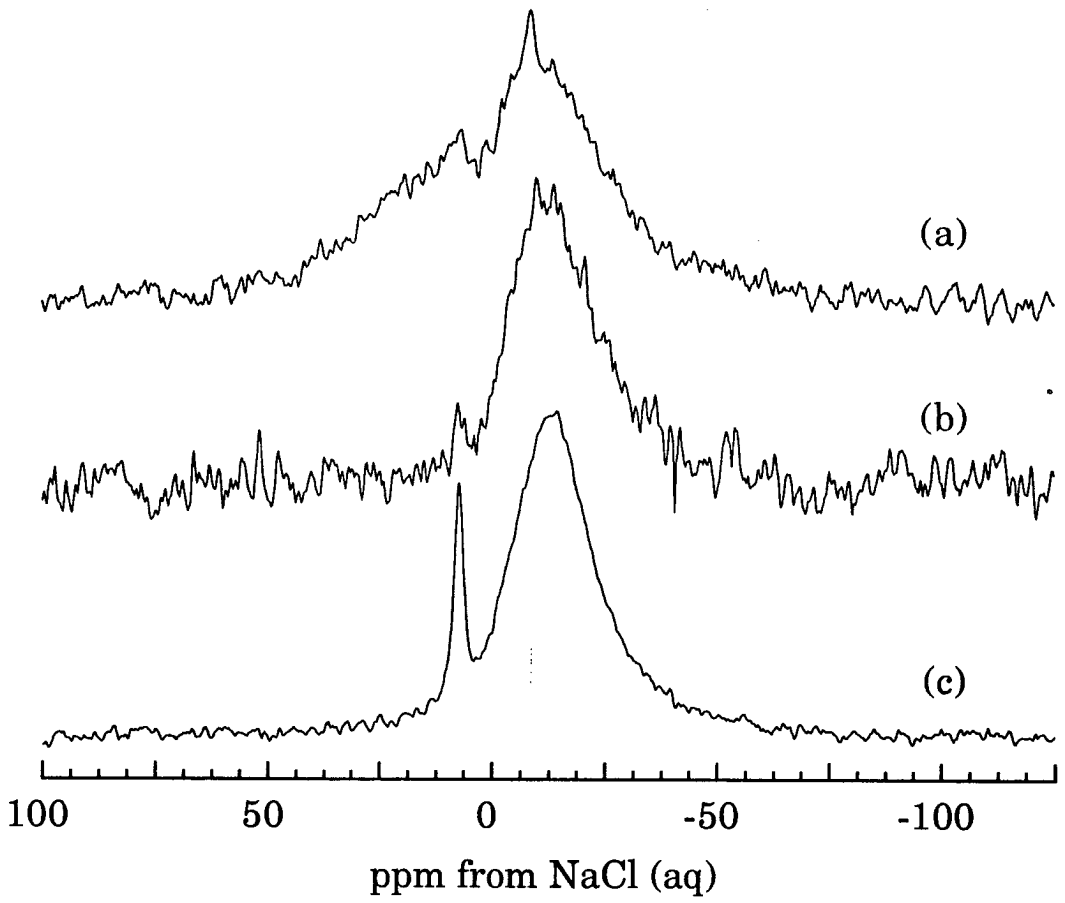

Figure 7-6: NMR spectra of a) M1-100 as synthesized b) M1-100 after casting from 95/5 THF/water at 0.5 wt% and c) NaSPS–1.7 after casting from 0.5 wt% 90/10 THF/water.

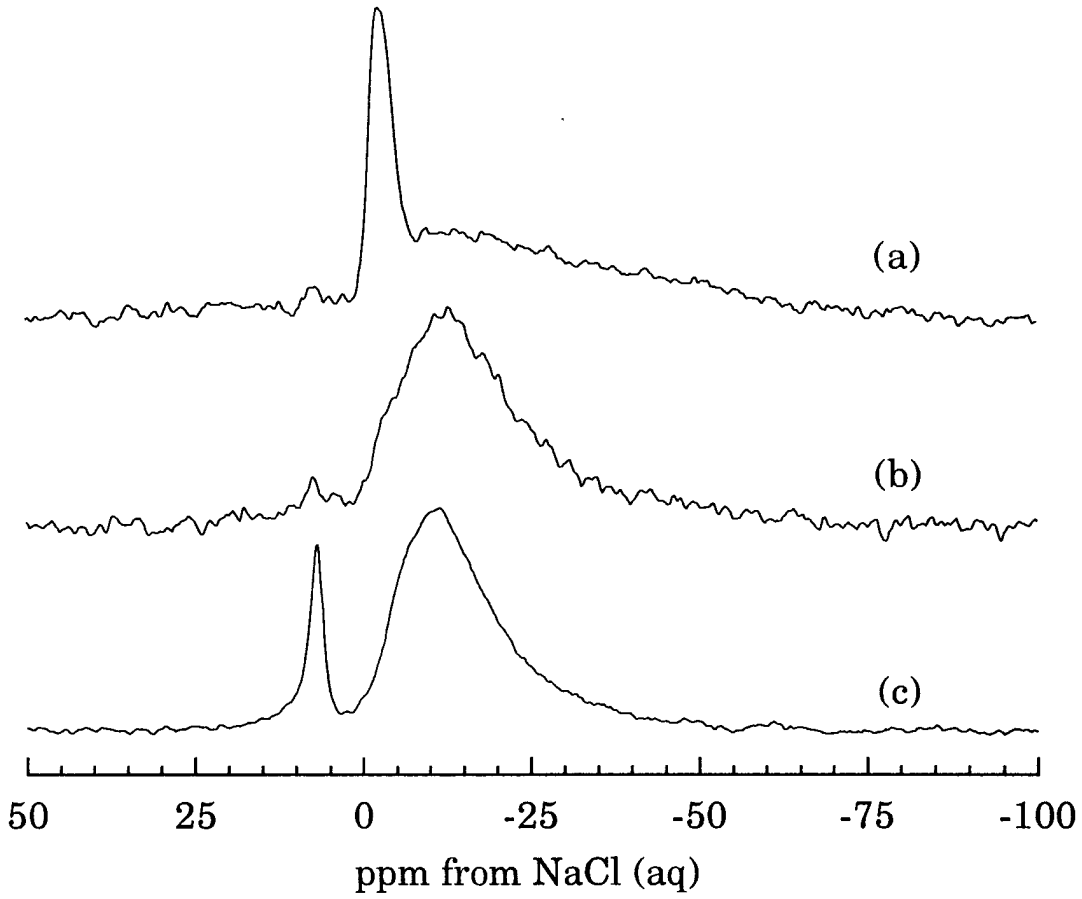

Figure 7-7: NMR spectra of a) M2-100 as synthesized and b) M2-100 after casting from 95/5 THF/water at 0.5 wt% and
c) NaSPS-2.7 after casting from 0.5 wt% 90/10 THF/water.

7.2.4 Blends of Monodisperse NaSPS

The monodisperse ionomers were mixed to determine if blending would remove the –2.7 ppm peak and create a spectrum more similar to that seen for the polydisperse ionomers, i.e. containing more isolated ions. Figures 7-8a and b show the result when the ionomers M3-900 and M4-35 were blended in a 1:1 ratio using THF/methanol and THF/water solutions, respectively. The result from the first cosolvent is essentially the sum of the spectra of the individual components, while the result from the THF/water solution shows dramatic changes. Apparently, the THF/methanol solution is not an effective solvent in terms of allowing complete mixing of the components. Similar results were shown in Chapter 5 for polydisperse NaSPS, in which THF/methanol cosolvents did not permit extensive redistribution of the sodium ions in and out of aggregates. Methanol solvates the sodium ions less completely than water does,[40] so the aggregates are not fully dissociated in the solution.

The lack of intensity around 7 ppm for the blend could be due to the high sulfonation level, which is close to the point at which all ions become aggregated in NaSPS (Chapter 4). Figure 7-8c shows a blend with three monodisperse ionomers, in which the ratio of M1-100:M3-900:M4-35 is 2:1:1, compared with the previous two-component blend. There is no increase in intensity around 7 ppm. It is likely that the concentrations in solution used in the blends are too low to permit the presence of isolated ions; however, low concentrations were needed to fully separate the ionomer chains and to ensure complete blending.

The three-component blend was then annealed at 155°C for 24 hours, a treatment which has been shown to create isolated ions in the polydisperse

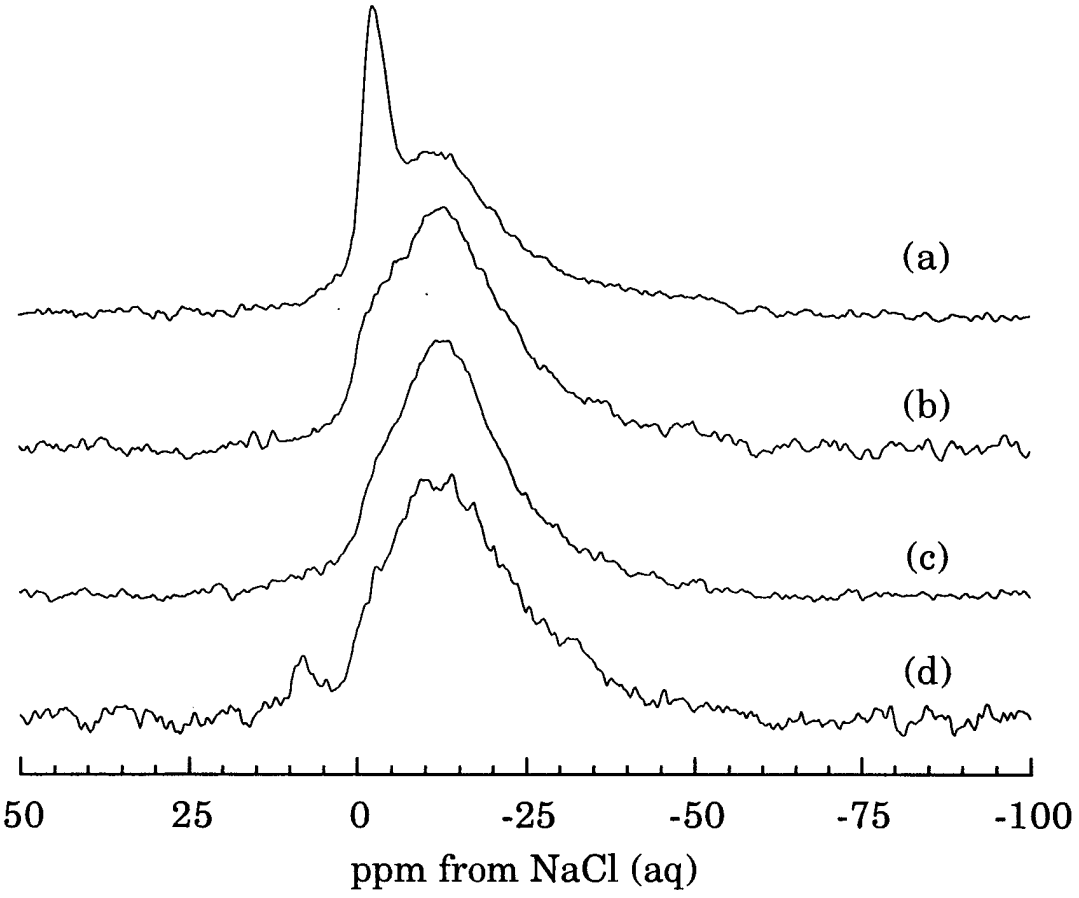

Figure 7-8: Spectra of a) 1:1 blend of M4-35:M3-900 blended in THF/MeOH solutions and cast b) sample (a) redissoved in THF/water and cast c) 2:1:1 M1-100:M3-900:M4-35 cast from THF/water; d) 7-8c annealed at 155°C 24 hrs

samples (Chapter 6). The results of this treatment are shown in Figure 7-8d. The fraction of isolated ions has indeed increased, as evidenced by the increase in intensity of the 7 ppm peak. However, this treatment noticeably discolored the blend of monodisperse ionomers, and to a higher degree than was observed for the polydisperse materials. These ionomers made from monodisperse polystyrene are more sensitive to annealing for long periods of time, perhaps because of the particular initiator used. Nevertheless, the similar behavior of monodisperse and polydisperse ionomers when subjected to both solvent casting and heat treatment shows that they are indeed chemically similar, and that the new Na^+ environment (–2.7 ppm peak) present in the monodisperse ionomers has a morphological cause related to different chain responses to sample processing for the monodisperse material. A possible cause is discussed below.

7.2.5 Discussion

The precise identification of the –2.7 ppm peak is not possible at this time. However, some observations on the characteristics of this new NMR peak are in order. The peak is narrow relative to the aggregated ions, but not compared to the isolated ions. Using the method of Kundla *et al.*,[41] an upper limit on the quadrupolar coupling constant (QCC) can be determined. The maximum QCC is ~900 kHz, significantly greater than the value reported for isolated ions (~160 kHz), but still substantially less than the value observed for aggregated ions (1.6 MHz). Additionally, while relatively narrow, the peak is not Lorentzian. As shown in the inset in Figure 7-4, there are several inflection points along the peak, indicating that this line is a heavily broadened quadrupolar powder pattern. Also, the spin-lattice relaxation time (T_1) of the

–2.7 ppm peak (2.3 s) is between the T_1's of the isolated (~6 s) and aggregated (<0.5 s) ions. The position of the peak is intermediate as well and since the second-order quadrupole shift is at most 3.3 ppm,[42] the main factor determining this peak position is the chemical shielding.

From the above considerations, it could be postulated that the environment represented by this peak is a distorted version of the isolated site, with the sodium ion becoming more shielded, causing an upfield shift. One possibility would be an isolated ion close to an aggregate or another isolated ion but sterically hindered from being incorporated into an aggregate. This would show an increased shielding from the higher electron density of another ion pair or aggregate nearby, compared to the shift observed for Na^+ isolated in a pure hydrocarbon environment.

The two phenomena, the –2.7 ppm peak and the lower fraction of isolated ions in cast MNaSPS, are interesting because the sulfonate groups are randomly located on the polymer chain, so the distance between ionic groups should not vary with chain length. However, it is also apparent that both phenomena are functions of chain length; in Figure 7-2 the –2.7 ppm peak in MNaSPS is not present for the ionomer of M_n=9,000 and this peak is only beginning to appear for the ionomer near the critic molecular weight for entanglements of polystyrene, M_n~35,000. Additionally, casting from the relatively polar cosolvent THF/water can remove the peak almost completely, with only a shoulder of intensity remaining, and annealing a blend of several monodisperse components allows this peak to entirely disappear.

These NMR results indicate that polydispersity affects the distribution of ions in sulfonated polystyrene so that more isolated ions are present in polydisperse NaSPS. Williams *et al.*[43] have compared SAXS patterns of

monodisperse Mg-neutralized telechelic polyisoprenes and polydisperse Mg-neutralized telechelic polybutadienes. They reported higher levels of electron density fluctuations in the polydisperse samples, which they attributed to a larger number of isolated ionic groups dissolved in the matrix of the polydisperse material. This is consistent with the results reported here.

It is likely that at constant ion content, entanglements or molecular weight play a role in the ionomer local morphology and in particular in the fraction of isolated ions seen in mono- and polydisperse materials. Table 7-1 shows the number of entanglements per chain (assuming an entanglement molecular weight $M_e=M_c/2\sim18,000$) for each material. In M2-100, all chains should have approximately 5 entanglements and 27 ion groups. In contrast, for polydisperse NaSPS–2.7, a polymer chain in the high molecular-weight tail might have an M~900,000 and would therefore have about 47 entanglements. The large number of entanglements may prevent some of the ionic groups from aggregating into domains.

In addition to the effects of high molecular-weight fractions, the lower molecular weight chains may also play a role in the appearance of isolated ions in polydisperse NaSPS. Plante *et al.*[44] studied the effects of low molecular weight ionic oligomers (MW 800) on the morphology and dynamic mechanical properties of carboxylated polystyrene (CPS) neutralized with either Cs or Ba. Addition of about 10 wt% of the Cs-neutralized oligomer to CsCPS caused the aggregate peak in the SAXS pattern to disappear; the peak reappeared at lower scattering angles (higher Bragg spacings) at higher oligomer content. Similar behavior was seen for BaCPS; the SAXS peak gradually shifted to lower scattering angles as the amount of oligomer increased. The authors suggested that the slight decrease in intensity of the

SAXS peak with increasing oligomer content could be due to destabilization of aggregates, leading to dispersion of some ionic groups into the matrix, as oligomer content increases. It appears that addition of low-molecular weight oligomers can alter the morphology of the aggregate. In a SAXS study comparing NaSPS of narrow and broad molecular weight distribution,[37] the SAXS peak of the narrow molecular weight sample is centered around 37Å while the SAXS peak of the polydisperse NaSPS is at 42Å, indicating a shift to lower scattering angle as dispersity increases. If in polydisperse NaSPS the lower molecular weight chains disrupt some of the aggregates, more isolated (unaggregated) ions would be expected.

The monodisperse (and polydisperse) materials are precipitated from the dichloroethane polymerization media into boiling water. It is likely that entangled chains prevent arrangement into a more-preferred morphology in such a short timescale. Dissolution in THF/water at these low concentrations allows the aggregates to be fully dissociated[38,39] and separates the entangled chains. Slow evaporation of the solvents permits rearrangement of the chains and ionic groups into a new, more preferred morphology. This local morphology consists primarily of aggregates. The greater chain uniformity of the monodisperse ionomers limits the plasticization of the aggregates by the low molecular weight components and permits more complete aggregation. In general, it appears that ionic aggregation in NaSPS is affected by ion concentration, molecular weight and polydispersity, among other factors. Various sample treatments such as solution casting and annealing affect the ionic group and polymer chain mobility during processing, which in turn affects the extent of aggregation achieved.

7.3 Conclusions

Ion content and molecular weight affect the ^{23}Na NMR spectra of monodisperse sulfonated polystyrene ionomers. At low ion contents, the fraction of NMR intensity due to isolated sodium ions is larger than at higher ionization levels, just as seen in polydisperse NaSPS. Many ions are too far apart to aggregate together and are left dispersed throughout the polystyrene matrix. A new NMR peak at –2.7 ppm appears at ionization levels ≥ 2.3% and molecular weights ≥ 35,000; this peak is not present in spectra of polydisperse NaSPS but is present in the fully sulfonated NaSPS polyelectrolyte. The effects of molecular weight on the NMR spectra are most noticeable below M_n~100,000; below this point, the fraction of intensity in the –2.7 ppm peak is less than what is seen in materials with larger molecular weights. The peak at –2.7 ppm is identified as due to morphological constraints since its intensity is a function of molecular weight and sample preparation. Casting from 95/5 THF/water cosolvents removed the –2.7 ppm peak from the NMR spectrum. Differences were apparent in the ^{23}Na NMR spectra of mono- and polydisperse materials due to the effects of entanglements and molecular weight on ionic aggregation. Blending two or more monodisperse materials did not replicate the NMR spectrum of a polydisperse material; however, the behavior of the blend with annealing paralleled that of polydisperse NaSPS.

References for Chapter Seven

1 Yarusso, D.J.; Cooper, S.L.; *Polymer*, 1985, **26**, 371.

2 Peiffer, D.G.; Weiss, R.A.; Lundberg, R.D. *J. Polym. Sci., Polym. Phys. Ed.* 1982, **20**, 1503.

3 Ding, Y.S.; Hubbard, S.R.; Hodson, K.A.; Register, R.A.; Cooper, S.L. *Macromol.* 1988, **21**, 1698.

4 Weiss, R.A.; Lefelar, J.A. *Polymer*, 1986, **27**, 3.

5 Galambos, A.F.; Stockton, W.B.; Koberstein, J.T.; Sen, A.; Weiss, R.A. *Macromol.* 1987, **20**, 3091.

6 Register, R.A.; Sen, A.; Weiss, R.A.; Cooper, S.L. *Macromol.* 1989, **22**, 2224.

7 Grady, B.P.; Cooper, S.L. *Macromol.* 1994, **27**, 6627.

8 Grady, B.P.; Cooper, S.L. *Macromol.* 1994, **27**, 6635.

9 Galambos, A.F.; Stockton, W.B.; Koberstein, J.T.; Sen, A.; Weiss, R.A.; Russell, T.P. *Macromol.* 1987, **20**, 3091.

10 Toriumi, H.; Weiss, R.A.; Frank, H.A. *Macromol.* 1984, **17**, 2104.

11 Hara, M.; Jar, P.; Sauer, J.A. *Polymer*, 1991, **32**, 1380.

12 Hara, M.; Jar, P.; Sauer, J.A. *Polymer*, 1991, **32**, 1622.

13 Hara, M.; Jar, P.; Sauer, J.A. *Macromol.*, 1988, **21**, 3186.

14 Bellinger, M.; Sauer, J.A.; Hara, M. *Macromol.* 1994, **27**, 1407.

15 Lantman, C.W.; MacKnight, W.J.; Peiffer, D.G.; Sinha, S.K.; Lundberg, R.D. *Macromol.*, 1987, **20**, 1096.

16 Lantman, C.W.; MacKnight, W.J.; Higgins, J.S.; Peiffer, D.G.; Sinha, S.K.; Lundberg, R.D. *Macromol.*, 1988, **21**, 1339.

17 Lantman, C.W.; MacKnight, W.J.; Sinha, S.K.; Peiffer, D.G.; Lundberg, R.D.; Wignall, G.D. *Macromol.*, 1988, **21**,1344.

18 Peiffer, D.G.; Kaladas, J.; Duvdevani, I.; Higgins, J.S. *Macromol.*, 1987, **20**, 1397.

19 Pedley, A.M.; Higgins, J.S.; Peiffer, D.G.; Rennie, A.R. *Macromol.* 1990, **23**, 2494.

20 Wu, J.L.; Hara, M. *Macromol.* 1994, **27**, 923.

21 Bodycomb, J.; Hara, M. *Macromol.* 1994, **27**, 7369.

22 Chu, B.; Wu, D.-Q.; MacKnight, W.J.; Wu, C.; Phillips, J.C.; LeGrand, A.; Lantman, C.W.; Lundberg, R.D. *Macromol.*, 1988, **21**, 525.

23 Onogi, S.; Masuda, T.; Kitagawa, K. *Macromol.* 1970, **3**, 109.

24 Masuda, T.; Kitagawa, K.; Onogi, S. *Macromol.* 1970, **3**, 116.

25 Graessley, W.W. *Adv. Polym. Sci.*, 1974, **16**, 3.

26 Ferry, J.D. *Viscoelastic Properties of Polymers*, 3rd Ed.;John Wiley & Sons: New York, 1980.

27 Nielson, L.E. *Polymer Rheology*; Marcel Dekker, Inc.: New York, 1977.

28 Soong, D.; Shyu, S.S.; Shen, M. *J. Macromol. Sci.-Phys.* 1981, **B19**, 49.

29 Wyman, D.P.; Elyash, L.J.; Frazer, W.J. *J. Polym. Sci. A*, 1965, **3**, 681.

30 Lee, C.L.; Polmanteer, K.E.; King, E.G. *J. Polym. Sci. A-2*, 1970, **8**, 1909.

31 Mills, N.J.; Nevin, A. *J. Polym. Sci. A-2*, 1971, **9**, 267.

32 Merz, E.H.; Nielson, L.E.; Buchdahl, R. *Ind. Eng. Chem.* 1951, **43**, 1396.

33 McCormick, H.W.; Brower, F.M.; Kin, L. *J. Polym. Sci.* 1959, **39**, 87.

34 Jackson, J.K; Winter, H.H. *Macromol.* 1995, **28**, 3146.

35 Watanabe, H.; Kotaka, T. *Macromol.* 1984, **17**, 2316.

36 Prest, W.M.; Porter, R.S. *Polym. J.* 1973, **2**, 154.

37 Wasserman, S.H.; Graessley, W.W. *J. Rheol.* 1992, **36**, 543.

38 Thomas, D.P.; Hagan, R.S. *Polym. Eng. Sci.* 1969, **9**, 164.

39 Chartoff, R.P.; Maxwell, B. *Polym. Eng. Sci.* 1969, **9**, 159.

40 Prest, W.M. *J. Polym. Sci. A-2*, 1970, **8**, 1897.

41 Yano, O.; Wada, Y. *J. Polym. Sci. A-2*, 1971, **9**, 669.

42 Callaghan, P.T.; Pinder, D.N. *Macromol.* 1985, **18**, 373.

43 Fleischer, G. *Polymer*, 1985, **26**, 1677.

44 Sharaf, M.A.; Mark, J.E.; Al-Ghazal, A.A.-R. *J. Appl. Polym. Sci., Appl. Polym. Symp.* 1994, **55**, 139.

45 Falender, J.R.; Yeh, G.S.; Mark, J.E. *J. Amer. Chem Soc.* 1979, **101**, 7353.

46 Falender, J.R.; Yeh, G.S.; Mark, J.E. *Macromol.* 1979, **12**, 1207.

47 Jérôme, R.; Broze, G. *Rubber Chem. Tech.* 1985, **58**, 223.

48 Tant, M.R.; Song, J.H.; Wilkes, G.L.; Horrion, J. Jérôme, R. *Polymer*, 1986, **27**, 1815.

49 Bagrodia, S.; Tant, M.R.; Wilkes, G.L.; Kennedy, J. *Polymer*, 1987, **28**, 2207.

50 Erhardt, P.F.; O'Reilly, J.M.; Richards, W.C.; Williams, M.W. *J. Polym. Sci. Symp.* 1974, **45**, 139.

51 Kim, J.S.; Yoshikawa, K.; Eisenberg, A. *Macromol.* 1994, **27**, 6347.

52 O'Connell, E.M.; Root, T.W.; Cooper, S.L. *Macromol.*, 1994, **27**, 5803.

53 O'Connell, E.M.; Root, T.W.; Cooper, S.L. *Macromol.*, 1995, **28**, 3995.

54 O'Connell, E.M.; Root, T.W.; Cooper, S.L. *Macromol.*, 1995, **28**, 4000.

55 Makowski, H.S.; Lundberg, R.D.; Singhal, G.S. U.S. Pat. 3,870,841 to Exxon Research and Engineering Company, 1975.

56 Toriumi, H.; Weiss, R.A.; Frank, H.A. *Macromol.* 1984, **17**, 2104.

57 Samoson, A.; Lippmaa, E. *Phys. Rev. B*, 1983, **28**, 6567.

58 Lippmaa, E.; Samoson, A.; Magi, M. *J. Am. Chem. Soc.* 1986, **108**, 1730.

59 Fitzgerald, J.J.; Weiss, R.A. *J. Polymer Sci., Phys. Ed.* 1990, **28**, 1719.

60 Lundberg, R.D; Phillips, R.R. *J. Polym. Sci., Phys. Ed.* 1982, **20**, 1143.

61 Lundberg, R.D., in *Structure and Properties of Ionomers*, Pineri, M.; Eisenberg, A., eds. D. Reidel Publishing Co.: Dordrecht, Holland, 1987.

62 Kundla, E.; Samoson, A.; Lippmaa, E. *Chem. Phys. Lett.* 1981, **83**, 229.

63 Samoson, A. *Chem. Phys. Lett.* 1985, **119**, 25.

64 Williams, C.E.; Russell, T.P.; Jérôme, R,; Horrion, J. *Macromol.* 1986, **19**, 2877.

65 Plante, M.; Bazuin, C.G.; Jérôme, R. *Macromol.* 1995, **28**, 1567.

Chapter Eight: Carboxylated Ionomers

8.1 Introduction

Several studies of carboxylated polystyrenes (CPS) have been reported in the literature.[1-8] In general, the carboxylic acid-based ionomers are considered to have weaker ionic aggregates than the sulfonated ionomers because of the differences in acid strength between the two anions. In studies comparing the two types of ionomers, Lundberg and Makowski[1] reported dramatically higher melt viscosities for NaSPS compared to NaCPS. In solution studies with relatively low polarity solvents, the reduced viscosity of NaSPS showed a significantly higher concentration dependence than NaCPS, and addition of polar cosolvents had a larger effect on the concentration dependence of NaSPS. Yarusso and Cooper[2] found that the size and concentration of aggregates did not vary with anion type for ZnSPS and ZnCPS, however, they did note that the thickness of the region of restricted mobility surrounding the aggregates was less for the carboxylate ionomers. Hird and Eisenberg[3] reported different sizes and interaggregate spacings (d) for NaSPS (d=37Å) and NaCPS (d=31Å). This discrepancy could be due to either cation type or sample preparation, since the CPS used by Yarusso and Cooper was synthesized by direct metalation of the polystyrene (identified here as NaCPS materials)[1,2] and the CPS used by Hird and Eisenberg was synthesized via a Friedel-Crafts acetylation reaction.[3] Tomita and Register reported differences in morphology and dynamic mechanical properties for CPS ionomers synthesized through free-radical polymerization of vinylbenzoic acid and styrene (identified here as VBA materials)[4] and CPS materials synthesized via carboxylation of poly(styrene co-bromostyrene) polymers.[5,6]

To determine the effects of anion type on the ^{23}Na NMR spectrum of polystyrene ionomers, ^{23}Na NMR experiments of three carboxylated polystyrene ionomers with ~2%, ~4% and ~8% COONa groups and of three carboxy-telechelic polystyrene ionomers are reported here. Results from proton NMR and molecular weight characterization of HCPS materials (samples identified as VBA) with ~0%, ~2%, ~4%, ~6% and ~8% COOH groups are also reported in this chapter.

8.2 Carboxylated Polystyrene

8.2.1 Characterization

Elemental analysis was completed by Galbraith Laboratories; the amount of sodium (wt% and mol%) in each ionomer is reported in Table 8-1. Since the ion content of the samples is slightly higher than to the ideal content, these ionomers are overneutralized. As was shown in Chapter 4, overneutralization may affect the ^{23}Na NMR spectra of these materials; however, the overneutralization levels are fairly small (~20%) and are less than the massive overneutralization required to produce a new Na^+ environment in NaSPS, so these samples are likely to be indicative of typical, fully-neutralized behavior.

Characterization of these NaCPS ionomers was complicated by the fact that the materials were not soluble in solvents normally used to dissolve ionomers (e.g. THF, toluene/methanol). This is probably due to a some crosslinking of the ionomer during the carboxylation reaction. Tomita and Register have reported similar problems with CPS synthesized in the same manner.[4] Because of this insolubility, solution-state ^{13}C NMR to determine

Table 8-1: Weight percent sodium in NaCPS

Sample Identification	Ideal wt% Na	Actual wt% Na
NaCPS–2	0.44	0.53
NaCPS–4	0.86	1.04
NaCPS–8	1.7	2.10

the carboxylic acid content could not be completed. Solid-state ^{13}C NMR was attempted for the 8% and 4% CPS samples. No distinct peak attributable to sodium-neutralized carboxylic acid sites could be identified in spectra using either cross polarization or direct observation (Figure 8-1a). The NMR spectrum of a carboxylated polyurethane clearly shows peaks due to both COOH and COONa (Figure 8-1b). These peaks are at 176 ppm and 181 ppm, respectively. Although some intensity in CPS may be present around 171 ppm in Figure 8-1a, peaks due to COOH or COONa cannot be clearly identified, so the exact ionization level is not known for these materials. Ion content could not be determined from ion exchange and titration because of insolubility.

8.2.2 Solid-State ^{23}Na NMR Studies

The ^{23}Na NMR spectra of NaCPS–2, –4, and –8 are shown in Figure 8-2. All three samples show the broad NMR peak at negative ppm values that is characteristic of aggregated ions. The peak appears to be more symmetric than the aggregate peaks in NaSPS. The exact position of this peak cannot be compared with that of the sulfonates because of the overneutralization, although they appear to be roughly comparable; NaCPS–4 appears upfield of NaSPS but the reverse is true for NaCPS–8 and NaSPS–6 (Figure 8-3). However, the NaCPS aggregate peaks are broader than the corresponding NaSPS materials. ^{23}Na NMR studies of TDI-based polyurethanes (Figure 8-4) show that the peak positions of the carboxylate and sulfonate ionomers are equivalent. Interestingly, the peak positions of the polyurethanes (~ –10 ppm) are farther downfield than the CPS and SPS ionomers, despite the fact that the ion contents of the polyurethane ionomers

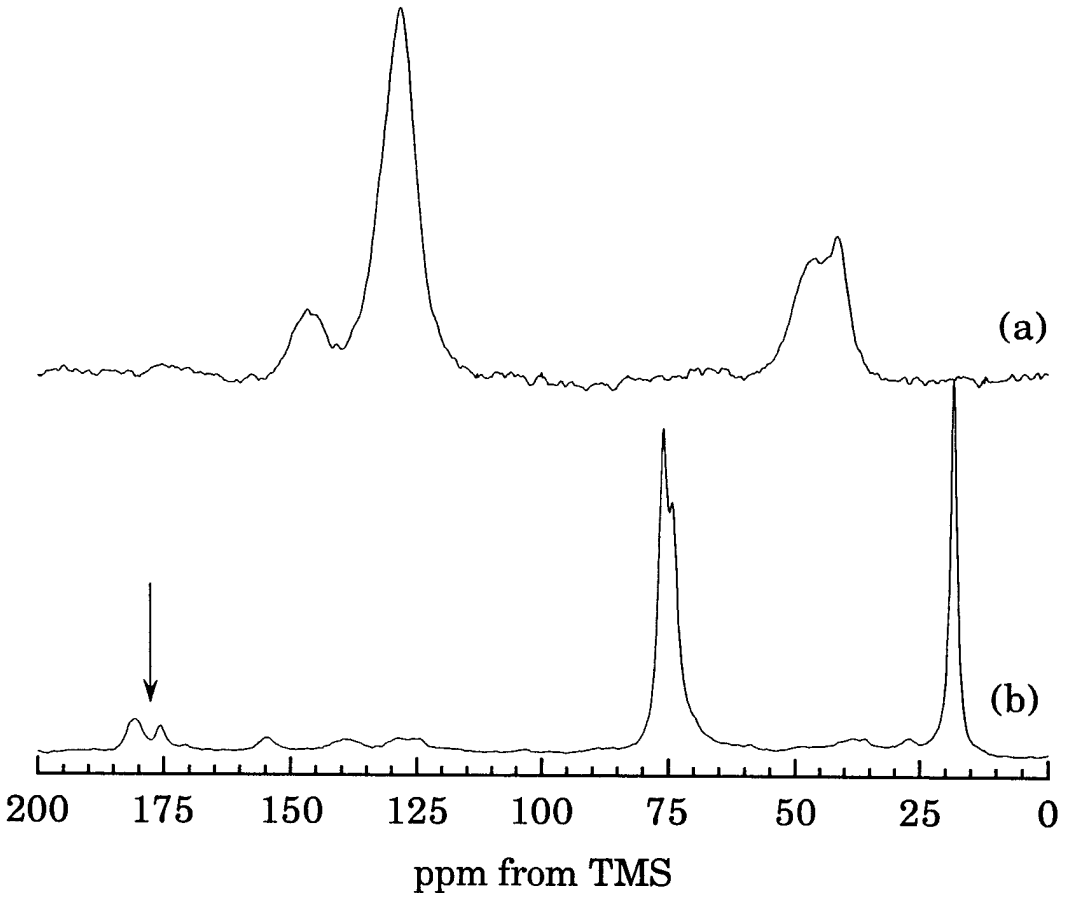

Figure 8-1: ^{13}C NMR spectra of a) NaCPS–8 and b) carboxylated PPO/TDI polyurethane.

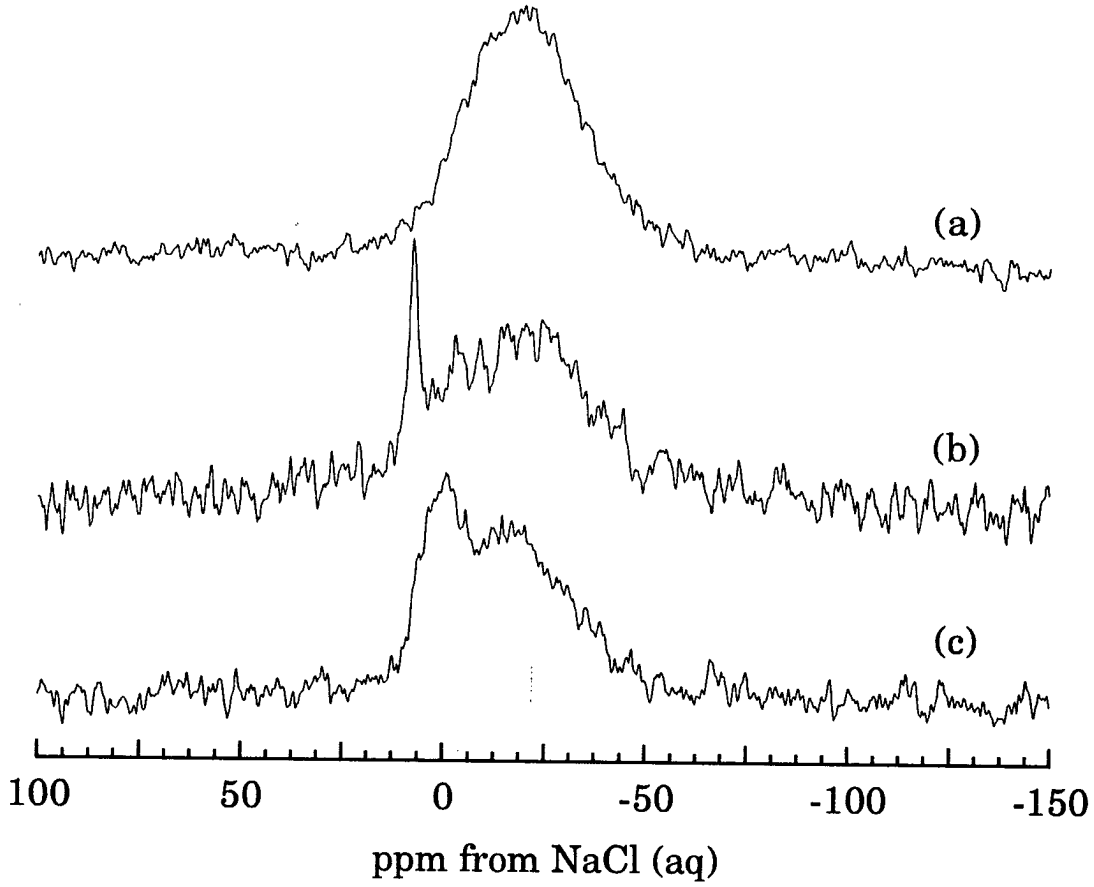

Figure 8-2: ^{23}Na NMR spectra of NaCPS at three ionization levels: a) 8%; b) 4%; c) 2%.

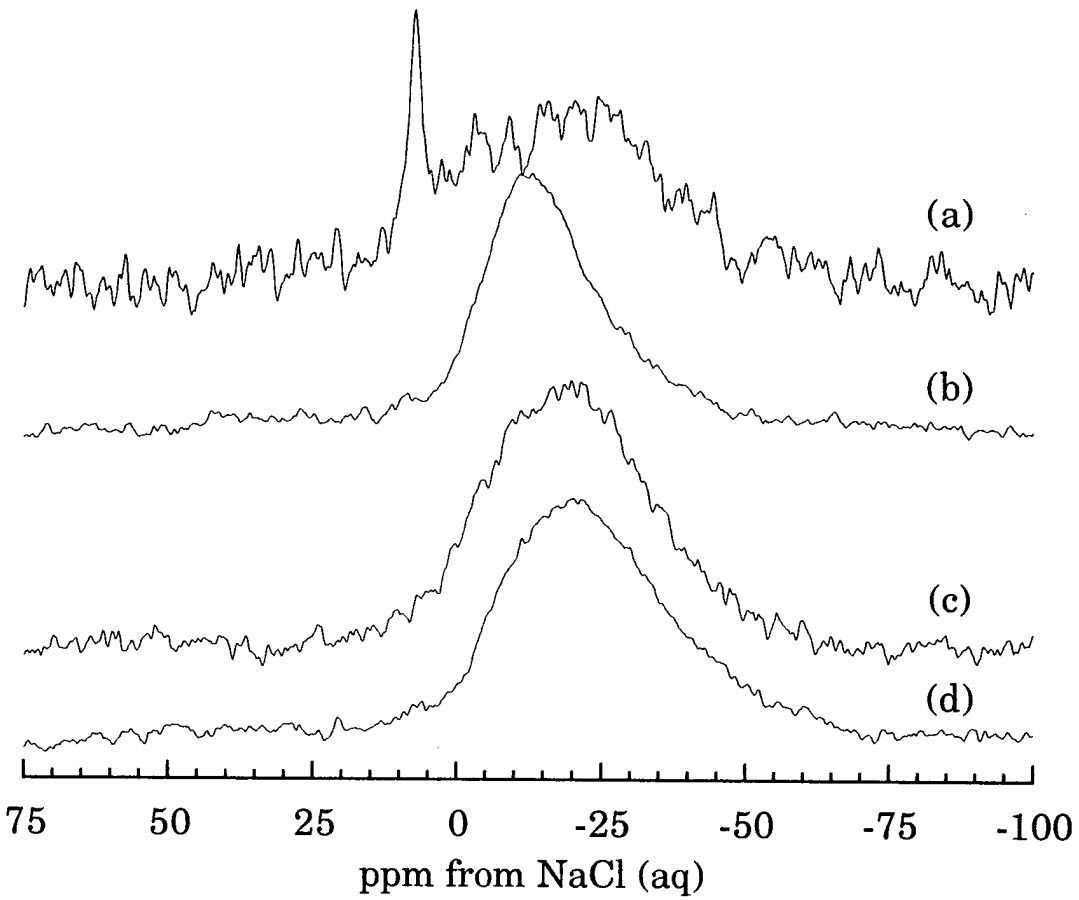

Figure 8-3: ^{23}Na NMR spectra of NaCPS and NaSPS:
a) NaCPS–4; b) NaSPS–4; c) NaCPS–8; d) NaSPS–6.

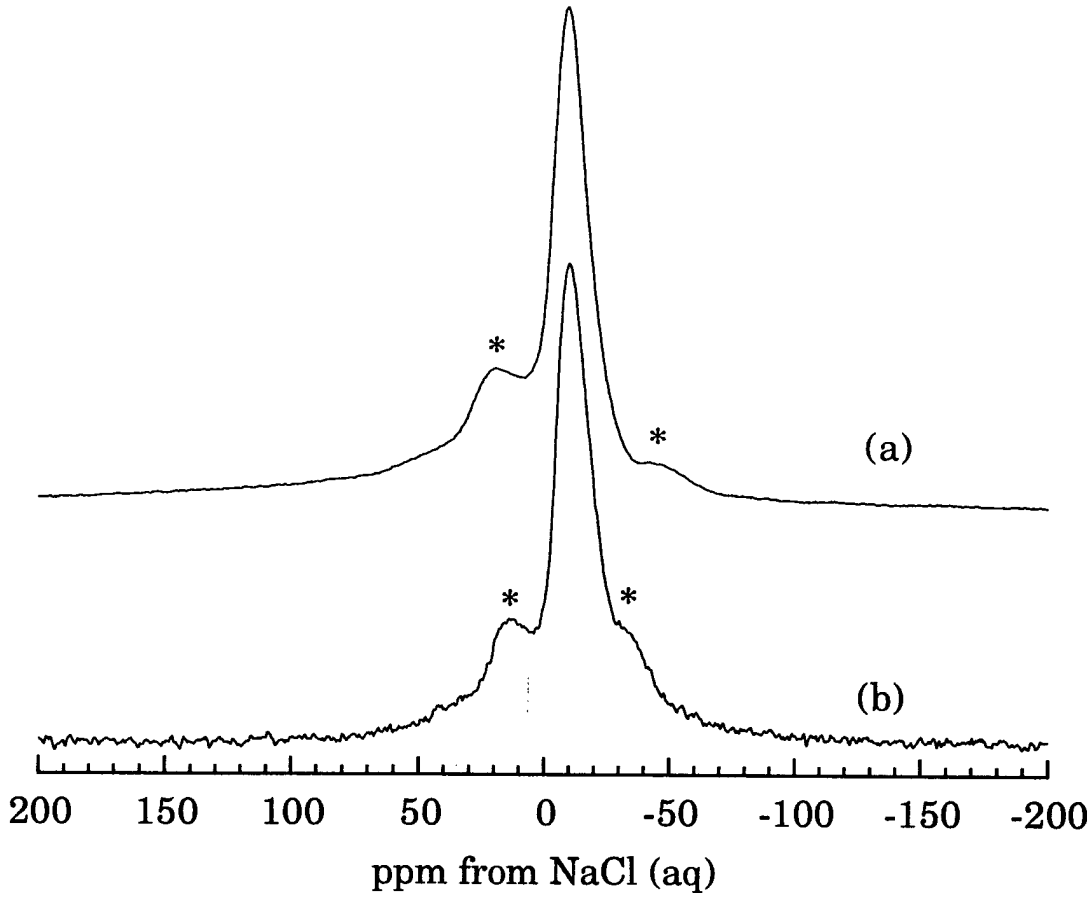

Figure 8-4: ^{23}Na NMR spectra of PPO/TDI polyurethane ionomers: a) sulfonated; b) carboxylated. The asterisks (*) denote spinning sidebands.

are higher (~1.5 meq/g for the polyurethanes; 0.16 to 0.54 meq/g for NaSPS–1.7 to –6.0). The differences could be due to backbone polarity, backbone T_g, or steric hindrances from the "side chain" to which the ionic groups is attached (alkyl chain versus styrene group).

Two other peaks are seen in the NMR spectra of NaCPS. NaCPS–2 shows a peak at 0 ppm similar to one in NaSPS that has been assigned to excess NaOH forming separate domains in the ionomer and indicative of overneutralization (Chapter 4). Since elemental analysis of this material does not indicate such a high overneutralization level, either the ion content is much lower than the desired 2% or neutralization was not uniform. NaCPS–4 also shows a second peak, but at 7 ppm. This narrow peak is at the same position as the peak due to isolated ions in NaSPS (Chapter 4); therefore, this peak is assigned to isolated ions in NaCPS. A second NaCPS–4 sample taken from the same synthesis batch shows far fewer isolated ions, indicating that the overall morphology of the batch is not uniform.

Although there may be some effect of cross-linking on the distribution of ions in NaCPS, it is important to note that at this ion content (4%) the sulfonated material (NaSPS) showed no isolated ions in the ^{23}Na NMR spectrum. The sample histories of the two materials are not different enough to account for this discrepancy; both samples are tested directly from post-polymerization ionization, precipitation, and drying. Therefore, the difference in the number of isolated ions in NaCPS–4 and NaSPS–4 is most likely due to the difference in electrostatic forces between sulfonate and carboxylate groups. Lefelar and Weiss[9] compared the packing of sodium ions around sulfonate and carboxylate groups and concluded that there is better packing of the ions in the sulfonate ionomers. Lundberg and Makowski[1] attributed

higher melt and solution viscosities of NaSPS to stronger ionic interactions of the sulfonate groups. Hird and Eisenberg[2] reported more well-defined plateau moduli for NaSPS ionomers than NaCPS materials and attributed the difference to greater stability of the sulfonate aggregates, again due to the greater electrostatic forces between sulfonate groups.

The positions of all ^{23}Na NMR peaks are relatively unchanged from NaSPS to NaCPS; therefore, the structure around the sodium ions, whether isolated or aggregated, are not dramatically altered when the anion type is changed. Similar results are seen when comparing the two anions in polyurethane ionomers. This is consistent with EXAFS studies[10,11] that have shown that SPS ionomers neutralized with certain monovalent cations (Rb^+ and Cs^+) have no discernible order in the aggregates. It is likely that disorder would average out the effects of different anion types. The increase in isolated ions as anion type is changed from sulfonate to carboxylate is also consistent with the lower electrostatic forces of the carboxylate anion.

8.3 Carboxy-Telechelic Polystyrene

Sodium-neutralized carboxy-terminated telechelic polystyrene ionomers (CTPS) at three different molecular weights were studied. Two ionic groups are present for each polymer chain, on each end of the chain. These telechelic ionomers have very regular spacings between ionic groups, however, the molecular weights of these model ionomers are relatively low when the ion contents are within the same range as random ionomers (1-10%). Figure 8-5 shows the spectra of CTPS–4000, –17,500, and –6000. The 6000 molecular weight material was synthesized at a different time that the other materials and has a dramatically different sample history, and so is expected to show a

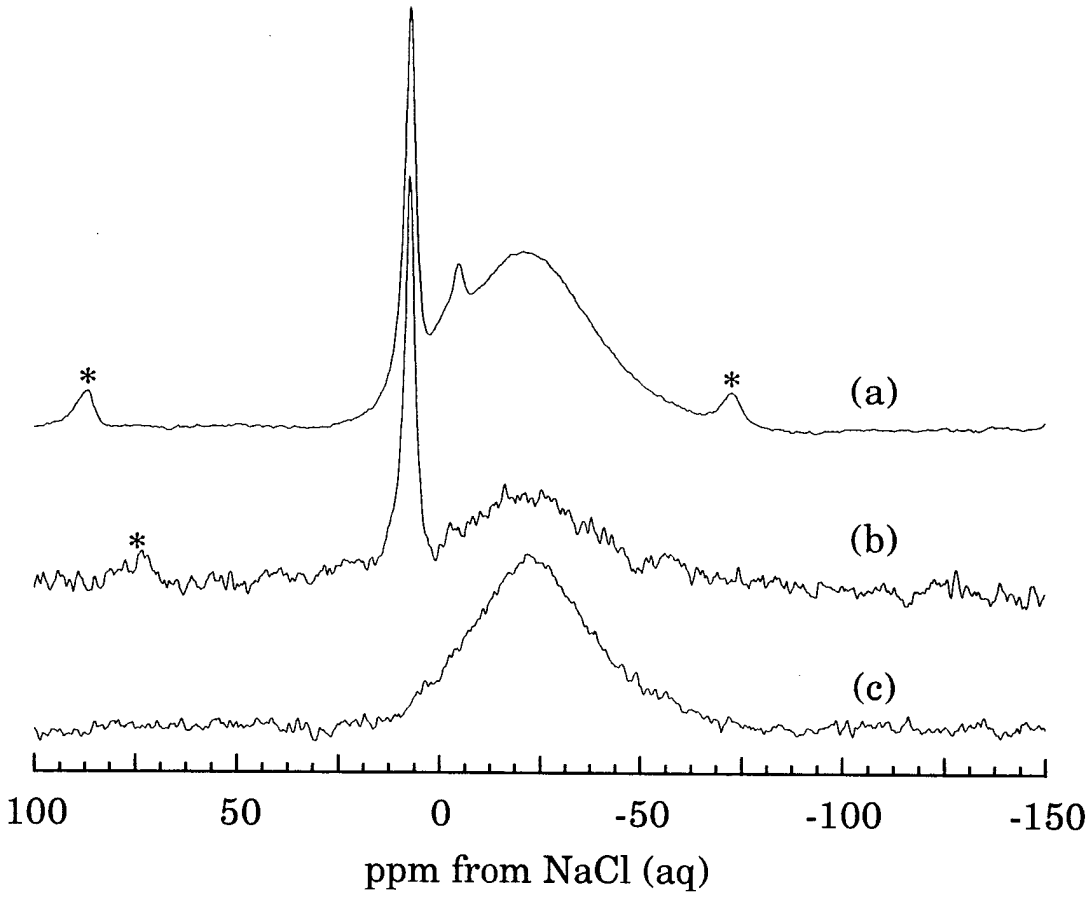

Figure 8-5: ^{23}Na NMR spectra of CTPS ionomers: a) M_n=4,000; b) M_n=17,000; c) M_n=6,000. (*) identifies spinning sidebands.

different morphology. The CTPS–4000 and 17,500 samples may have been dissolved in toluene for solution studies,[7] but this is not expected to change the morphology of the ionic aggregates (Chapter 5).

Both the CTPS–4000 and –17,500 materials in Figure 8-5 contain isolated ions (roughly 38% and 27%, respectively). The ionomer with the higher molecular weight, and correspondingly lower ion content, has a higher fraction of isolated ions. These telechelic ionomers also show a larger fraction of isolated ions than do the sulfonated ionomers (NaSPS) at the same ion contents, supporting the idea that the carboxylic acid anion is not as effective in forming aggregates. The peak due to isolated ions is shifted slightly from that seen in the NaCPS materials, to 7.8 ppm.

The CTPS–4000 material also shows a peak around –4.3 ppm, which has not been reported before. It was initially anticipated that this peak is due to overneutralization, but most overneutralized materials do not show isolated ions (see NaCPS–2 in Figure 8-2), and the neutralizing agent, CH_3ONa, has a peak near 0 ppm, has a width at half height of more than 10 ppm, and shows a broadened quadrupolar shape. This new peak in CTPS–4000 has no quadrupolar pattern. It is at a different position than the NMR peak seen in monodisperse NaSPS (Chapter 7), and appears at an M_n well below the entanglement molecular weight for polystyrene. Finally, the peak does not appear in the CTPS–6000 or 17,500. More study would be needed to determine if this peak is related to the polymer morphology or is an artifact due to sample contamination.

As seen for NaCPS, the aggregate peaks in CTPS are more symmetrical than the peaks in NaSPS. In addition, the peak maxima are shifted farther upfield than either the NaCPS or NaSPS materials and do not

vary greatly with ion content. This shift to lower ppm compared to the random ionomers could be due to more structured aggregates. Telechelics are considered to be more well-ordered than random ionomers because of their low molecular weight (reducing entanglements) and regular spacings between ionic groups. Williams *et al.*[12] showed that monodisperse telechelic polyisoprene ionomers have narrow interfaces between the two phases. The researchers referred to EXAFS studies[13,14] that showed two coordination shells around metal cations in telechelic ionomers and concluded that these materials have a high degree of local order in the aggregates. The overall morphology of the ionomers was also considered to be well-ordered, with the spacing between aggregates controlled by the polymer chain molecular weight.[12]

8.4 Other ionomers

An alternative synthesis for NaCPS is copolymerization of vinylbenzoic acid and styrene to form HCPS, which can then be neutralized. This procedure has been detailed by Register and Tomita.[4] One downside to this procedure is that the backbone molecular weight is not constant as ion content is changed, since incorporation of the carboxylic acid group occurs during polymerization, not post-polymerization as in the synthesis of the materials in section 8.2. However, if the molecular weight is high enough and does not vary widely from sample to sample, its effects on properties should be minimized. An additional drawback of this procedure is that the reaction is free-radical, so the final materials will be polydisperse.

The molecular weights of the HCPS materials were determined though viscometric experiments. Plots of reduced viscosity (η_{sp}/c) versus ionomer concentration in THF are shown in Figure 8-6. The data are fitted to the

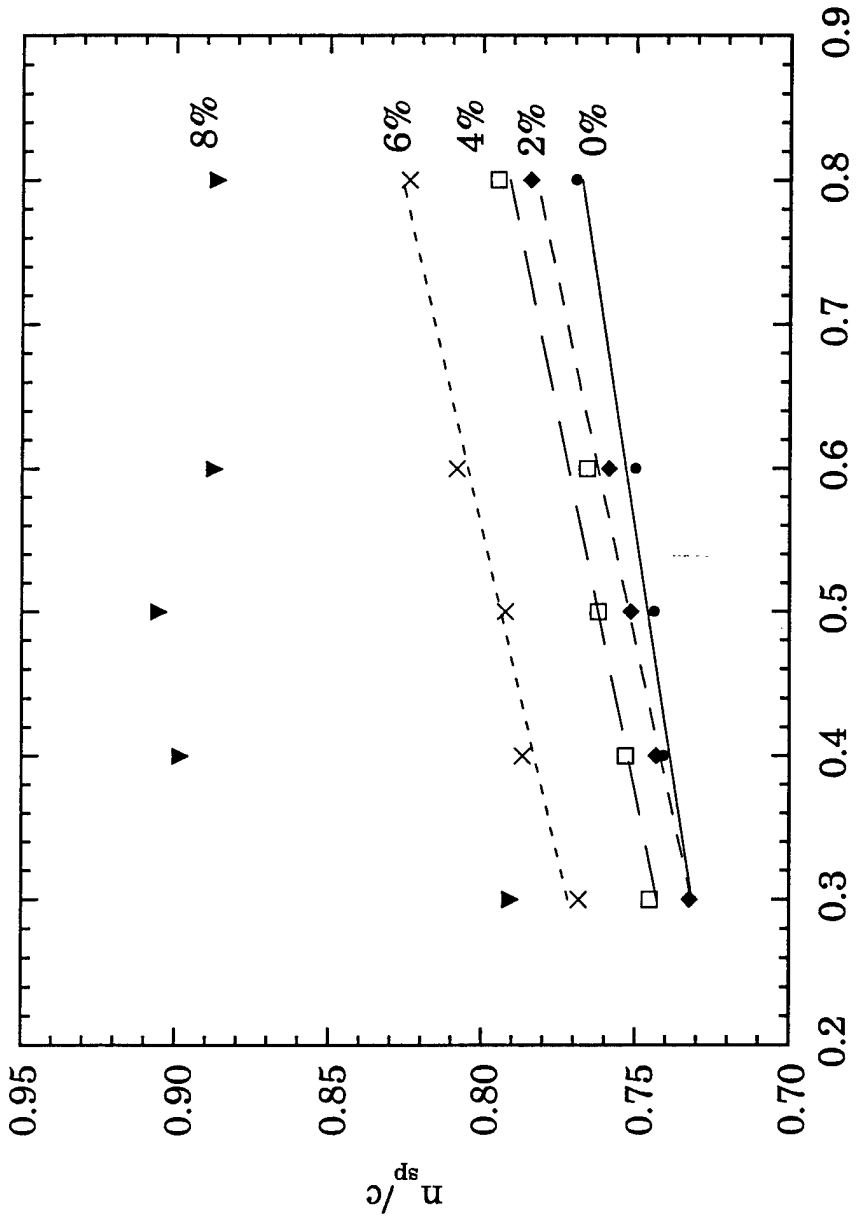

Figure 8-6: Plots of reduced viscosity versus concentration for polystyrene (VBA–0) and four HCPS (VBA) samples. The lines correspond to fitting the data to the Huggins equation, as discussed in the text.

Huggins equation[12] (Chapter 3). The intrinsic viscosity ([η]) of the material can be determined from the intercept of the fitted line; then, the viscosity average molecular weight can be determined from [η] using the Mark-Houwink equation. For the VBA–0,–2, and –4 materials, $M_v \sim 190{,}000$ (see Table 8-2). Even at high dilutions VBA–6 is at the upper limit of HCPS solubility in THF; VBA–8 showed micellar behavior in the viscosity experiments (Figure 8-6). The samples with higher ionic content (10%) are not soluble in THF, but are expected to have similar molecular weights. The values of k_1 from the Huggins equation give an indication of the polymer-solvent interactions. Good polymer-solvent conditions are demonstrated by $k_1 \leq 0.3$; $k_1 > 0.5$ indicates association.

Carboxylic acid content for the VBA samples can be determined through solution-state ^1H NMR. The carboxyl proton, which does not appear in VBA–0, appears between 7.6 and 7.9 ppm for VBA–6. This is next to the range for the aromatic protons, 6.3 to 7.3 ppm. The ionic content of the VBA materials can be approximated using the ratio of areas of the carboxyl and aromatic peaks. In the case of VBA–6, the NMR indicates an ion content near 5%. Therefore, the actual ion content achieved through this synthetic route is close to the desired ion level.

A standard synthetic route for the production of NaCPS has not yet been determined. Many different procedures have been proposed and studied.[3,4] For low ion contents (< 2%), the procedure of Lundberg and Makowski is acceptable, but for higher ion contents the product is insoluble in solvents typically used with ionomer systems.[4] The procedure of Tomita and Register[4] leads to a soluble acid-form of the ionomer with a molecular weight

Table 8-2: Viscosity-average molecular weights and Huggins parameters for NaCPS

Sample Identification	[η] dl/g	M_v	k_1
VBA–0	0.710	194,000	0.143
VBA–2	0.714	196,000	0.190
VBA–4	0.701	191,000	0.207
VBA–6	0.740	206,000	0.199

that can be reproduced reliably, but the procedure is limited to polydisperse ionomers.

8.5 Conclusions

NaCPS ionomers have been studied with ^{23}Na NMR and compared to similar NaSPS materials that were discussed earlier (Chapters 4-7). For the random ionomers, the two types of materials have the approximately the same peak positions for the aggregated sodium ions, but the shapes are somewhat different. In NaCPS, the aggregate peaks are broader and more symmetrical. The position of the isolated ions is equivalent in the two materials. At a given ion content, NaCPS has more isolated ions than NaSPS because of the weaker electrostatic interactions of the carboxylate anions. Carboxy-telechelic polystyrene ionomers also show more isolated ions than NaSPS for the same ion contents. Additionally, CTPS materials show more symmetrical peak shapes and upfield chemical shifts for the peak due to aggregated ions relative to the NaSPS materials. The ^{23}Na NMR characterization of the carboxylated and sulfonated polystyrene ionomer shows behavior consistent with previous studies comparing the morphology and behavior of ionomeric materials containing the two anions.

References for Chapter Eight

1 Lundberg, R. D.; Makowski, H.S. *Am. Chem. Soc. Adv. Chem.* 1980, **187**, 21.

2 Yarusso, D. J.; Cooper, S.L. *Polymer*, 1985, **26**, 371.

3 Hird, B; Eisenberg, A. *J. Polym. Sci., Polym. Chem. Ed.* 1993, **31**, 1377.

4 Tomita, H.; Register, R.A. *Macromol.* 1993, **26**, 2791.

5 Brockman, N.L.; Eisenberg, A. *J. Polym. Sci. Polym. Chem. Ed.* 1983, **21**, 3563.

6 Brockman, N.L.; Eisenberg, A. *J. Polym. Sci. Phys. Phys. Ed.* 1985, **23**, 1145.

7 Clas, S.-D.; Eisenberg, A. *J. Polym. Sci. Phys. Phys. Ed.* 1986, **24**, 2767.

8 Karayianni, E.; Cooper, S.L. *I&EC Research*, 1994, **33**, 2492.

9 Lefelar, J.A.; Weiss, R.A. *Macromol.* 1984, **17**, 1145.

10 Yarusso, D.J.; Ding, Y.S.; Pan, H.K.; Cooper, S.L. *J. Polym. Sci., Polym. Phys. Ed.* 1984, **22**, 2073.

11 Pan, H.K.; Knapp, G.S.; Cooper, S.L. *Coll. Polym. Sci.* 1984, **262**, 734.

12 Williams, C.E.; Russell, T.P.; Jérôme, R.; Horrion, J. *Macromol.* 1986, **19**, 2877.

13 Galland, D.; Belakhovsky, M.; Medrignac, F.; Pinéri, M.; Vlaic, G.; Jérôme, R. *Polymer*, 1986, **27**, 883.

14 Jérôme, R,; Vlaic, G.; Williams, C.E. *J. Phys. Lett.* 1983, **44**, 717.

Chapter Nine: Characterization of Polyurethanes Blended with Metal Acetates

9.1 Introduction

Polyurethanes are linear block copolymers that are classified as thermoplastic elastomers. Thermoplastic elastomers are phase-separated materials in which one phase consists of rubbery or "soft" domains and the other glassy or semi-crystalline "hard" domains. Incompatibility of the hard and soft segments leads to phase separation, with the hard domains acting as physical crosslinks and reinforcing filler.

Recently, researchers have studied blends of polymers, including thermoplastic elastomers, which contain complexing agents. One of the most commonly used polymers for complexation is poly(4-vinylpyridine) (P4VP), or poly(styrene co-4-vinylpyridine) (PSVP), because the pyridine nitrogen is believed to coordinate readily with transition metal ions. Agnew[1] first presented evidence of interactions in blends of metal chlorides with vinylpyridines and P4VP. Peiffer *et al.*[2,3] showed interaction in blends of a zinc-neutralized sulfonated thermoplastic elastomer (Zn S-EPDM) and PSVP. Blending the interacting components led to marked improvements in tensile properties, melt viscosity, and dynamic mechanical properties compared to a blend of Zn S-EPDM and polystyrene. Belfiore *et al.*[4] used ^{13}C NMR to study interactions in polymer systems by tracking the chemical shift of the acetate carbonyl site as zinc acetate was blended with P4VP at several different ratios. FTIR and ^{13}C NMR were also used to study cobalt, nickel and ruthenium complexes.[5]

In two papers studying the effects of complexation in phase-separated polymers, a new polyurethane containing a pendant pyridine group was presented.[8,9] Enhancements in tensile and dynamic mechanical properties were seen when these new materials were blended with transition-metal acetates; for example, the moduli of the blends were 10–35 times that of the precursor material.[8] The morphology of the material, as studied by small-angle x-ray scattering (SAXS), was not dramatically affected by the blending (Figure 9-1); the position of the SAXS peak did not shift appreciably with blending. EXAFS studies were undertaken to determine the local structure surrounding the cations in the blends, but results were inconclusive.[9]

This chapter describes a continued molecular-level approach to understand the causes behind the improved properties of the blends. ^{13}C and ^{15}N nuclear magnetic resonance were used to study the carbon and nitrogen sites in the urethane linkage and the pyridine chain extender, as well as the carbon nuclei in the acetate complexing agent. IR studies were also undertaken to identify changes in the pyridine C–N stretching region and urethane nitrogen region with blending. The goal was to correlate the effects of blending to changes in the chemical shifts and relaxation times for the carbon and nitrogen sites on the pyridine group that are proposed to interact with the metal salts. The results can be used to explain the mechanical and morphological properties acquired from tensile testing and small-angle x-ray scattering. In this way the structure-property relationships of the blends can be determined.

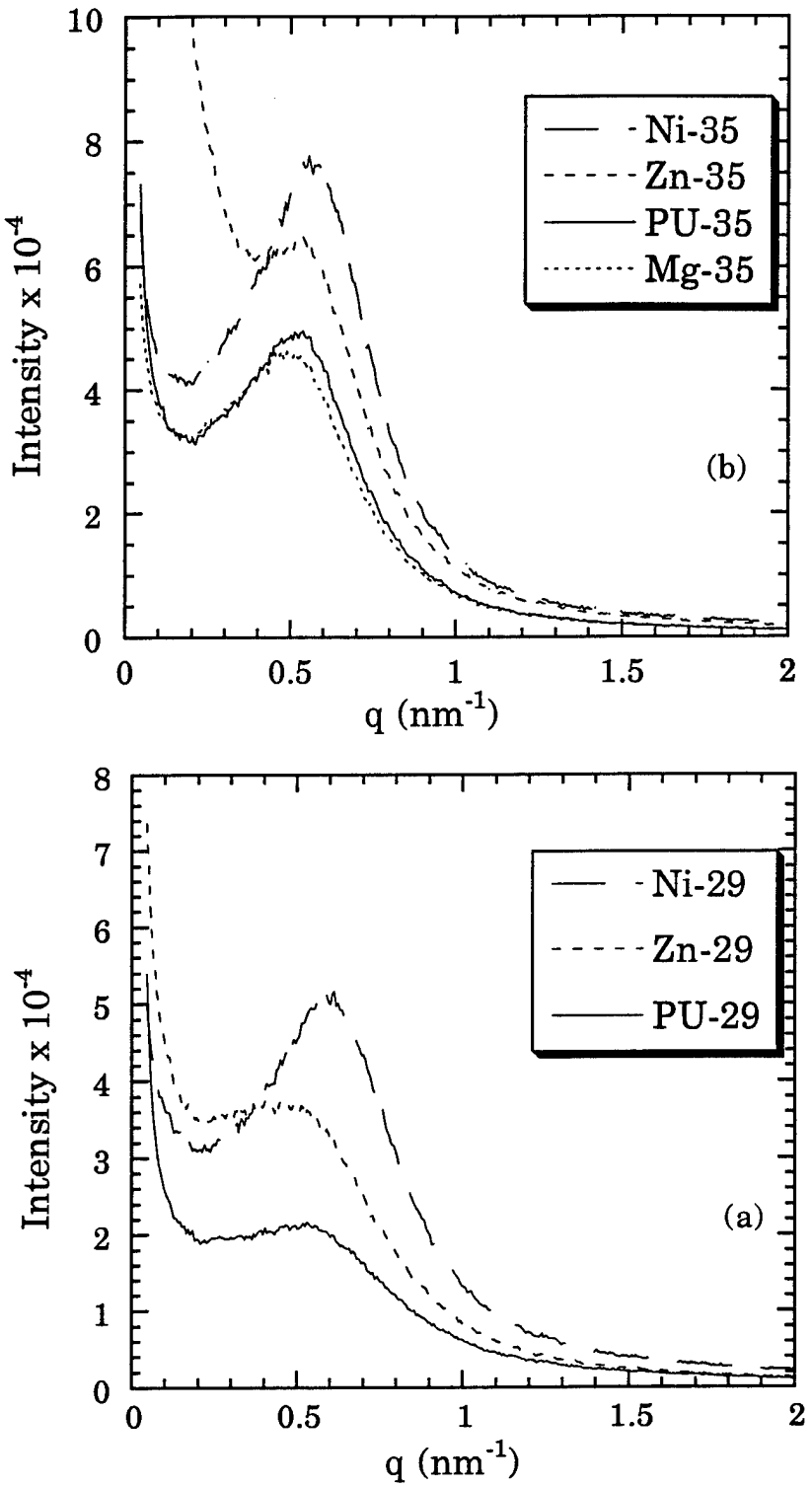

Figure 9-1: SAXS patterns for a) PU–29 and its blends with metal acetates and b) PU–35 and its blends with metal acetates.

9.2 Results and Discussion

In an earlier article[8] a morphology for the pyridine-containing polyurethane was proposed. The proposed morphology of the PU-35 material was that of an interconnected hard-domain, while PU-29 possessed a dispersed hard-domain morphology, with the soft domain as the continuous phase. Addition of the metal acetates to PU-35 improved the hard-domain cohesion and strength dramatically but only slightly affected the phase separation. For PU-29, it was suggested that addition of the metal ions increased the number of physical crosslinks, but again altered the phase separation only slightly. This was confirmed with SAXS experiments (Figure 9-1); the precursor polymers were phase-separated materials, and addition of the metal acetates did not dramatically change the morphology. The position of the SAXS peak shifts slightly to higher scattering angles (smaller Bragg spacings) after blending, indicating a small improvement in phase separation, and the peak sharpens, indicating a more narrow distribution of domain spacings. The peak is near 0.5 nm^{-1}; based on this position and the hard-segment content of the polyurethanes, the morphology is considered to be lamellar. The increase in scattered intensity for most blends is due to the increased electron density of the metal ions in the hard domain. Only one SAXS peak is present, so any pyridine:acetate complex does not create ionic-like domains, as are typically seen at higher scattering vectors in polyurethane ionomers.[6,7] The SAXS peak in the PU-35 material is sharper than in the PU-29 sample, indicating a more well-developed morphology; this is expected since PU-35 has a higher hard-segment content.

A schematic of the components of PU-35 and a poly(ether-urethane) are shown in Figure 9-2. The traditional polyurethane does not contain the

(a) Soft Segment, PTMO

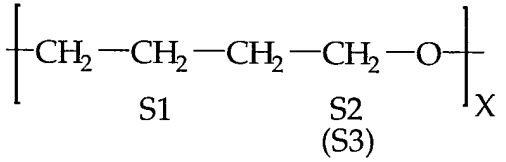

(b) Hard Segment, MDI/BD

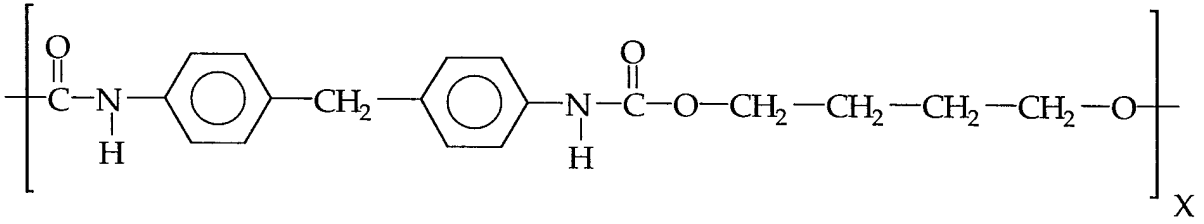

(c) Hard Segment, MDI/BIN

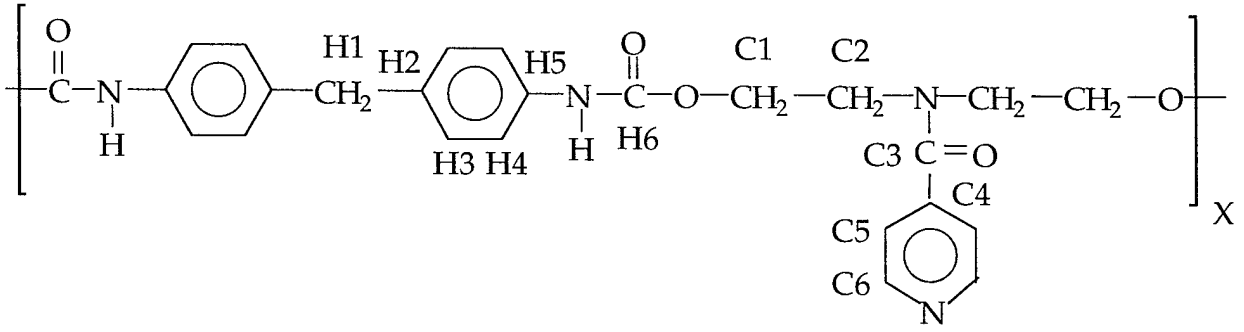

Figure 9-2: Schematics of a) PTMO, b) MDI/BD and c) MDI/BIN

pyridine group in the chain extender. Figure 9-3 shows the stress-strain curves of PU-35 and its blend with several transition-metal acetates.[8] It is apparent that blending dramatically improves both the modulus and ultimate strength of the polyurethane. It is proposed that the improvements in mechanical strength are due to the metal acetate complexing with the pyridine nitrogen on a molecular level. This supposition can be tested using spectroscopic methods.

9.2.1 Infrared Spectroscopy

Infrared spectroscopy (IR) is used extensively in the study of specific interactions in polymer blends.[10,11] Figure 9-4 shows the infrared spectrum of PU-35 compared with the spectrum of a commercial poly(ether-urethane) (Pellethane,® having a component ratio of 3/2/1 MDI/BD/PTMO), which does not contain the pyridine group. Likewise, an MDI/BIN hard segment-only material is compared to an MDI/BD hard segment in Figure 9-5. The peak due to the C–N stretch of the pyridine group is near 1630 cm^{-1}. Pyridine C–N and urethane N–H band positions for several of the polyurethane blends are shown in Table 9-1. Other researchers have studied pyridine-containing polymers; their IR bands and identifications for the pyridine groups are shown in Table 9-2. Identification of the other bands found in polyurethanes can be found elsewhere.[16]

Incorporation of the pyridine group into the polyurethanes affects the hydrogen bonding in the materials. The ratios of free and hydrogen-bonded carbonyls (1730 and 1703 cm^{-1}, respectively)[17] change when the pyridine-containing chain extender is incorporated into the material, although some of the change in the carbonyl ratio is due to the presence of the chain-extender

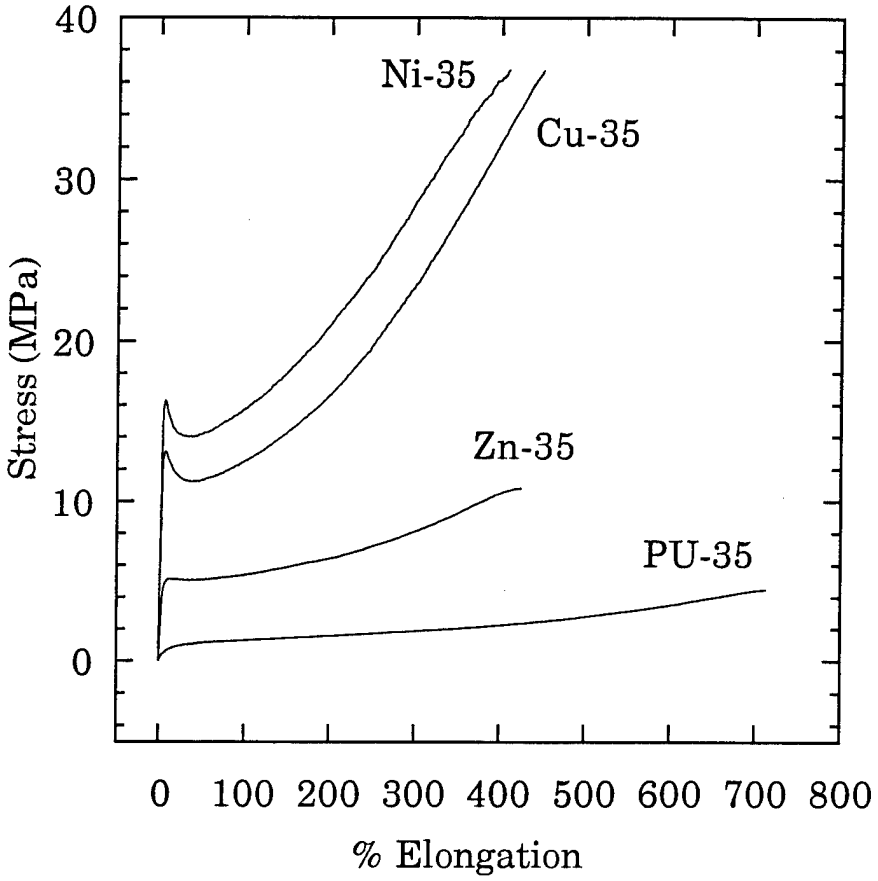

Figure 9-3: Stress-strain curves for PU–35 and its blends.[6]

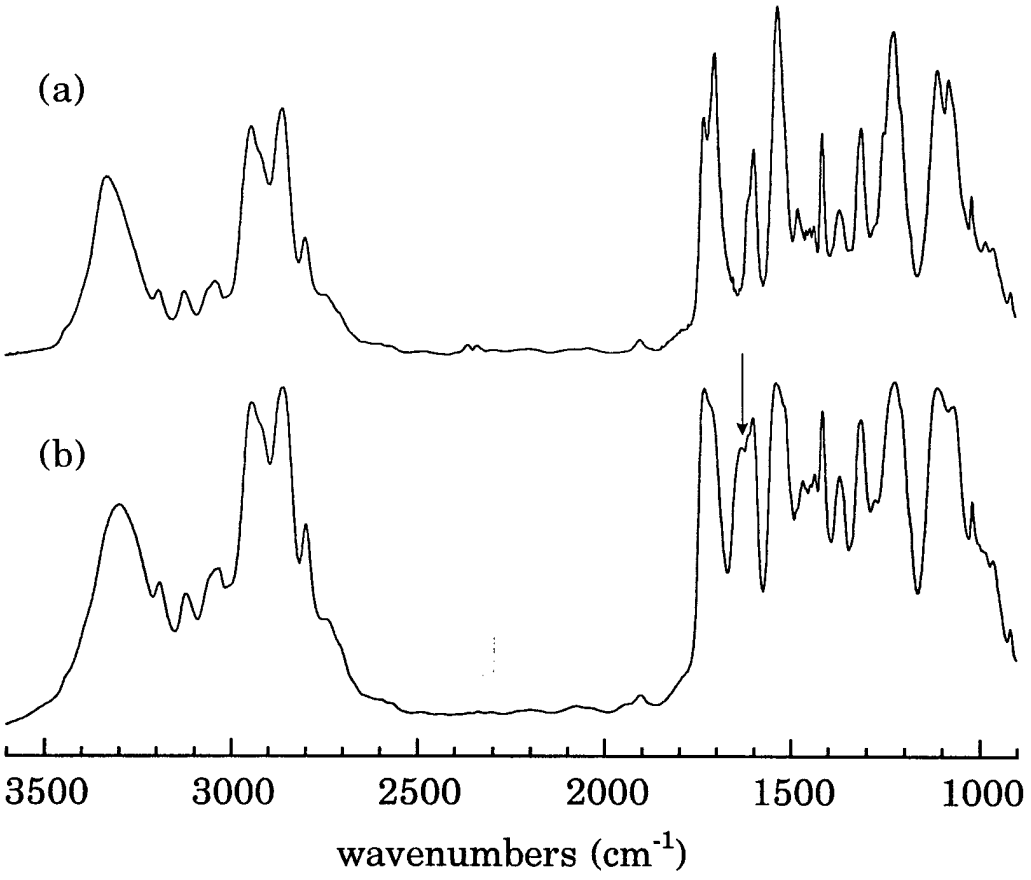

Figure 9-4: FTIR spectra of a) Pellethane, a commercial poly(ether-urethane) and b) PU–35. The arrow points to the pyridine C–N stretch.

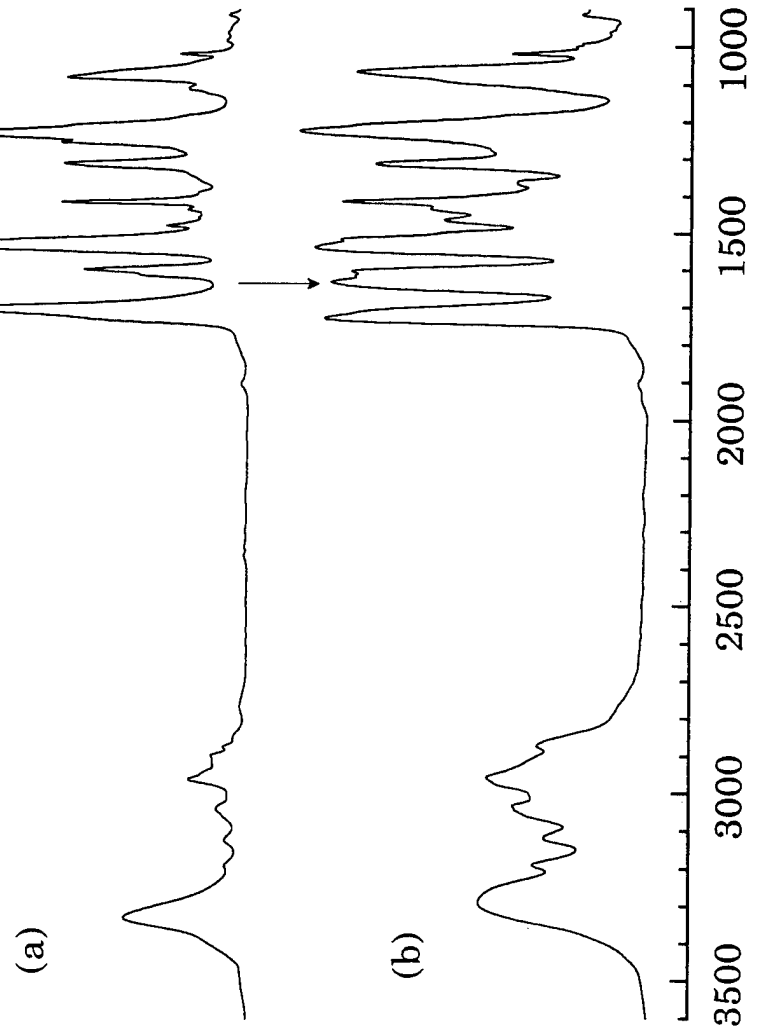

Figure 9-5: FTIR spectra of a) MDI/BD hard segment material and b) MDI/BIN. The arrow points to the pyridine C–N stretch.

Table 9-1: FTIR band positions for pyridine-containing polyurethanes and blends

Sample Identification	wavenumber, C=N stretch (cm^{-1})	wavenumber, H–bonded N–H
MDI/BD	–	3328
MDI/BIN	1630	3287
MDI/BIN/Zn	1634	3301
MDI/BIN/Mg	1633	3300
MDI/BIN/Na	1629	3293
Pellethane®	–	3329
Pu-29	1630	3296
Zn-29	1644	3304
Ni-29	1635	3303
Pu-35	1630	3295
Zn-35	1632	3302
Mg-35	1626	3300
Na-35	1626	3300
Ni-35	1632	3300

Table 9-2: FTIR band assignments

Author Material Description	wavenumber (cm^{-1})
Smith and Eisenberg[10]	
P4VP, C=C stretch in pyridine	1555
P4VP, C=N stretch in pyridine	1596
P4VP, band proportional to 4VP content	1414
$P4VPH^+$ pyridinium ion	1636
Sakurai *et al.*[11,12]	
pyridine stretching band in EAVP	1602
ring vibration of pyridinium cation	1638
pyridine stretching band in ZnSPS/EAVP blend	1621
Ng *et al.*[13]	
free pyridine ring stretch in EAVP	1598
pyridine stretch in EAVP/Zn-S-PET blends	1618
Peiffer *et al.*[2]	
pyridine ring C=N stretch in Zn-S-EPDM/PSVP blends	1615
Belfiore *et al.*[4]	
P4VP C=N stretch	1596
P4VP blended with zinc acetate, C=N stretch	1617

*EAVP is poly(ethyl acrylate-co-4-vinyl pyridine)

*Zn-S-PET is zinc-neutralized sulfonated poly(ethylene terephthalate)

*Zn-S-EPDM is zinc-neutralized sulfonated EPDM

carbonyl. The maximum of the broad N–H band shifts as well, indicating a change in the relative ratios of types of N–H stretches. Different band positions for the N–H stretching region indicate free N–H groups (around 3440 cm^{-1})[16] and hydrogen-bonded N–H groups (a range near 3300 cm^{-1}), which can be in various environments, such as hydrogen bonded to urethane carbonyl groups[16,17] or bonded to ether groups in the soft segment.[18,19] In MDI/BD and Pellethane,® the N–H groups are at ~ 3328 cm^{-1}; this position is similar to reported values for MDI-based poly(ether-urethanes).[16-18,20,21] When BIN is incorporated into the polyurethane as the chain extender, the maximum in the N–H stretch shifts to lower wavenumbers and the breadth of the peak increases significantly. Coleman and Painter report that the presence of crystallinity in a semi-crystalline polyamide is demonstrated by narrowing of the N–H band,[22] and that shifts to lower frequency of C=O····H–N interactions indicate an increase in the strength of the overall hydrogen bonding.[21] Other researchers suggest that band shifts to lower frequency are due to an increase in the degree of hard domain order, such as crystallinity.[23] Still others have proposed that increases in crystallinity and hard-segment order lead to both peak narrowing and band shifts to lower frequency.[24] Addition of BIN is expected to disrupt any existing hard-domain crystallinity and decrease hard domain order; this is consistent with the increase in breadth of the N–H stretching band seen in Figures 9-4 and 9-5. Therefore, the shift to lower wavenumbers is not due to improvements in hard-domain order. Additionally, there is no soft domain in the hard segment materials, and both the polyurethanes and the hard segment materials show the same trends, so it is unlikely that the urethane N–H band shifts are due to a change in hydrogen bonding from within the hard domain in MDI/BD-based

polyurethanes to with the ether oxygens in the soft domain in the MDI/BIN-based materials.

It is more likely that some urethane nitrogens are interacting to the C-O-C urethane linkages of the $\overset{O}{\overset{\|}{C}}$–O–C groups in the BIN-containing polyurethanes. The urethane C-O-C stretching band is at roughly 1080 cm^{-1} for traditional polyurethanes[16,20] as can be seen in Figures 9-4a and 9-5a. Bandekar and Klima[20] studied polyurethanes with several hard segments and concluded that shifts in the C-O-C region from ~1080 cm^{-1} to ~1060 cm^{-1} were due to changes in the hydrogen-bonding interactions from between the urethane carbonyls and N–H groups to between the urethane alkoxy oxygens and N–H groups. Shifts from ~3320 cm^{-1} to 3295 cm^{-1} were seen in the N–H stretching region, for the same reason. In MDI/BD and Pellethane,® the maximum of the C-O-C stretch is at 1080 cm^{-1}, with a shoulder near 1065 cm^{-1}. In MDI/BIN the main peak is at 1065 cm^{-1}, and the shoulder is at 1080 cm^{-1}. In both PU-29 and PU-35, the entire region is covered by a broad peak. As supporting evidence for this change in hydrogen bonding, the carbonyl band would have to show increased intensity for the free carbonyls, and this is seen in Figures 9-4 and 9-5. Although some of this intensity is due to the chain-extender carbonyl, it is apparent that the trends in the carbonyl region are consistent with the proposed changes in hydrogen bonding. The N–H peak is broader in the BIN-extended polyurethanes, indicating that there is a larger distribution of bonding sites in these materials than in the traditional polyurethane. Skrovanek *et al.*[22] have proposed that breadth in the N–H stretching region is due to a distribution of N–H····O=C distances. Therefore, addition of other bonding sites and disruption in the order imposed

blending with transition metals such as zinc and nickel leads to a slight increase in wavenumbers of the C–N stretching band. (Note that the IR spectrum of PU-29 is very similar to that of PU-35 in Figure 9-4b.) Blending the polyurethane materials with other metals, such as magnesium and sodium, leads to mixed results. The slight increase in the wavenumbers of the transition-metal blends is in the same direction as the band shifts seen in P4VP (Table 9-2); however, the shifts reported here are much smaller than the examples shown in Table 9-2.

9.2.2 ^{13}C NMR Chemical Shifts

The solid-state ^{13}C NMR spectrum of PU-35 is shown in Figure 9-8; the corresponding peak identification is in Table 9-3. Peak identification is based on known polyurethane spectra,[27,28] small molecules,[29,30] and the ^{13}C solution state spectrum.[8]

The ^{13}C CPMAS NMR spectra of PU-35 and Zn-35 are shown in Figure 9-9. There is an additional peak at 181 ppm in Zn-35 due to the carbonyl carbon of the zinc acetate group; the methyl group is incorporated into the 27 ppm peak. The peak position of the acetate carbon is 3 ppm upfield from unblended zinc acetate (184 ppm). Blends with the chain extender and hard segment also show this carbonyl shift (Table 9-4). A similar shift in zinc acetate has been seen previously[4] in blends of P4VP and zinc acetate. This peak shift was atrributed to transition-metal complexation. Additionally, there are other qualitative changes in the polyurethane spectrum after blending. The peak at 144 ppm (due to the pyridine quaternary aromatic carbon) has shifted, probably downfield. According to Levy *et al.*,[30] protonation of a pyridine nitrogen will increase the chemical shift

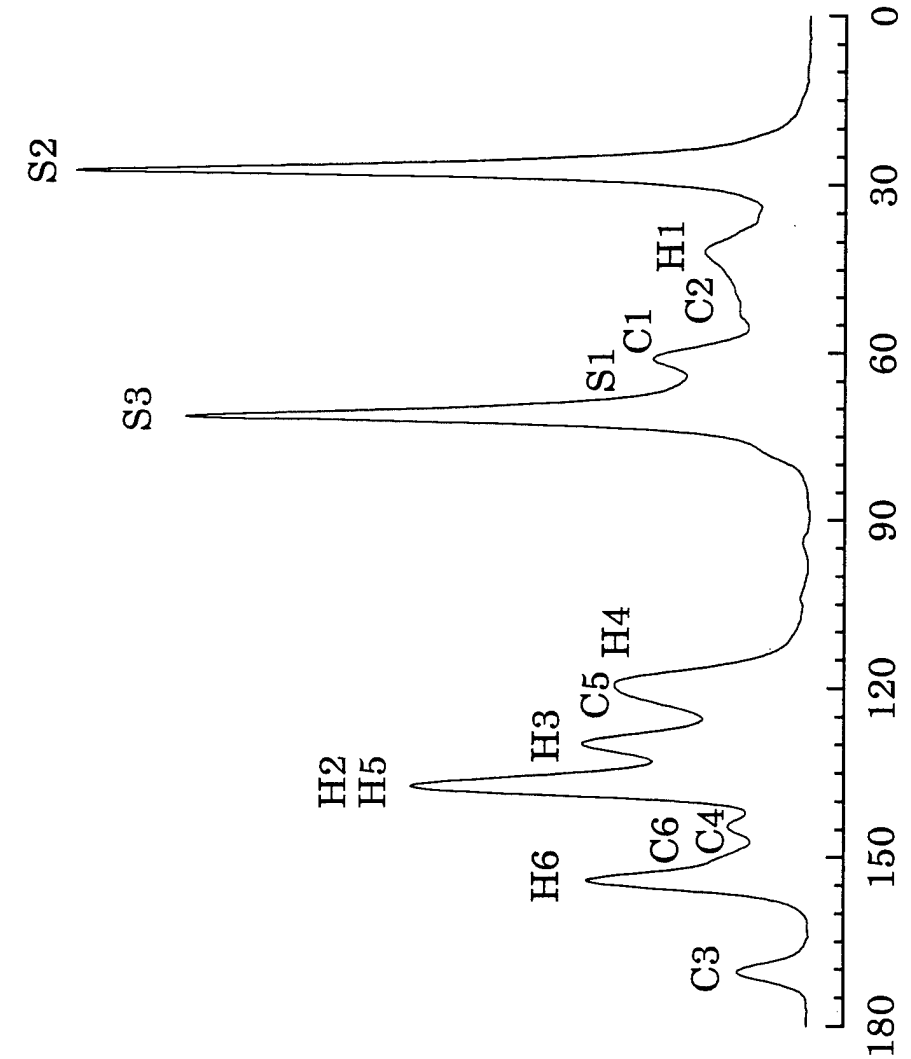

Figure 9-8: ^{13}C NMR spectrum of PU–35.
Peak identification corresponds to Table 9-3 and Figure 9-2.

Table 9-3: ^{13}C NMR peak assignments for PU-35

Carbon Site	Carbon Label	Shift (ppm)
PTMO external CH_2 adjacent to urethane	S1	65
PTMO internal CH_2	S2	27
PTMO external CH_2	S3	71
MDI CH_2	H1	41
MDI quaternary ring	H2/H5	137
MDI internal protonated ring	H3	129
MDI external protonated ring	H4	119
MDI urethane carbonyl	H6	154
Chain-extender external CH_2-O	C1	61
Chain-extender internal CH_2-N	C2	49
Chain-extender carbonyl	C3	170
Pyridine quaternary aromatic	C4	144
Pyridine protonated aromatic	C5	123
Pyridine protonated aromatic adjacent to nitrogen	C6	150

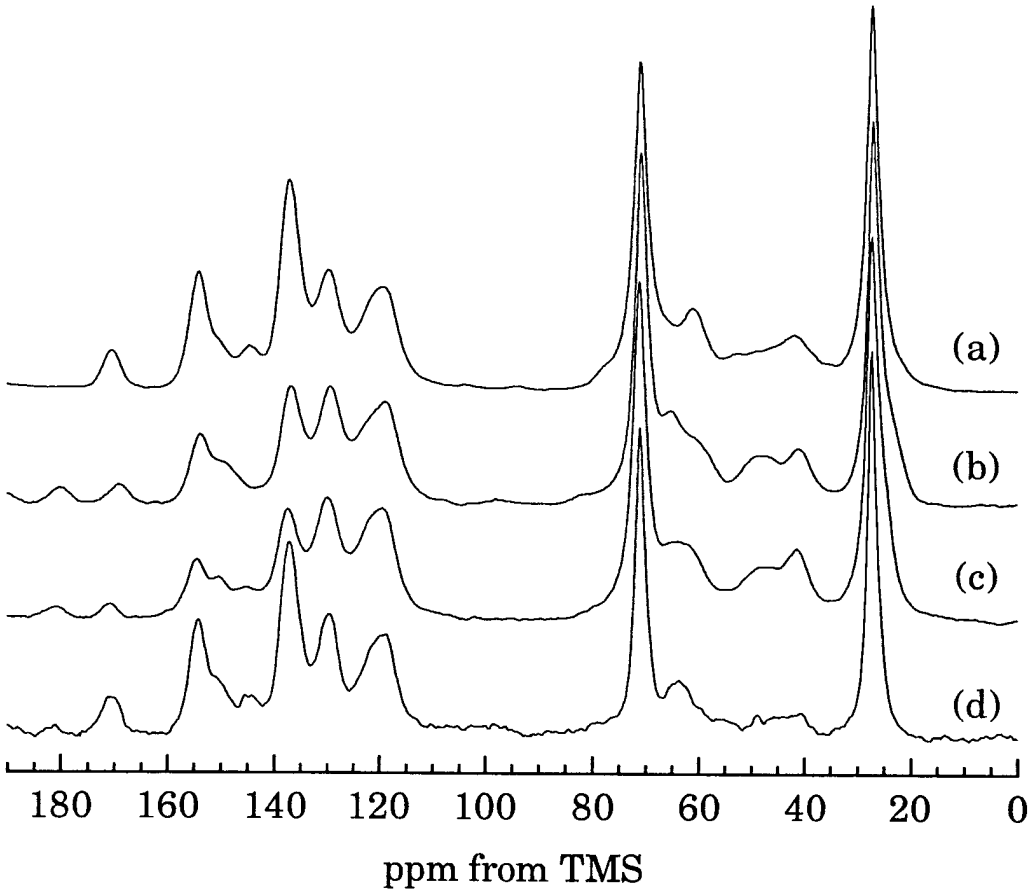

Figure 9-9: ^{13}C NMR spectra of a) PU–35; b) Zn–35; c) Mg–35; d) Na/2–35.
Contact times were either 0.5 or 1 ms.
Spectrum (d) was collected with a 2 ms spin-lock time.

Table 9-4: Chemical shifts (widths) for the metal acetates

	Neat	Blend with BIN	Blend with MDI/BIN	Blend with PU-35
zinc acetate	184 (0.5)	179 (1.3) 183.5 (0.8)	179.5 (1.9)	181 (1.9)
magnesium acetate	183 (0.5)	180.5 (3.2)	179.5 (2.5)	181 (2.0)
sodium acetate	182 (0.5)	–	183 (1.5)	183 (2.5) 182 (1.4)*

*sample Na/2, with half the stoichiometric amount of sodium acetate

of the carbon in the para position (Figure 9-10). Complexation with zinc should cause a shift in the same direction. The peak at 150 ppm (due to the carbon adjacent to the pyridine nitrogen) has sharpened and shifted slightly upfield, which is also consistent with data from Levy *et al.*[30] The other pyridine ring carbons overlap with the MDI carbons of the polyurethane. Finally, the position of the chain-extender carbonyl peak has shifted upfield ~ 1 ppm, to 169 ppm. Similar results are seen in the hard segment materials.

The cross-polarization dynamics have changed in the aromatic region upon the addition of zinc acetate, leading to a change in the ratios of the peaks. Changes such as these can also be caused by drying the samples thoroughly so that most water is removed. With this type of drying procedure, the intensity of the peak at 144 ppm is suppressed, but not removed, because the residual water provides nearby protons for cross polarization of the quaternary carbon.

When the materials are exposed to equivalent humidity levels so the effects of water content are minimized, blending causes changes in the cross-polarization dynamics of the aromatic region, as seen in Figure 9-9. The peaks in the range 30-70 ppm have changed as well; the peak due to the chain-extender CH_2–N has become more prominent and the peaks due to the chain-extender CH_2–O carbons and the PTMO end groups (61 and 65 ppm, respectively) have either shifted or broadened. These changes can only be discussed qualitatively, however, because the spinning sidebands of the aromatic regions overlap with these sites. Obviously, blending has affected the dynamics and local electron structure of the polyurethane. The effect of blending on the chemical shifts and cross-polarization dynamics can be taken as indirect evidence of complexation.

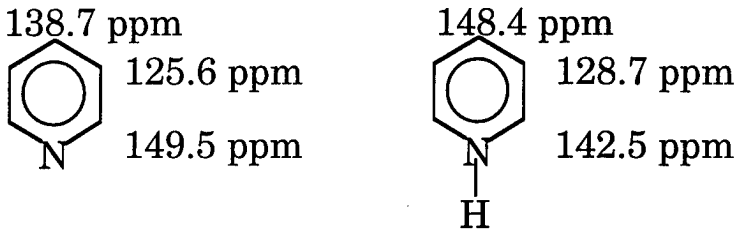

Figure 9-10: Peak identification of carbon sites in pyridine and pyridinium ion

9.2.3 ^{13}C Relaxation Times

Spin lattice relaxation times in the rotating frame ($T_{1\rho}$) were acquired to determine the effects of blending on the kilohertz frequency motions of the polyurethane carbon nuclei. $T_{1\rho}$ values have been shown to give the most information on motions in polyurethane and polyurethane-urea systems.[27,31] Polyurethanes are phase-separated systems and because of that they generally have two relaxation times for each type of carbon nucleus. The $T_{1\rho}$ relaxation plots were fit using a two-component model:

$$M(t)= M_f \exp\left(-\frac{t}{T_{1\rho f}}\right) + M_s \exp\left(-\frac{t}{T_{1\rho s}}\right) \qquad (9\text{-}1)$$

Where M_f and M_s are the magnetizations of the two different components (fast and slow) and $T_{1\rho,f}$ and $T_{1\rho,s}$ are the corresponding relaxation times. For example, the urethane carbonyl may have two components to the relaxation curve. In that case, one component is likely due to the carbonyl carbons in the hard domain, while the other is due to carbonyls at the interface of the hard and soft domains or dissolved in the soft phase. Previous work in this laboratory[27] concluded that the longer $T_{1\rho}$ component in poly(ether-urethanes) could be assigned to carbons in the hard domain. The pyridine group is expected to disrupt hard-segment crystallinity, so the long $T_{1\rho}$ is due to amorphous hard-domain material in PU-35. Since this work focuses on changes in the hard domain of the polyurethane, the emphasis will be on these longer $T_{1\rho}$ times.

The ^{13}C $T_{1\rho}$ relaxation times of the two polyurethanes, PU-29 and PU-35, were compared to determine if relaxation times were sensitive to the

changes in segmental motion that should occur in polyurethanes as hard-segment content is increased from 42% (PU-29) to 54% (PU-35). Tables 9-5 and 9-6 contain the relaxation times ($T_{1\rho,s}$ and $T_{1\rho,f}$), the amount of magnetization related to the species with the particular relaxation time (M_s and M_f), and the fraction of magnetization due to the slowly-relaxing component (M_s/M_t). The $T_{1\rho,s}$ times for PU-35 are all lower or approximately equal to the relaxation times of PU-29. This means that most carbon nuclei in PU-29 are on the low correlation-time side of the $T_{1\rho}$ minimum, so as the correlation time increases (as the hard phase becomes more cohesive) the relaxation time decreases.[32,33] The fraction of magnetization due to the slowly-relaxing component increases substantially as hard-segment content increases, indicating that more hard-segment carbons are in the hard phase and there is less phase-mixing or interfacial material.

Blending with zinc acetate also has an effect on the relaxation dynamics of the polyurethane. Tables 9-6 and 9-7 contain both components of the $T_{1\rho}$ relaxation curves for PU-35 and Zn-35 and the fractions of the slowly-relaxing components from the relaxation curves. Blending increases all relaxation times, in contrast to the relaxation behavior when hard-segment content was increased from PU-29 to PU-35. Therefore, the $T_{1\rho}$ values of PU-35 are probably very near the minimum value of the relaxation curve. Addition of the zinc acetate decreases the segmental motion near the 45 kHz spin-locking frequency; the correlation times of the carbon nuclei increase and move past the $T_{1\rho}$ minimum, so the $T_{1\rho}$ values increase again.

The relative fractions of carbon sites in the slow-component regime have either remained constant or increased slightly after the addition of zinc acetate, indicating that the amount phase separation may increase slightly

Table 9-5: Spin-Lattice Relaxation Times in the Rotating Frame ($T_{1\rho}$) for PU-29

Carbon site	shift (ppm)	M_f	$T_{1\rho,f}$ (ms)	M_s	$T_{1\rho,s}$ (ms)	M_s/M_t
MDI external protonated ring	119	24600	1.06	2080	22.1	0.078
MDI internal protonated ring	129	37000	1.11	2400	27.7	0.061
MDI quaternary ring	137	18600	1.80	13200	23.9	0.415
MDI urethane carbonyl	154	6520	3.87	6620	28.6	0.504
Pyridine protonated aromatic	122	25700	0.70	2400	24.5	0.085
Pyridine quaternary aromatic	145	582	0.58	792	25.2	0.576
Pyridine protonated aromatic adjacent to nitrogen	150	4010	1.81	498	34.3	0.110
Chain-extender carbonyl	170	1040	6.31	1400	28.7	0.574
Acetate salt carbonyl	181	–	–	–	–	–

Table 9-6: Spin-Lattice Relaxation Times in the Rotating Frame ($T_{1\rho}$) for PU-35

Carbon site	shift (ppm)	M_f	$T_{1\rho,f}$ (ms)	M_s	$T_{1\rho,s}$ (ms)	M_s/M_t
MDI external protonated ring	119	42100	1.16	18800	15.7	0.309
MDI internal protonated ring	129	73600	1.33	24400	12.1	0.248
MDI quaternary ring	137	35500	0.56	83900	20.6	0.703
MDI urethane carbonyl	154	8430	0.36	38700	23.4	0.821
Pyridine protonated aromatic	122	41600	1.02	12200	16.7	0.227
Pyridine quaternary aromatic	145	1160	0.57	3440	31.0	0.748
Pyridine protonated aromatic adjacent to nitrogen	150	17200	0.94	8680	19.8	0.335
Chain-extender carbonyl	170	1920	0.32	10000	24.9	0.839
Acetate salt carbonyl	181	–	–	–	–	–

Table 9-7: Spin-Lattice Relaxation Times in the Rotating Frame ($T_{1\rho}$) for Zn-35

Carbon site	shift (ppm)	M_f	$T_{1\rho,f}$ (ms)	M_s	$T_{1\rho,s}$ (ms)	M_s/M_t
MDI external protonated ring	119	14600	2.00	7030	20.8	0.325
MDI internal protonated ring	129	17800	2.09	9780	15.8	0.355
MDI quaternary ring	137	5480	2.53	17300	33.9	0.759
MDI urethane carbonyl	154	1270	2.56	8400	37.8	0.869
Pyridine protonated aromatic	122	6410	1.58	3600	23.4	0.360
Pyridine quaternary aromatic	145	–	–	–	–	–
Pyridine protonated aromatic adjacent to nitrogen	150	3440	2.45	5630	27.2	0.621
Chain-extender carbonyl	170	614	2.21	2600	44.3	0.809
Acetate salt carbonyl	181	–	–	–	–	–

but has not changed dramatically with blending. This is consistent with previous studies on these materials.[8,9] The fraction M_s/M_t for the pyridine carbon adjacent to the nitrogen (150 ppm) has increased substantially, about 85%. This carbon is closest to the nitrogen, which is the proposed site of the complexation, so it is not surprising that this carbon is the most affected, since more pyridine groups are motionally restricted after blending than before. The other protonated aromatic carbon in the pyridine ring also shows an increase in the fraction of slow component. Finally, the carbonyl carbon of the chain extender, while not affected dramatically in M_s/M_t, does show substantial increases in both $T_{1\rho}$ values. If the pyridine ring flips are suppressed by the complexation, this may decrease the fluctuating magnetic fields near the carbonyl carbon and cause an increase in the relaxation time.

9.2.4 ^{15}N NMR Chemical Shifts and Cross-Polarization

IR and ^{13}C NMR give indirect evidence for complexation in these blends. A much more direct probe is ^{15}N NMR of the possible complexing nucleus, the pyridine nitrogen. Figure 9-11 shows the natural-abundance (0.37% of all nitrogens) ^{15}N CPMAS NMR spectrum of the MDI/BIN hard segment material. The polyurethanes were not attempted because of the prohibitively low amount of ^{15}N in them. At different cross-polarization times, different peaks are emphasized. ^{15}N peaks are seen at –276 ppm, –320 ppm, and possibly –405 ppm. The peaks were identified by comparing the positions to other urethane- and pyridine-containing materials. Figure 9-12 shows the NMR spectra of MDI/BD, which contains only urethane nitrogens at –281 ppm, and the NMR spectrum of BIN, the chain extender. The two spectra contain all the peaks present in the MDI/BIN material.

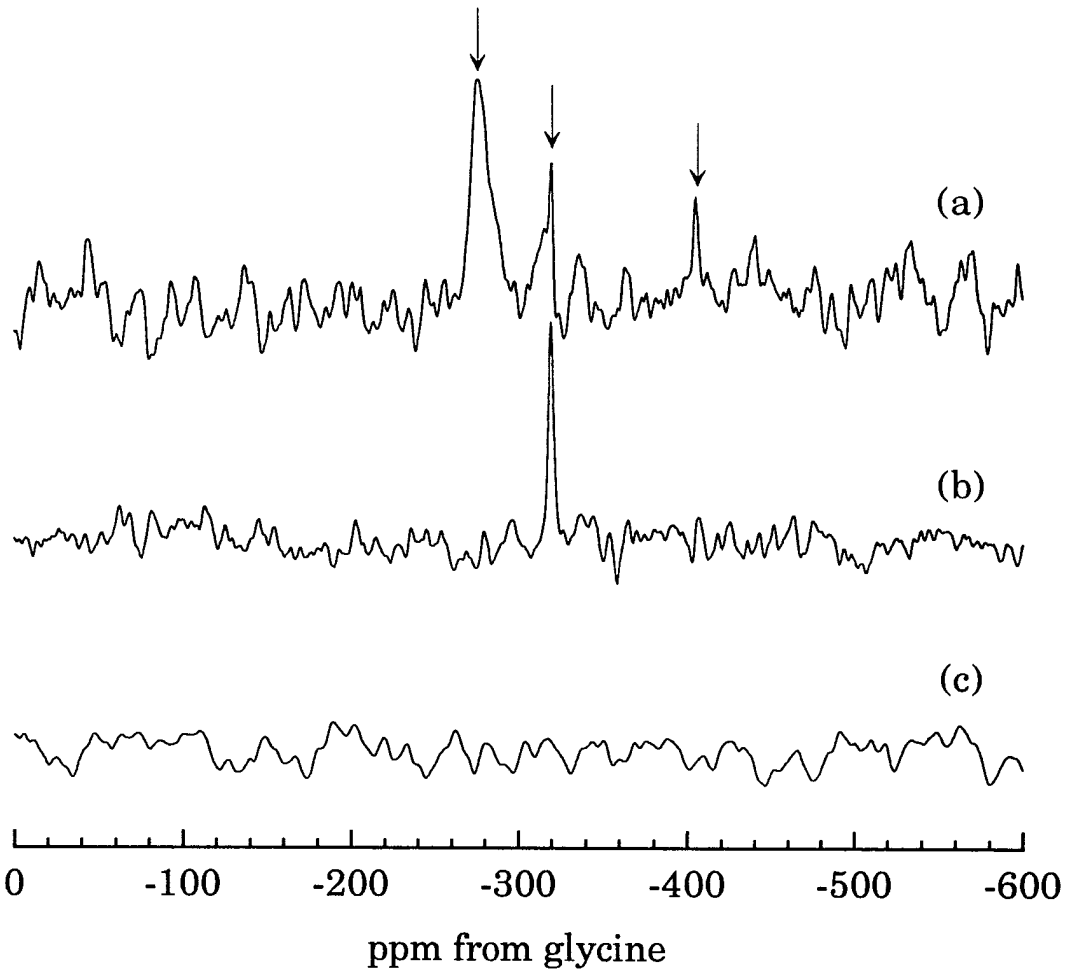

Figure 9-11: ^{15}N NMR spectra of MDI/BIN at three contact times: a) 0.5 ms; b) 2 ms; c) 3 ms.

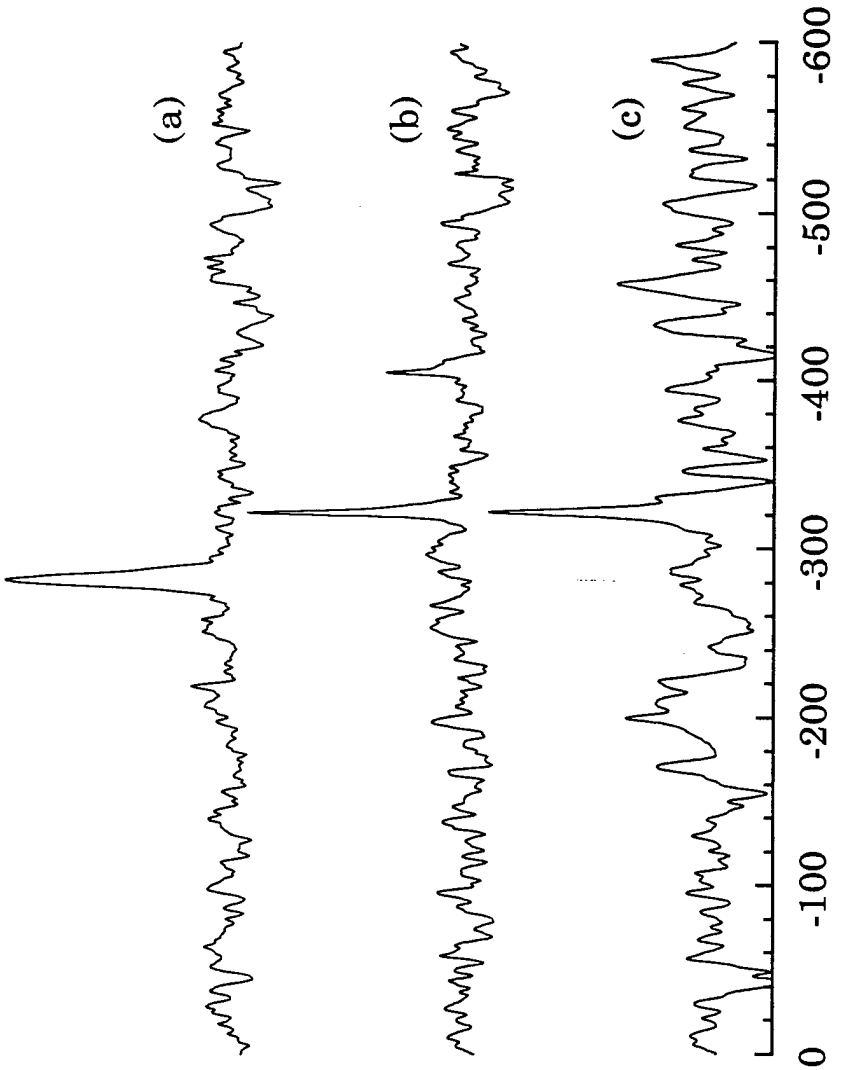

Figure 9-12: ^{15}N NMR spectra of a) MDI/BD; b) BIN; c) P4VP.

Therefore, the –276 ppm peak is assigned to the urethane nitrogens; this assignment agrees with many in the literature.[34] The slight shift of the urethane nitrogen, from –281 to –276 ppm, may be an artifact of the signal-to-noise level, or it may be due to the different types of hydrogen bonding in the two materials.

The spectrum of P4VP is shown in Figure 9-12c. It shows a single peak at –322 ppm, which is comparable to one of the peaks seen in BIN, and so, this peak is assigned to the pyridine peak in BIN. The last peak, at –405 ppm, is unassigned at this time. It could be due to the amine nitrogen in the chain extender, but is far upfield from most amine shifts.[34,35] It is also possible that the –405 ppm peak is due to a pyridinium-type nitrogen that is hydrogen-bonded to OH groups (in BIN) or urethane N–H groups (in MDI/BIN). The pyridinium ion resonates about 100 ppm upfield from pyridine nitrogen,[35] and a hydrogen-bonded pyridine group may show a slightly smaller shift compared to the pyridinium ion. Therefore, the ~80 ppm shift from pyridine is certainly reasonable for this species. The IR experiments indicate the presence of hydrogen-bonding to the pyridine nitrogen, so it is most likely that this peak is due to hydrogen-bonded pyridine nitrogen. If this –405 ppm peak is hydrogen-bonded pyridine nitrogen, then the amine nitrogens are not detected with these cross-polarization parameters. However, it is the pyridine nitrogen peak which is of greatest interest in this study.

MDI/BIN was blended with zinc acetate and the ^{15}N NMR spectra were acquired. ^{13}C NMR spectra were taken to ensure that little if any residual solvent (DMF) was present. (DMF appears as a ^{15}N NMR peak near –260 ppm and ^{13}C NMR peaks at 31, 36, and 162 ppm) Figure 9-13 shows the blend compared with the original hard-segment material. Other

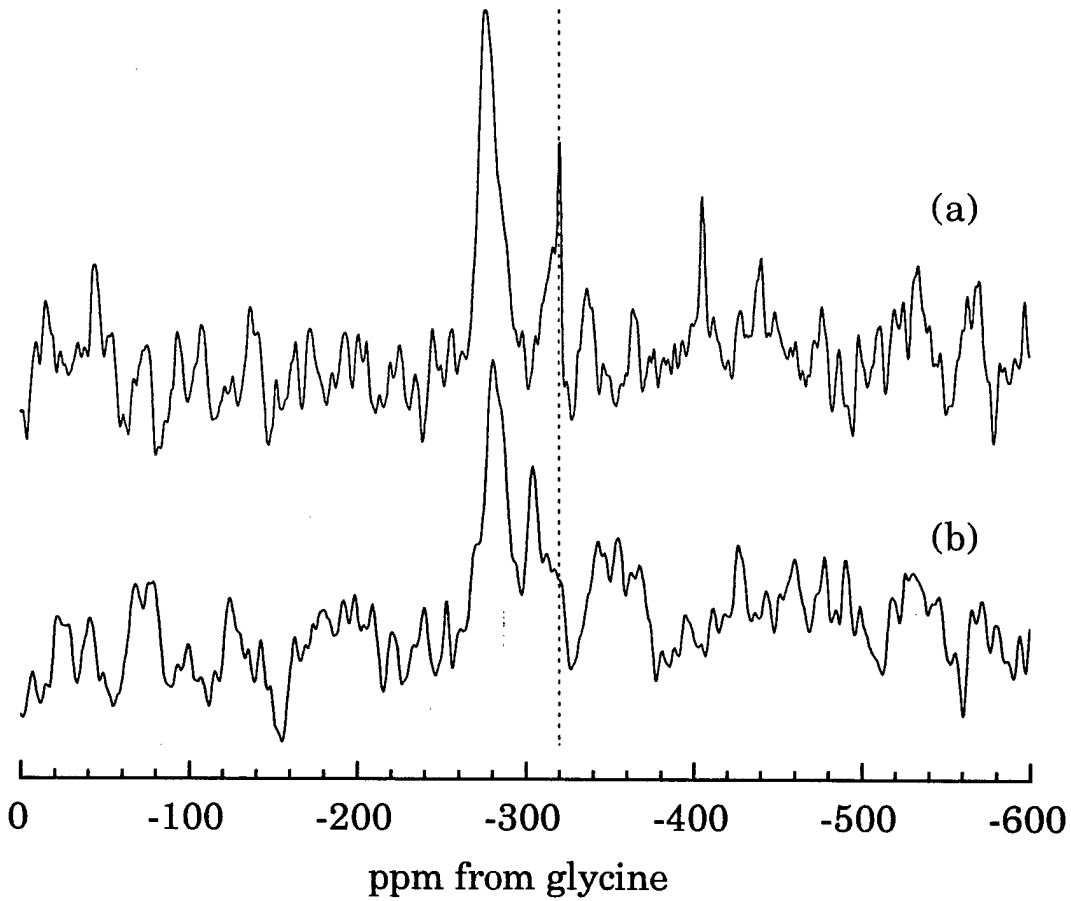

Figure 9-13: ^{15}N NMR spectra of a) MDI/BIN at a contact time of 0.5 ms b) MDI/BIN/Zn at a contact time of 5.5 ms.

researchers[36] have proposed that interactions can take place at either the urethane carbonyl carbon or the pyridine nitrogen. Since no significant shift is apparent in the urethane carbonyl group (Figure 9-9) or the urethane nitrogen immediately neighboring it, the interaction is not at that site. Instead, the peak due to the pyridine nitrogen has shifted significantly downfield, from –320 ppm to –304 ppm. This is direct evidence that complexation has taken place at the pyridine site.

Blending also affects the cross-polarization dynamics of the polyurethane. Figure 9-11 shows the ^{15}N NMR spectra of MDI/BIN at several different contact times. The urethane nitrogen cross polarizes at shorter contact times than the pyridine carbon, and both signals are short-lived, vanishing by a contact time of 3 ms. In contrast, Figure 9-14 shows the spectra of MDI/BIN/Zn at several contact times. The dynamics are quite different than what was seen for MDI/BIN. Once again the urethane nitrogen cross-polarized at shorter contact times than the pyridine group, however, the peak persists to much higher contact times in the blend. Additionally, the contact time at which the pyridine nitrogen appears has increased dramatically; now the peak appears at much longer times (5.5 ms). The increase in the contact time for the pyridine nitrogen is due to the complexation; nearby protons have been displaced by the zinc atom, and cross polarization is more difficult. The change in the contact time dynamics of the urethane nitrogen is probably due to the change in hydrogen bonding that affected the N–H stretch in the IR spectra.

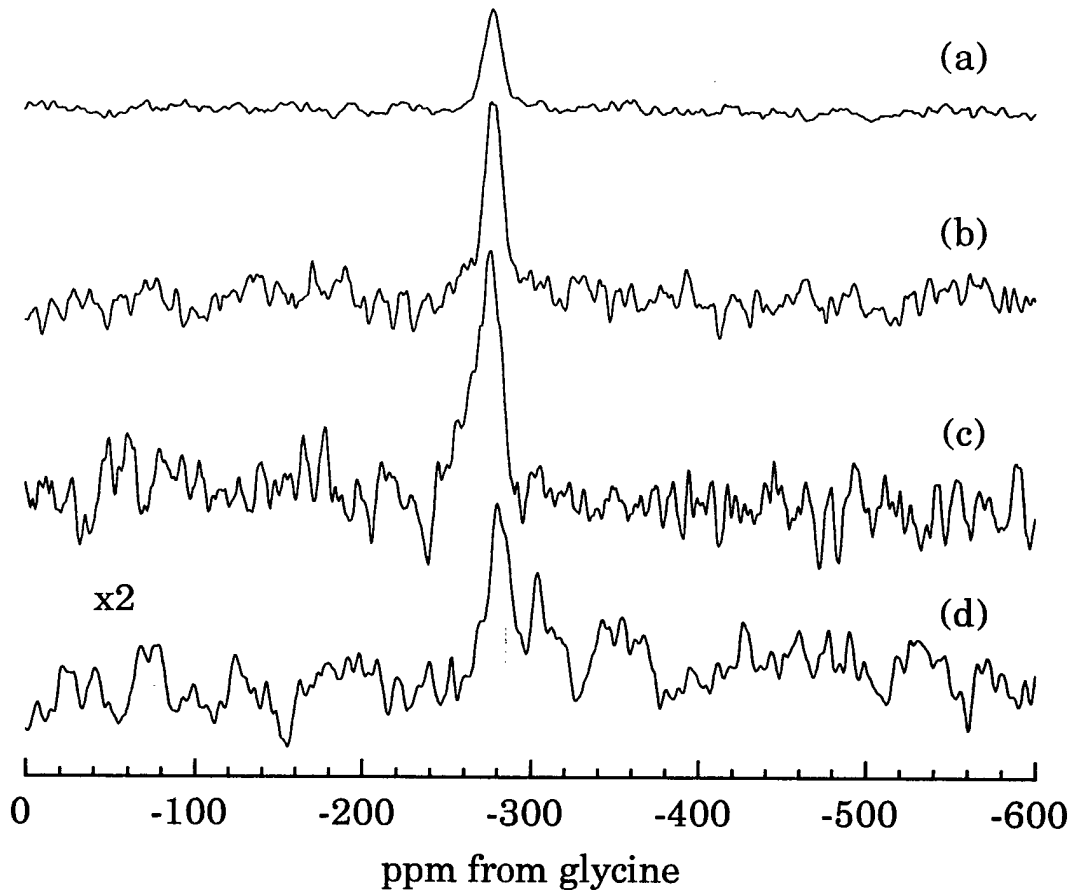

Figure 9-14: ^{15}N NMR spectra of MDI/BIN/Zn at four contact times: a) 0.7 ms; b) 1.7 ms; c) 3 ms; d) 5.5 ms. Spectral intensities are normalized.

9.2.5 Blends with Non-Transition Metals

The previous studies on pyridine-containing blends have focused mainly on transition-metal complexes. One of the purposes of this chapter is to determine the local interactions of a transition metal (zinc) with the pyridine nitrogen. Additionally, however, the effects of a non-transition metal (magnesium) on the properties of this polyurethane are also of interest. In previous studies of poly(4-vinyl pyridine),[2-4] magnesium did not complex with the pyridine nitrogen. Belfiore *et al.*[4] reported ^{13}C NMR chemical shifts of the acetate carbonyl peak in blends of zinc acetate and P4VP as an indication of complexation, and no such shifts were present in blends of magnesium acetate and P4VP. In the PU-35 system, however, a distinct shift in the acetate peak is apparent when neat magnesium acetate is compared to its blend with PU-35 (Table 9-4). However, the qualitative changes in the spectrum of Mg-35 after blending are not as distinctive as in the blend with zinc acetate. In particular, the pyridine C–N carbon at 144 ppm and chain-extender carbonyl at 170 ppm are not affected as dramatically (Figure 9-9). Additionally, SAXS experiments (Figure 9-1b) showed no changes in the SAXS pattern of PU-35 when blended with magnesium acetate.

Tensile tests indicate that magnesium does affect the tensile properties of the polyurethane, albeit slightly. Figure 9-15 shows the stress-strain curves for PU-35 blended with Ni, Zn, Mg and Na acetates. These curves are different than those shown in Figure 9-3;[8] this is most likely due to aging of the polyurethanes and possibly the effects of annealing since these samples were dried at 50-60°C both in air and under vacuum to completely remove the solvent, DMF. Young's modulus of the PU-35 sample is noticeably higher than in the previous study. The strain-hardening seen in PU-35 and Zn-35 is likely

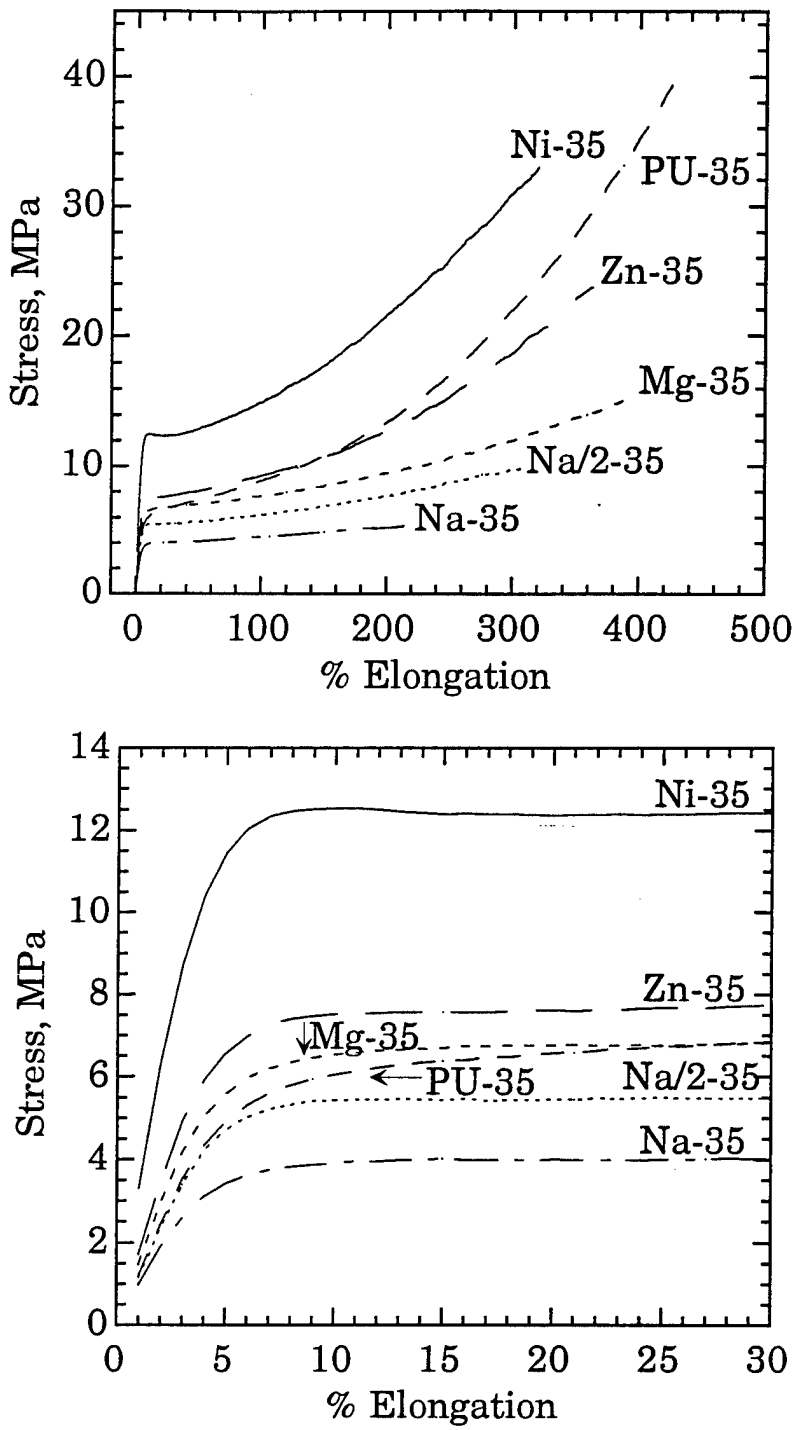

Figure 9-15: Stress-strain curves for PU–35 and its blends with nickel, zinc, magnesium, and sodium acetates. Sample Na/2–35 contains half the stoichiometric amount of sodium. The upper plot contains the full curves, while the lower plot shows the initial slopes.

due to crystallization of the PTMO soft segment; this was not seen in the earlier study, although strain hardening was apparent in the blends with nickel and copper acetates (Figure 9-3). Table 9-8 contains the moduli, ultimate strength and elongation of the polyurethane and its blends. Blending with Ni and Zn increases the modulus of the polyurethane, as expected. However, blending with magnesium increases the modulus as well, although not to as high a value. The effects on ultimate strength cannot be compared because of the large errors involved. The increase in modulus for the magnesium blend is not considered to be a filler effect because the ^{13}C NMR data indicate that the acetate peak shifts from 183 ppm to 181 ppm, similar to the shift in Zn-35 (Table 9-4 and Figure 9-9). Additionally, blending with sodium acetate decreases the modulus of the material. The NMR position of the sodium acetate carbonyl does not change after blending with sodium acetate; if anything, it actually shifts in the opposite direction from what seen in all other blends (Table 9-4).

It is possible that the magnesium ion interacts with a group other than the pyridine nitrogen, such as the amine nitrogen or the carbonyl carbon. Interaction with the urethane carbonyl is unlikely since its chemical shift at 154 ppm is unchanged from PU-35 (Figure 9-9). The ^{15}N NMR of MDI/BIN/Mg is shown in Figure 9-16. The pyridine nitrogen shifts 11 ppm relative to MDI/BIN, to ~ –309 ppm. This shift is even substantial for the zinc blend, in which the pyridine peak shifted to –304 ppm. It appears that magnesium does affect the pyridine nitrogen, but the interaction is not as strong as in the blend with zinc acetate. Additionally, the cross-polarization dynamics of the urethane nitrogen in the blend with magnesium acetate (Figure 9-16) are different from that in the blend with zinc acetate

Table 9-8: Tensile Properties for PU-35 and blends with metal acetates

Sample	Modulus (MPa)	% Elongation	Stress at break (MPa)
PU–35	122 ± 12	441 ± 14	25.2 ± 19.6
Mg–35	146 ± 7	420 ± 15	12.3 ± 5.9
Zn–35	174 ± 2	396 ± 31	26.7 ± 3.6
Ni–35	327 ± 47	341 ± 26	24.6 ± 19.4
Na–35	96.9 ± 7.7	246 ± 27	4.82 ± 1.18
Na/2–35	115 ± 9	342 ± 29	6.47 ± 4.11

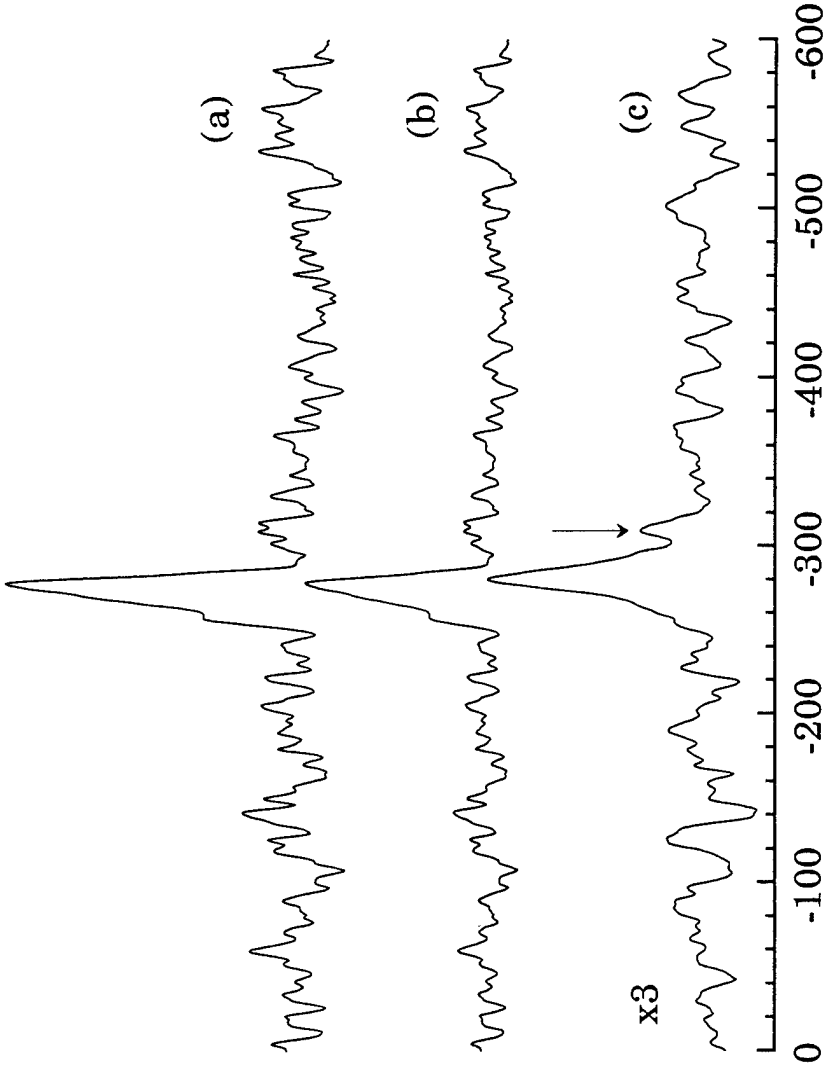

Figure 9-16: ^{15}N NMR spectra of MDI/BIN/Mg at three contact times: a) 0.7 ms; b) 2 ms; c) 5.5 ms. Spectral intensities are normalized.

(Figure 9-14). In MDI/BIN/Mg, the maximum intensity is found near a contact time of 0.7 ms. This maximum in the cross-polarization curve of the urethane nitrogen is much closer to the maximum seen in MDI/BIN (near 0.5 ms, Figure 9-11) than in MDI/BIN/Zn (near 3 ms, Figure 9-14). In both blends the signal persists to much higher contact times than in the original unblended hard segment material. Lu and Weiss[37] found miscible, interacting blends of certain ratios of Zn and Na-neutralized SPS and PSVP blended in DMF, cast, and annealed. One glass-transition temperature (T_g) was seen for some ratios, and for other ratios the individual T_g's were functions of composition, indicating some interaction. From their study and the present ^{13}C and ^{15}N NMR chemical shifts, interactions between pyridine and non-transition metal ions such as magnesium are shown to be possible, but the mechanism is different and the interaction is weaker than that in transition-metal blends.

In Figure 9-15, the polyurethane blended with sodium acetate shows decreased mechanical properties compared to the unblended polymer. Sodium is a monovalent ion that probably needs to cluster in order to form physical crosslinks. Unlike ionomers, the sodium incorporated into these materials is due to a separate molecule and not ionically bonded to the polymer chain. Aggregation of the sodium groups could lead to clusters of sodium acetate that would not crosslink the polymer chains, but instead would lower the mechanical properties of the polyurethane.

The FTIR data in Table 9-1 and Figure 9-17 show the band shifts of the pyridine C–N stretch and the urethane N–H group when sodium is incorporated into the polyurethane PU-35 and the hard segment material. The C–N bands in the blends with sodium acetate appear at lower wavenumbers than in MDI/BIN, PU-35, and most other blends. Only Mg-35

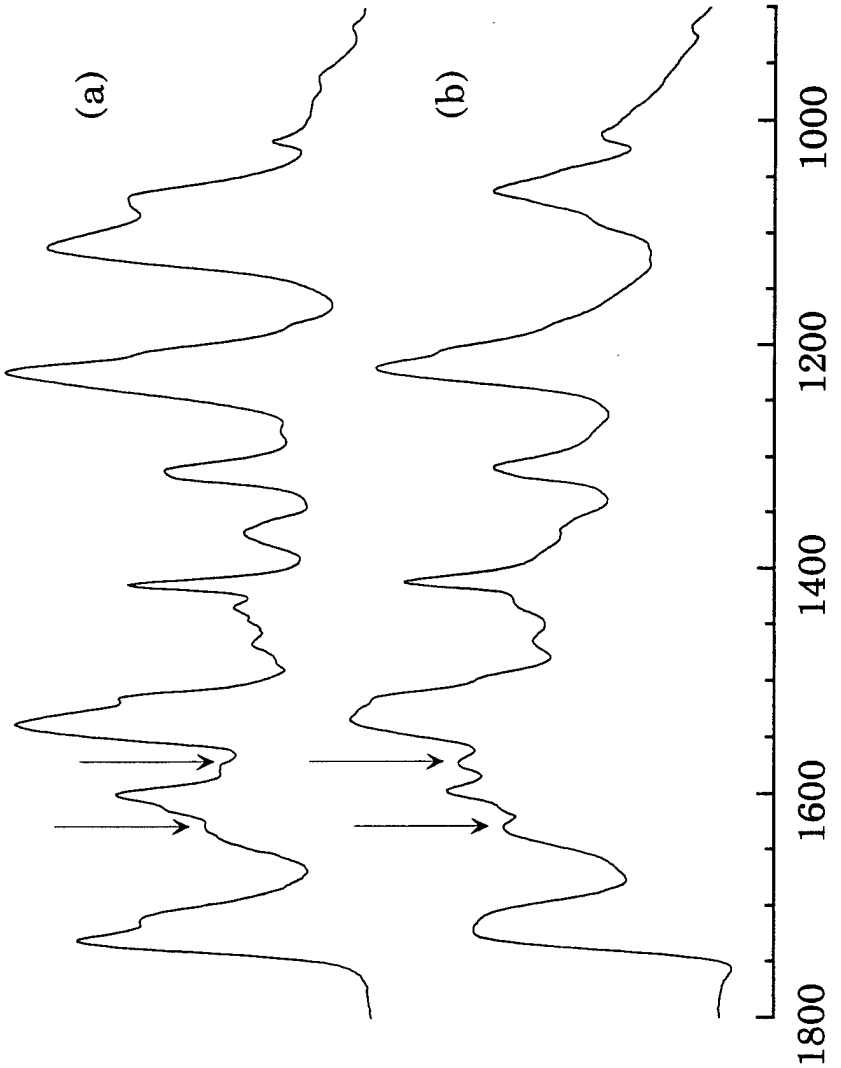

Figure 9-17: FTIR spectra of a) Na–35 and b) MDI/BIN/Na

has an equivalent band position to Na-35; in the hard segments all other blends, including magnesium, have higher band positions. The position of the maximum in the N–H stretching band is also lower in MDI/BIN/Na than in all other hard segment blends. This probably indicates that the metal-pyridine interaction that increased the band position in the other bands in not present in the sodium blend. Finally, the sodium-containing materials have an additional peak at 1572 cm^{-1}, which is not present in any other starting polymer or blend. Carboxylate anion peaks are generally found around 1550 cm^{-1}.[38] In sodium-neutralized ethylene-methacrylate polymers, Brozoski *et al.*[38] saw two IR bands in this region, at 1547 cm^{-1} and 1568 cm^{-1}. They reported that the position of this peak is a function of cation type and local structure. The appearance of this peak in only the sodium blends could indicate that the local structure in these blends is different than in the other metal-containing materials.

^{23}Na NMR experiments were completed on the sodium-containing polyurethane materials to determine the environment of the sodium in these materials. Figure 9-18 shows the results of these experiments. Sodium acetate (Figure 9-18a) is characterized by a broadened quadrupolar lineshape centered near 0 ppm. After blending with PU-35 the main peak is shifted slightly downfield and is Lorentzian in shape, but there is also a very small amount of intensity at lower ppm (Figure 9-18 inset), characterized by a broad peak. The narrow peak is most likely due to amorphous sodium acetate; the loss of crystalline structure would lead to a more average environment around the sodium and a decrease in the quadrupole coupling constant. The broad peak is probably equivalent to the aggregated sodium ions in NaSPS ionomers. (Chapters 4-7). Evidently there are relatively few

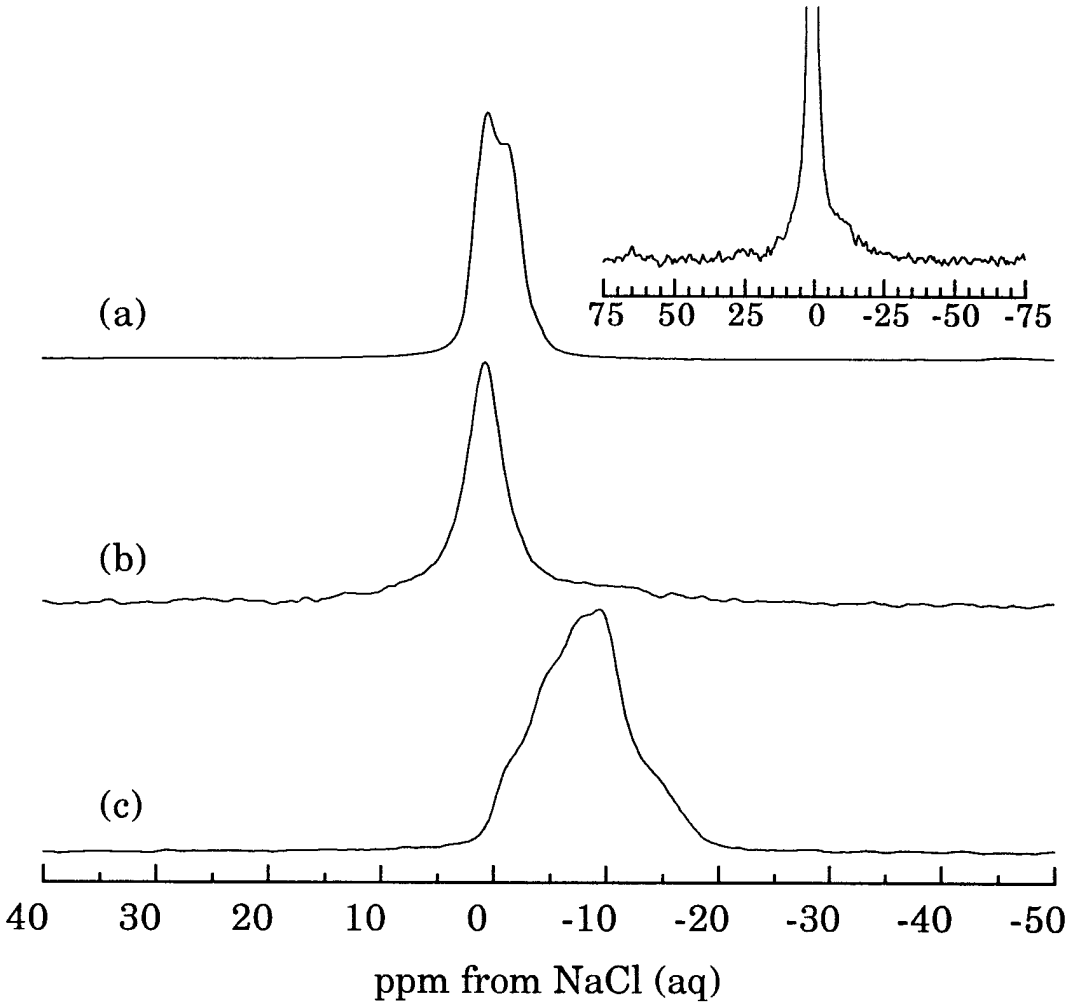

Figure 9-18: ^{23}Na NMR spectra of a) sodium acetate; b) Na–35; c) MDI/BIN/Na. The inset is an expanded view of (b).

clustered sodium ions in this polyurethane blend, so the sodium acetate is not contributing significantly to mechanical properties. It is possible any clusters that do exist could lead to early failure of the material, however. The behavior in the hard segment material is quite different, however (Figure 9-18c). The sodium acetate has a different structure and the peak shifts upfield from the neat sodium acetate, similar to the behavior of the ionomers. This shift could be due to some clustering or phase-separation of the sodium acetate. This hard-segment blend was more opaque than all other blends, possibly due to poor compatibility of the sodium acetate and the polyurethane. Agarwal *et al.*[3] reported a gradual decrease in clarity for blends of PSVP and metal-neutralized S-EPDM when the metal was varied from zinc to magnesium and then to sodium, the last of which was completely opaque. The PSVP blends with magnesium and sodium as the cations did not show any indications of complexation.

^{13}C NMR studies of both MDI/BIN/Na and Na-35 were undertaken. Incorporation of sodium does not affect the ^{13}C spectrum of the polyurethane materials in the same way blending with zinc or magnesium acetate does. The peak at 144 ppm is still present for the sodium blends and the 150 ppm carbon is also unaffected (Figure 9-9). Additionally, the acetate carbonyl in Na-35 has not changed position compared to the neat sodium acetate peak (Table 9-4). The carbonyl in sodium acetate also has a much lower cross-polarized intensity than the carbonyls in all other blends, indicating that its environment is not equivalent to the others. The acetate carbonyl in MDI/BIN/Na may have shifted slightly downfield compared to the unblended salt, but the peak width is larger than the possible shift, so the extent of the shift is near the limit of resolution. Finally, ^{15}N NMR results showed a very

weak CPMAS peak at ~ –323 ppm with a contact time of 9 ms. Therefore, the position of the pyridine nitrogen in MDI/BIN does not change when the polyurethane is blended with sodium, and no complex is formed.

^{23}Na, ^{13}C and ^{15}N NMR data indicate that the sodium acetate in these blends is not forming any complex with the pyridine nitrogen of the chain extender. In order to form physical crosslinks, most likely the sodium ions must form aggregates similar to those seen in ionomers; however, because the sodium is monovalent and part of an acetate group, it cannot coordinate with other acetate groups and the pyridine nitrogen. Instead, it remains mostly isolated in the case of Na-35, in which the number of sodium acetates per gram of polymer is much lower than in the hard segment material. In the hard-segment material, the sodium acetates manage to aggregate together, probably into separate domains.

9.3 Conclusions

^{15}N NMR gives direct evidence for metal-pyridine interactions in blends of pyridine-containing polyurethanes and metal acetates. After blending with zinc acetate, the pyridine nitrogen peak shifts from –320 ppm to –304 ppm. In ^{13}C NMR studies, the acetate carbonyl and pyridine ring carbons shift after blending, giving indirect evidence of complexation. Relaxation studies show increases in $T_{1\rho}$ values when zinc acetate is blended with the polyurethane. This is due to complexation with the metal cation which decreases segmental motions of the hard-domain carbons in the kilohertz frequency range. The effects of incorporation of the pyridine group on the hydrogen-bonding within the hard domain are apparent in IR experiments. BIN-containing polymers show evidence of hydrogen bonding to urethane C-O-

C oxygens and pyridine nitrogens. Effects of blending on the hard-domain hydrogen-bonding were evident in IR and ^{15}N NMR contact-time experiments. The IR N–H stretching band shifts to higher wavenumbers and the ^{15}N NMR N–H signal persists to higher contact times for the blend. Blends of polyurethanes and magnesium acetate also cause shifts in the ^{13}C and ^{15}N NMR spectra, but not to the extent seen in blends with zinc acetate. Sodium acetate does not complex with the BIN-containing polyurethanes; no shifts in the ^{13}C NMR signal for the acetate carbonyl or in the ^{15}N NMR for the pyridine nitrogen are apparent.

References for Chapter Nine

1 Agnew, N.H. *J. Polym. Sci. Polym. Chem. Ed.* 1976, **14**, 2819.

2 Peiffer, D.G.; Duvdevani, I.; Agarwal, P.K.; Lundberg, R.D. *J. Polym. Sci. Polym. Lett. Ed.* 1986, **24**, 581.

3 Agarwal, P.K.; Duvdevani, I.; Peiffer, D.G.; Lundberg, R.D. *J. Polym. Sci. Polym. Phys. Ed.* 1987, **25**, 839.

4 Belfiore, L.A.; Pires, A.T.N.; Wang, Y.; Graham, H.; Ueda, E. *Macromol.* 1992, **25**, 1411.

5 Belfiore, L.A.; McCurdie, M.P.; Ueda, E. *Macromol.* 1993, **26**, 6908.

6 Lee, D.-C.; Register, R.A.; Yang, C.-Z.; Cooper, S.L. *Macromol.* 1988, **21**, 998.

7 Ding, Y.S.; Register, R.A.; Yang, C.-Z.; Cooper, S.L. *Polymer*, 1989, **30**, 1213.

8 Yang, C.-Z.; Zhang, X.; O'Connell, E.M.; Goddard, R.J.; Cooper, S.L. *J. Appl. Polym. Sci.* 1994, **51**, 365.

9 Grady, B.P.; O'Connell, E.M.; Yang, C.-Z.; Cooper, S.L. *J. Polym. Sci., Polym. Phys. Ed.* 1994, **32**, 2357.

10 Coleman, M.M.; Graf, J.F.; Painter, P.C. *Specific Interactions and the Miscibility of Polymer Blends*; Technomic Publishing Co.: Lancaster, PA, 1991.

11 Coleman, M.M.; Painter, P.C. *Appl. Spectr. Rev.* 1984, **20**, 255.

12 Smith. P.; Eisenberg, A. *Macromol.* 1994, **27**, 545.

13 Sakurai, K.; Douglas, E.; MacKnight, W.J. *Macromol.* 1992, **25**, 4506.

14 Sakurai, K.; Douglas, E.; MacKnight, W.J. *Macromol.* 1993, **26**, 208.

15 Ng, C.-W.A.; Lindway, M.J.; MacKnight, W.J. *Macromol.* 1994, **27**, 3027.

16 Srichatrapimuk, V.W.; Cooper, S.L. *J. Macromol. Sci.-Phys.* 1978, **B15**, 267.

17 Seymour, R.W.; Estes, G.M.; Cooper, S.L. *Macromol.* 1970, **3**, 579.

18 Lee, H.S.; Wang, Y.K.; Hsu, S.L. *Macromol.* 1987, **20**, 2089.

19 Goddard, R.J.; Cooper, S.L. *Macromol.* 1995, **28**, 1390.

20 Bandekar, J.; Klima, S. *J. Mol. Struct.* 1991, **263**, 45.

21 Coleman, M.M.; Lee, K.H.; Shrovanek, D.J.; Painter, P.C. *Macromol.* 1986, **19**, 2149.

22 Skrovanek, D.J.; Painter, P.C.; Coleman, M.M. *Macromol.* 1986, **19**, 699.

23 Pollack, S.K.; Shen, D.K.; Hsu, S.L.; Wang, Q.; Stidham, H.D. *Macromol.* 1989, **22**, 551.

24 Brunette, C.M.; Hsu, S.L.; MacKnight, W.J. *Macromol.* 1987, **15**, 71.

25 Skrovanek, D.J.; Coleman, M.M. *Polym. Eng. Sci.* 1987, **27**, 857.

26 Seymour, R.W.; Cooper, S.L. *Macromol.* 1970, **6**, 48.

27 Okamoto, D.T.; O'Connell. E.M.; Cooper, S.L.; Root, T.W. *J. Polym. Sci., Polym. Phys. Ed.*, 1993, **31**, 1163.

28 Meadows, M.D.; Christenson, C.P.; Howard, W.L.; Harthcock, M.A.; Guerra, R.E.; Turner, R.B. *Macromol.* 1990, **23**, 2440.

29 *Handbook of 13C NMR Spectra*; Toda, F., ed.; Sanyo: Tokyo, 1981.

30 Levy, G.C.; Lichter, R.L.; Nelson, G.L. *Carbon-13 Nuclear Magnetic Resonance Spectroscopy*, 2nd. ed.; John Wiley & Sons: New York, 1980.

31 Okamoto, D.T.; Cooper, S.L.; Root, T.W. *Macromol.* 1992, **25**, 1068.

32 *High Resolution NMR spectroscopy of Polymers in Bulk*; Komoroski, R.A., ed. VCH Publishers, Inc.: Deerfield Beach, FL., 1986.

33 Sudmeier, J.L.; Anderson, S.E.; Frye, J.S. *Concepts in Mag. Res.* 1990, **2**, 197.

34 Duncan, T.M. A *Compilation of Chemical Shift Anisotropies*; The Farragut Press: Chicago, 1990.

35 Levy, G.C.; Litcher, R.L. *Nitrogen-15 Nuclear Magnetic Spectroscopy*; John Wiley & Sons: New York, 1979.

36 Kwei, T.K.; Dai, Y.K.; Lu, X.; Weiss, R.A. *Macromol.* 1993, **26**, 6583.

37 Lu, X.; Weiss, R.A. *Macromol.* 1991, **24**, 5763.

38 Brozoski, B.A.; Coleman, M.M.; Painter, P.C. *Macromol.* 1984, **17**, 230.

Chapter Ten: Conclusions and Recommendations

10.1 Summary of Conclusions

The local environment, or "local morphology" of sodium cations in sodium-neutralized sulfonated polystyrene (NaSPS) can be characterized using ^{23}Na nuclear magnetic resonance. This technique can measure the distribution of sodium ions based on quantitative detection of those held in aggregates and those dispersed throughout the matrix. Up to three environments are seen in polydisperse NaSPS: isolated $Na^+SO_3^-$ groups at 7 ppm, hydrated $Na(H_2O)_4^+$ groups at 0 ppm, and aggregated sodium ions at –12 to –23 ppm. The ionic aggregates are physical crosslinks, so NMR is a useful technique in determining the efficiency of ionic crosslinking of the pendant sulfonate groups in polystyrene ionomers.

^{23}Na NMR is used to follow the changes in ion distribution as a function of sample composition, such as ionization level and neutralization level. As the sulfonation level increases, the fraction of sodium ions held in isolated ion pairs decreases to zero while the fraction of ionic species in aggregates increases. This is because the distance between sulfonate groups decreases at higher ionization levels. The attractive force between dipoles depends inversely on the fourth power of the distance between the ion groups, so the sodium sulfonate ion pairs are more likely to aggregate at higher ion concentrations. This coincides with a shift in the peak position of the aggregated sodium ions to lower frequency, indicative of increased quadrupolar interactions. As the neutralization level is increased at a constant 3.4% sulfonate content, the aggregate peak shifts to higher frequency due to incorporation of the neutralizing agent, NaOH, into the aggregates. At

neutralization levels above stoichiometric, a separate NMR peak characteristic of phase-separated NaOH appears. At this point, the mechanical properties of the material are compromised.

The effects of sample history, such as type of solvent used in solvent casting, level of humidification, and extent of annealing can also be determined. Solution casting has a significant effect on the local morphology of NaSPS. NaSPS with 1.7% sulfonate groups cast from solutions of DMF or THF/water at low concentrations show more aggregated ions than those samples cast from relatively nonpolar solvents such as THF and THF/methanol mixtures. The polar component solvates the ions and dissociates the aggregates, permitting redistribution of the ions into more favored arrangements upon film formation. Additionally, casting from a relatively nonpolar cosolvent, in which the nonpolar component has the higher boiling point, increases the fraction of isolated ions. No changes due to sample history appear for more highly sulfonated samples (4.2% styrene sulfonate groups). At this ion content, ion-pair interactions are strong enough to ensure that all ions reside in aggregates regardless of solvent history. The changes in morphology due to solution casting appear to have reversible character; redissolving a sample in different casting solvents can cause the isolated ions to appear or disappear repeatedly.

Fully dried NaSPS at 1.7% sulfonation shows two peaks, indicating isolated and aggregated sodium ions. Once humidified, a third peak appears at 0 ppm. With humidification of 1.7% NaSPS at 80°C, all sodium ions are in hydrated sites, $Na(H_2O)_4^+$, demonstrating that all ion pairs – isolated or aggregated – are readily hydrated. The extent of hydration is a function of humidification temperature. At low temperatures (40°C), most aggregated

ions and some isolated ions are not hydrated after 72 hours and the peak due to hydrated ions at 0 ppm is not distinct. This is due to both time and temperature effects; a sample stored at room temperature and humidity for several years showed a significant fraction of humidified ions. The ionomers show a redistribution of ions on subsequent drying, with more ions residing in aggregates. Water swells the aggregates, increasing mobility and allowing this redistribution to occur.

Annealing ionomers at temperatures above the glass transition temperature of the polymer leads to an increase in the number of isolated ions and a shift in the peak position of the aggregate peak. The creation of isolated ions indicates some dissociation of the aggregates with heating. A reversible first-order rate expression describes the isolated-ion variation with annealing treatment, with a heat of reaction of 6.3 kcal/mol. The effects of annealing are reversible if the sample is cast from a cosolvent of THF and water; however, cosolvents such as toluene/methanol serve to increase the fraction of isolated ions further. Thus, the distribution of sodium ions between isolated sites and aggregated sites can be varied widely depending only on sample processing history.

The role of molecular weight polydispersity in ionomer local morphology is also significant. In monodisperse NaSPS, a fourth NMR peak at -2.7 ppm appears at ionization levels above 1.2% and molecular weights of at least 35,000. The fraction of NMR intensity due to this peak is relatively constant above M_n~ 100,000. It is proposed that this peak is due to a distorted version of an isolated site. Along with the new -2.7 ppm peak, the monodisperse materials also have far fewer isolated ions than the corresponding polydisperse ionomers. It is possible that the greater chain uniformity of the

monodisperse ionomers prevents plasticization of the aggregates by low molecular weight components and limits steric hindrances from high molecular weight components, permitting more complete aggregation of the ionic groups. The new NMR peak intensity can be reduced to a shoulder by casting from a cosolvent of THF/water but not by casting from THF/methanol. Blending two or more monodisperse materials in solution followed by annealing results in an NMR spectrum similar to that of a polydisperse material; however, the behavior of the blend without annealing does not replicate that of polydisperse NaSPS.

The investigation into the effects of incorporating ions into polymers can be extended from ionomers to blends of polymers containing interacting groups with small metal-containing molecules. Polyurethanes are excellent candidates for incorporation of these interacting groups through their chain-extenders. Once such example is a pyridine-containing polyurethane. Blends with transition-metal ions such as Zn^{2+} (in the form of zinc acetate) show significant improvement in mechanical properties compared to the unblended polyurethane. ^{15}N NMR offers direct evidence of complexation of the zinc cation with the pyridine nitrogen in these materials; the NMR peak due to the pyridine nitrogen shifts from –320 ppm to –304 ppm after blending. Cross-polarization dynamics of the nitrogen nuclei are affected as well; the peak due to the pyridine nitrogen appears at a much higher cross-polarization time after blending. Complexation with zinc acetate would displace nearby hydrogen-bonded protons and make cross polarization less facile. Additionally, the urethane nitrogen peak persists to much longer contact times. This increase could indicate changes in the hydrogen bonding or motion within the hard phase. Similar results are seen for a blend of the polyurethane and

magnesium acetate, but the shift of the NMR peak and the effects on the cross-polarization dynamics are not as significant as those in the blend with zinc acetate. Blends with a monovalent ion, sodium, show no indications of complexation in either the mechanical properties or NMR spectra.

IR and ^{13}C NMR spectra also give indications of interactions between the polyurethane and metal acetate. IR studies show that incorporation of the pyridine-containing chain extender into the polyurethane disrupts the hard-segment crystallinity and alters the hydrogen bonding in the hard domain. Blending with metal acetates does not have as dramatic an effect, but both the urethane nitrogen and the pyridine nitrogen bands shift. The acetate carbonyl ^{13}C NMR peak shifts upfield with blending, and the carbon sites on the pyridine ring are affected as well. The relaxation times of all carbon sites in the hard domain increase when the polyurethane is blended with zinc acetate. This indicates that the kilohertz-frequency motions are being restricted. Additionally, the fraction of slowly-relaxing sites of the carbon closest to the pyridine nitrogen increases by 85% after blending. This is a consequence of the interaction between the zinc cation and the pyridine nitrogen, in which more pyridine groups are motionally restricted because of the complexation.

10.2 Recommendations

The recommendations for future research described in this section are an extension of the work in this thesis. ^{23}Na NMR of ionomers has produced interesting results on the distribution of ions among different environments in NaSPS. NMR can identify the individual cation environments, such as isolated and aggregated ions. Extended X-ray absorption fine structure

(EXAFS) work in this laboratory[1-4] has shown that this technique can give very detailed information on the composition and arrangement of atoms in the ionic aggregates. EXAFS is an excellent tool for determining the coordination numbers and distances of nearby atoms for an average cation environment. In combination, these two complementary techniques provide a more complete picture of the structure and morphology of the aggregates.

EXAFS studies of monovalent ions in ionomers have given little, if any, information on the number and type of ions surrounding the cation of interest.[1,5] NMR experiments of other monovalent ions, such as potassium or rubidium, would be expected to give similar results to sodium. However, as was discussed in Chapters 5 and 6, the behavior of divalent ions with sample processing appears to be different than that of monovalent ions. Differences in materials neutralized with monovalent and divalent ions have been noted in studies using infrared spectroscopy,[6-8] SAXS[9] and mechanical properties[10,11] as probes. Divalent ions are tethered to two polymer chains in the solid state, and are already individual cross links before aggregation. Therefore, both the increased ionic interactions between the divalent ions and the steric effects of the additional polymer chains attached to the ions should affect the behavior of the divalent ion. Using this argument, the behavior of trivalent ions will be different from sodium as well. Studying ionomers neutralized with these ions could result in a complete picture of the behavior of ionomers neutralized with nearly any cation. Therefore, parallel EXAFS and NMR experiments of di- and trivalent ions could give the most information on the effect of valency on the behavior seen in NMR and on the structure and morphology of the ionomer systems.

Many of the ions accessible to EXAFS are not NMR active or are of very low abundance. However, two cations are excellent candidates for both experiments: cadmium and aluminum (^{113}Cd and ^{27}Al). Using NMR, studies on the difference in ion distribution at various ionization levels and sample preparation conditions for cadmium- and aluminum-neutralized sulfonated polystyrene can be completed and compared to the results of NaSPS samples prepared in equivalent ways. Then, the NMR spectra of the three materials can be used to gain insight into the local ion environments and the macroscopic properties of samples neutralized with these cations.

The NMR results will also allow the determination of the ion concentration where all ions are aggregated, so the EXAFS studies will be focused on only aggregated ions, not a distribution of both isolated and aggregated ions. SAXS and EXAFS studies of cadmium-neutralized sulfonated polystyrene and polyurethane ionomers have been published.[3,4,12,13] These previous studies reported the presence of the characteristic scattering peak in SAXS, but only one coordination shell around the Cd^{2+} cation in EXAFS, so no clear structure could be elucidated from the data. NMR could be used to determine the best sample composition and preparation conditions for constructing a structure for CdSPS. It is possible that the presence of isolated ions or water masked the second shell of the EXAFS spectrum. By using NMR to determine the presence or absence of water and isolated ions in samples prepared for EXAFS, the effects of these parameters on the intra-aggregate order can be determined. In this way the advantages of and information obtained from each technique can be maximized.

Following the completion of the combined EXAFS/NMR experiments on ionomers neutralized with di- and trivalent cations, similar studies can be completed on mixed cation systems. For example, sodium can be diluted with another NMR-active monovalent nucleus such as rubidium and the NMR structure of both cations can be studied. Many questions are still unanswered about these types of systems, such as how would the difference in cation size affect the packing? Would the interactions between Rb and Na be dramatically different than Na–Na interactions? How are the mechanical properties affected by the choice of cations and the compositional ratio? Similar work can be completed on divalent ions such as cadmium combined with any one of a number of cations, such as zinc. In this case, NMR would give useful information on the extent of aggregation and how it is affected by the second cation. EXAFS could supply data on the identity of nearest neighbors in the aggregates to determine if the two cations cluster into mixed aggregated or segregated aggregates. Finally, investigations on systems of mixed monovalent and divalent ionomers can be completed. For mixed systems such as cadmium and sodium, it will be interesting to determine whether the mechanical properties of the mixed system are intermediate, increased or decreased relative to the ionomers with either type of cation. EXAFS can determine whether or not the cations form mixed aggregates and if they do, EXAFS can determine what order, if any, is present. NMR can again show the extent of aggregation and the effects of the additional cation on the aggregation. The ability to probe both cation species with these two techniques will be a distinct advantage in terms of defining the aggregate structure in the materials.

References for Chapter Ten

1 Yarusso, D.J.; Ding, Y.S.; Pan, H.K.; Cooper, S.L. *J. Polym. Sci.. Phys. Ed.* 1984, 22, 2073.

2 Visser, S.A.; Cooper, S.L. *Polymer*, 1992, **33**, 930.

3 Grady, B.P.; Cooper, S.L. *Macromol.* 1994, **27**, 6627.

4 Grady, B.P.; Cooper, S.L. *Macromol.* 1994, **27**, 6635.

5 Pan, H.K.; Knapp, G.S.; Cooper, S.L. *Coll. Polym. Sci.* 1984, **262**, 734.

6 Brozoski, B.A.; Coleman, M.M.; Painter, P.C. *Macromol.* 1984, **17**, 230.

7 Brozoski, B.A.; Painter, P.C.; Coleman, M.M. *Macromol.* 1984, **17**, 1591.

8 Han, K.; Williams, H.C. *J. Appl. Polym. Sci.* 1991, **42**, 1845.

9 Weiss, R.A.; Lefelar, J.A. *Polymer*, 1986, **27**, 3.

10 Hara, M.; Jar, P.; Sauer, J.A. *Macromol.* 1990, **23**, 4465.

11 Hara, M.; Jar, P.; Sauer, J.A. *Polymer*, 1991, **32**, 1625.

12 Register, R.A.; Foucart, M.; Jérôme, R.; Ding, Y.S.; Cooper, S.L. *Macromol.* 1988, **21**, 1009.

13 Ding, Y.S.; Register, R.A.; Yang, C.-Z.; Cooper, S.L. *Polymer*, 1989, **30**, 1221.